TECHNICAL REPORT STANDARD TITLE PAGE

1. Report No.	2. Government Accession No.	3. Recipient's Catalog No.
FHWA/TX-86/07+306-2F		

4. Title and Subtitle	5. Report Date
THE APPLICATION OF CUMULATIVE DAMAGE FATIGUE THEORY TO HIGHWAY BRIDGE FATIGUE DESIGN	November 1984
	6. Performing Organization Code
7. Author(s)	8. Performing Organization Report No.
Kurt D. Swenson and Karl H. Frank	Research Report 306-2F
9. Performing Organization Name and Address	10. Work Unit No.
Center for Transportation Research The University of Texas at Austin Austin, Texas 78712-1075	11. Contract or Grant No. Research Study 3-5-81-306
	13. Type of Report and Period Covered
12. Sponsoring Agency Name and Address Texas State Department of Highways and Public Transportation; Transportation Planning Division P. O. Box 5051 Austin, Texas 78763	Final
	14. Sponsoring Agency Code

15. Supplementary Notes

Study conducted in cooperation with the U. S. Department of Transportation, Federal Highway Administration. Research Study Title: "Determination of the Influence of Low-Level Stress Ranges on the Fatigue Performance of Steel Weldments"

16. Abstract

The influence of small stress cycles caused by the dynamic response of a bridge upon the fatigue life of welded components was studied. Various loading waveforms were used to load a cantilever welded tee specimen. The fatigue life was measured and means of transforming the loading waveform to constant amplitude waveform producing the same damage were investigated. The waveforms investigated included actual stress histories measured on an in-service bridge loaded with both a single test vehicle and under normal traffic.

The results of the study indicate that the small stress cycles cause considerable fatigue damage and cannot be ignored in the design and evaluation of steel bridges for fatigue. Based on the results of the experimental study and an evaluation of the stress histories of three bridges, a simple means for estimating the damage done by these small cycles was developed using a fatigue factor. The design stress range including the normal AASHTO impact fraction for a single vehicle passage should be multiplied by a fatigue factor of 1.15 to include the fatigue damage done by these minor cycles.

The factor of 1.15 is the best estimate for medium span girder bridges. Other type and span bridges may produce different values according to their dynamic behavior. The most accurate means of obtaining this value is through field stress measurements of the actual bridge.

17. Key Words	18. Distribution Statement
small stress cycles, dynamic response, bridge fatigue life, welded components, loading waveforms, design	No restrictions. This document is available to the public through the National Technical Information Service, Springfield, Virginia 22161.

19. Security Classif. (of this report)	20. Security Classif. (of this page)	21. No. of Pages	22. Price
Unclassified	Unclassified	240	

Form DOT F 1700.7 (8-69)

THE APPLICATION OF CUMULATIVE DAMAGE FATIGUE THEORY TO HIGHWAY BRIDGE FATIGUE DESIGN

by

Kurt D. Swenson and Karl H. Frank

Research Report 306-2F

Research Project 3-5-81-306

"Determination of the Influence of Low-Level Stress Ranges on the Fatigue Performance of Steel Weldments"

Conducted for

Texas
State Department of Highways and Public Transportation

In Cooperation with the
U.S. Department of Transportation
Federal Highway Administration

by

CENTER FOR TRANSPORTATION RESEARCH
BUREAU OF ENGINEERING RESEARCH
THE UNIVERSITY OF TEXAS AT AUSTIN

November 1984

The contents of this report reflect the views of the authors who are responsible for the facts and accuracy of the data presented herein. The contents do not necessarily reflect the official views or policies of the Federal Highway Administration. This report does not constitute a standard, specification, or regulation.

There was no invention or discovery conceived or first actually reduced to practice in the course of or under this contract, including any art, method, process, machine, manufacture, design or composition of matter, or any new and useful improvement thereof, or any variety of plant which is or may be patentable under the patent laws of the United States of America or any foreign country.

P R E F A C E

This report presents the results of the third and final phase of Research Project 3-5-81-306, "Determination of the Influence of Low Level Stress Ranges on the Fatigue Performance of Steel Weldments." This research was sponsored by the Texas State Department of Highways and Public Transportation and the Federal Highway Administration. Specimen testing was performed at the Phil M. Ferguson Structural Engineering Laboratory of The University of Texas at Austin.

The authors are grateful to Dr. Joseph A. Yura for his help, to Peter G. Hoadley for his collection of useful field data, and to John M. Joehnk for the foundation he laid in the first phase of the project. Special thanks are extended to Farrel Zwerneman for taking time to familiarize the author with testing and analysis procedures. Special thanks are also extended to Bahram (Alex) Tahmassebi whose computer software allowed for the development of the complicated loading histories used in the study.

S U M M A R Y

The influence of small stress cycles caused by the dynamic response of a bridge upon the fatigue life of welded components was studied. Various loading waveforms were used to load a cantilever welded tee specimen. The fatigue life was measured and means of transforming the loading waveform to constant amplitude waveform producing the same damage were investigated. The waveforms investigated included actual stress histories measured on an in-service bridge loaded with both a single test vehicle and under normal traffic.

The results of the study indicate that the small stress cycles cause considerable fatigue damage and cannot be ignored in the design and evaluation of steel bridges for fatigue. Based on the results of the experimental study and an evaluation of the stress histories of three bridges, a simple means for estimating the damage done by these small cycles was developed using a fatigue factor. The design stress range including the normal AASHTO impact fraction for a single vehicle passage should be multiplied by a fatigue factor of 1.15 to include the fatigue damage done by these minor cycles.

The factor of 1.15 is the best estimate for medium span girder bridges. Other type and span bridges may produce different values according to their dynamic behavior. The most accurate means of obtaining this value is through field stress measurements of the actual bridge.

I M P L E M E N T A T I O N

The results of this study indicate that the design of steel bridges for a finite life (bridges with design stress ranges greater than the over 2 x 10^6 cycles stress ranges in the AASHTO Specifications) needed to be designed using a design stress range greater than that calculated using the AASHTO Specification. The design stress ranges should be multiplied by 1.15 to account for the influence of the small stress cycles upon the fatigue life of a weldment. In bridge designs which satisfy the over 2 x 10^6 allowable stress ranges, the present AASHTO Specifications are adequate.

The fatigue factor of 1.15 should also be used when evaluating in-service bridges. However, the most accurate method to determine the remaining life of a bridge is to perform a field stress measurement on the bridge to determine its actual behavior. The rainflow counting method and damage models developed in this study can then be used to evaluate the reamining life of the bridge.

TABLE OF CONTENTS

TABLE OF CONTENTS (continued)

LIST OF TABLES

LIST OF TABLES (continued)

LIST OF FIGURES

LIST OF FIGURES (continued)

LIST OF FIGURES (continued)

LIST OF FIGURES (continued)

LIST OF FIGURES (continued)

N O T A T I O N

A	N axis intercept on log-log S_R-N curve
a	Empirical factor used in mean stress damage theory
ADTT	Average daily truck traffic
CF	Correction factor used in stress interaction damage theory
D_L	Design life in days
F	Damage factor
F_{EXP}	Experimental damage factor
F_G	Damage factor calculated using Gurney's theory
F_M	Damage factor calculated Miner's theory
F_{NLM}	Damage factor calculated using Joehnk's theory
F_{PRED}	Damage factor calculated by any method
F_{SI}	Damage factor calculated using stress interaction method
GVW	Gross vehicle weight of truck
I	Impact fraction
I_F	Fatigue factor
L	Bridge span length, feet
m	Slope of log-log S_R-N curve
n_c	Number of stress cycles in a complex cycle
n_i	Number of stress cycles applied at S_{Ri}
N_c	Number of complex cycles to failure
N_D	Number of stress cycles in a design life
N_i	Number of stress cycles to failure at S_{Ri}
N_{MAX}	Number of stress cycles to failure at S_{RMAX}

N O T A T I O N (continued)

P_i	Ratio of S_{Ri} and S_{RMAX}
R	Ratio of minor cycle maximum stress to major cycle maximum stress
S_{MEAN}	Mean stress of a cycle
S_{MAX}	Maximum stress of a cycle
S_{Rd}	Stress range distribution = $S_{RM} - S_{RMIN}$
S_{RD}	Design stress range
S_{REC}	Complex effective stress range
S_{REQ}	Equivalent stress range, represents truck passage
S_{Ri}	Stress range of i^{th} cycle
S_{RM}	Modal stress range
S_{RMAX}	Maximum stress range in a complex cycle
S_{RMIN}	Minimum stress range
S_{RS}	Static component of equivalent stress range
V_i	Number of stress excursions at S_{Ri} in a complex cycle
w_c	Work done by a complex cycle
w_i	Work done by n_i cycles
W	Work done at failure
x_i	Total number of excursions in a complex cycle equal to or exceeding P_i
z	Stress range of minor excursion in complex cycle
Z_{EFF}	Effective stress range of a minor excursion in a complex cycle calculated by Joehnk
α	Reduction factor used in AASHTO specifications

β Elastic constant relating load and stress

δ_i Frequency of occurrence of $(GVW)_i$

λ Stress interaction factor, used in calculation of CF

ϕ_i $(GVW)_i$ / $(GVW)_{design}$

C H A P T E R I

INTRODUCTION

1.1 Background

In addition to dead loads, a highway bridge is subjected to a large number of cyclic live loads during its design life. The primary source of these cyclic live loads is vehicle traffic with truck traffic producing the most damaging loads. The cyclic stresses produced by a truck, as shown in Fig. 1.1, contain one major stress cycle with smaller superimposed stress cycles. Throughout the design life of the bridge random truck traffic imposes a random series of cyclic loads on the bridge similar to the one shown in Fig. 1.1. The addition of cyclic live loads to the loading of a bridge introduces the problem of fatigue failure into highway bridge design. Therefore, present design specifications limit the allowable live load stresses to prevent premature fatigue failure.

The first comprehensive fatigue design specificatin was adopted by AASHTO in 1973. Since that time, the specification has been revised in 1975, 1976 and 1977. The latest revision was made necessary by studies of existing highway bridges which indicated that the assumed fatigue limit of 2,000,000 cycles was not adequate [2]. The reevaluation, which produced the current AASHTO Fatigue Tables 1.7.2A1 and 1.7.2B shown here in Tables 1.1 and 1.2 respectively, was based on the following two assumptions: 1) the minor cycles contained in a truck loading may be neglected, and 2) the fatigue life can be accurately

TABLE 1.1 AASHTO Fatigue Table 1.7.2A1.

Category (See Table 1.7.2A2)	Allowable Range of Stress, F_{sr}							
	For 100,000 Cycles		For 500,000 Cycles		For 2,000,000 Cycles		For over 2,000,000 Cycles	
	ksi	MPa	ksi	MPa	ksi	MPa	ksi	MPa
REDUNDANT LOAD PATH STRUCTURES[1]								
A	60	413.69	36	248.21	24	165.47	24	165.47
B	45	310.26	27.5	189.60	18	124.10	16	110.31
C	32	220.63	19	131.00	13	89.63	10 12*	68.95 82.74*
D	27	186.16	16	110.31	10	68.95	7	48.26
E	21	144.79	12.5	86.18	8	55.15	5	34.47
F	15	103.42	12	82.74	9	62.05	8	55.15
NONREDUNDANT LOAD PATH STRUCTURES[2]								
A	36	248.21	24	165.47	24	165.47	24	165.47
B	27.5	189.60	18	124.10	16	110.31	16	110.31
C	19	131.00	13	89.63	10 12*	68.95 82.74*	9 11*	62.05 75.84*
D	16	110.31	10	68.95	7	48.26	5	34.47
E	12.5	86.18	8	55.15	5	34.47	2.5	17.24
F	12	82.74	9	62.05	8	55.15	7	48.26

* For transverse stiffener welds on girder webs or flanges.

[1]Structure types with multi-load paths where a single fracture in a member cannot lead to the collapse. For example, a simply supported single span multi-beam bridge or a multi-element eye bar truss member have redundant load paths.

[2]Structure types with a single load path where a single fracture can lead to a catastrophic collapse. For example, flange and web plates in one or two girder bridges, main one-element truss members, hanger plates, caps at single or two column bents have nonredundant load paths.

TABLE 1.2 AASHTO Fatigue Table 1.7.2B.

Main (Longitudinal) Load Carrying Members				
Type of Road	Case	(*ADTT*)*	Truck Loading	Lane Loading†
Freeways, expressways, major highways and streets	I	2,500 or more	2,000,000**	500,000
	II	Less than 2500	500,000	100,000
Other highways and streets not included in Case I or II	III	–	100,000	100,000

Transverse Members and Details Subjected to Wheel Loads				
Type of Road	Case	(*ADTT*)*	Truck Loading	Lane Loading
Freeways, expressways, major highways and streets	I	2,500 or more	Over 2,000,000	–
	II	Less than 2,500	2,000,000	–
Other highways and streets	III	–	500,000	–

*Average daily truck traffic (one direction).

**Members shall also be investigated for "over 2 million" stress cycles produced by placing a single truck on the bridge distributed to the girders as designated in Article 1.3.1(B) for one traffic lane loading.

†Longitudinal members should also be checked for truck loading.

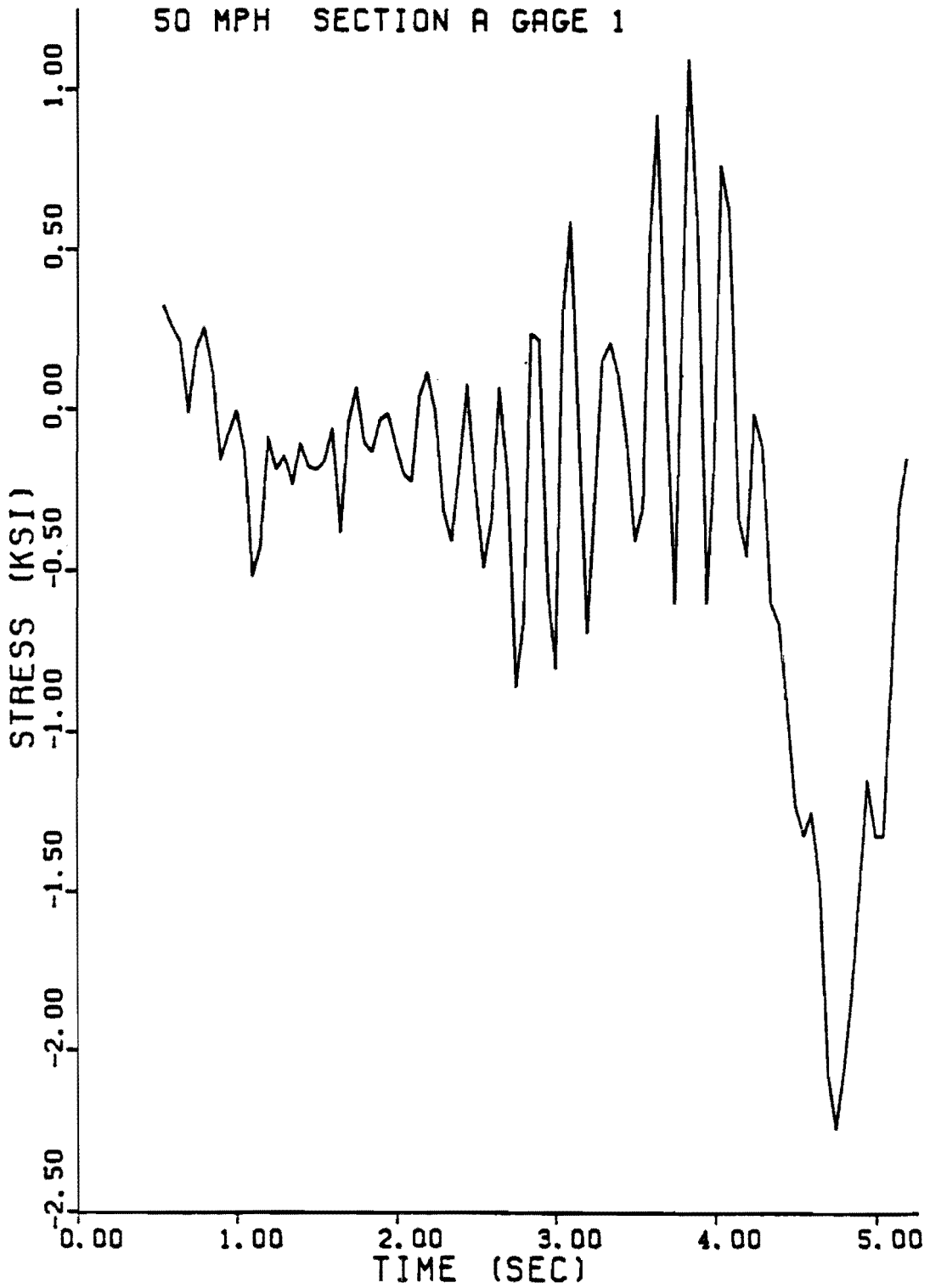

Fig. 1.1 Stress cycles produced by truck passage.

calculated using a linear accumulation of the fatigue damage of each truck as proposed by M. A. Miner [11]. The first assumption leads to the concept that a truck loading can be simulated by one cycle in design. This assumption is questionable because the reevaluation of the specifications was caused by concern over the amount of fatigue damage caused by small stress cycles in the loading history of a bridge [2].

1.2 The Use of One Cycle Per Truck in Design

The concept of one cycle per truck passage was used by the designer in the calculation of an applied stress range before the reevaluation which resulted in the 1977 specifications. It was also used in the determination of allowable design stress ranges in the 1977 specifications.

The bridge designer calculates an equivalent stress cycle to represent the design truck loading as shown schematically in Fig. 1.2. The stress cycle contains the following two components: 1) a static component whose magnitude is based on the gross vehicle weight (GVW) of the design truck; and 2) a dynamic component whose magnitude is based on the bridge span. The static component is calculated by static structural analysis. The dynamic component, given by the impact fraction I, is calculated by the following equation:

$$I = (50)/(L + 125); \; I \leq 0.30 \qquad (1.1)$$

where L is the span length in feet. Thus, the magnitude of the equivalent stress cycle is given by:

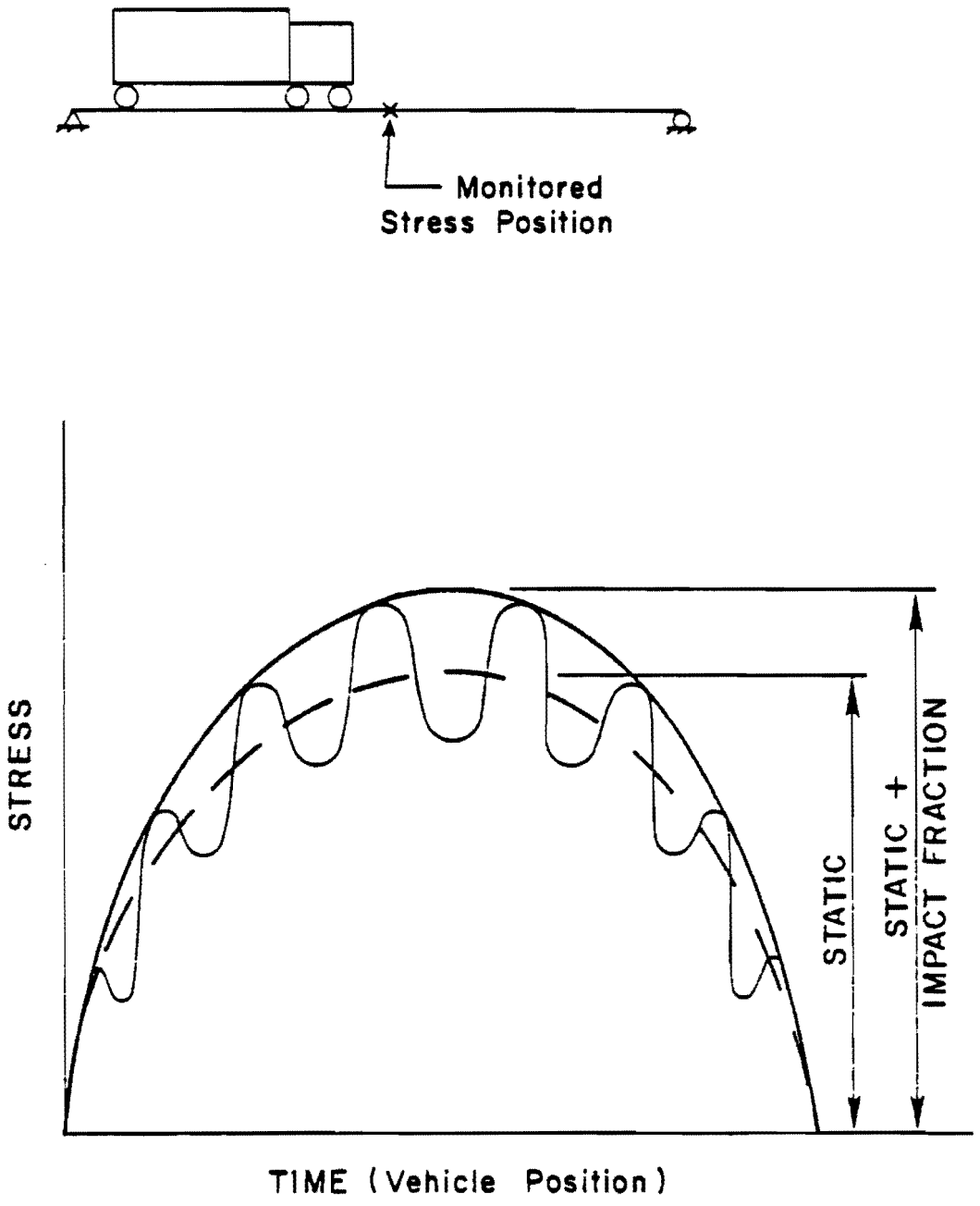

Fig. 1.2 Plot showing the two components of S_{REQ}.

$$S_{REQ} = S_{RS} (1.0 + I) \qquad (1.2)$$

S_{REQ} is the equivalent stress range and S_{RS} of the stress range produced by the static loading.

The relation demonstrated in Eq. (1.2) is shown graphically in Fig. 1.2. The application of this impact fraction to the static load is assumed to accurately predict the peak stresses imposed on the bridge. However, the impact fraction given by Eq. (1.1) does not account for the fatigue damage caused by the minor cycles in a truck loading.

The allowable design stress ranges presented in the Fatigue Table 1.7.2A1 of the AASHTO specifications were derived with the use of a linear cumulative damage theory. The validity of this procedure is discussed further in the next section. However, the damage calculations were made on stress histories which were developed with the assumption of one cycle per truck. The relationship between stress range and GVW was considered linear. Thus, the stress range was expressed as:

$$S_{Ri} = \alpha\beta \, (GVW) \qquad (1.3)$$

where β is an elastic constant based on structural analysis and α is a reduction factor. The use of the reduction factor is based on results of measurements on actual bridges which indicated that the actual peak stress ranges are always less than calculated values. As before, all minor cycles were neglected in the calculation of an equivalent stress range. Thus, the fatigue damage caused by these minor cycles is neglected in the determination of allowable design stress ranges.

The assumption that minor cycles in the truck loading can be neglected in fatigue design is based on the idea that the minor cycles are not large enough to drive a fatigue crack. This assumption has never been experimentally verified. Because including the minor cycles in testing lengthens testing times, and measuring the minor cycles in the field is very difficult. However, recent research by Joehnk [14], Tilly [28], and Fisher [21] suggest that these minor cycles may produce fatigue damage and neglecting them will produce unconservative results.

1.3 Use of Miner's Theory in Design

In developing Tables 1.7.2A1 and 1.7.2B in the AASHTO specification, it was assumed that the fatigue damage produced by random truck traffic could be calculated with Miner's damage theory. This cumulative fatigue damage model is expressed as:

$$\Sigma n_i/N_i = 1.0 \qquad (1.4)$$

at failure, where:

N_i = number of cycles to failure at S_{Ri}

n_i = number of cycles applied at S_{Ri}

Fatigue studies [19] have shown that N_i is related to S_{Ri} for steels by the following equation:

$$N_i = A\ S_{Ri}^{-3} \qquad (1.5)$$

where A is the N axis intercept for a log-log S_R-N curve for a specific detail. As discussed in Section 1.2, S_{Ri} was determined without

accounting for the fatigue effects of the minor cycles of a truck loading. In the AASHTO analylsis, S_{Ri} is given by Eq. (1.3).

Combining Eqs. (1.3), (1.4), and (1.5), the AASHTO specification determined that the fatigue life under random traffic could be written as:

$$\frac{(\alpha)^3}{A} \Sigma n_i [\beta (GVW)_i]^3 = 1.0 \qquad (1.6)$$

When $(GVW)_i$ is expressed in terms of a design vehicle weight $(GVW)_D$, and n_i is expressed as the frequency of occurrence of $(GVW)_i$; Eq. (1.6) becomes:

$$\frac{(\alpha)^3}{A} [\beta (GVW)_D]^3 \ (ADT)(D_L) \ \Sigma \gamma_i \phi_i^3 = 1.0 \qquad (1.7)$$

where:

ADTT = average daily truck traffic

D_L = design life in days

ϕ_i = $(GVW)_i/(GVW)_D$

γ_i = frequency of occurrence of $(GVW)_i$

Miner's cumulative damage theory is represented by the summation in Eq. (1.7). The value of the summation set by AASHTO was influenced by two factors. First, the value of the summation was calculated based on the 1970 FHWA Loadometer Survey shown in Fig. 1.3. However, as stated earlier, there was concern over the amount of damage done by cycles below the fatigue limit. Research done by Tilly [28] and Fisher [21] indicated that if the design stress range is below the fatigue limit, then no fatigue damage occurs. In order to ensure an

Fig. 1.3 GVW distribution from 1970 FHWA Loadometer Survey.

adequate fatigue life for bridges subjected to a large number of truck passages, Eq. (1.7) was used to set a limit on the average daily truck traffic for a finite life design. The allowable stress ranges for bridges with an average daily truck traffic greater than 2500 are set in order to produce an infinite fatigue life.

In Eq. (1.7), the design stress range S_{Rd} is given by the term $(GVW)_D$. An additional expression for S_{Rd} can be derived from Eq. (1.5):

$$(S_{Rd})^3 = A/N_D \tag{1.8}$$

where N_D is the number of constant amplitude cycles in the design life. By combining Eqs. (1.7) and (1.8) the following expression for N_D in terms of ADTT is derived:

$$N_D = \frac{(ADTT)(D_L)(n)^3}{2.85} \tag{1.9}$$

The values of N_D present in AASHTO Fatigue Table 1.7.2B are based on the relationship expressed in Eq. (1.9). The allowable design stress ranges which correspond to N_D and a specific detail presented in Table 1.7.2A1 are defined by Eq. (1.8).

Miner's cumulative damage theory has been supported by the results of several experimental investigations [11,12,20]. However, because Miner's model has no basis in fracture mechanics, its applicability is based only on available experimental data. Empirical results are often used as a basis of design; however, the loadings used to test Miner's theory have little in common with actual highway bridge

loadings. In addition, there is no experimental data generated using actual measured highway bridge loadings.

Researchers in highway bridge fatigue have used loading patterns which only simulate actual bridge loadings. As mentioned in the previous section, all researchers have assumed that the minor cycles in a truck loading could be neglected, so these stress cycles were not included in testing. The most commonly used loading patterns are the 1) block and 2) random discrete loading patterns. Reference 1 provides a detailed description of each loading. Two examples of block loading are shown in Fig. 1.4. Research done using block loadings include work done by Alder [20], Miner [11], Fisher [21], and Albrecht and Yamada [16]. An example of random discrete loading is shown in Fig. 1.5. Research done using random discrete loadings include NCHRP Project 12-12 [12] and work done by Fisher [21].

The ability of the two loading patterns to adequately test the applicability of Miner's theory in design is limited by two factors. First, the minor cycles in a truck loading are neglected; consequently, the histograms of test loadings do not resemble those of actual loadings. Second, both loading patterns have a constant mean or minimum stress unlike actual bridge loadings (see Fig. 1.1). Research done by Zwerneman [1] indicates that the level of the mean stress of the minor cycles affects the amount of fatigue damage they produce. Since a constant mean or minimum stress level imposes artificial stress levels on the minor cycles, loadings with a constant mean or minimum stress will not simulate loadings without a constant stress level. Measured

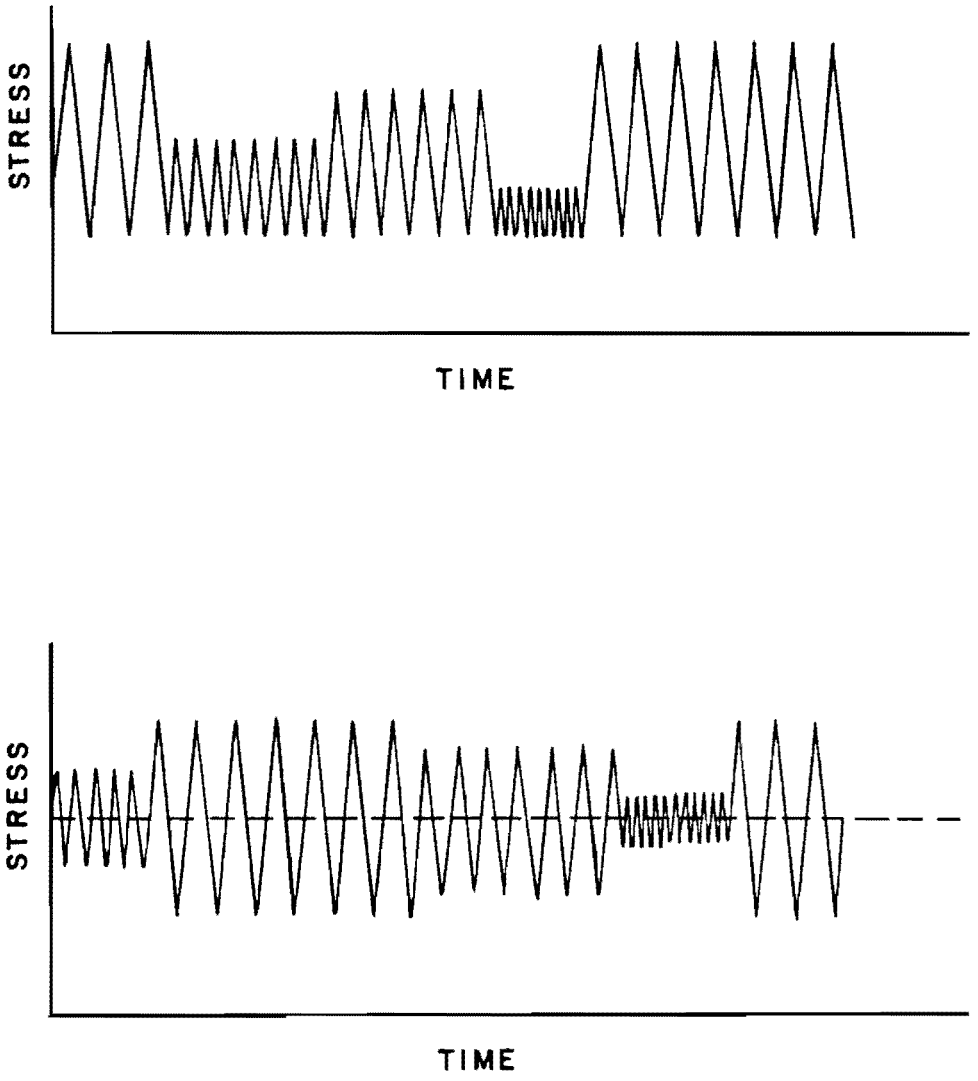

Fig. 1.4 Two examples of block loading pattern.

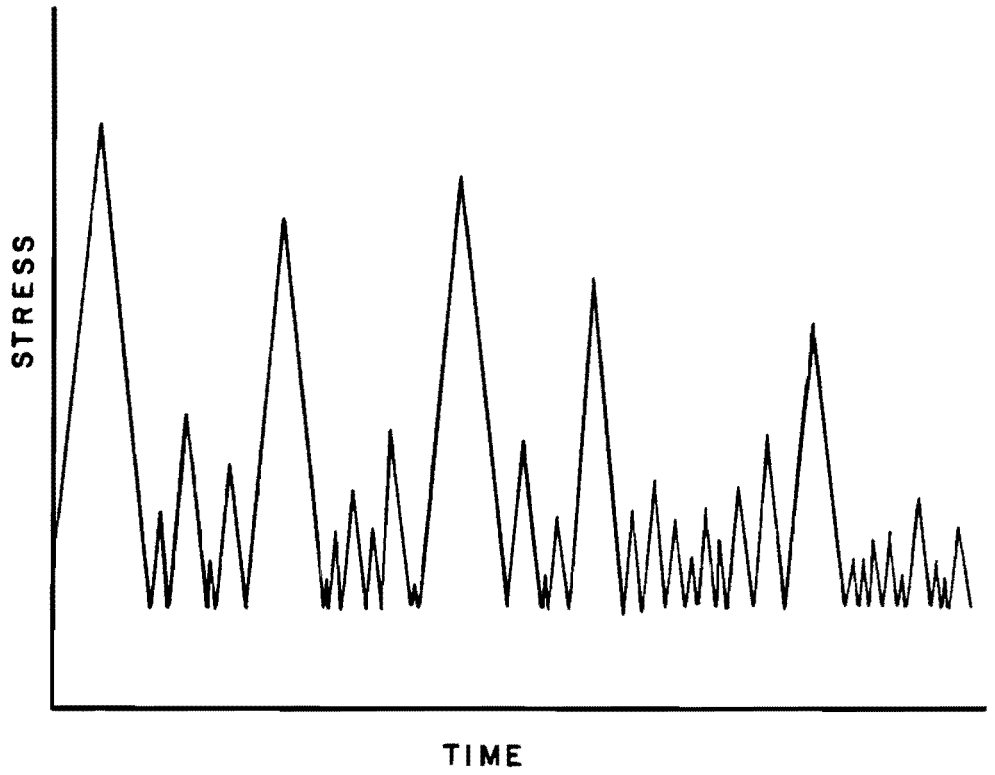

Fig. 1.5 Example of random discrete loading pattern.

bridge loadings do not possess any constant stress levels [18]. Therefore, block and random discrete loadings may not simulate actual bridge loadings adequately.

Because past experimental stress histories which validate the use of Miner's rule in design do not represent actual stress histories, the use of Miner's rule in design is still questionable. In addition, recent research by Gurney [13], Joehnk [14], and Zwerneman [1] indicates that Miner's cumulative damage theory produces unconservative fatigue life predictions for some loadings. Thus, testing using measured bridge loadings is necessary to determine if it is safe to use Miner's rule in design.

1.4 Problem Statement

This study is part of an ongoing investigation of variable amplitude fatigue in highway bridges. The main objective of the investigation is to determine the soundness of present AASHTO fatigue specifications. To fulfill this objective, the fatigue behavior of specimens loaded with measured highway bridge stress histories is compared to the behavior predicted by the analyses used in the AASHTO specifications.

The first stage of the investigtion was the gathering of field data. This was done by Peter G. Hoadley [18] in a previous research project. Two types of load histories were measured. One was produced by the passage of a single test truck and one was produced by normal vehicle traffic. Hoadley developed a design method which combined Miner's rule and a modified rainflow cycle counting technique which

accounted for the minor cycles in the loading history. However, there was no experimental verification of this method of analysis.

The next phase of the study was completed by John M. Joehnk [14]. Joehnk attempted to verify Hoadley's analysis experimentally, and investigate the amount of fatigue damage caused by minor cycles. Several superimposed sine stress histories were used in this set of tests. The results of Joehnk's experiments indicated that the use of Miner's rule and modified rainflow counting produces unconservative results. In addition, the results showed that minor cycles produce a significant amount of fatigue damage. From his experimental results, Joehnk developed a nonlinear damage model to be used with modified rainflow counting.

In the third phase of the investigation, Zwerneman conducted experiments using a measured stress history produced by the passage of a single test truck [1]. The results of Zwerneman's testing showed that Miner's rule was again unconservative, and Joehnk's model as well as one proposed by T. R. Gurney [13] were overly conservative. In addition, the results indicated that the minor cycles in the measured truck loading produced a significant amount of fatigue damage. Further testing by Zwerneman demonstrated that the amount of fatigue damage produced by the minor cycles is effected by their mean stress levels.

At this point in the study two procedures in the AASHTO fatigue analyses have been challenged by experimental data. First is the assumption that highway bridge fatigue life can be calculated by Miner's cumulative fatigue damage theory. Second is the use of one cycle per

truck passage without accounting for the fatigue damage produced by the minor cycles in the truck loading. In addition, Zwerneman's investigation into mean stress effects indicates that a large portion of past research using a constant mean or minimum stress may not be applicable to design.

1.4 Research Objectives

1. Determine the applicability of Miner's cumulative damage theory in design using measured bridge loadings.

2. Develop a method of representing the passage of a single truck in design which accounts for the fatigue damage caused by the minor cycles.

3. Determine the ability of random discrete load patterns to simulate actual highway bridge loadings.

C H A P T E R I I

VARIABLE AMPLITUDE FATIGUE ANALYSIS

Variable amplitude fatigue analysis can be divided into three steps: (1) development of a finite load history which represents the loads imposed on the structure; (2) calculation of an equivalent constant amplitude load history to replace the variable load history; and (3) determination of the fatigue life using a curve developed from constant-amplitude stress range tests. This report deals with steps (1) and (2). In this chapter, step (2) will be discussed in detail.

The calculation of an equivalent constant amplitude load history requires two steps: (1) cycle counting and (2) calculating fatigue damage. In cycle counting, the variable amplitude history is described as a number of stress cycles. The total fatigue damage is calculated by summing the fatigue damage done by each stress cycle. The summation is based on a cumulative damage theory which relates the damage done by each stress cycle to the damage done by a constant amplitude history of the same magnitude.

Presently, there are two ways to characterize the equivalent constant amplitude load history described in step (2). Use of either of the terms will produce the same fatigue life. However, the terminology can become confusing.

In this chapter, the terms used to describe the equivalent constant amplitude history will be defined. Then, several cycle

counting methods and cumulative damage theories will be presented and evaluated.

2.1 Terminology

In this study, the finite load history described in step (1) of the variable amplitude fatigue analysis will be referred to as a "complex" cycle. The load history of a structure is described by repetition of the "complex" cycle. Thus, the load history can be treated as a constant amplitude history in which each cycle is a "complex" cycle. This terminology has direct application in highway bridge design. The passage of a truck causes a variable amplitude loading which can be defined as one "complex" cycle. The "complex" cycle concept allows for the fatigue life to be described in "complex" cycles or truck passages while still accounting for damage done by minor cycles. However, the "complex" cycle concept causes some confusion when used with more traditional terminology.

The confusion occurs in attempting to characterize the equivalent constant amplitude load history. The effective stress range is the most common method of relating a variable history and its equivalent constant amplitude history. The effective stress range is defined as the constant amplitude stress range which produces the same fatigue damage as the variable stress ranges in the same number of cycles. Thus, "n" variable stress cycles can be replaced by "n" constant amplitude stress cycles, as shown schematically in Fig. 2.1a.

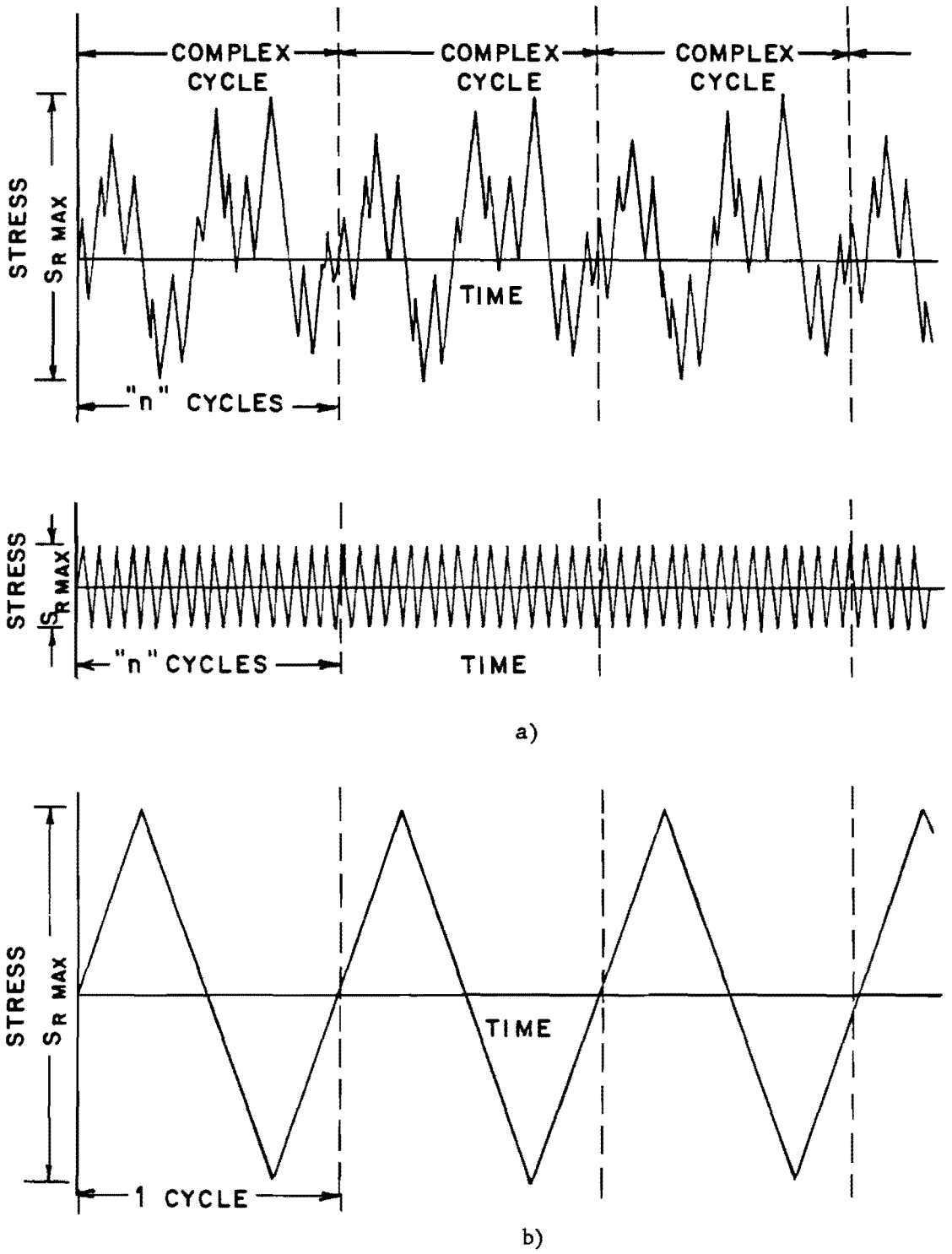

Fig. 2.1 Definition of simple and complex effective stress ranges.

This effective stress range will be referred to as the simple effective stress range (S_{RES}), as it treats each cycle of the load history as a simple, independent cycle.

When using the "complex" cycle concept, there are two ways to relate variable load histories and their equivalent constant amplitude loadings. The first is with an effective stress range similar to the simple effective stress range. The second is using a damage factor which indicates the amount of fatigue damage done by the minor cycles of the load history.

The effective stress range used in combination with "complex" cycles will be referred to as the complex effective stress range (S_{REC}) since it describes complex cycles. The complex effective stress range is defined as the constant amplitude stress range which produces the same fatigue damage as the variable stress ranges in the complex cycle with only one cycle. Thus, "n" variable stress cycles defined as a "complex" cycle can be replaced by one stress cycle as shown schematically in Fig. 2.1b.

The two effective stress ranges can be compared mathematically through a third variable known as the damage factor. The damage factor was used by Zwerneman [1] to describe the damage done by the minor cycles in a variable amplitude history. The damage factor F is defined as the ratio of the fatigue life of the structure under a constant amplitude stress history at the maximum stress range of the complex cycle and the fatigue life under the variable amplitude stress history. In general form, the damage factor can be expressed as:

$$F = N_{MAX}/N_c \qquad (2.1)$$

where N_{MAX} = number of constant amplitude cycles to failure at S_{RMAX}, N_c = number of complex cycles to failure, and F = damage factor.

F is a function of the shape of the load history, not its magnitude. This fact makes F an excellent way to compare the fatigue behavior of different types of stress histories. A high damage factor means the small minor cycles in the complex cycle cause much more fatigue damage than a constant amplitude history of the same magnitude. Since the addition of minor cycles to a constant amplitude loading can only increase the fatigue damage caused by the stress history, F is always greater than 1.0.

The fact that fatigue life is proportional to stress range means that the damage factor can be used to determine the effective stress ranges. The relationship between the damage factor and the effective stress ranges can be expressed as follows:

$$S_{RES} = S_{RMAX} (F/n_c)^{1/m} \qquad (2.2)$$

$$S_{REC} = S_{RMAX} (F)^{1/m} \qquad (2.3)$$

So,
$$S_{REC} = S_{RES} (n_c)^{1/m} \qquad (2.4)$$

where

S_{RMAX} = maximum stress range in the finite load history

F = damage factor

n_c = total number of cycles in the complex cycle

m = slope of log N vs. log S_r curve

A development of the effective stress range and damage factor is presented in Appendix A.

Equations (2.2) and (2.3) show the difference between the simple effective stress range and the complex effective stress range. First, the simple effective stress range accounts for the length of the load history while the complex effective stress range does not. Since F is always greater than 1.0, the complex effective stress range is always greater than S_{RMAX}. A minor cycle can never cause as much fatigue damage as a major cycle so F/n_c is always less than 1.0. So, the simple effective stress range is always less than S_{RMAX}. Equation (2.4) shows the exact relation between the simple and complex effective stress range. Since n_c is always greater than 1.0, S_{REC} is always greater than S_{RES}. In addition, as the number of cycles in the load history increases, S_{REC} increases in relation to S_{RES}.

2.2 Cycle Counting

The clear definition of a stress cycle within a variable amplitude stress history is obviously crucial to a variable amplitude fatigue analysis. However, the definition of a stress cycle is not obvious in most variable amplitude stress histories. For waveforms using a constant minimum stress or constant mean stress, cycles are easily defined without a cycle counting method, as shown in Figs. 2.2a and 2.2b. The stress histories used in this study which are similar to those applied to highway bridges have variable minimum and mean stresses. In these

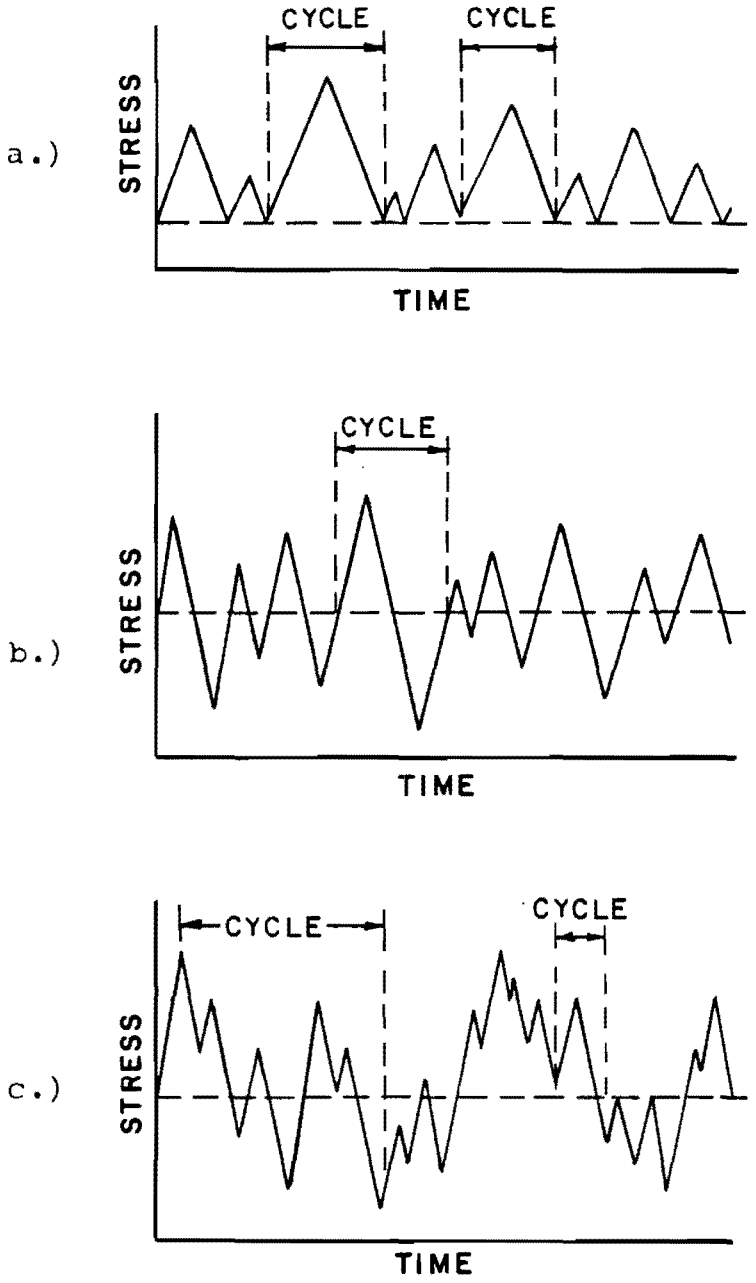

Fig. 2.2 Schematic definition of a stress cycle in various waveforms.

complicated stress histories, the definition of a cycle is vague as shown in Fig. 2.2c. Therefore, a cycle counting procedure is required to define the stress cycles.

There are several methods of defining a stress cycle in a variable stress history. A detailed explanation of the various counting procedures is supplied by Dowling [3], and Wirshing and Shehata [4]. Only a brief discussion of the methods will be presented here. The methods used for cycle counting have been grouped according to their basic definition of a cycle.

1. Peak counting methods--Peak counting methods define a cycle using the maximum and minimum peaks in the stress history. In the peak count method, each peak represents a cycle. This definition tends to magnify stress cycles. The zero crossing peak count method defines a cycle as a maximum or minimum peak between two zero crossings. This technique neglects minor cycles in the stress history.

2. Range counting methods--In range counting, a cycle is defined by pairing half-cycles. A half-cycle is the difference between a minimum stress peak and the next consecutive maximum stress peak. There are two techniques which utilize range counting methods, the range count and the range pair methods. Both methods yield some unpaired half-cycles which cannot be included in the fatigue analysis. In addition, the range counting methods will not account for some low frequency large stress cycles when high frequency small stress cycles are superimposed on them.

3. Rainflow counting method--This method defines a cycle as a closed hysteresis loop in the stress-strain history [5], as shown in Fig. 2.3. The rainflow technique defines half-cycles from a stress-time diagram. The half-cycles are paired to form stress cycles as with the range counting methods. This method produces unpaired half-cycles but it accounts for all parts of the stress history.

4. Modified rainflow counting method--A modification to the stress history can eliminate the unpaired half-cycles that result from rainflow, as well as range pair counting. The elimination of unpaired half-cycles is accomplished by reordering the stress history. The portion of the stress history occurring before the absolute maximum is moved to the end of the stress history. Thus, the stress history shown in Fig. 2.4a will become the history in Fig. 2.4b. A rainflow or range pair count done on the modified history will not have unpaired half-cycles. This modification in the stress history leads to another counting method known as the reservoir counting method.

5. Reservoir counting method--The reservoir counting method is based on the stress-strain hysteresis loop as the rainflow counting method. However, this technique works only with a modified stress history. The load history is considered to be a "reservoir" as shown in Fig. 2.5b. Stress cycles are counted by draining the "reservoir" at the relative minimum stresses from the lowest to the highest. Each time the reservoir is drained defines a stress cycle. The height of "water" drained determines the stress range of the cycle.

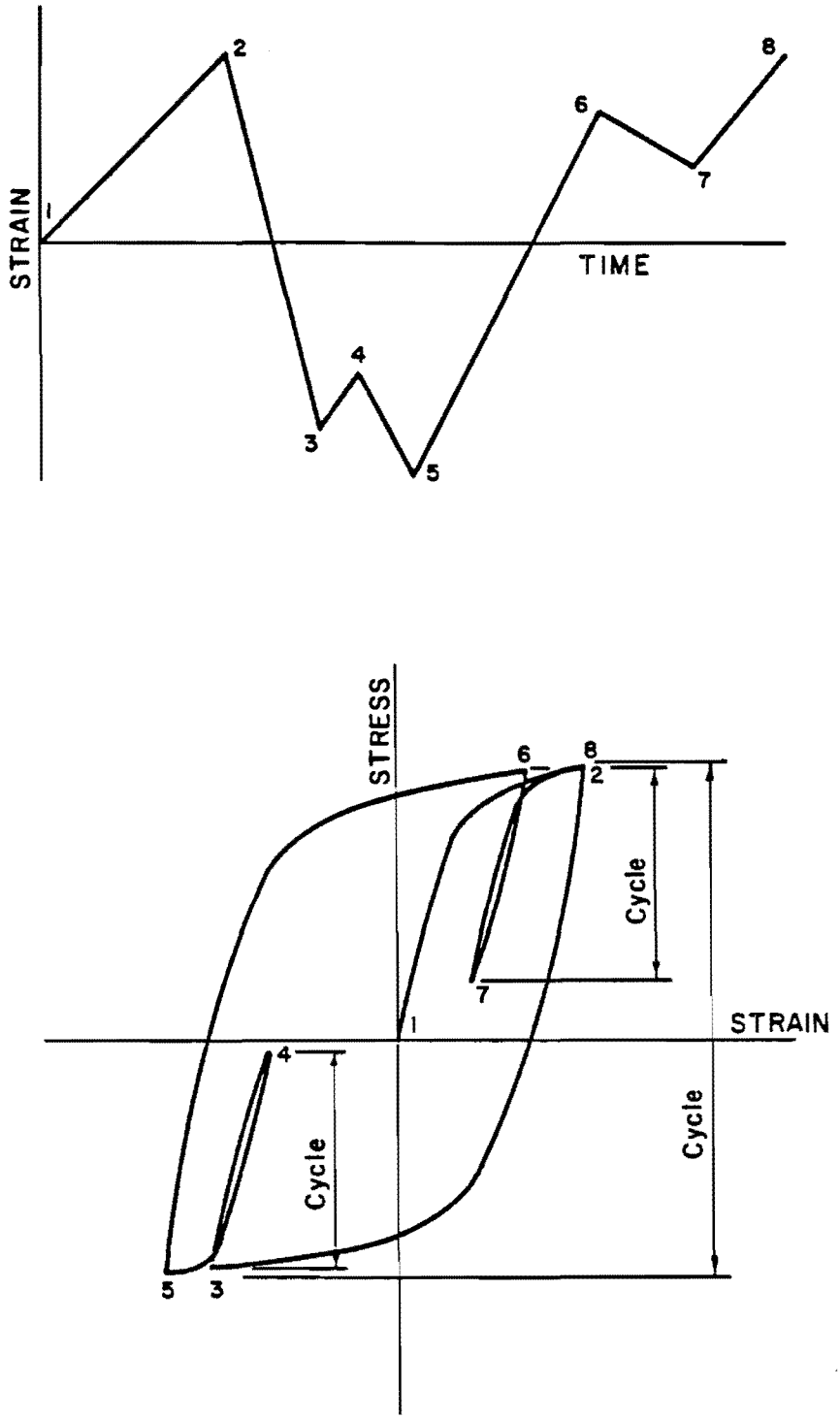

Fig. 2.3 Definition of a cycle by the rainflow counting method.

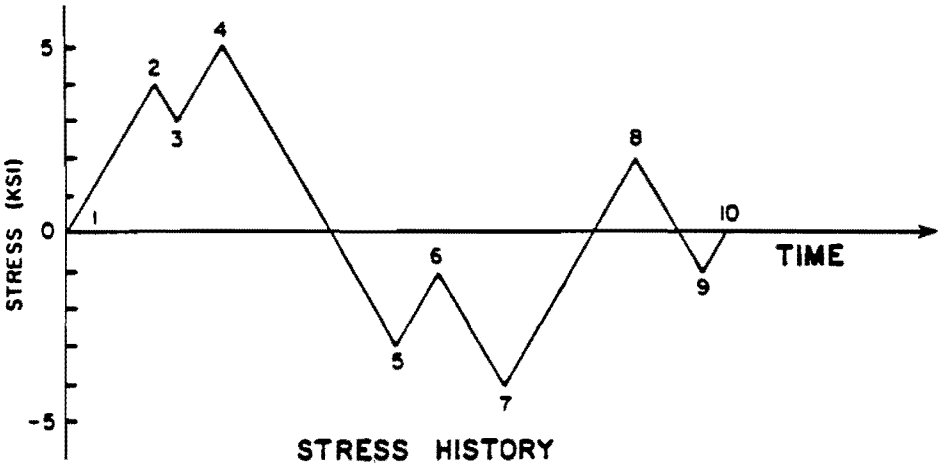

(a)

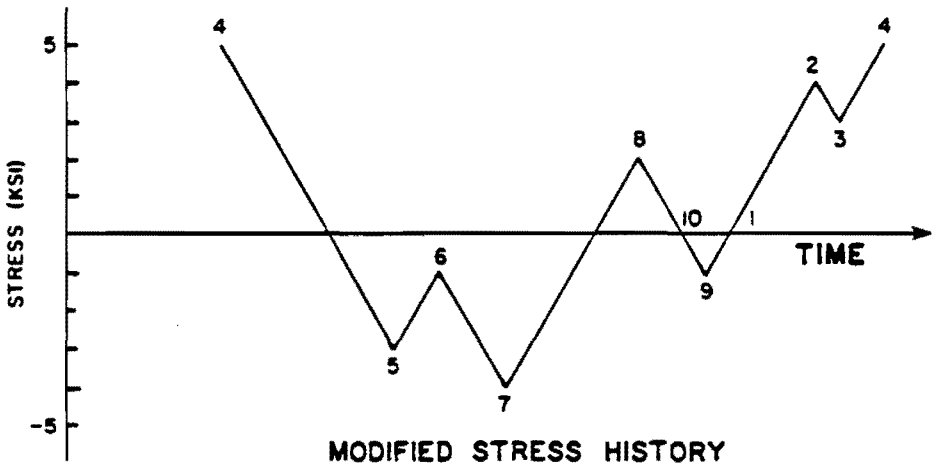

(b)

Fig. 2.4 Example of modified stress history.

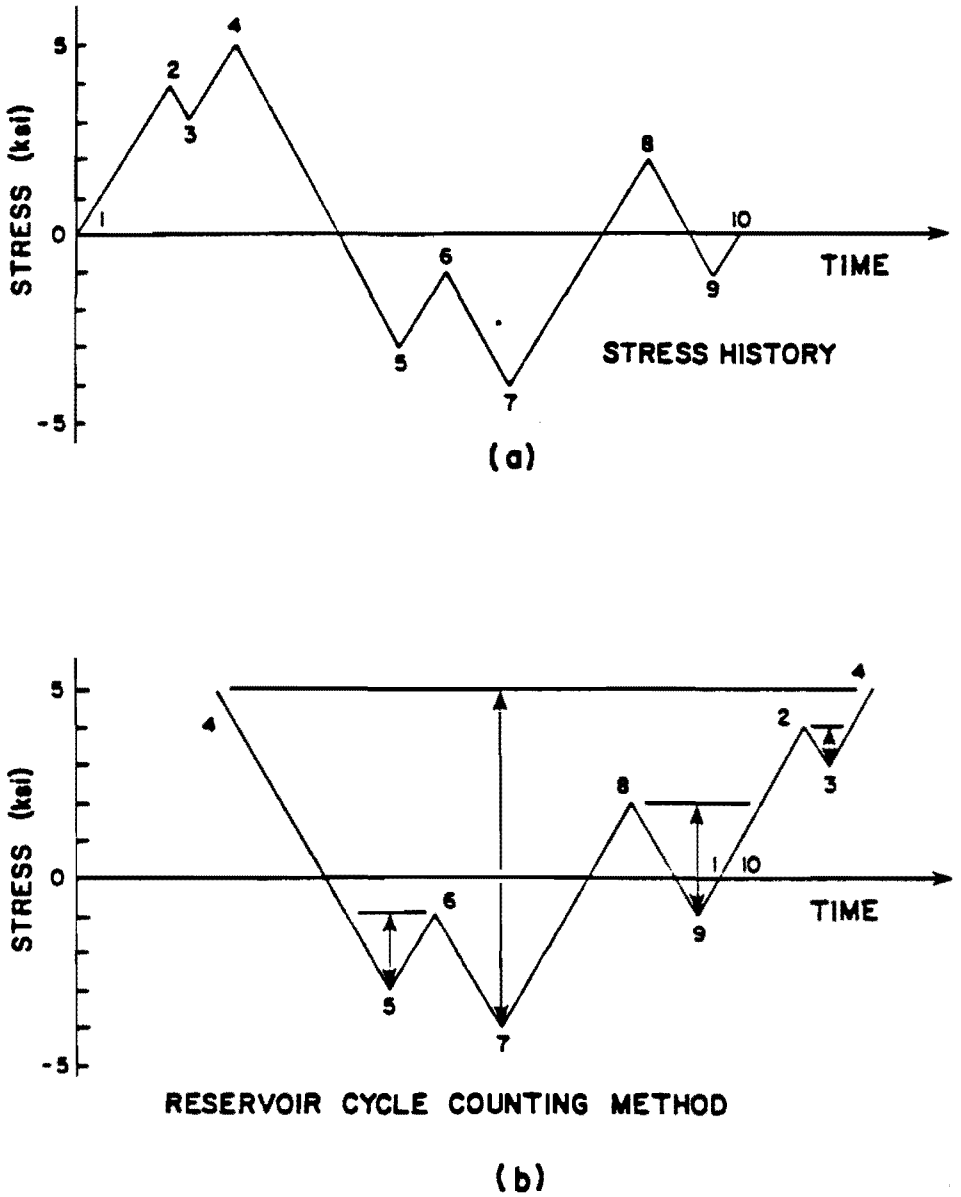

Fig. 2.5 Example of reservoir cycle counting method.

The modified rainflow and the reservoir counting methods produce the same number and size stress cycles. The rainflow counting technique is generally considered accurate for wide band stress histories similar to those produced by highway bridge traffic [6]. However, since both methods yield identical histograms, either may be used.

It should be noted that the use of any one of these counting schemes will scramble the order in which the stresses are applied. As shown in Fig. 2.6, this means that the maximum stress of a cycle may not be adjacent to the minimum stress of the cycle. In the waveform shown in Fig. 2.6a, the maximum peak (1) and minimum peak (8) define stress cycle 1. Intuitively, there is some question concerning the equivalence of cycle 1 in Fig. 2.6a and cycle 1 in Fig. 2.6b. The intermediate stress cycles 2 through 4 will have some effect on the crack front and thus will alter the fatigue damage caused by the cycle.

In this report, the reservoir counting method is used for cycle counting. The decision to use the reservoir counting method was based on the following three conditions: (1) the procedure describes the entire stress history; (2) the procedure gives the stress range and mean stress of each cycle; and (3) the procedure is most easily translated into a computer algorithm. This report does not attempt to determine the validity of any counting method on its own merit. Only the accuracy of a combination of a counting method and a cumulative damage theory in the fatigue design procedure is under investigation.

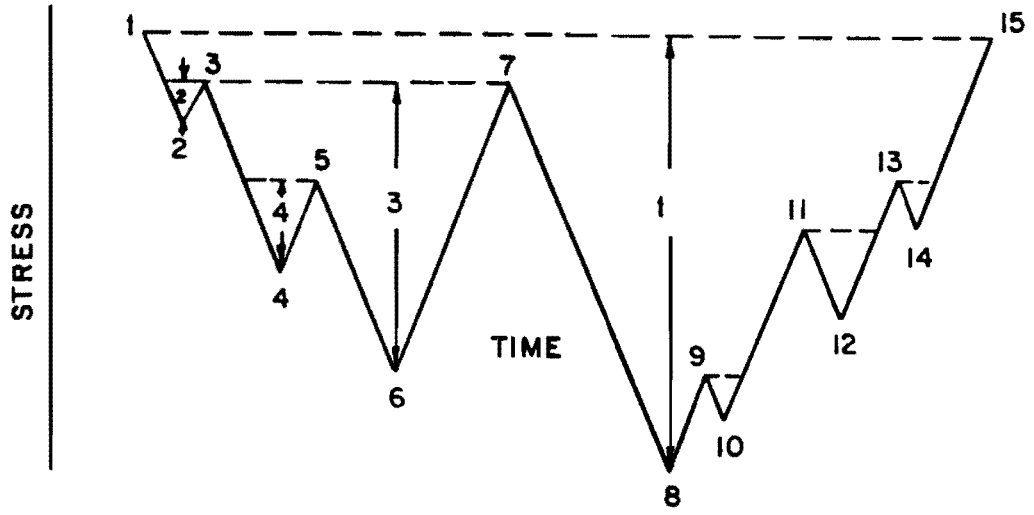

a) before counting

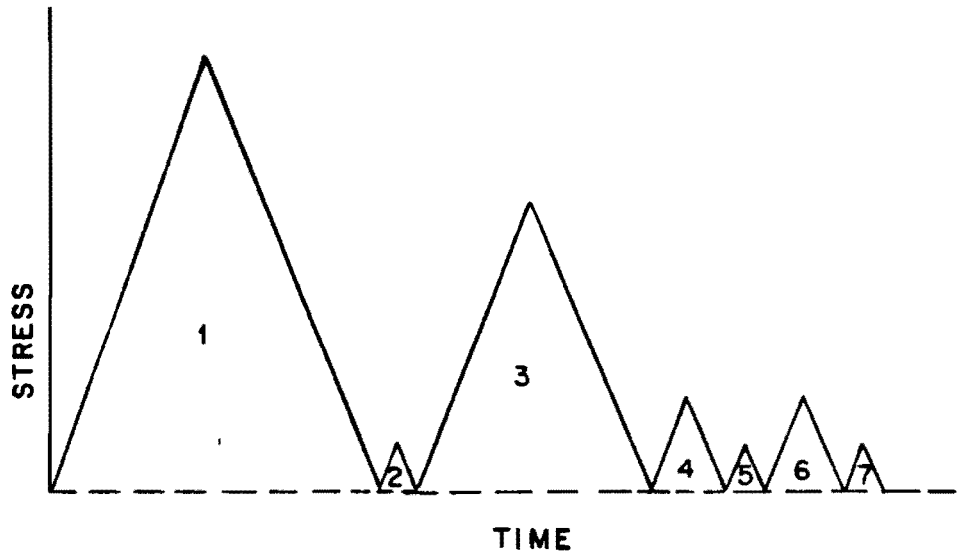

b) after counting

Fig. 2.6 Variable amplitude loading before and after cycle counting.

2.3 Cumulative Damage Theories

The fatigue damage caused by a constant amplitude stress cycle is easily quantified by comparing the number of cycles applied to the fatigue life of the structure as determined experimentally. In variable amplitude fatigue analysis, the variable stress history is defined as a group of constant amplitude stress cycles by cycle counting. Thus, the fatigue damage caused by the variable amplitude stress history is a summation of the fatigue damage of the constant amplitude stress cycles. The summation of fatigue damage is done using a cumulative damage theory.

Cumulative damage theories can be divided into two groups, depending on whether they are based on (1) fracture mechanics or (2) empirical constant amplitude fatigue data. The fracture mechanics theories typically use a cycle-by-cycle integration of the crack propagation over the stress history to calculate the fatigue damage. The "empirical" theories assume that the fatigue damage done by a cycle is proportional to the damage caused by the cycle in a constant amplitude stress history.

The fracture mechanics theories of cumulative fatigue damage include those developed by Willenburg [7], Wheeler [8], and Bell and Wolfman [9]. In these models, the damage caused by a cycle is a function of [10]:

1. the crack geometry,
2. the material properties at the crack tip, and
3. the stress range of the cycle.

The crack propagation caused by each cycle is calculated based on the above variables, and then the crack growth caused by each cycle is summed to determine the total fatigue damage caused by the stress history.

The theories based on fracture mechanics can be very accurate in a controlled setting. However, when they are applied to highway bridge fatigue design, the following three problems arise:

1. the order of cycles which will determine the state of stress at the crack tip is destroyed in cycle counting;
2. the design is usually controlled by the fatigue of a weldment, and the stresses in this region are very complicated due to residual stresses; and
3. it is impossible to predict the load history over the life of the bridge, so the accuracy produced by the cycle-by-cycle integration of crack growth is destroyed.

Therefore, the cumulative damage theories using fracture mechanics will not be investigated further as they are not presently applicable to design.

The cumulative damage theories based on empirical data are easily applied to highway bridge fatigue design. These methods relate the fatigue damage caused by a stress cycle on a specific detail to the fatigue life of the same detail when loaded by the stress cycle alone. This fatigue analysis eliminates the need to know the stresses present in each detail to be designed. However, the resulting design is purely empirical and holds only for the details tested. This limits the applicability of the method, but, with the limited number of details used in highway bridges, the empirical analysis leads to a very efficient design procedure.

Because of their applicability to fatigue design, four theories which incorporate the constant amplitude fatigue data will be considered in this report.

2.3.1 Miner's Cumulative Damage Theory. M. A. Miner presented his theory of cumulative fatigue damage in 1945 [11]. Miner's theory is derived from the assumption that accumulated fatigue damage is proportional to the net work absorbed by the material. From this assumption, Miner developed a relation between the percentage of the total work required for failure done by a stress cycle to the fatigue life of the specimen under a constant amplitude stress history of the same magnitude. This can be presented mathematically by

$$w_i/W = n_i/N_i \tag{2.5}$$

where w_i = work done by n_i cycles

W = work required for failure

n_i = number of cycles at stress range S_{ri}

N_i = number of cycles to failure at S_{ri}

[It should be noted that Miner assumed the major stress variable in the fatigue analysis to be the maximum stress. Further experimentation has shown that stress range should be the major stress variable so it has been substituted for maximum stress in Miner's calculations.] With this notation, failure is defined by

$$\Sigma w_i = W \tag{2.6}$$

or in another form

$$\Sigma(w_i / W) = 1.0 \tag{2.7}$$

Combining Eqs. (2.7) and (2.5) yields the more familiar expression of Miner's theory.

$$\Sigma(n_i / N_i) = 1.0 \tag{2.8}$$

This theory can be used to develop an expression for the effective stress ranges and damage factor for a complex cycle which were presented in section 2.1.

$$S_{RES}(M) = [(\Sigma n_i S_{ri}^{m} / n_c)]^{1/m} \tag{2.9}$$

$$S_{REC}(M) = [\Sigma n_i S_{ri}^{m}]^{1/m} \tag{2.10}$$

$$F_M = \Sigma n_i p_i^{m} \tag{2.11}$$

where S_{ri} = stress range of a cycle

n_i = number of cycles at S_{ri} in the complex cycle

n_c = number of cycles in complex cycle

m = slope of the constant amplitude log-log S_r-N curve for the detail in question

p_i = S_{ri} / S_{RMAX}

An extensive study sponsored by the National Highway Transportation Board [12] determined that Miner's theory is sufficiently accurate. However, several studies have shown that Miner's theory will produce unconservative results [13, 14, 6]. In addition, other studies

have proven Miner's rule to be conservative [15, 16]. The contradiction is a result of the differences in the spectrums which were used in testing. The contradictions result from the weak theoretical basis for Miner's model.

Miner's relation between the percentage of work done and the number of stress cycles applied assumes a linear accumulation of fatigue damage. This assumption is incorrect for two reasons: (1) crack growth is not linear. The amount of crack propagation also depends on the crack length. As the crack grows, the rate of crack propagation increases. This relationship is shown in Fig. 2.7 [17]; and (2) a linear summation of fatigue damage does not account for any interaction between stress cycles.

These two inconsistencies in the development of Miner's cumulative damage theory make its general application in fatigue design questionable. Therefore, empirical verification of Miner's rule is required for each new spectrum.

2.3.2 Non-Linear Miner's Cumulative Damage Theory. Joehnk developed this cumulative damage theory based on testing done on welded tees with the superimposed sine wave stress histories similar to the one shown in Fig. 2.8. The results of his testing indicated that minor cycles produce more fatigue damage than Miner's linear damage theory predicted. This indicated that the relation between stress range and fatigue damage was not linear for the minor cycles. Joehnk made a modification in Miner's theory according to the test results to account

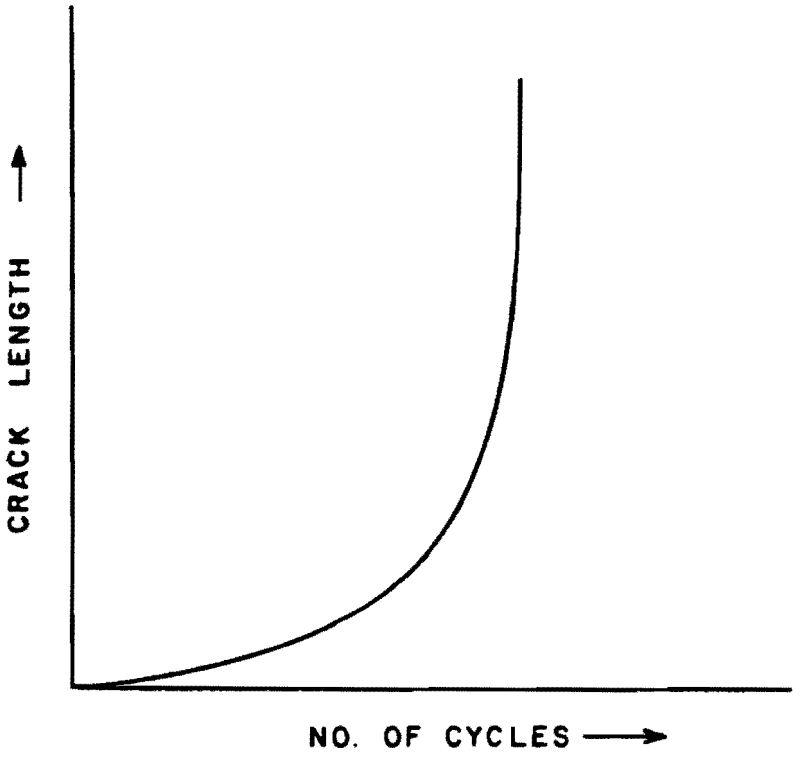

Fig. 2.7 Plot of crack growth vs. number of cycles applied.

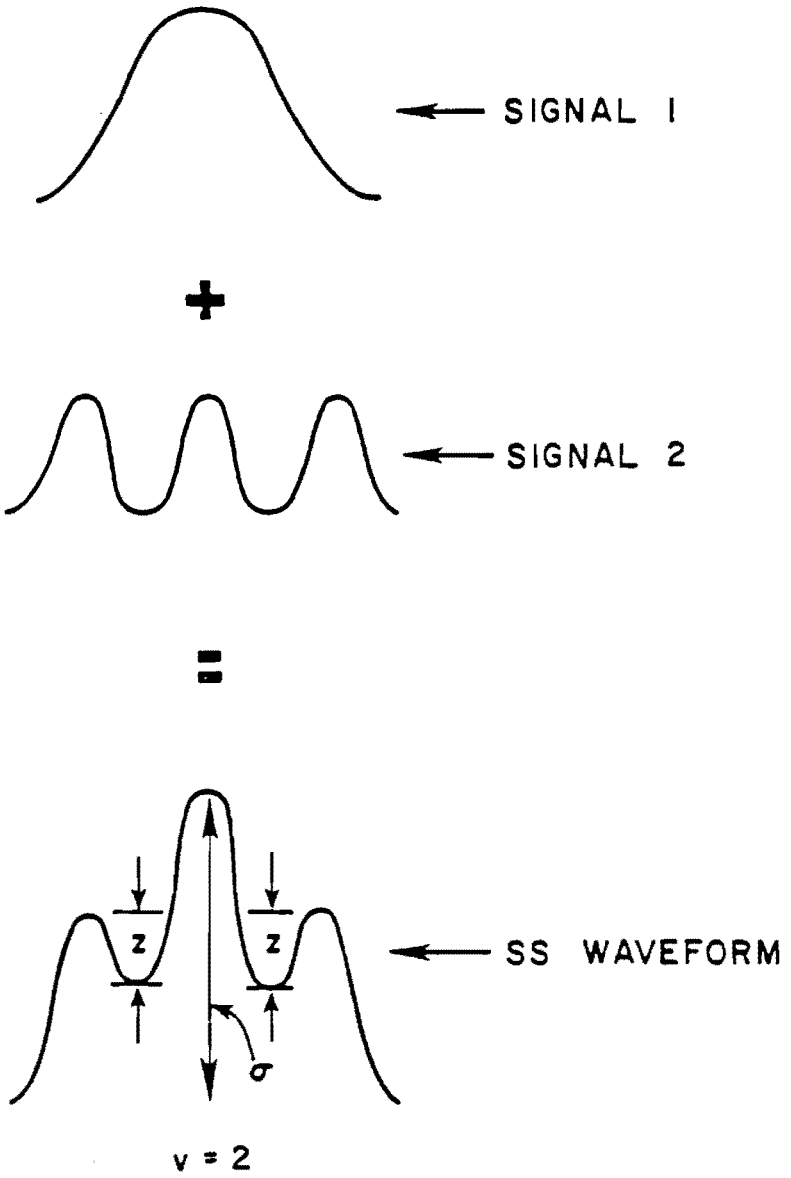

σ = Major Stress Range

z = Minor Stress Excursion

v = Number of Minor Excursions, z

Fig. 2.8 Example of Joehnk's superimposed sine stress histories.

for the non-linear behavior and labeled it non-linear Miner's damage theory.

From the experimental data, Joehnk developed an effective stress cycle to replace a minor stress cycle in a variable stress history. The stress range of this effective cycle can be expressed in the following form:

$$Z_{eff} = Z\ (S_{RMAX} / Z)^{1/2} \tag{2.12}$$

where Z = stress range of the minor cycle

Z_{eff} = stress range of the effective cycle

Equation (2.12) shows that as the stress range of a minor cycle decreases, its relative fatigue damage increases. The relation is shown graphically in Fig. 2.9. As Z_{eff} / Z increases, the relative damage done by a minor cycle, Z, increases.

After accounting for this stress interaction, Joehnk returned to Miner's format by substituting the number of cycles to failure with the new effective stress cycle $N_{i(eff)}$ for N_i in Eq. (2.5). Thus, at failure,

$$\Sigma(n_i / N_{i(eff)}) = 1.0 \tag{2.13}$$

This theory can also be used to determine effective stress ranges and a damage factor for a complex cycle.

$$S_{RES(NLM)} = \left\{ \Sigma \frac{n_i}{n_c} \left[\left(\frac{1}{P_i} \right)^{\frac{1}{2}} S_{Ri} \right]^m \right\}^{1/m} \tag{2.14}$$

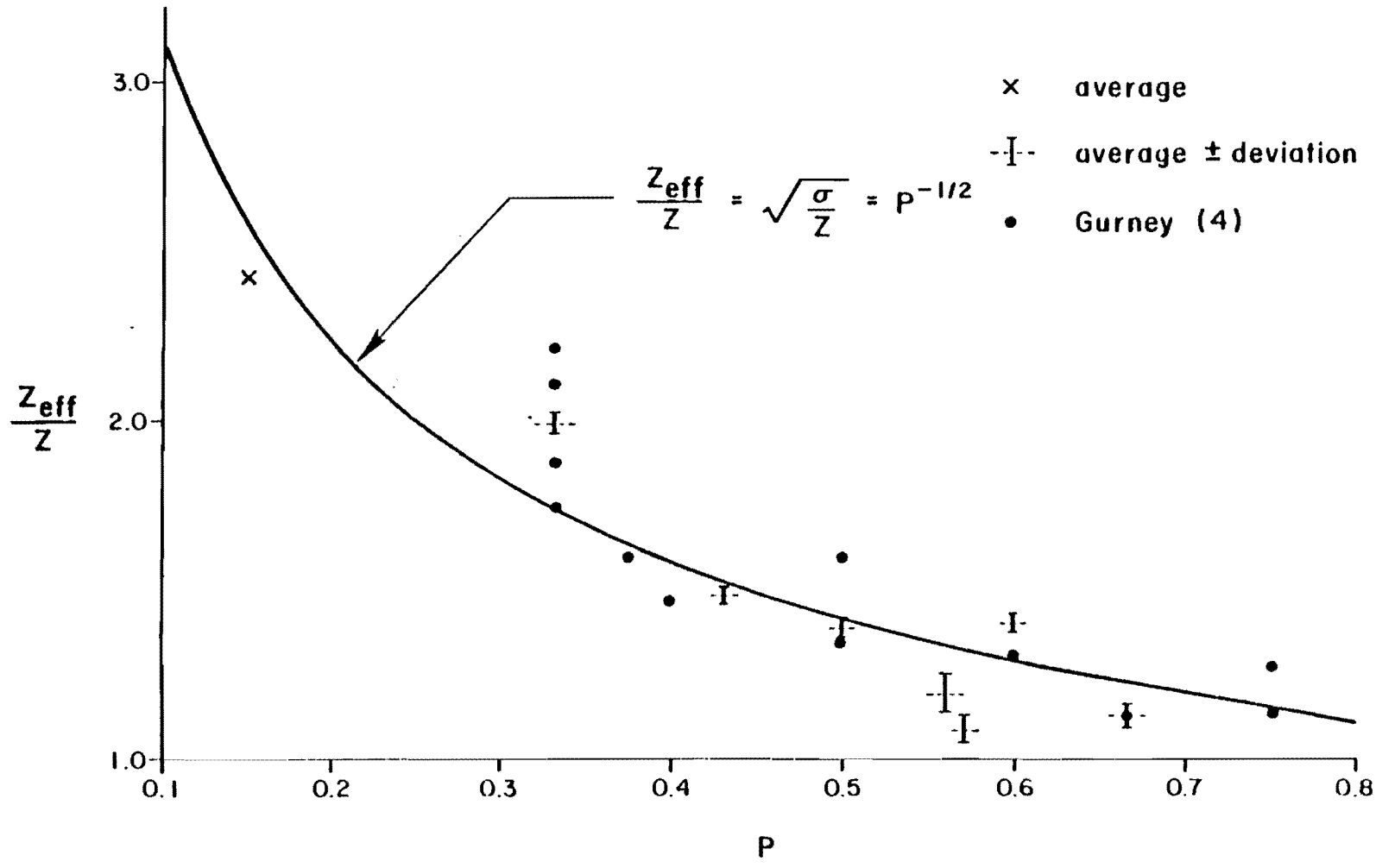

Fig. 2.9 Plot of Z_{EFF}/Z vs. P developed by Joehnk.

$$S_{REC(NLM)} = \left\{ \Sigma\, n_i \left[\left(\frac{1}{P_i} \right)^{1/2} S_{Ri} \right]^m \right\}^{1/m} \qquad (2.15)$$

$$F_{NLM} = \Sigma n_i\, p_i{}^{m/2} \qquad (2.16)$$

Non-linear Miner's theory is very accurate for the stress histories used in Joehnk's experiments. The theory also produced accurate fatigue life predictions for seven stress histories used in T. R. Gurney's research [13]. However, Joehnk's cumulative damage model has no basis in material behavior. The model was derived to "fit" the limited experimental data which was available. Recent testing by Zwerneman [1] showed that non-linear Miner's cumulative damage model produced overconservative fatigue life predictions. This illustrates the model's limited applicability.

Joehnk's cumulative damage model is based on limited empirical data, so its application in design is also limited. Further testing on actual design spectrums is required before this theory can be used with confidence.

2.3.3 Gurney's Cumulative Damage Theory. T. R. Gurney developed a cumulative damage model by investigating the fatigue damage caused by minor cycles at their limiting stress ranges [13]. A minor cycle produces no fatigue damage as p, the ratio of the minor cycle stress range to S_{RMAX}, approaches zero, so the fatigue life is not affected. As p approaches 1.0, the minor cycle becomes a major cycle and the fatigue life approaches the constant amplitude faituge life, accounting for the additional major cycles.

Gurney described a variable amplitude stress history as a constant amplitude stress history with a number of stress cycle excursions, z, as shown in Fig. 2.10. So, each major cycle and its excursions were defined as a "complex" cycle. Gurney used eight different "complex" cycles in his research, which are shown in Fig. 2.11.

Given the definition of the "complex" cycle, when p = 0 the complex cycle reduces to a single constant amplitude cycle. When p = 1.0, the "complex" cycle becomes v + 1 constant amplitude cycles, where v is the number of excursions. This reasoning leads to a linear relationship between p and the fatigue life in "complex" cycles, N_c, as shown in Fig. 2.12. The relation can be expressed mathematically as

$$N_c = N_{MAX} \, (v_i + 1)^{-p_i} \tag{2.17}$$

where N_c = number of complex cycles to failure

N_{MAX} = number of constant amplitude cycles to failure when $p_i = 0$

v_i = number of excursions of magnitude z_i

p_i = z_i / S_{RMAX}

It follows that the fatigue life for a "complex" cycle with excursions of k different magnitudes is expressed by

$$N_c = \left[\prod_{2}^{k} \left(\frac{x_{(i-1)}}{x_i} \right)^{p_i} \right] N_{MAX} \tag{2.18}$$

where $x_i = (1 + v_1 + v_2 + v_3 + \ldots + v_i)$

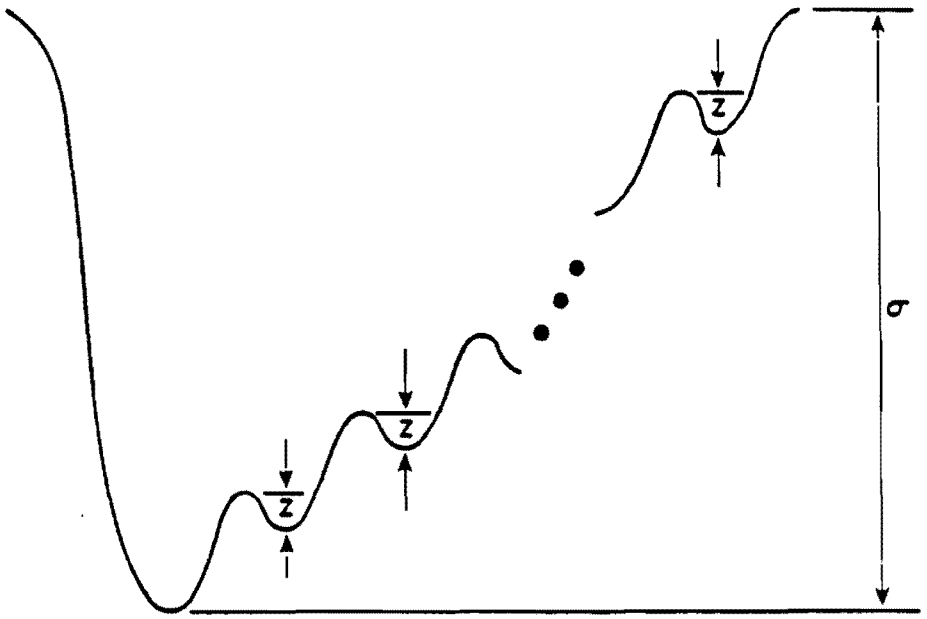

Fig. 2.10 Gurney's description of a variable stress history.

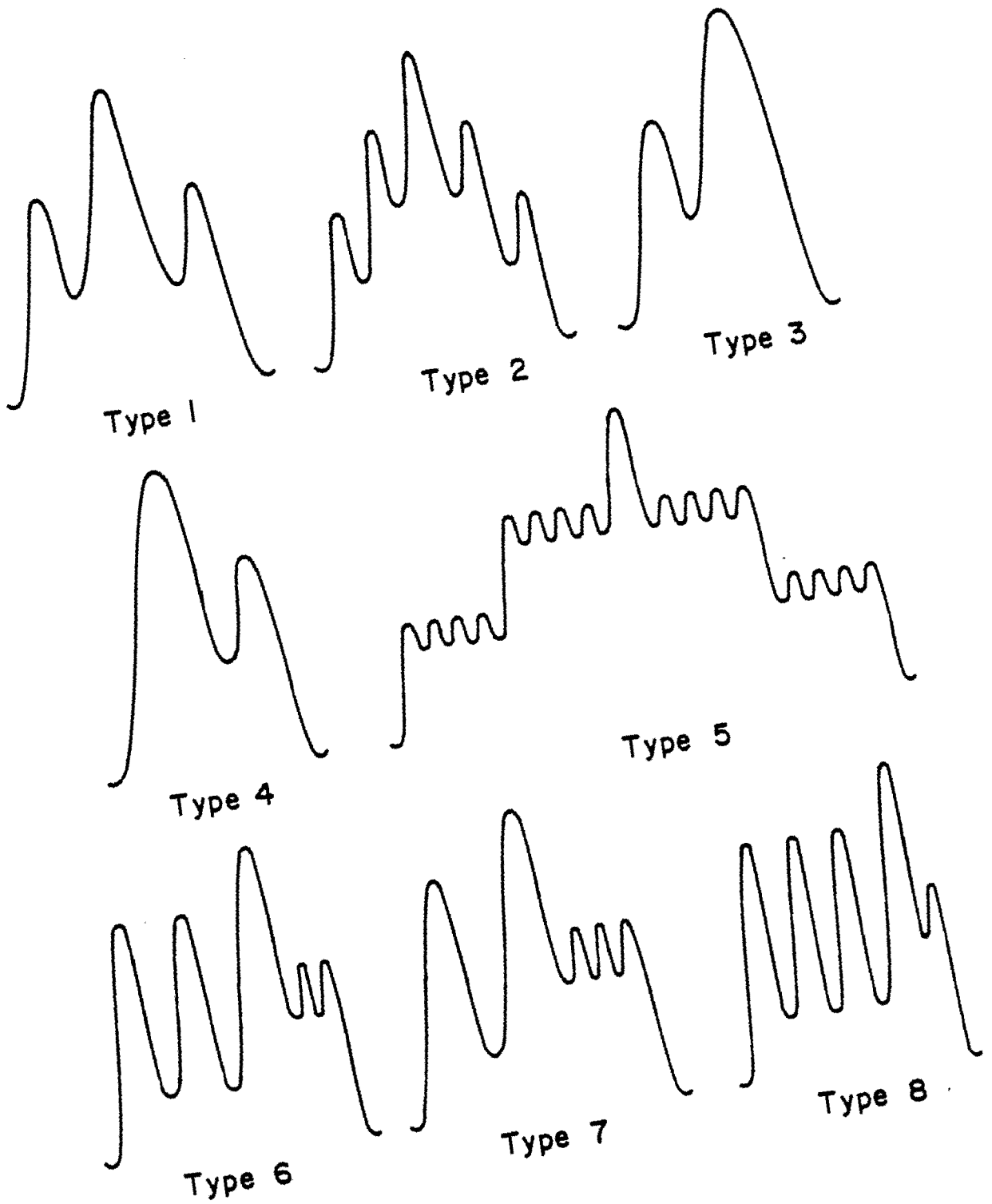

Fig. 2.11 Gurney's experimental stress histories.

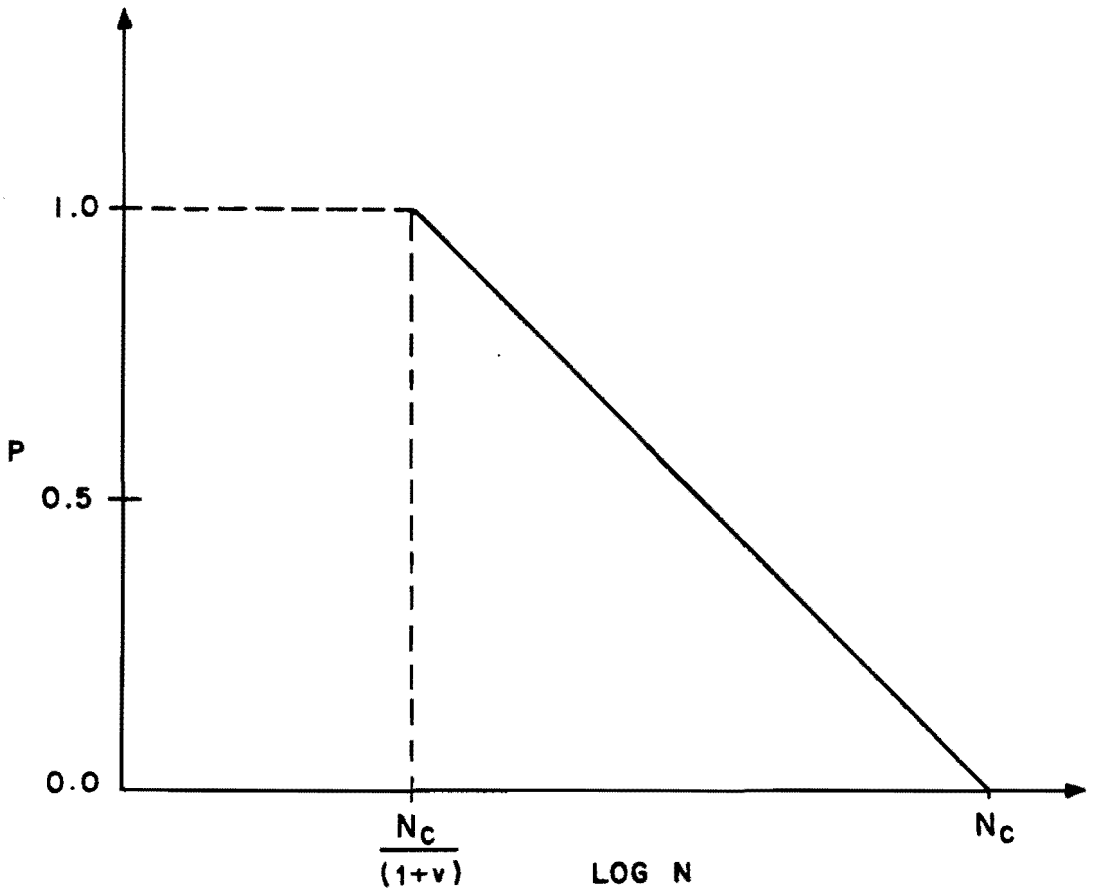

Fig. 2.12 Relation between P and N derived by Gurney.

For example, when the "complex" cycle contains three excursions of different magnitudes, the fatigue life is given in complex cycles by

$$N_c = \left[\left(\frac{1}{1+V_1}\right)^{P_1}\left(\frac{1+V_1}{1+V_1+V_2}\right)^{P_2}\left(\frac{1+V_1+V_2}{1+V_1+V_2+V_3}\right)^{P_3}\right]N_{MAX} \qquad (2.19)$$

where $p_1 < p_2 < p_3$.

The effective stress ranges and the damage factor corresponding to Gurney's cumulative damage theory are given by

$$S_{RES(G)} = \left\{\left[\prod_{2}^{K}\left(\frac{x_{(i-1)}}{x_i}\right)^{P_i}\right] n_c\right\}^{-1/m} S_{RMAX} \qquad (2.20)$$

$$S_{REC(G)} = \left[\prod_{2}^{K}\left(\frac{x_{(i-1)}}{x_i}\right)^{P_i}\right]^{-1/m} S_{RMAX} \qquad (2.21)$$

$$F_G = \prod_{2}^{K}\left(\frac{x_{(i-1)}}{x_i}\right)^{P_i} \qquad (2.22)$$

Gurney's cumulative damage model predicted the fatigue life of the stress histories used in his research very well. The model also produced accurate predictions of fatigue life for the superimposed sine spectrums used by Joehnk. It is interesting to note that Gurney and Joehnk produce almost the same fatigue life predictions for Joehnk's stress histories, as shown in Fig. 2.13 through entirely different methods. However, Zwerneman's research on measured stress histories caused by truck traffic indicates that Gurney's, like Joehnk's, damage model produces overly conservative results.

Zwerneman noticed the similarity of Joehnk's and Gurney's damage models, and noted that the relationship of the two theories

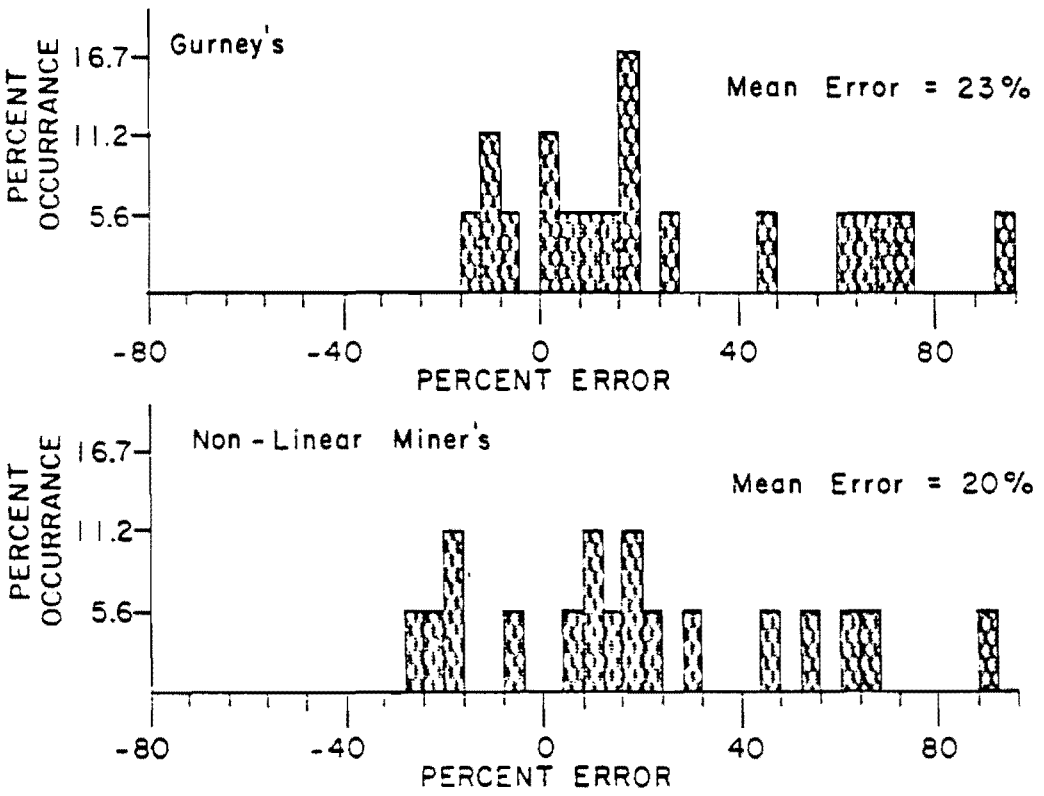

Fig. 2.13 Comparison of Joehnk's and Gurney's models predictions on Joehnk's stress histories.

varies with v and m. The results of the study show that (1) as v increases, Gurney's model predicts less damage than non-linear Miner's; and (2) as m increases, the difference between the two models decreases. These trends can be seen in Figs. 2.14 through 2.21.

2.3.4 Mean Stress Cumulative Damage Theory. The mean stress cumulative damage theory was developed by Zwerneman [1]. Zwerneman investigated the effect of the stress level of the minor cycles relative to that of the major cycle on the fatigue life of a welded detail. Experiments using the stress histories in Fig. 2.22 showed that the fatigue damage done by a minor cycle varies with the stress level in the history.

In Zwerneman's study, he introduced the damage factor F as discussed in section 2.2. He proposed that the damage factor may be written in the following form:

$$F = \Sigma n_i \, p_i^{a} \qquad (2.23)$$

where a is an empirical factor which varies with the number of minor cycles n_i and the relative stress level of those minor cycles.

From the limited amount of data he generated, a relationship was developed between the relative stress level of the minor cycles R, the number of minor cycles n_i, and the exponent a. This relation is illustrated in Fig. 2.23. This curve was used to predict fatigue lives for Gurney's and Joehnk's, as well as Zwerneman's, stress histories. The accuracy of this method was comparable to Gurney's, and the non-

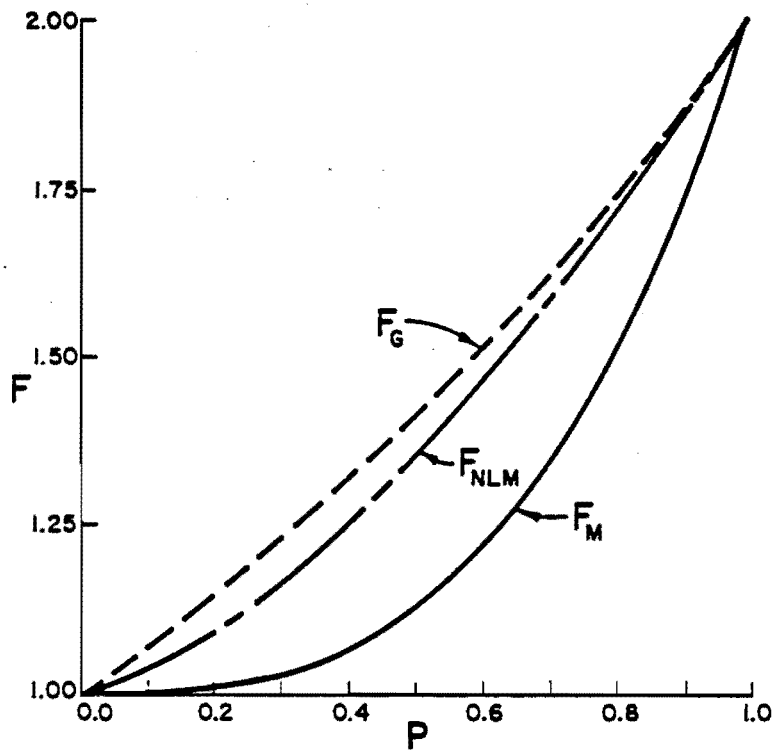

Fig. 2.14 Comparison of damage factors with m = 3 and v_2 = 1.

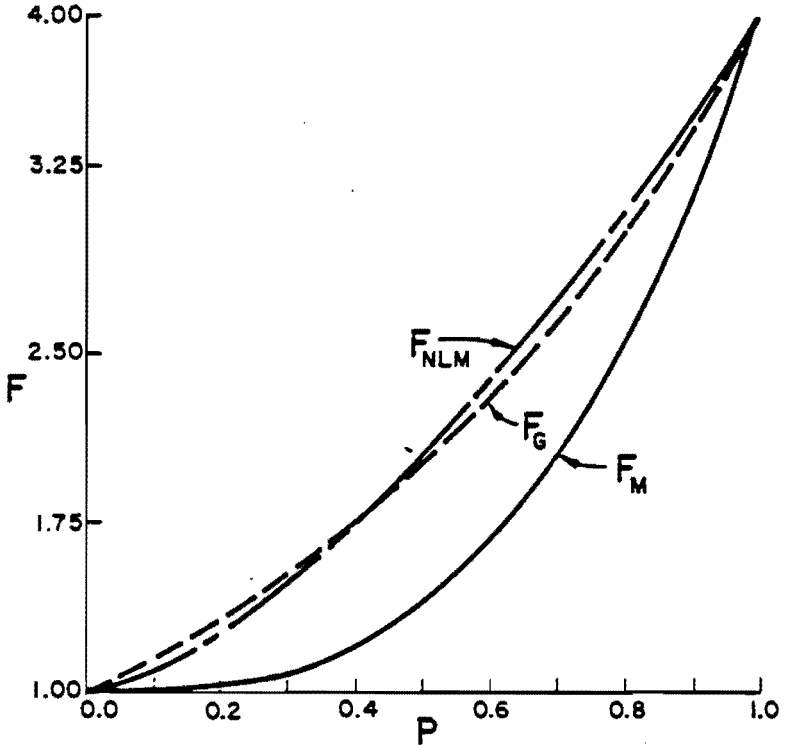

Fig. 2.15 Comparison of damage factors with m = 3 and v_2 = 3.

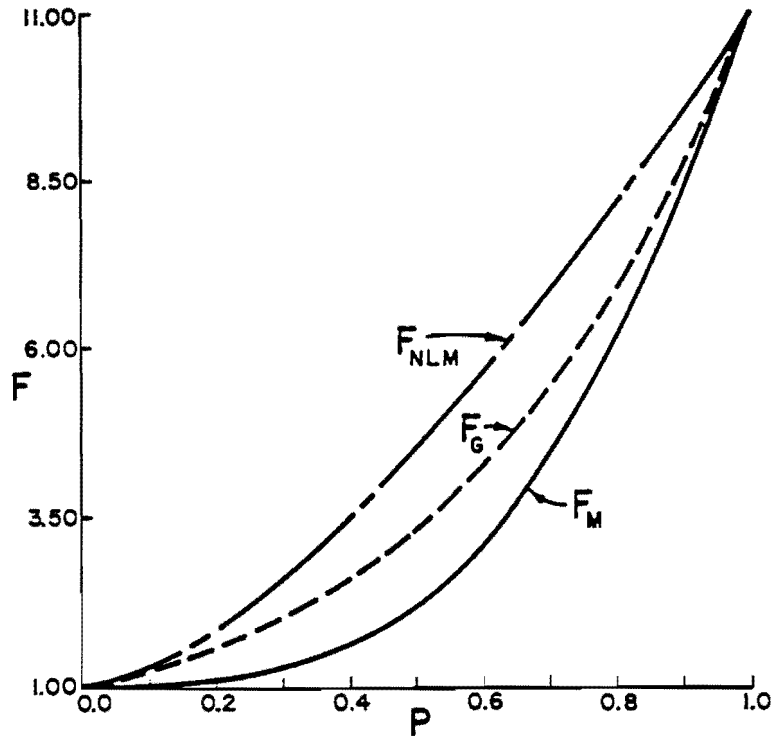

Fig. 2.16 Comparison of damage factors with m = 3 and v_2 = 10.

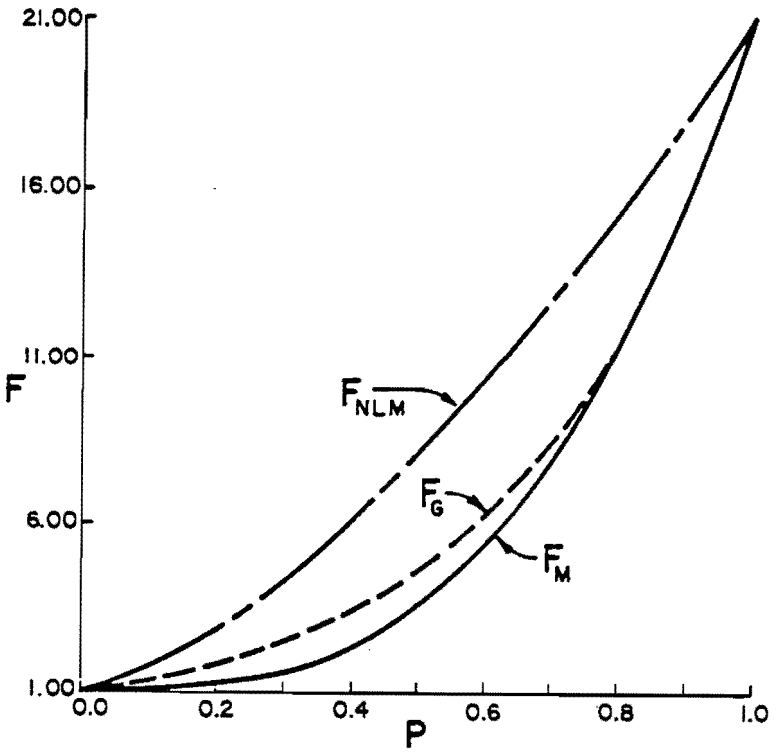

Fig. 2.17 Comparison of damage factors with m = 3 and v_2 = 20.

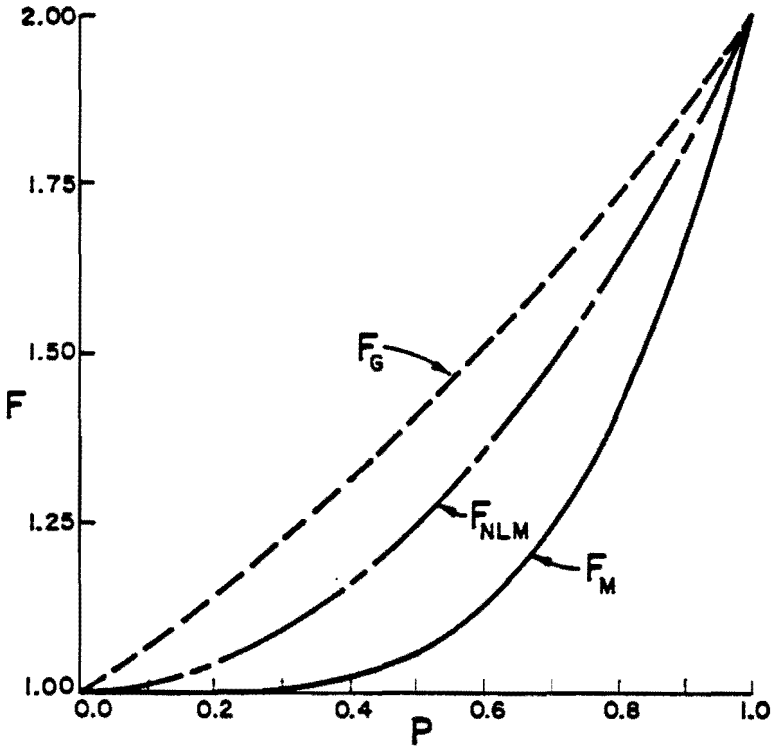

Fig. 2.18 Comparison of damage factors with m = 4 and v_2 = 1.

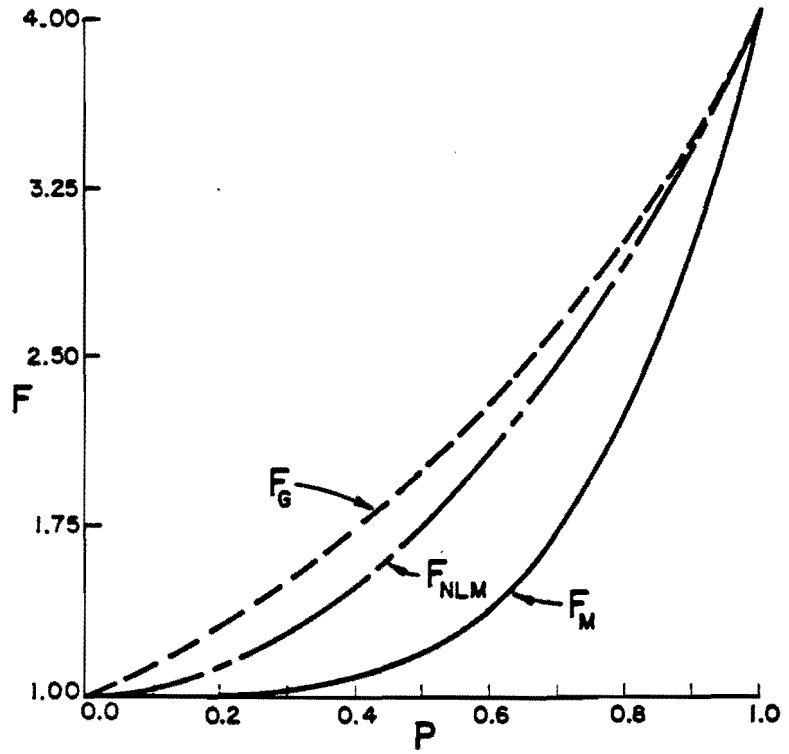

Fig. 2.19 Comparison of damage factors with m = 4 and v_2 = 3.

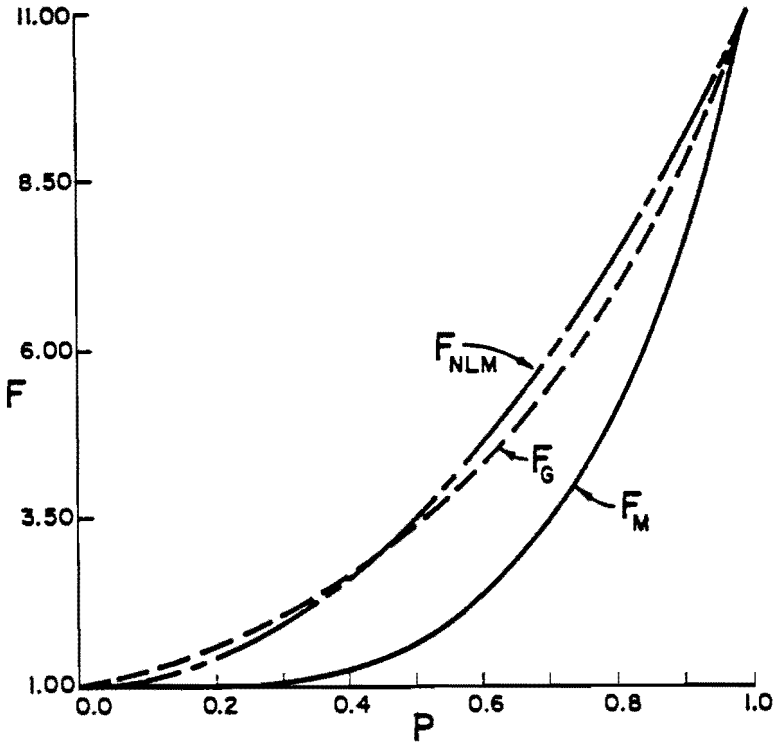

Fig. 2.20 Comparison of damage factors with m = 4 and v_2 = 10.

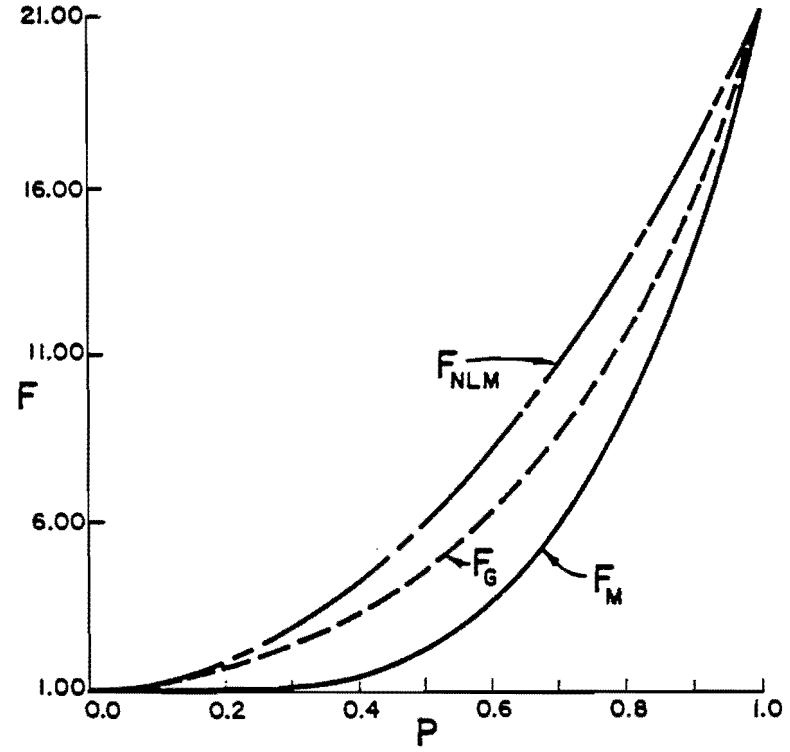

Fig. 2.21 Comparison of damage factors with m = 4 and v_2 = 20.

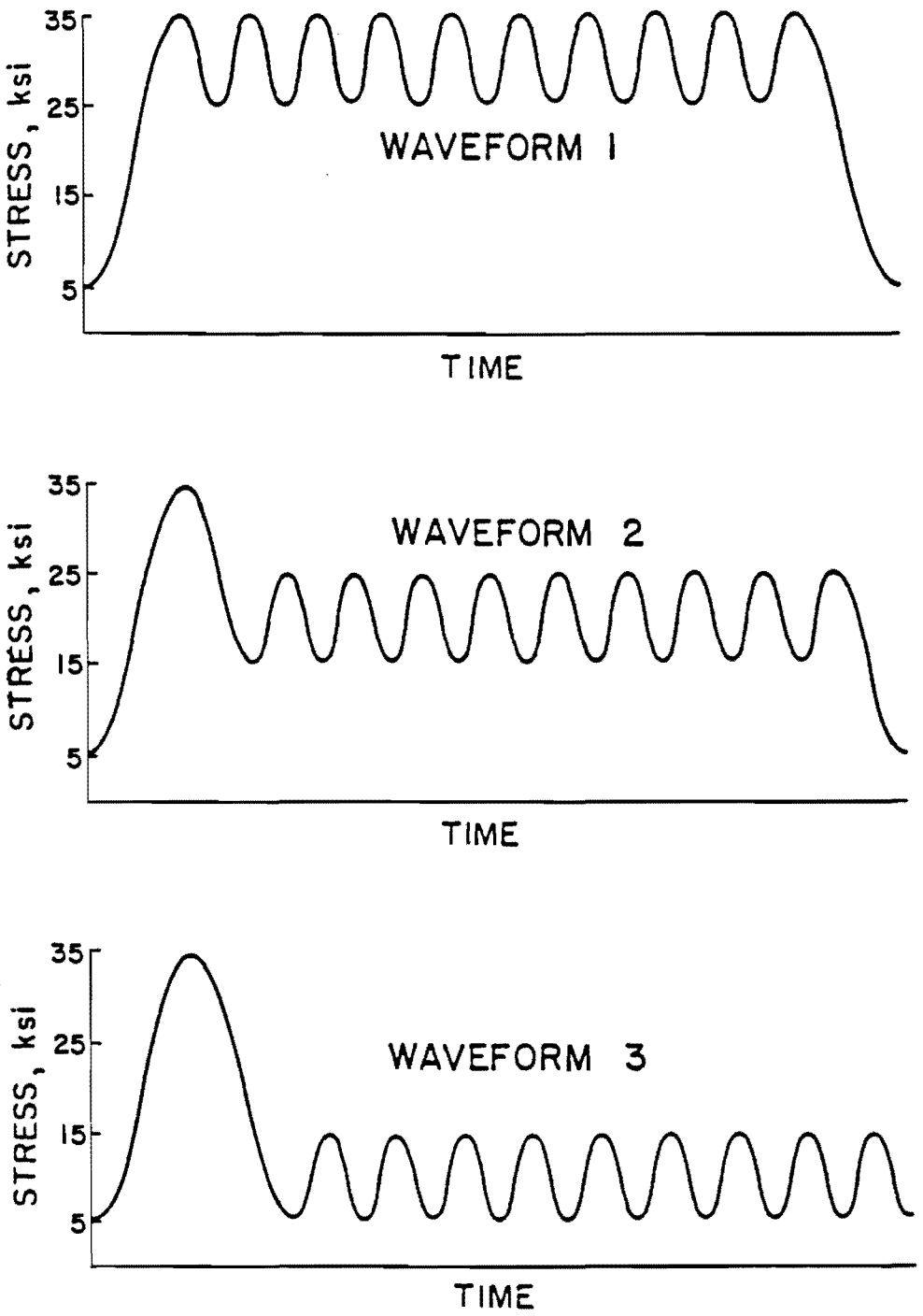

Fig. 2.22 Zwerneman's mean stress histories.

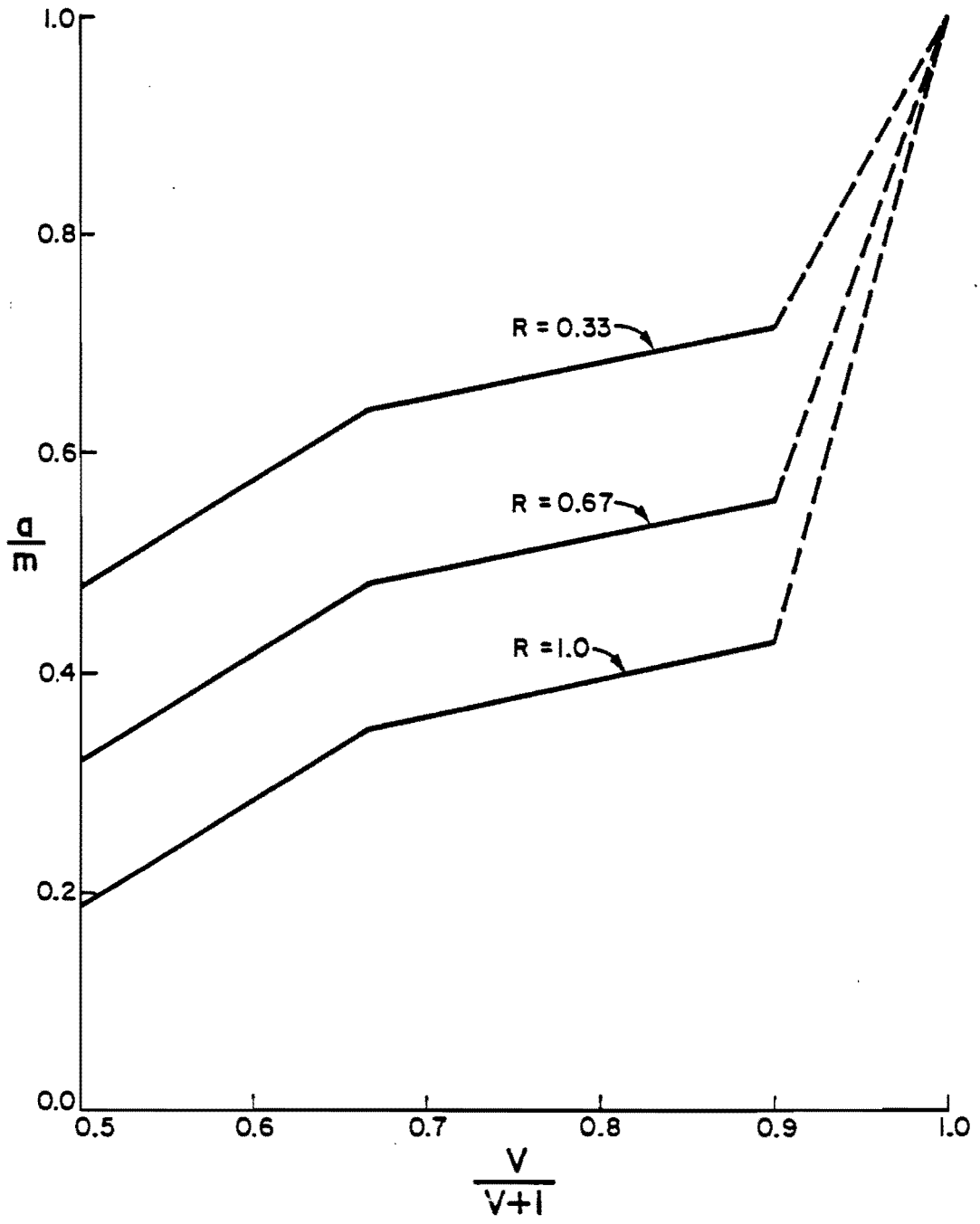

Fig. 2.23 Relation between V, R, and a developed by Zwerneman.

linear Miner's theory, but it was also accurate for the mean stress test histories while Gurney's and Miner's non-linear theories were not.

The mean stress cumulative damage model takes one step farther than the other theories by accounting for the relative stress level of the minor cycles, but further research is required to develop a reliable method of determining a. In addition, the method is very complicated with only a marginal increase in accuracy. This reduces the effectiveness of the method when applied to fatigue design.

2.4 Variable Amplitude Fatigue Analysis Procedure

In the first step of the analysis, development of a finite load history, the present AASHTO specifications use the concept of one cycle per truck passage. The magnitude of the applied stress cycle is calculated using Eq. (1.2) which predicts the peak stress or S_{RMAX}. However, AASHTO does not account for minor cycle fatigue damage in Eq. (1.3). Thus, an additional factor to account for the damage caused by the minor cycles. The resulting stress range is equivalent to S_{REC}. With a frequency distribution of GVW and the factor for the fatigue effects it is easy to develop a finite load histogram for use in design. One objective of this research is to determine the value of the factor which accounts for the fatigue damage of the minor cycles.

The second part of analysis, calculation of an equivalent constant amplitude or design stress range, is completed in the AASHTO specifications by applying Miner's rule to the histogram produced in Step 1. This procedure is equivalent to calculating S_{RES}. However, there are several models for calculating S_{RES}. The results of this

study are directed toward determining which cumulative damage theory is most appropriate for use with highway bridge loadings.

C H A P T E R I I I

EXPERIMENTAL PROGRAM

This chapter will describe how the experimental data used in this study was generated. The generation of the experimental data consisted of several procedures: 1) development of load histories; 2) design and fabrication of test specimen; and 3) physical testing. An analysis of experimental error was also completed to aid in the interpretation of the data.

3.1 Load Histories

Six different load-time histories were used in the test program. These six histories can be divided into the following three categories:

1. test truck history;
2. traffic histories; and
3. constant minimum stress histories.

The test truck history was produced by a three-axle dump truck. The traffic histories tested were three load-time histories which were developed from a stress history produced by normal vehicle traffic. Two different constant minimum stress histories were tested. Both constant minimum stress histories are random discrete loadings with a constant minimum stress. One history was developed from a histogram of the test truck loading, the other from a histogram based on the Rayleigh function

used in NCHRP Project 12-12 (see Ref. 12). The experimental program is presented in Table 3.1.

3.1.1 Test Truck History. The test truck history represents the passage of a three-axle dump truck over a highway bridge. This history was selected to provide some basic information on the amount of damage caused by the minor cycles in a stress history produced by truck traffic. A single "test" truck was used because this produced a relatively simply waveform of a manageable length with which to begin the study of fatigue damage caused by vehicle traffic.

This test history was developed by Zwerneman [1] from strain data recorded as the test truck crossed an instrumented bridge [18]. The test truck was a three-axle dump truck loaded with sand and traveling at a speed of 50 MPH. The strains were measured by strain gages placed at four cross sections of the bridge with four gages at each cross section. The history used in this study was taken from one cross section where all gages performed satisfactorily. The data from three strain gages at the cross section were used to generate the test history. The three strain-gage-time histories were normalized and averaged to eliminate any random electronic "noise" to produce a single stress history which is shown in Fig. 3.1.

Once a single stress history was produced, several steps were required to place this data into a form which was compatible with the function generator used in testing. First, the stress history was described as a series of discrete endpoints. Then, the endpoints were digitized as a percentage of the maximum stress. To reduce testing

TABLE 3.1 Experimental Program

Test Group	Spectrum	S_{RMAX} (ksi)	Specimen Number
Test truck	Test truck	33.46	FD5605
	"	28.71	FD5706
	"	28.65	FD5707
	"	20.00	FD6909
Traffic	Traffic 1	35.0	TT7105
	"	35.0	TT7112
	Traffic 2	35.0	TT7207
	"	35.0	TT7208
	"	35.0	TT7211
	Traffic 3	35.0	TT7209
	"	35.0	TT7210
Constant Minimum	CMS 1	35.0	BL6610
	"	35.0	BL6611
	CMS 2	35.0	USS612
	"	35.0	USS713

time, a constant loading rate was adopted and used to determine the time to program between endpoints. The use of a constant loading rate accounts for the response of the testing system to the command signal with increasing testing speed. This alteration in loading rate does not significantly affect the fatigue characteristics of the stress history. Finally, a Haversine loading function was used to connect the endpoints of the stress history. The resulting stress history which was used in testing is shown in Fig. 3.2.

The values of P of the stress cycles produced by a reservoir count on the load history used in testing are presented in Table 3.2. A stress range histogram is shown in Fig. 3.3. A more detailed discussion of the acquisition of the field data and the development of the load history used in testing is presented in Appendix B.

3.1.2 Traffic Histories. The traffic histories represent the stress histories produced on a highway bridge by vehicle traffic. The traffic histories were included in the experimental program to produce data on the fatigue behavior of welds under highways traffic loadings.

The loading histories included in this category were developed from strain data measured on the same bridge as the test truck loading. The strain data was recorded for a period of ten minutes while the bridge was loaded by normal vehicle traffic [18]. The field data was reduced in the same manner as the test truck data to produce a single stress-time history which was used to develop the load histories used in testing.

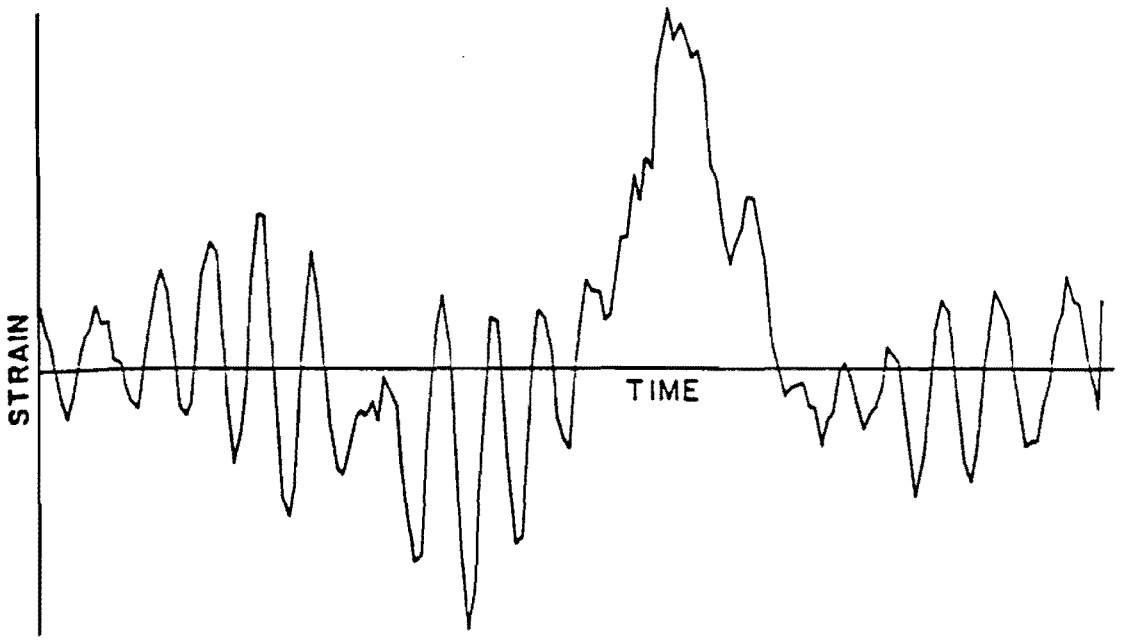

Fig. 3.1 Normalized, average strain data produced by test truck.

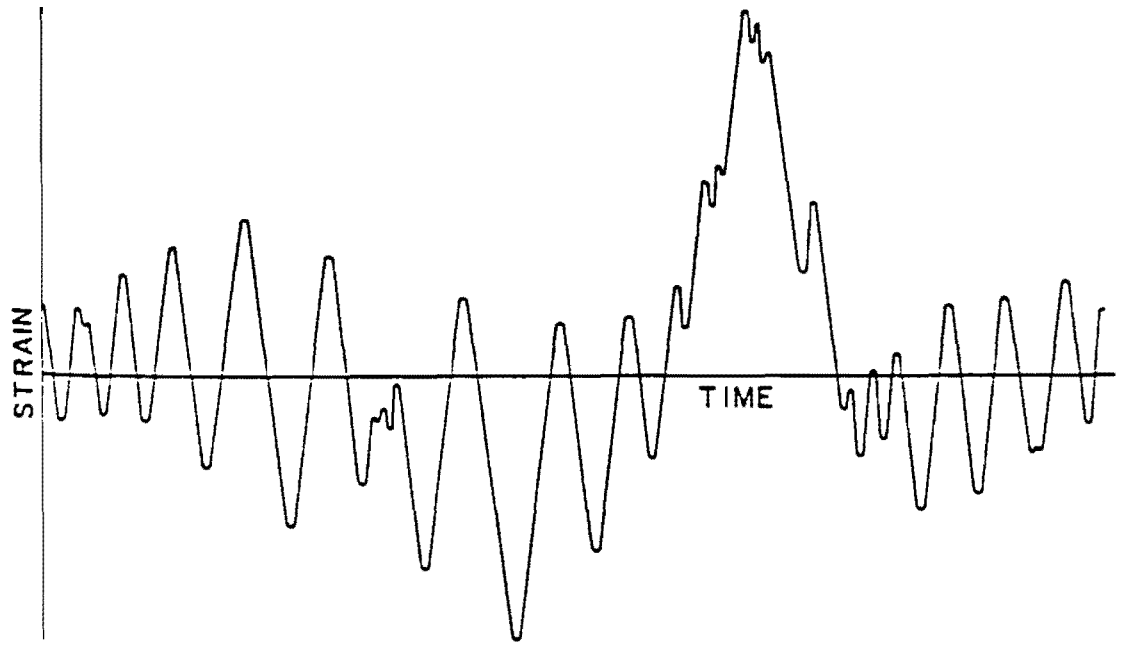

Fig. 3.2 Actual test truck stress history used in testing.

TABLE 3.2 P Values for Test Truck History.

CYCLE NO.	p
1	1.000
2	0.460
3	0.430
4	0.428
5	0.367
6	0.355
7	0.298
8	0.250
9	0.235
10	0.227
11	0.225
12	0.173
13	0.170
14	0.166
15	0.159
16	0.112
17	0.112
18	0.066
19	0.043
20	0.032
21	0.027
22	0.023
23	0.020
24	0.014
25	0.009
26	0.007
27	0.002

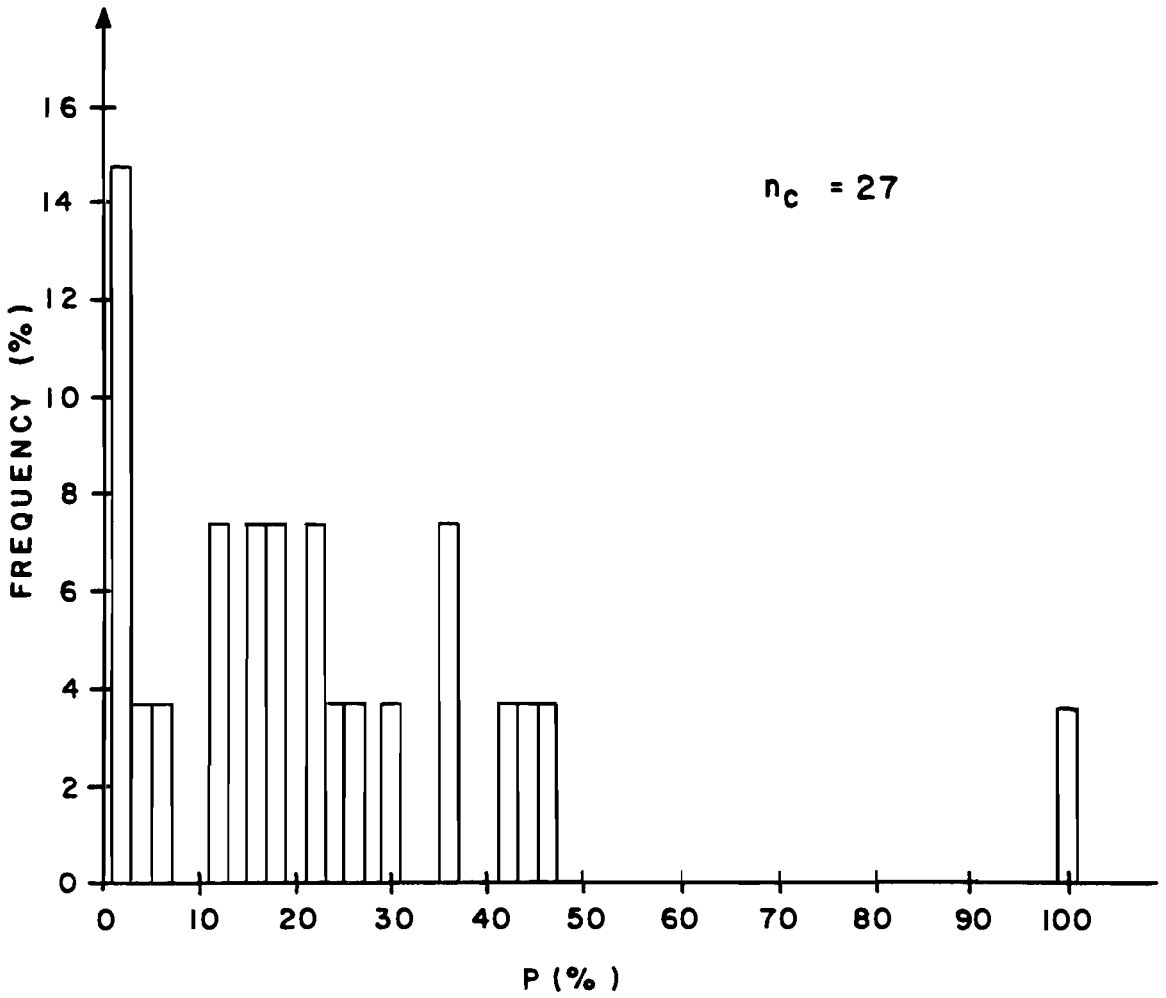

Fig. 3.3 Stress range histogram of test truck stress history.

The measured strain history contained over 4900 endpoints. This was an unmanageable record length; therefore, the history was edited to produce three more efficient and manageable traffic histories which were used in testing. Nine "significant" events in the total history were defined by visual inspection of a plot of strain vs. time in combination with a vehicular traffic count taken in the field test. The nine events correspond to the passage of single truck or multiple trucks. During the testing period sixteen trucks crossed the bridge. An additional event was designated as a "quiet" period and corresponds to periods when the bridge was not loaded by a truck. The three load histories used in testing were developed by linking these events in various combinations.

A "significant" event was defined as a segment of the recorded strain history with larger strain cycles than the surrounding history. Figure 3.4 illustrates the definition by showing a portion of the total history containing a "significant" event. A plot of the stress-time history, and stress range histogram, resulting from a reservoir count for each event are presented in Appendix C.

Traffic History 1. The first traffic load history was generated by arranging the nine "significant" events (2-10) in five random sequences. Event (1), designated as a "quiet" period, was used as a transition between each "significant" event. In testing, the five sequences were recycled. A listing of the events used in each sequence is presented in Table 3.3. A stress range histogram developed by a reservoir count is presented in Fig. 3.5.

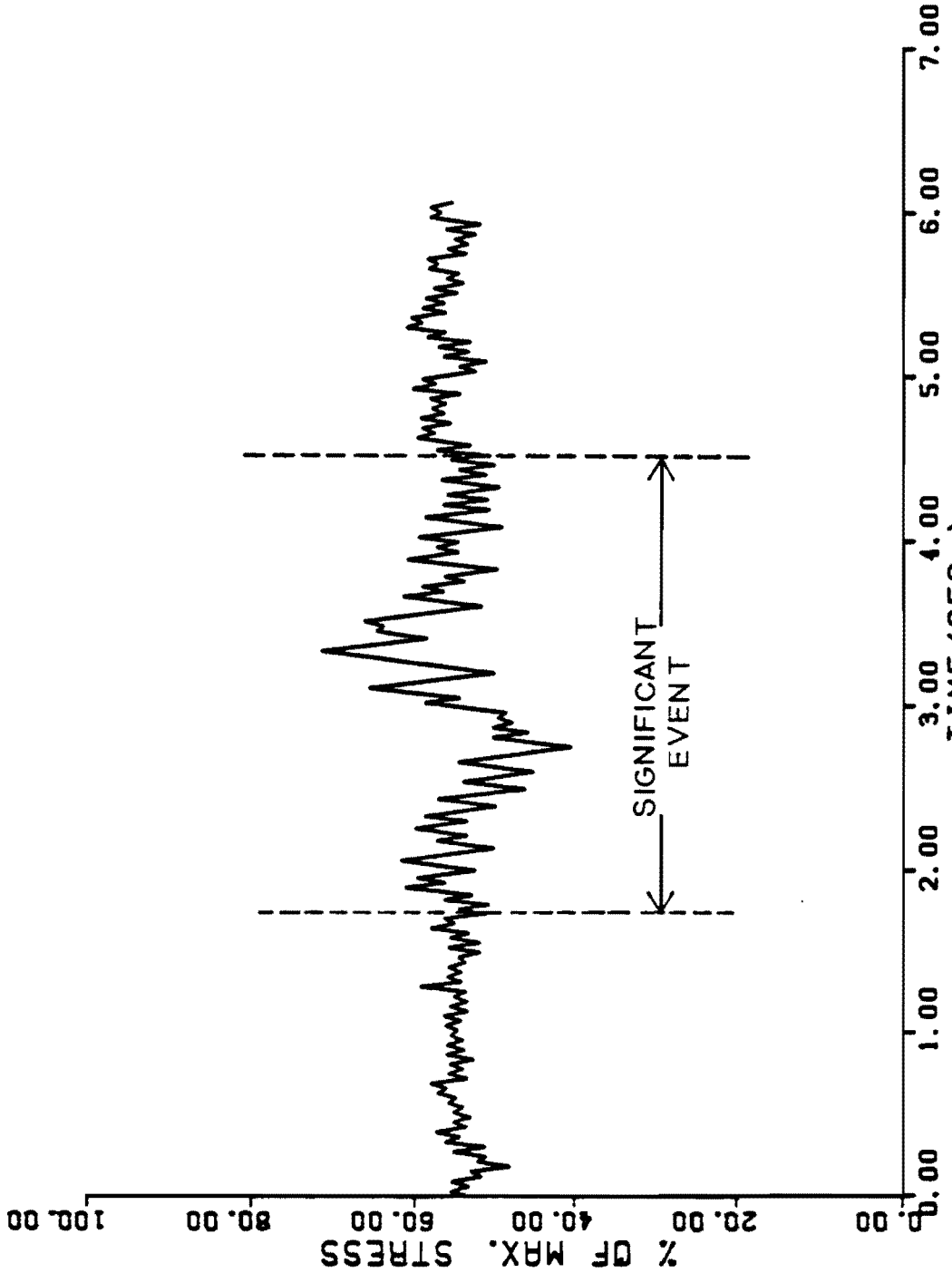

Fig. 3.4 Example of a "significant" event.

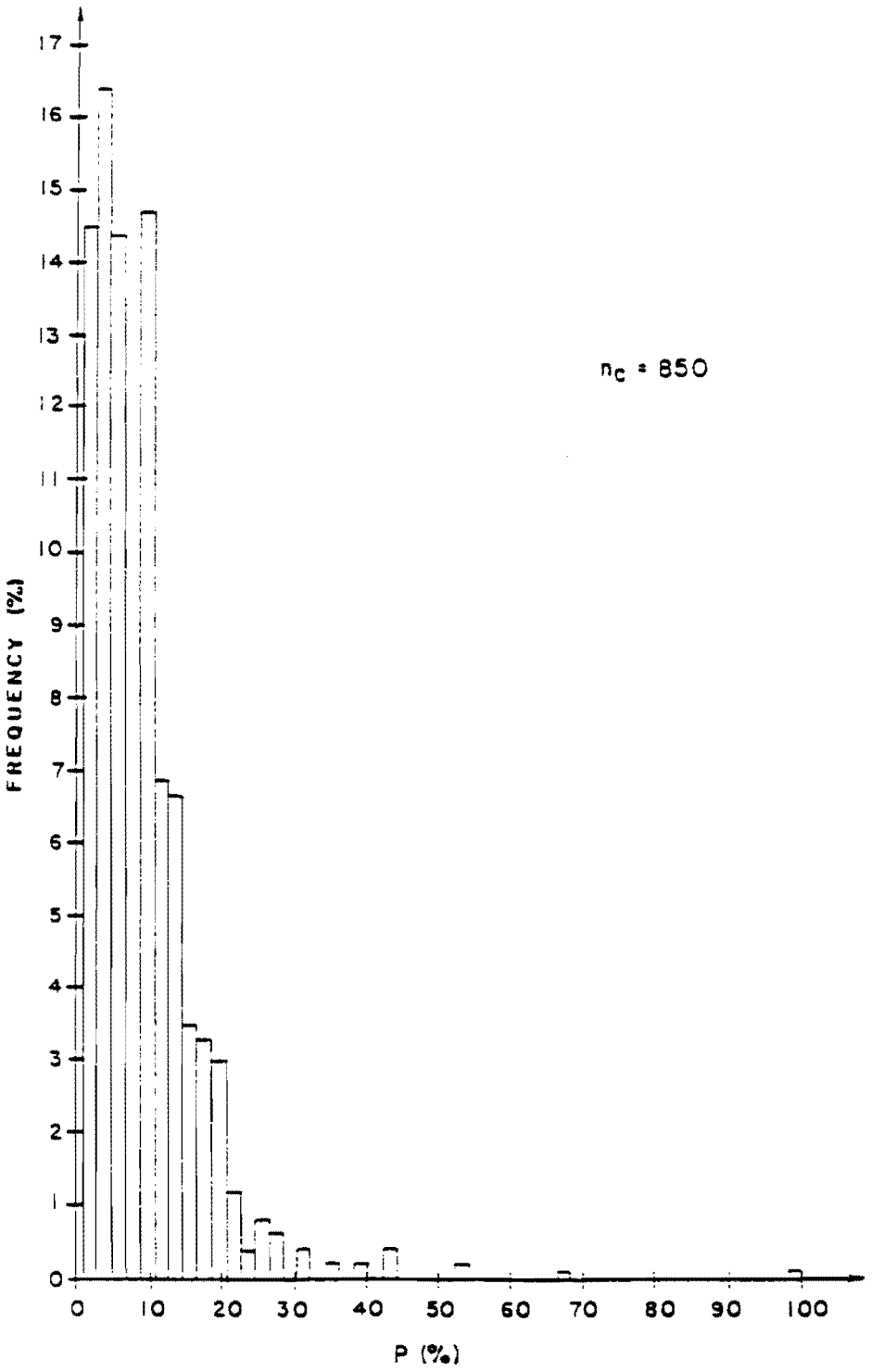

Fig. 3.5 Stress range histogram of Traffic History 1.

This test history was developed to simulate the stress history measured on the bridge. For this reason, all "significant" events were included in Traffic History 1. The use of Event 1 between each significant event increased the number of small cycles, thus shifting the frequency distribution toward the lower stress ranges. A stress range histogram of the measured stress history is presented in Fig. 3.6 for comparison. The difference in the two histograms occurs because a large number of small cycles (less than 10 percent of S_{rmax}) were not used in Traffic History 1 due to restrictions in testing time. The significance of this difference can be measured by comparing the complex effective stress range of each history. The complex effective stress range was calculated using Miner's cumulative damage rule with m = 3.0. The result were S_{rec} = 11.01 ksi for the measured stress, while S_{rec} = 11.13 ksi for Traffic History 1. This is a negligible difference of 1.1 percent.

Traffic History 2. The second traffic history was generated in the same manner as Traffic History 1; however, Event 6 was not used in Traffic History 2. A listing of the events used in each sequence of Traffic History 2 is presented in Table 3.4. A stress range histogram generated by a reservoir count is presented in Fig. 3.7.

The magnitude of the maximum stress range in Event 6 was twice as large as any other event in the history. This fact combined with the shape of the waveform (see Appendix C) makes it apparent that Event 6 represents the passage of multiple trucks. Traffic history 2 was included in the experimental program for the following two reasons: 1)

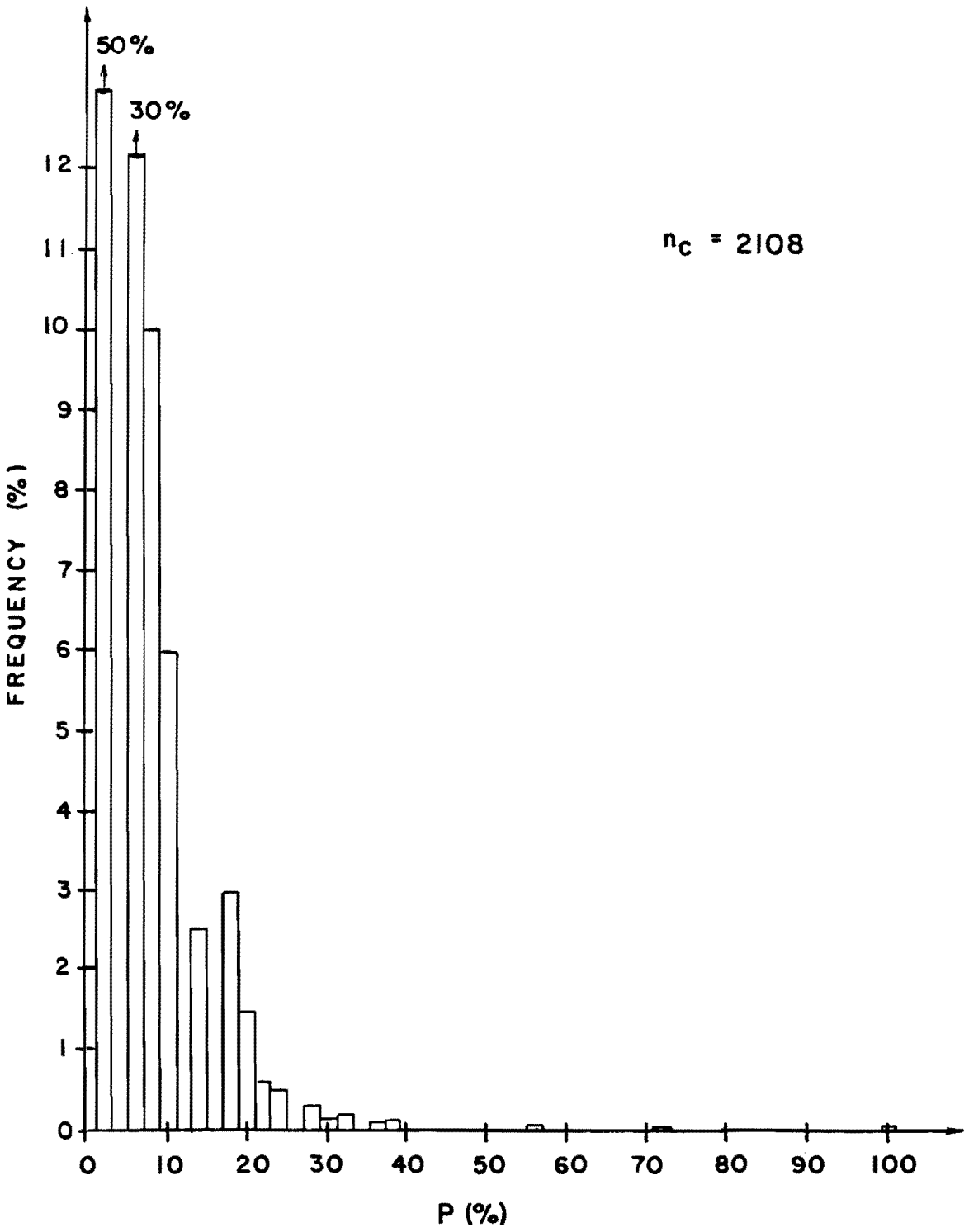

Fig. 3.6 Stress range histogram of measured traffic history.

TABLE 3.3 Listing of Events in Traffic History 1

Order	Events in Sequence
1	5-1-6-1-3-1-10-1-8-1-9-1-4-1-2-1
2	3-1-8-1-4-1-5-1-2-1-7-1-6-1-9-1-10-1
3	8-1-9-1-2-1-6-1-4-1-10-1-7-1-3-1-5-1
4	9-1-7-1-10-1-2-1-5-1-6-1-4-1-8-1-3-1
5	5-1-7-1-6-10-1-8-1-2-1-3-1-9-1-4-1

TABLE 3.4 Listing of Events in Traffic History 2

Order	Events in Sequence
1	5-1-3-1-10-1-8-1-9-1-3-1-2-1
2	3-1-8-1-4-1-5-1-2-1-7-1-9-1-10-1
3	8-1-9-1-2-1-4-1-10-1-7-1-3-1-5-1
4	9-1-7-1-10-1-2-1-5-1-4-1-8-1-3-1
5	5-1-7-1-10-1-8-1-2-1-3-1-9-1-4-1

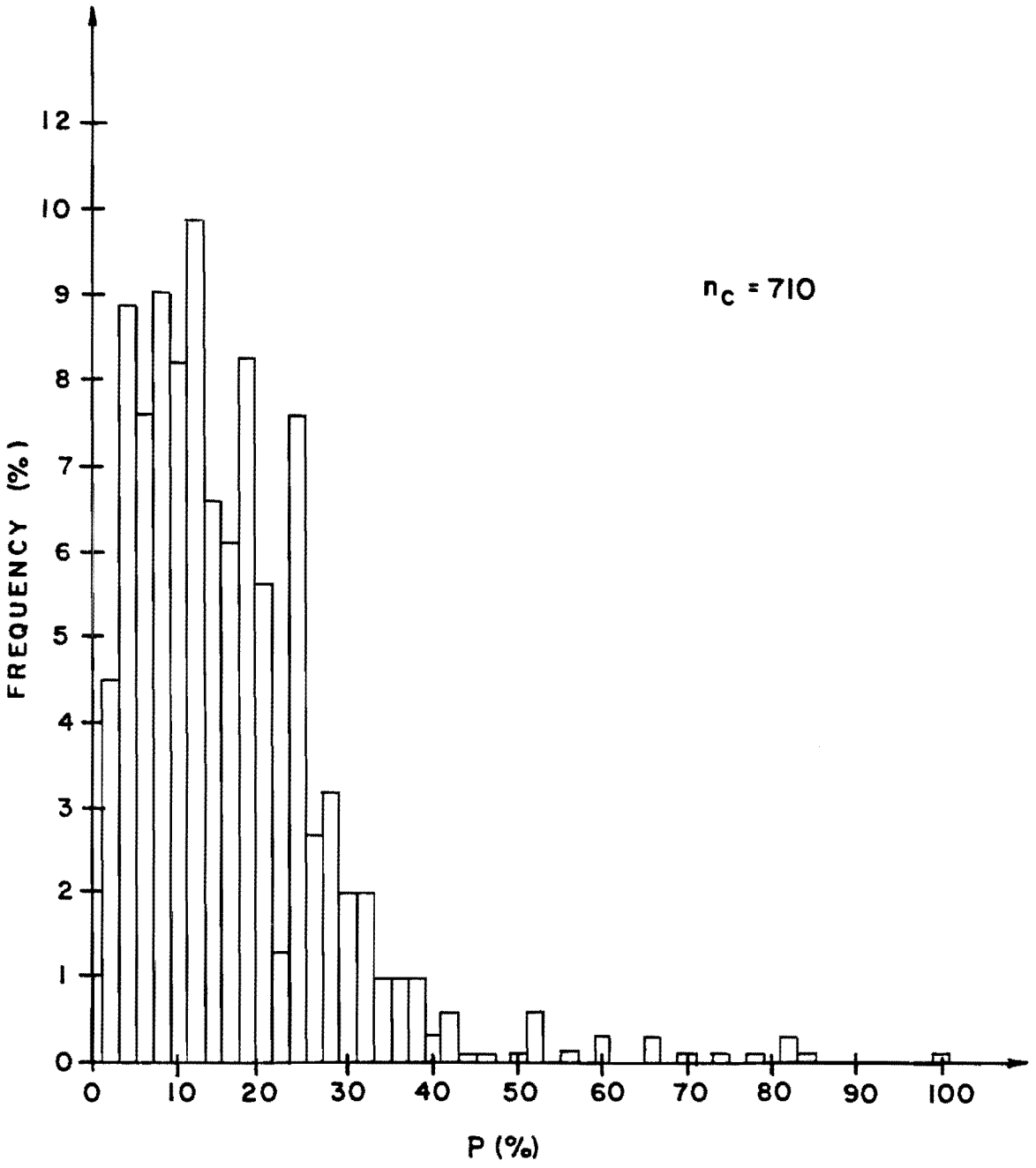

Fig. 3.7 Stress range histogram of Traffic History 2.

to produce information on the difference in damage done by segments of the history individually and as a part of the stress history, and 2) to produce a waveform which better simulates overall vehicle traffic. The difference in the fatigue lives of specimens loaded with Traffic History 1 and those of specimens loaded with Traffic History 2 which did not included Event 6 is a measure of the fatigue damage done by Event 6 as part of the total stress history. In Traffic History 1, Event 6 occurred once in every ten events. This is equivalent to one multiple truck passage in every ten truck passings. Field studies have shown that this percentage is much too high [16]. Therefore, overall vehicle traffic was better simulated by neglecting Event 6.

Traffic Test 3. This load history was generated by recycling Event 6 alone. Traffic Test 3 was included in the experimental program to produce information concerning the summation of fatigue damage caused by trucks in the life of a highway bridge. The idea being tested by use of this traffic history in combination with traffic histories 1 and 2 is that the fatigue damage caused by each individual truck passage can be summed to predict the fatigue damage produced by all truck passages. Comparison of the results of the experiments done with traffic histories 1, 2 and 3 indicates the difference in the fatigue damage caused by Event 6 when applied alone and as a part of the stress history. A stress range histogram of Traffic Test 3 is presented in Fig. 3.8.

3.1.3 Constant Minimum Stress Histories. The constant minimum stress histories are random discrete loadings. A random discrete loading consists of discrete load cycles which are applied in a random

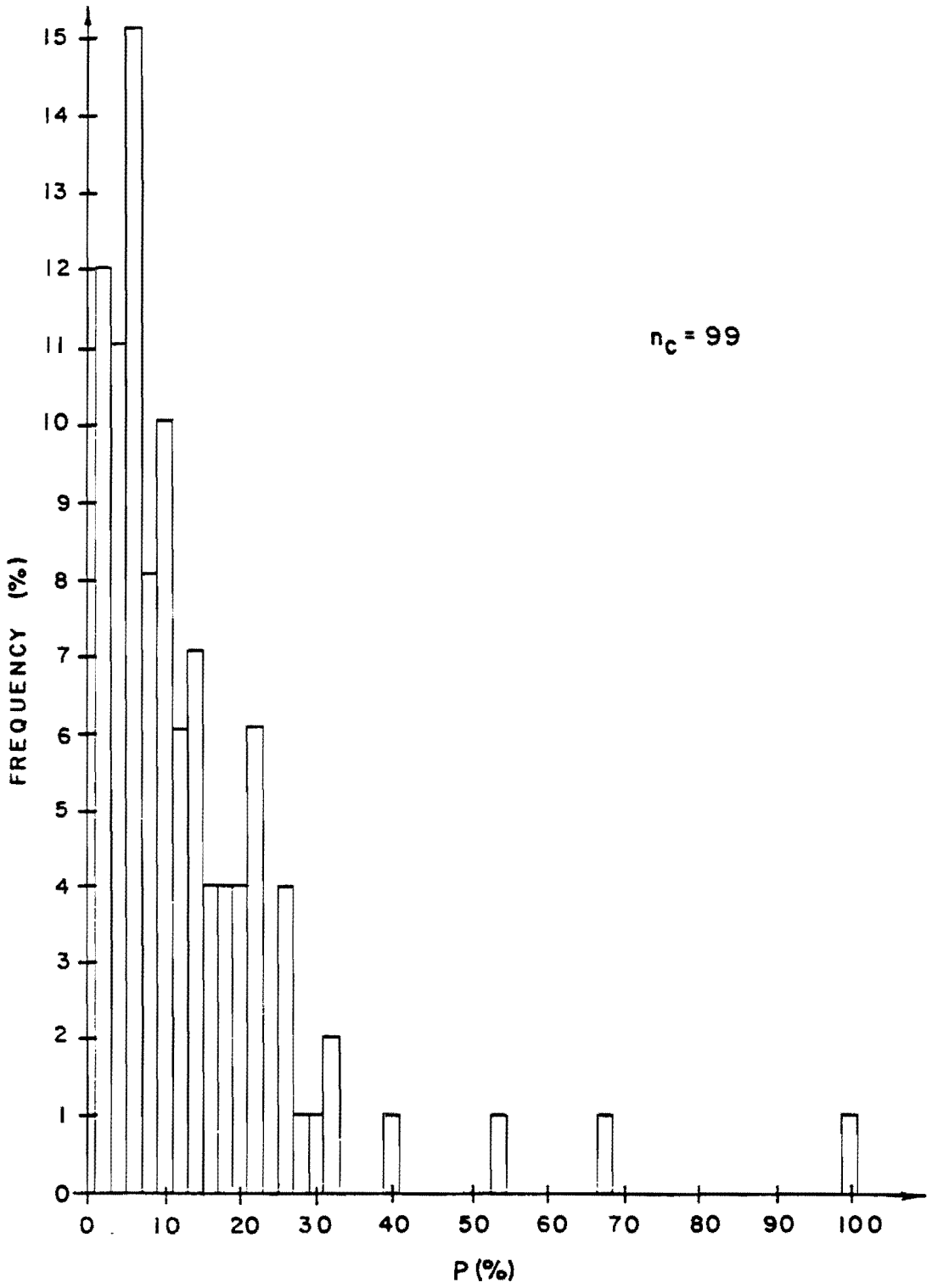

Fig. 3.8 Stress range histogram of Traffic History 3.

sequence. In this study, as the name of the category implies, the load cycles are applied with a constant minimum stress. The order in which the cycles were applied was determined by using a random number table. Two loading histories were included in this category.

Constant Minimum Stress History 1. The stress range histogram of the test-truck history (see Fig. 3.3) was used to determine the magnitude and number of stress cycles in this history. Using a random number table, the cycles were arranged in five random sequences. In testing, the sequences were recycled.

Constant Minimum Stress (CMS) History 1 was included in the experimental program to test the ability of a random discrete loading pattern to simulate actual traffic loadings. CMS History 1 was designed to have the same stress cycles as the test truck history. Thus, the fatigue lives of specimens loaded by CMS History 1 should be the same as those of specimens loaded with the test truck history if random discrete loadings are accurate models of actual loadings.

Constant Minimum Stress History 2. This loading history was developed from one of the histories used by United States Steel's researchers in NCHRP Project 12-12 [12]. The distribution of stress ranges in the history is based on a probability-density curve described by the Rayleigh function:

$$P' = 1.001\, x' e^{-1/2(x')} \qquad (3.1)$$

where P' = nondimensional probability density

e = Napierian base (2.7183)

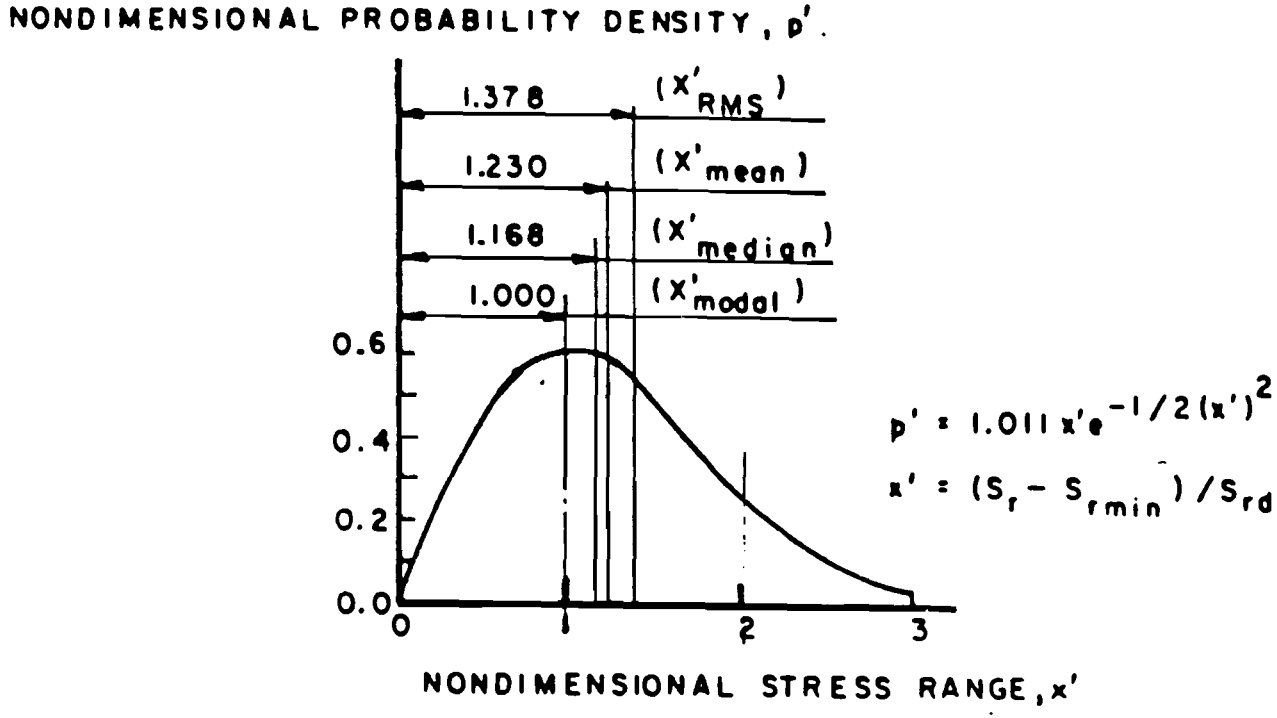

Fig. 3.9 Rayleigh function used to develop CMS History 2.

$$x' = (S_r - S_{rmin}) / S_{rd} \qquad (3.2)$$

S_r = independent stress range

S_{rmin} = minimum stress range in the history

$$S_{rd} = S_{rm} - S_{rmin} \qquad (3.3)$$

S_{rm} = modal stress range

A plot of the Rayleigh function used to develop CMS 2 is shown in Fig. 3.9.

The stress history contains 500 cycles; thus, the frequency of occurrence of each cycle is 1/500. The value of x_n' which corresponds to x' of the n^{th} cycle is calculated by integrating Eq. (3.1) from 0 to x_n' and equating the result to the desired frequency, $(n - 1/2)/500$. This results in the following equation for x_n':

$$x_n' = \sqrt{-2Ln\ [1 - 0.001978\ (n - 0.5)]} \qquad (3.4)$$

The stress range of the n^{th} cycle, S_{rn}, is then calculated from Eq. (3.2) with the value of x_n'.

To program this history for the function generator, each stress range was described as a percentage of the maximum stress range, P_n. The following equation for P_n was developed by combining Eqs. (3.2) and (3.3) and the relation $S_{rmax} = S_{rm} + 2\ S_{rd}$:

$$P_n = \frac{1 + [(x_n' - 1)(S_{Rd}/S_{Rm})]}{1 + 2(S_{Rd}/S_{Rm})} \qquad (3.5)$$

where x_n' is given by Eq. (3.4) and the ratio $S_{rd}/S_{rm} = 1.0$. $S_{rd}/S_{rm} = 1.0$ was used to develop CMS History 2 because it produced a wide band spectrum which best represented traffic data. Once P_n was determined for each cycle, the 500 cycles were arranged in three random sequences. In testing, the sequences were recycled.

CMS History 2 was included in the experimental program to correlate the results of the tests of this study done on welded tees to the results of the tests done by U.S. Steel on full-sized bridge girders [12].

3.2 Test Specimen

3.2.1 Specimen Design.

The specimen shape, support conditions, point of load application, and location of the fatigue crack are shown in Fig. 3.10. The specimen used in this testing program has the following attributes:

1. fatigue cracking at the weld toe;
2. ability to be tested at high frequency;
3. easy installation and removal of specimen; and
4. identical weld toe geometries to minimize test scatter.

The crack location and the direction of crack propagation are constant in all tests. The consistent mode of failure improves the repeatibility of test results, thus increasing the confidence in the comparison of test results between experiments using different loading histories.

3.2.2 Specimen Fabrication.

The specimens used in this study were constructed by Joehnk as part of his fatigue study [14]. The

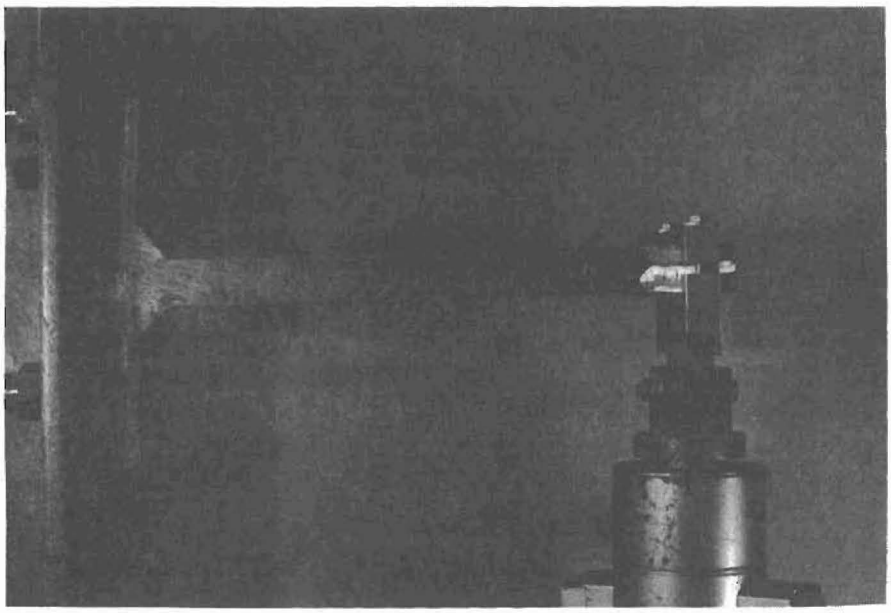

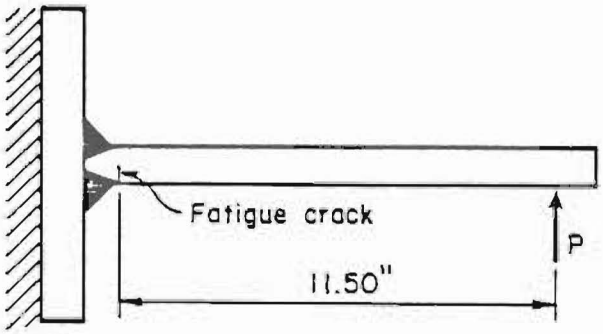

Fig. 3.10 Specimen shape, support conditions, load application point, and crack location.

specimens were taken from two groups left untested by Joehnk and Zwerneman [1].

The specimens were fabricated from 1-in. thick plates of A572 Grade 50 steel. All plates were of the same mill plate whose chemical composition is presented in Table 3.5. A 5/16-in. double bevel was flame cut along one edge of the plate used as the cantilever. A manual shielded metal arc welding process was used to join the cantilever plate to the support plate. The welding sequence is shown in Fig. 3.11. Thirteen 3-in. wide specimens were cut from each weldment with a saw after 1/2 in. was trimmed from each end of the weldment to eliminate the end of the welds. Two holes were drilled in the support plate of each specimen to provide a method for bolting the specimen to the testing frame. The specimen geometry is shown in Fig. 3.12.

To differentiate between weldments, each one was marked with a unique pattern painted on the edge of the support plate before cutting. The painted edge was used to define the loading direction so the same weld toe was tested within each weldment. The rolling direction is the same with respect to the loading direction within a weldment but not necessarily between weldments.

3.3 Testing Apparatus

The testing apparatus used in this study consists of two interrelated systems, 1) the support system and 2) the loading system. The apparatus is pictured in Fig. 3.13.

3.3.1 Support System.

The support system is a structurally determinate system which holds the specimen and hydraulic ram in position during testing. This unit consists of 1) a load frame of

TABLE 3.5 Base Metal Chemical Composition.

Steel Grade: A572-50

Chemical Composition

	C	Si	Mn	P	S	Cr	Ni	Mo	V	Cu	Nb
Mill Ladle Analysis (%):	0.19	0.23	1.12	0.019	0.019				0.007		0.030
Mill Product Analysis (%):	0.18	0.22	1.09	0.018	0.016						0.029
[1]Laboratory Analysis (%):	0.17	0.23	1.11	0.013	0.022	0.18	0.02	0.01		0.01	0.027
ASTM Heat Analysis (Type 1) Requirements	0.23 max	0.40 max	0.80-1.65	0.04 max	0.05 max						0.005-0.05

[1]Chicago Spectro Service Laboratory, Inc.

Mechanical Strength (Mill Test Results)

	Tensile Test	ASTM Required
Yield Point:	58 ksi	50 ksi
Tensile Strength:	81.2 ksi	65 ksi

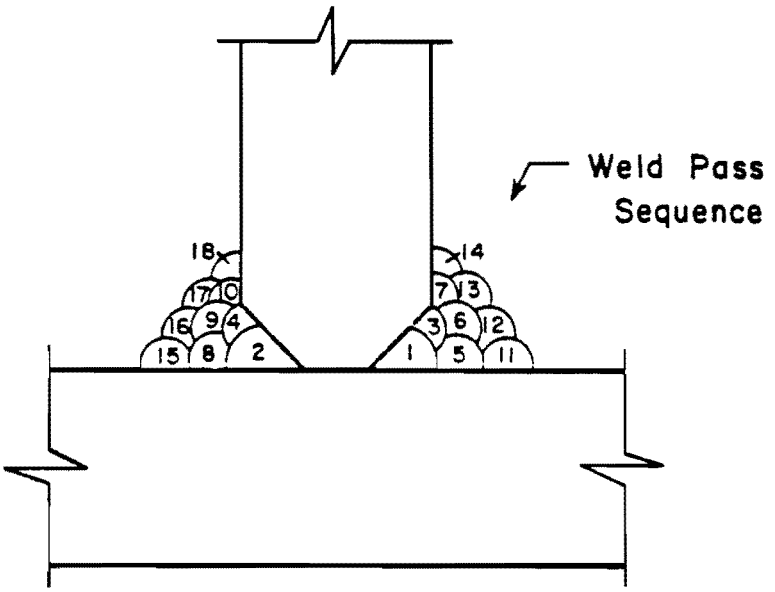

Weld Pass No.	Electrode	Current, Amps	Voltage, Volts DC
1 & 2	3/32"-7018 Low Hydrogen	100	26
3 - 18	1/8"-7018 Low Hydrogen	150	27

Fig. 3.11 Specimen weld sequence.

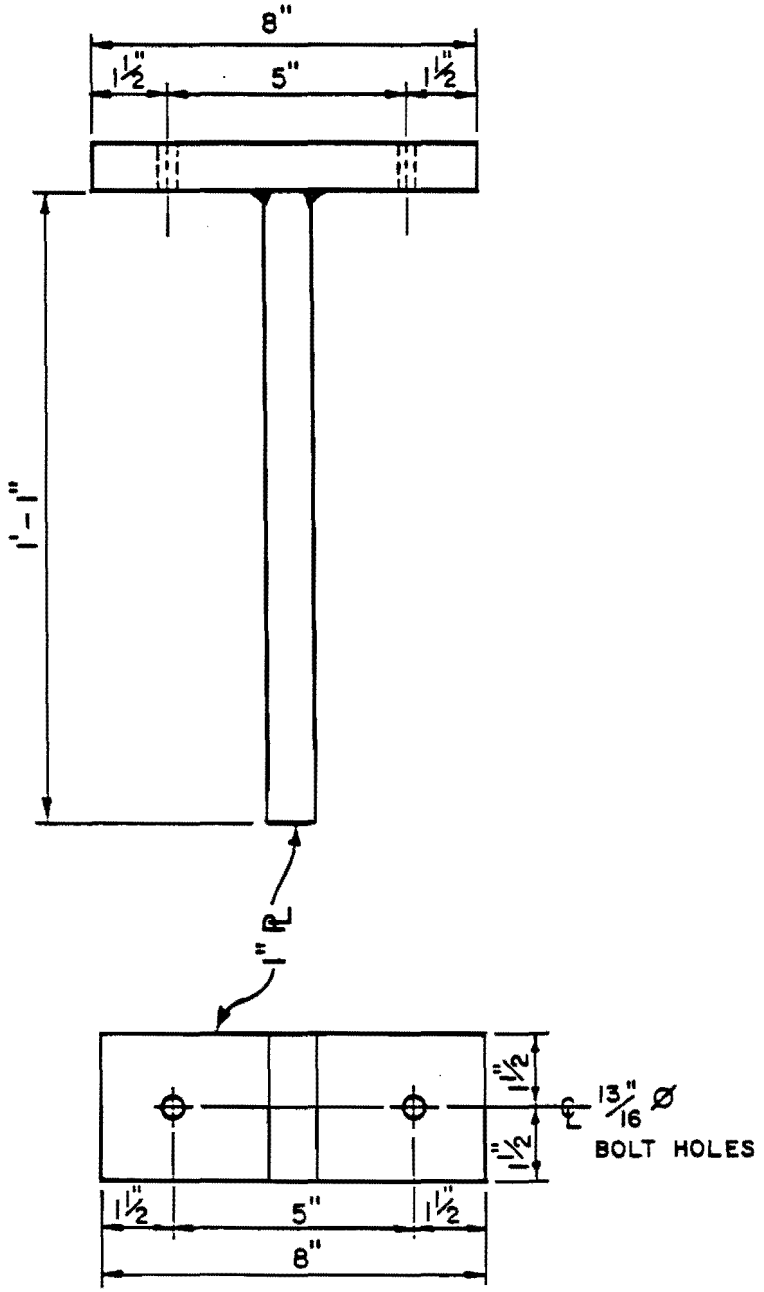

Fig. 3.12 Specimen geometry.

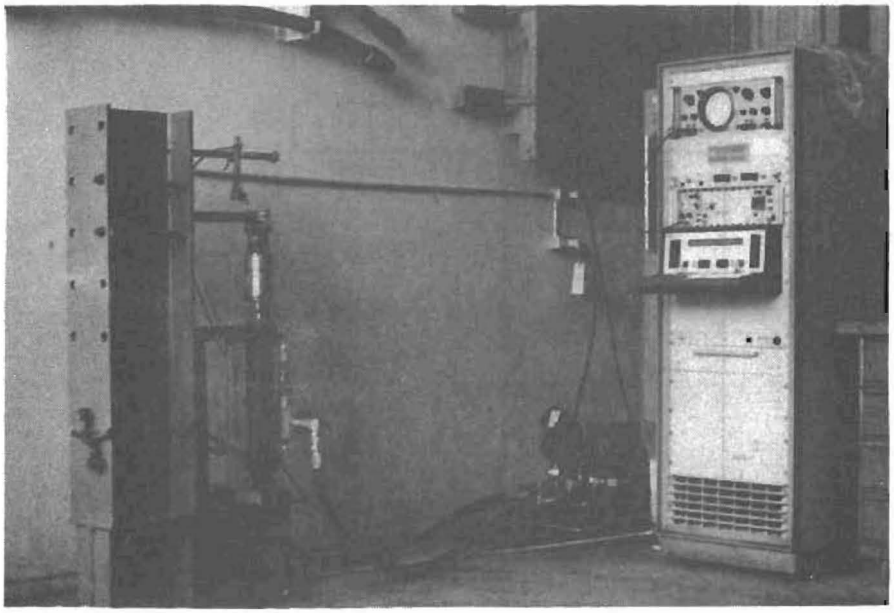

Fig. 3.13 Testing apparatus.

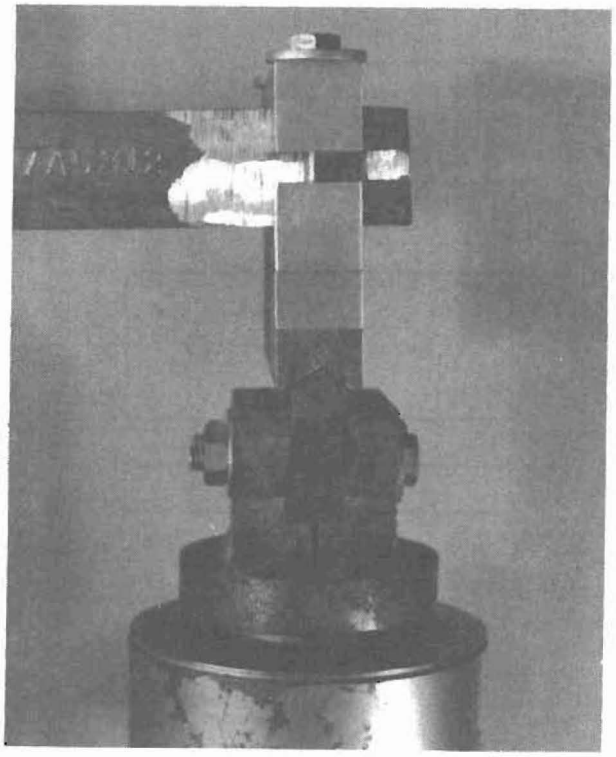

Fig. 3.14 Knife-edged loading attachment.

structural steel and 2) a knife-edged loading attachment which connects the ram to the specimen. The knife-edged loading, shown in Fig. 3.14, eliminates the possibility of load reversals, and the transfer of moments.

3.3.2 Loading System. The load on the specimen was supplied with a standard closed-loop servo-controlled hydraulic system. In this system, however, a microcomputer was used as a function generator. This alteration allowed the generation of the complicated stress histories required by the test program.

3.4 Testing Procedure

The testing procedure can be divided into two tasks, 1) test preparation and 2) test maintenance.

3.4.1 Test Preparation. Test preparation begins by programming the function generator to produce the desired waveform. This waveform is based only on percentages of maximum voltage applied. Then, measurements of thickness and width of the specimen are made to determine section properties. With the section properties, loading configuration and the desired maximum stress range, the required load was calculated to produce the desired stress range at the weld toe. The load is converted to a maximum voltage which is used to set the electronic servo-system.

Next, the testing speed must be set. As discussed in Section 3.1.1 concerning the development of the loading histories, the waveform possesses a constant loading rate. To provide a way to vary the actual testing speed, the function generator has a control which sets the

testing speed as a percentage of the speed originally programmed. The operator can set the test to run at a rate from 0 to 499 percent of the original testing speed. Since the hydraulic system response lags behind the command signal, the rate of testing was somewhat restricted by the response of the hydraulic system. Overprogramming of the command signal allowed for an increased testing rate. For most experiments, the testing speed was set at a rate of 200 percent.

To begin testing, the specimen was placed in the supporting frame and aligned with the hydraulic ram. The desired loading was applied using the servo controller in combination with the microcomputer function generator. A limit was then set on the feedback to stop testing in case of a system failure. In addition, a limit was set on the error i.e., difference between the command signal and the feedback signal, to stop testing as the specimen lost stiffness.

3.4.2 Test Maintenance. Once the test is started, test maintenance consisted of 1) adjusting the command signal to ensure that the desired loading was maintained, and 2) restarting the test after system failures. The monitoring of the test continued at regular intervals until the specimen failed.

Adjustments in the command signal during testing was necessary because the loading supplied by the hydraulic ram lags behind the electronic signal as the specimen fatigues. As the specimen fatigues, it becomes less stiff and a greater displacement is required to maintain the load. Thus, the hydraulic ram must move farther which slows the response of the hydraulic system. This condition is corrected

by overprogramming the servo controller which drives the ram so that the desired load is maintained.

Restarting the test was required in two situations: 1) a system failure due to a mechanical failure, i.e., hydraulic pump overheating, or 2) a system failure due to electrical failure. In case of a mechanical failure, loading was restarted from the last position in the load history. An electrical failure disables the function generator, requiring reprogramming and a restart of the loading at the beginning of the history. This situation results in the application of partial complex cycles. However, the effect of these partial cycles was negligible because electrical failures were infrequent.

To ensure an accurate measurement of fatigue life, two conditions for failure were adopted: 1) the specimen stiffness decreases 10 percent, and 2) a visible crack occurs through 1/3 to 1/2 of the specimen thickness. The first condition was used to automatically stop testing before absolute failure as defined by the second condition. Therefore, the limit set on the error was 10 percent greater than the error produced by the uncracked specimen. The system was automatically shut down at this point. From this point, the test was resumed and monitored more closely than previously until the second condition of failure was reached. Two examples of the crack lengths at failure are shown in Fig. 3.15.

3.5 Experimental Error

The experimental error in the study is defined as an error in determining the fatigue life of the load history used in the test. The

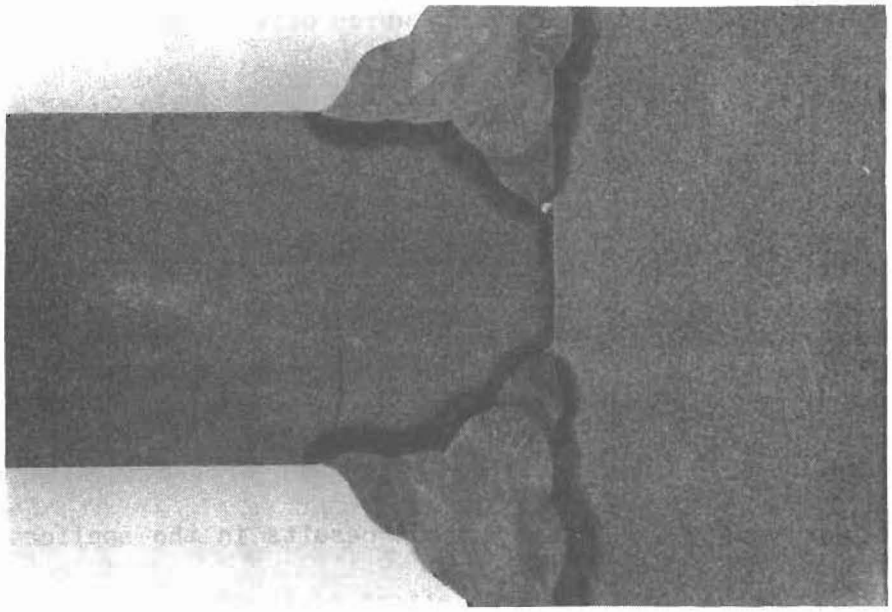

(a) Specimen opened transverse to crack

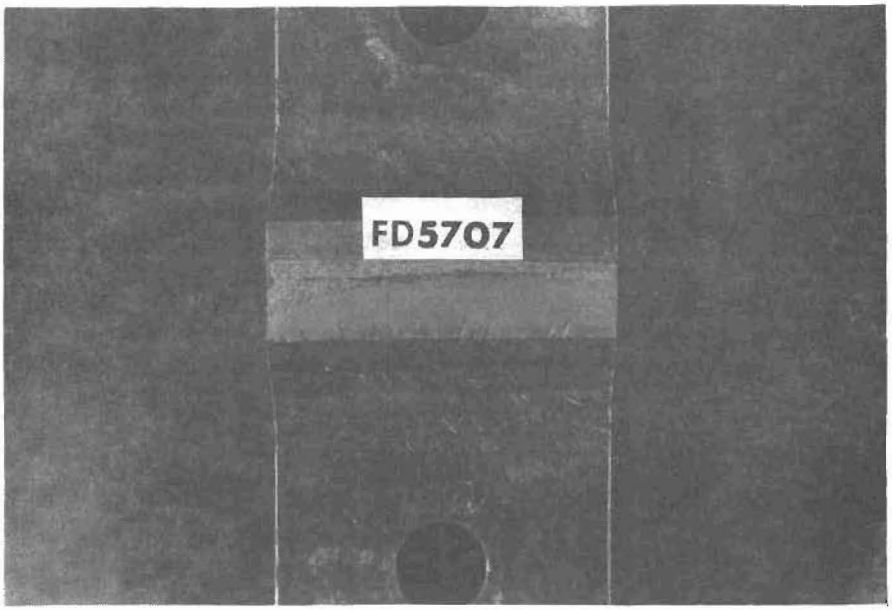

(b) Specimen opened in plane of crack

Fig. 3.15 Example of crack length at failure.

experimental error enters the testing in two areas: 1) the application of the desired load history, and 2) the definition of fatigue life.

The sources of error in the application of the load history are: 1) the determination of required command signals; 2) the inaccuracy of the electronics; and 3) the lag between the electronic signal and the hydraulic response. Three measurements were required to determine the command signals. The thickness and width of the specimen and the distance from the applied load to the weld toe were used to calculate the signals required.

The inaccuracy of the electronics is defined as the difference between the programmed signal and the signal that is actually produced. The load cell and the electronic monitoring equipment were calibrated before testing and were accurate to within 1.6 percent.

Due to the lag time between the electronic signal from the servo controller and the response of the hydraulics, some of the smaller minor cycles were not applied to the specimen. This occurred when the system was run at high speeds. A comparison of the command and feedback signals was made for several testing speeds using an Explorer III oscilloscope by Nickolet as described below.

An example of the two signals at a loading rate of 200 is shown in Fig. 3.16. The global maximum and minimum points in the load history were set to desired levels using a peak detector, so there is no error in these values due to the lag in the system. The error occurs in the application of intermediate loads. The error is not a constant one, so to determine the effect of the lag in response, a reservoir count was

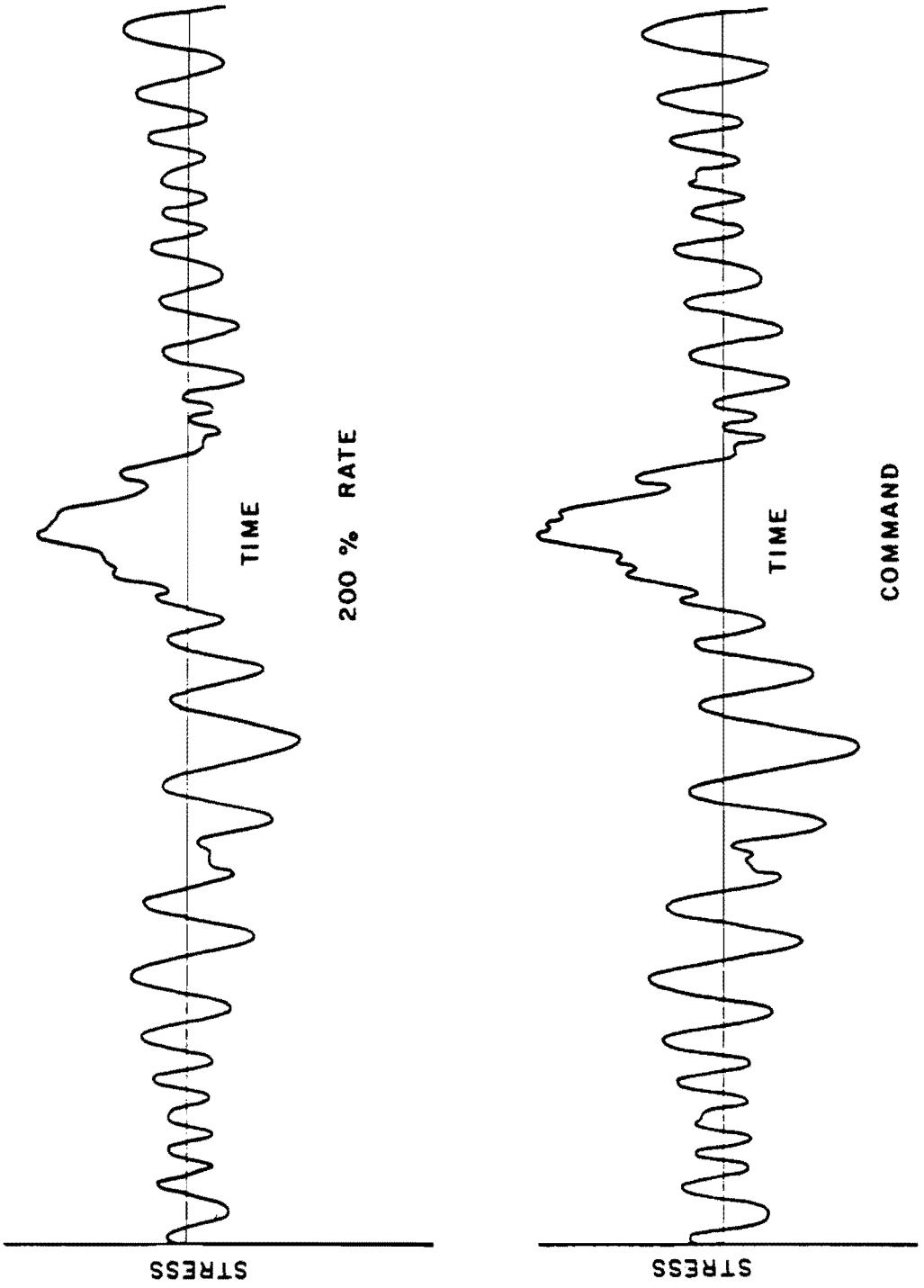

Fig. 3.16 Comparison of command and feedback signals.

done and the damage factors for the command and feedback signals were calculated for the truck test history. The results of these calculations are shown in Tables 3.6 and 3.7. From comparisons of the damage factors and the feedback signals, it was concluded that further testing would be done a a rate of 200 percent of the originally programmed testing speed. At this testing speed the difference between the command waveform and the applied waveform is negligible. Use of this rate allowed for a decrease in testing time while assuring accurate load application. In addition, the errors in previous testing were compensated for in the comparison of experimental to predicted data.

Combining the sources of error in the application of the load history, the maximum error (as determined by Zwerneman [1]) is approximately 2.9 percent. the more probable value is closer to 1.5 percent.

The error in the definition of failure is caused by the vagueness of the crack length at failure. The crack length was determined by the naked eye. For the test histories used in this study, the variation of crack size used to define failure resulted in a maximum error of 2.8 percent. A more probable value of the error is 1.4 percent.

The total experimental error is a combination of the errors in applying the load history and in defining failure. Therefore, the total error will be estimated by the square root of the sum of the squares of these two components. For the maximum errors of 2.9 and 2.8 percent, the total error is 4.0 percent. For the more probable errors of 1.5 and 1.4 percent, the total error is 2.1 percent.

TABLE 3.6 Comparison of P Values for Test Truck History at Various Test Speeds

Cycle No.	Command	Feedback Rate (%) 100	200	320	499
1	1.00	1.00	1.00	1.00	1.00
2	0.46	0.46	0.46	0.47	0.46
3	0.43	0.43	0.43	0.44	0.43
4	0.43	0.43	0.43	0.44	0.42
5	0.37	0.37	0.37	0.37	0.37
6	0.35	0.35	0.36	0.37	0.34
7	0.30	0.30	0.31	0.31	0.28
8	0.25	0.25	0.26	0.26	0.25
9	0.24	0.24	0.24	0.24	0.21
10	0.23	0.23	0.23	0.23	0.20
11	0.22	0.22	0.23	0.22	0.20
12	0.17	0.20	0.18	0.21	0.15
13	0.17	0.18	0.17	0.17	0.13
14	0.17	0.17	0.16	0.14	0.11
15	0.16	0.17	0.16	0.14	0.11
16	0.11	0.12	0.11	0.11	0.06
17	0.11	0.11	0.10	0.09	0.04
18	0.07	0.07	0.07	0.06	0.01
19	0.04	0.04	0.03	0.02	
20	0.03	0.03	0.02	0.02	
21	0.03	0.02	0.01	0.01	
22	0.02	0.02	0.01	0.01	
23	0.02	0.02	0.01		
24	0.02	0.02	0.01		
25	0.01	0.01			
26	0.01	0.003			
27	0.002	0.003			

TABLE 3.7 Comparison of F Values for Test Truck History at Various Speeds

Linear Model	Command	Feedback Rate (%) 100	200	320	499
F (Miner)	1.217	1.216	1.217	1.234	1.219
F (NLM)	2.499	2.509	2.499	2.536	2.505

C H A P T E R I V

ANALYSIS OF TEST RESULTS

The results and analysis of the results of fatigue experiments on welded tees loaded in bending are presented in this chapter. Seven different loading histories were included in the test program. The loading histories include a constant amplitude history, the test truck history, three traffic histories, and two constant minimum stress histories.

The constant amplitude tests were used to develp a log-log S-N curve for the specimen. The test truck and traffic histories tests are included to investigate the applicability of the cumulative damage models to measured loadings. The results of these tests are also used to study the amount of fatigue damage produced by minor cycles. A comparison of the results of tests using the test truck loading and CMS History 1 is used to demonstrate the ability of random discrete loading patterns to model actual loadings. The results of tests using CMS History 2 are compared with the results of the U.S. Steel study [12] to determine the applicability of the results of this study to full scale bridge girder design. Finally, to increase the data base of this study, the results of the U.S. Steel study [12] are presented in terms of S_{RMAX} and experimental damage factors.

A damage model is developed from an analysis of the test results. This damage model applies a correction factor based on a

stress interaction term to Joehnk's cumulative damage calculation. To conclude this chapter, modifidations to the present design procedure are proposed.

4.1 Test Results

4.1.1 Constant Amplitude. Constant amplitude tests were performed on several specimens from each weldment in order to correlate test results across weldments. While all tests were run with a minimum stress of 5 ksi, stress ranges from 35 to 12.5 ksi were included in the experimental program. A total of thirty constant amplitude tests were performed. All constant amplitude testing was completed by Joehnk [14] and Zwerneman [1] in earlier phases of this research.

The results of the constant amplitude tests are plotted in Fig. 4.1. The least squares linear regression was done to determine the S-N curve and the 95% confidence band which are presented on Fig. 4.1. It should be noted that only data from specimens tested to failure were included in the regression analysis. The equation of the S-N curve provides the values of the variable m used in Eqs. (2.2) through (2.4), (2.9) through (2.11), (2.14) through (2.16), (2.20) and (2.21); and the constant used to calculate N in Eq. (1.5). The equation of the S-N mean curve as determined by regression is:

$$N = (2.09 \times 10^{11}) (S_R)^{-3.76}$$

Thus, $A = 2.09 \times 10^{11}$ and $m = 3.76$. Since a fatigue failure occurred with $S_R = 12.5$ ksi, the threshold stress range (S_{RTH}) must be below this level. Assuming conservatively that $N = 5 \times 10^7$ defines the fatigue

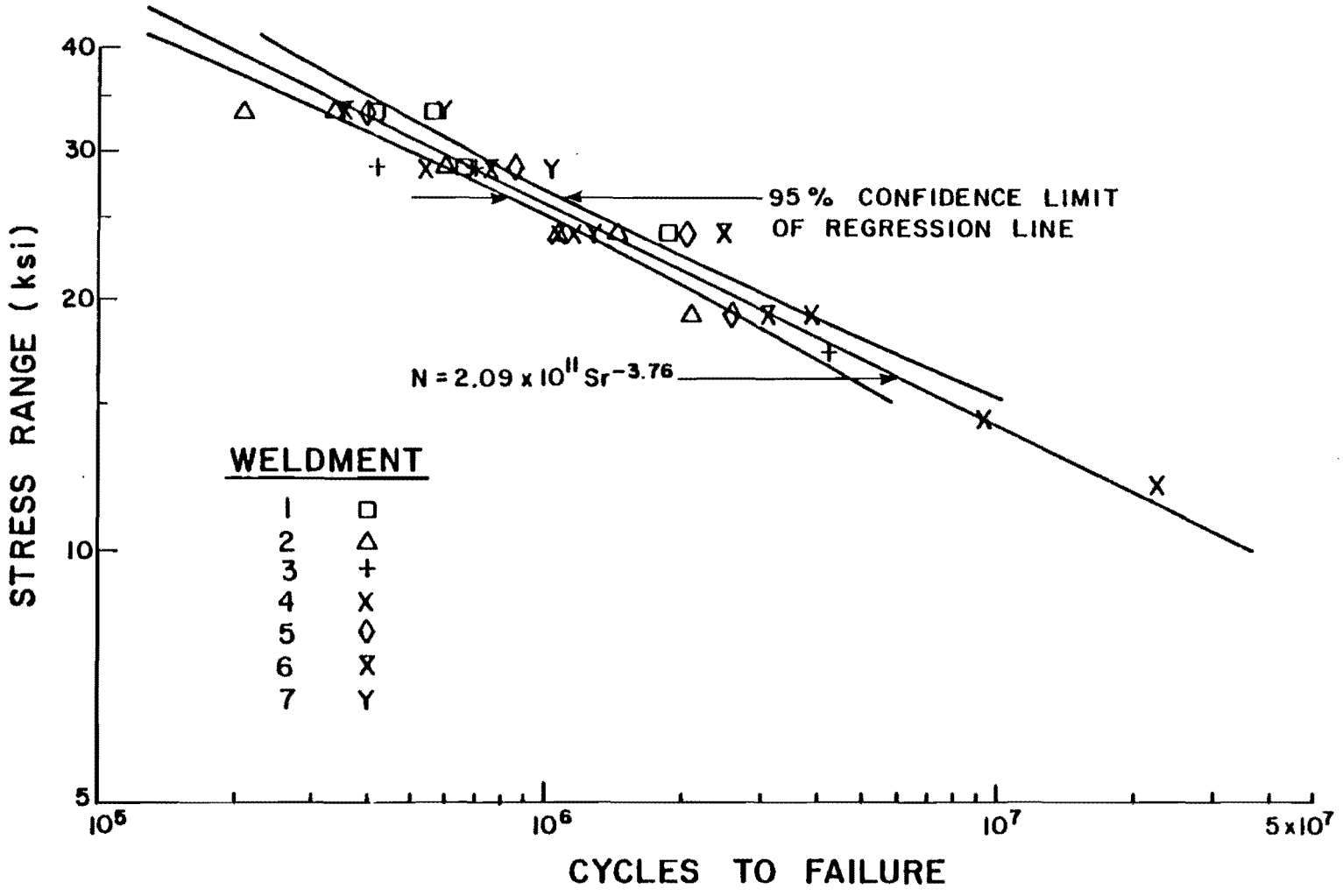

Fig. 4.1 Constant amplitude test results.

limit, then S_{RTH} = 9.19 ksi. This should represent the minimum value of S_{RTH}. Assuming that N = 3 x 10^7 defines the fatigue limit, then S_{RTH} = 10.52 ksi. Thus, the threshold stress range should exist from between 10.5 and 9.2 ksi.

The S-N curve derived from the regression analysis provides a reference from which to measure the fatigue damage produced by the minor cycles in a variable amplitude history. In addition, the determination of the damage factor is dependent on the variables produced by the S-N curve. Therefore, the cumulative damage models can be no more accurate than the initial S-N curve. If the S-N curve was perfectly accurate, then the values of the experimental damage factor (F_{EXP}), experimental fatigue life divided by value from mean regression line, would be 1.0 for all constant amplitude tests. Figure 4.2 presents a histogram of the values of F_{EXP} for all constant amplitude tests. The average value of F_{EXP} is 1.04. The maximum and minimum values of F_{EXP} are 1.82 and 0.55 respectively. This range of values demonstrates the amount of experimental scatter inherent in fatigue testing.

4.1.2 Test Truck History. The loading used in this series of tests was developed from strain data measured during the passage of a single test truck. A plot of the loading is presented in Fig. 3.2. All tests in this series were done by Zwerneman [1] except specimen FD6909. As with the CA tests, a minimum stress of 5 ksi was using in testing. A summary of test results, along with the ratio of experimental damage factor (F_{EXP}) to the predicted damage factor (F_{PRED}) for the respective damage models is provided in Table 4.1. For this relationship, a value

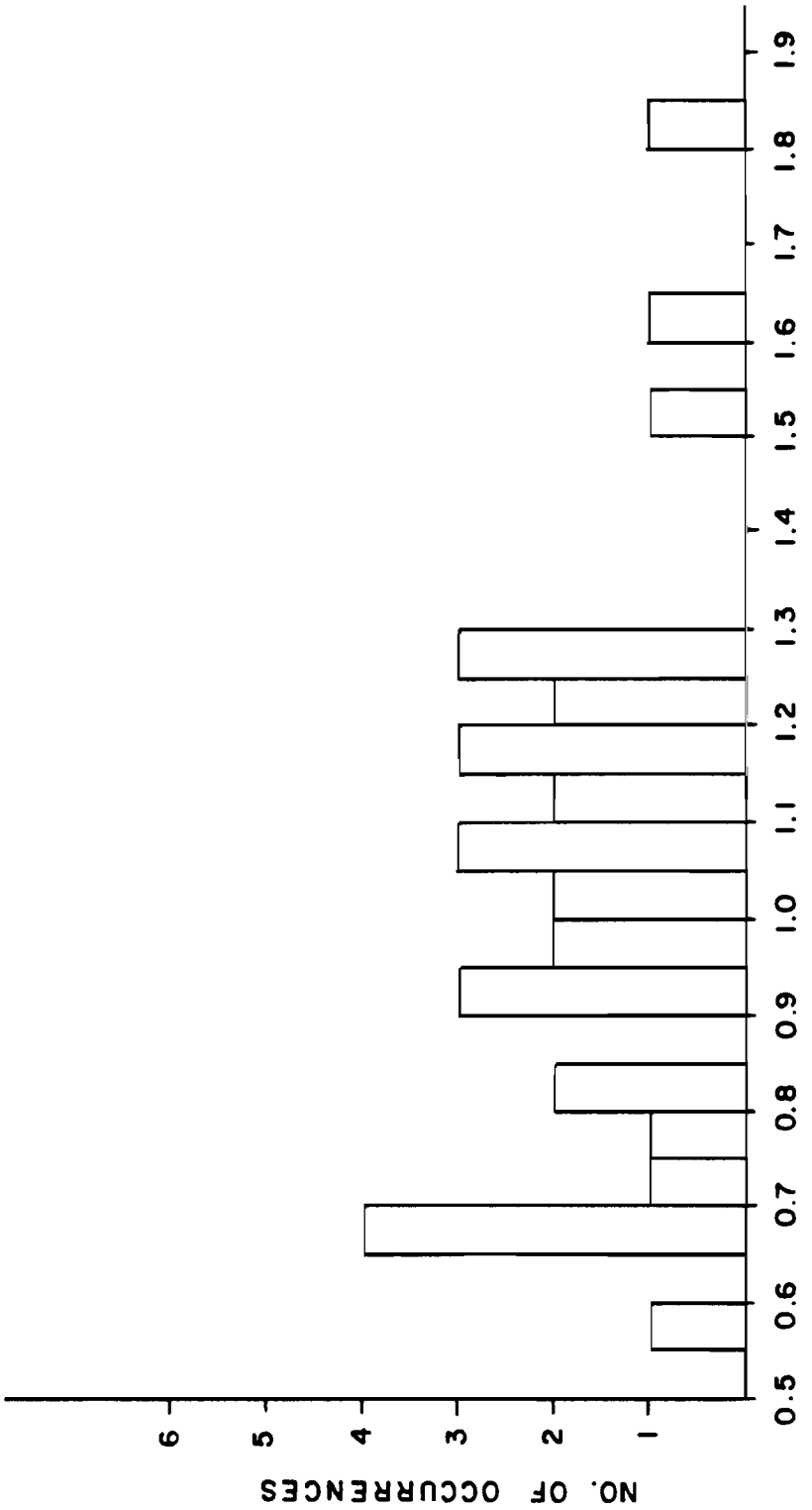

Fig. 4.2 Histogram of F_{EXP} for CA tests.

TABLE 4.1 Test Truck Test Results

Specimen	S_{RMAX} (ksi)	N_c x 10^3	F_{EXP}	$\frac{F_{EXP}}{F_M}$	$\frac{F_{EXP}}{F_{NLM}}$	$\frac{F_{EXP}}{F_G}$
FD5605	33.46	206.5	1.85	1.50	0.73	0.67
FD5706	28.71	329.7	2.07	1.68	0.82	0.75
FD5707	28.71	356.2	1.92	1.56	0.62	0.70
FD6909	20.00	1581.6	1.70	1.42	0.73	0.67

of F_{EXP}/F_{PRED} greater than 1.0 is unconservative as the predicted fatigue damage is less than the experimental, while F_{EXP}/F_{PRED} less than 1.0 is conservative.

The experimental damage factor, F_{EXP}, is given by the ratio N_c/N_{MAX} where $N_{MAX} = 2.09 \times 10^{11} (S_{RMAX})^{-3.76}$, the maximum stress range is set for each test, and N_c is determined experimentally. The predicted damage factors by Miner's (F_M), nonlinear Miner's (F_{NLM}), and Gurney's (F_G) models are determined by Eqs. (2.11), (2.16), and (2.22) respectively.

The values of F_{EXP}/F_{PRED} for this test series are plotted against S_{RMAX} in Fig. 4.3. The distribution of points in Fig. 4.3 indicates that none of the three damage models accurately predict the fatigue damage produced by this stress history. Miner's theory is unconservative in all cases and underestimates the fatigue damage by an average of 54%. Nonlinear Miner's and Gurney's damage models were more accurate and produced conservative predictions of fatigue damage, but the average errors of 28 and 30 percent respectively are not acceptable.

The values of F_{EXP} presented in Table 4.1 are a measure of the fatigue damage produced by the minor cycles in the truck loading. The experimental damage factors range from 1.70 to 2.07 with an average of 1.89. Neglecting the minor cycles would result in an F_{PRED} of 1.0; therefore, neglecting the fatigue damage produced by the minor cycles would produce an underestimation of fatigue damage of approximately 90 percent. This error translates into an overprediction of fatigue life of approximately 11 times.

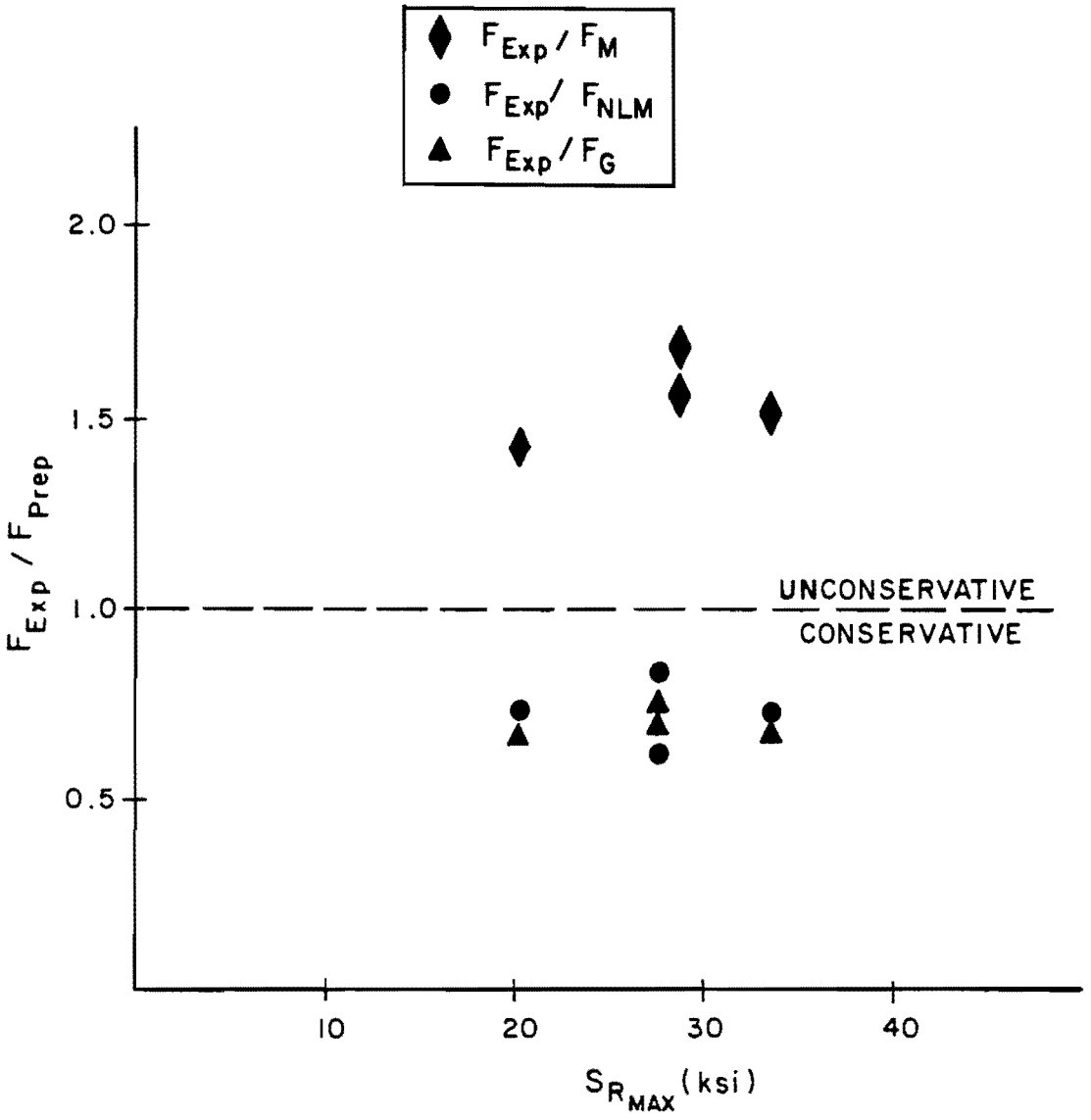

Fig. 4.3 F_{EXP}/F_{PRED} for test truck tests.

The values of F_{EXP} in Table 4.1 indicate that there is little variation of fatigue damage with the maximum stress range. In addition, from Fig. 4.3 it can be observed that the accuracy of the damage models is not affected by the maximum stress range. For this same range of tests, the percentage of cycles below S_{RTH} (assumed 9.20 ksi) varies from 74 for S_{RMAX} = 33.46 ksi to 96 for S_{RMAX} = 20.00 ksi. Thus, the fatigue limit does not seem to have an effect on the damage caused by the minor cycles. The fact that F_{EXP} and F_{EXP}/F_{PRED} do not vary with S_{RMAX} is important because it eliminates the need to test at low stress ranges which significantly increase testing time.

4.1.3 Traffic Histories. This series of tests includes experiments using Traffic Loading Histories 1, 2 and 3. These loading histories were developed from strain data measured while normal vehicle traffic passed over an instrumented bridge. The development as well as the stress range histograms of the traffic histories are presented in Section 3.1. As before, all tests were run with a minimum stress of 5 ksi. In order to reduce testing time and since the test truck results showed that S_{RMAX} is not a major variable, all tests in this series were run with S_{RMAX} = 35 ksi. The results of this test series and the values of F_{EXP}/F_{PRED} are presented in Table 4.2. The value of F_{EXP} is determined in the same manner as for the test truck history tests. A plot of the values of F_{EXP}/F_{PRED} or the three histories is presented in Fig. 4.4.

Observation of Fig. 4.4 reveals that Miner's cumulative damage model is the most accurate for all three traffic loadings. Nonlinear

TABLE 4.2 Traffic Test Results

Specimen	Traffic History	N_c x 10^3	F_{EXP}	$\frac{F_{EXP}}{F_M}$	$\frac{F_{EXP}}{F_{NLM}}$	$\frac{F_{EXP}}{F_G}$
TT7015	1	167.9	1.95	0.90	0.13	0.26
TT7112	1	181.5	1.80	0.83	0.12	0.24
TT7208	2	65.1	5.02	0.74	0.15	0.24
TT7207	2	114.6	2.85	0.42	0.08	0.14
TT7211	2	37.0	8.83	1.31	0.26	0.43
TT7209	3	183.1	1.79	1.20	0.43	0.44
TT7210	3	240.0	1.36	0.91	0.33	0.33

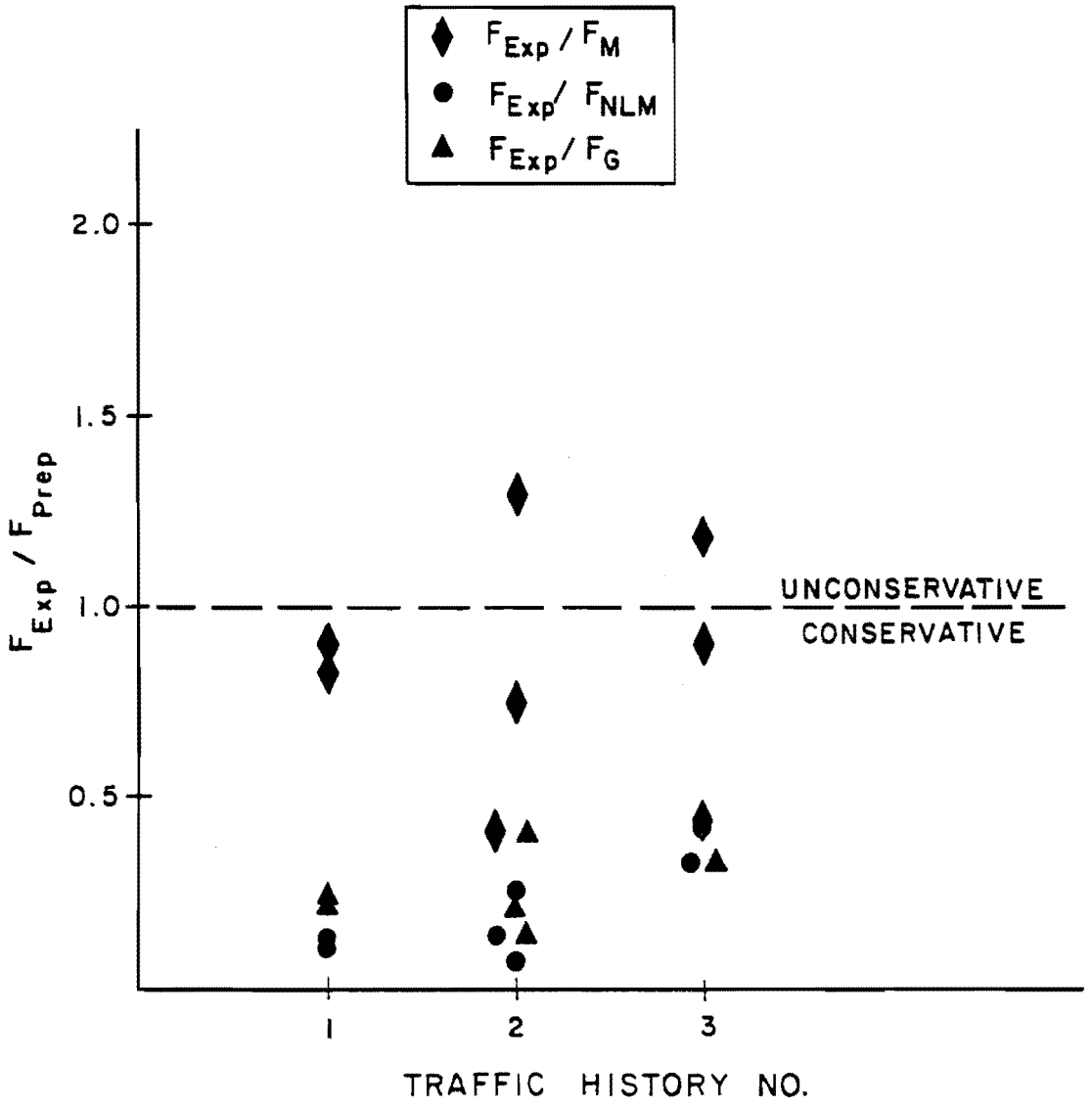

Fig. 4.4 F_{EXP}/F_{PRED} for traffic tests.

Miner's and Gurney's models overestimated fatigue damage by a factor of 2.0 or more in every test. The differences in the apparent scatter in data between values for F_{EXP}/F_M and for F_{EXP}/F_{NLM} and F_{EXP}/F_G are a result of the properties of the variable F_{EXP}/F_{PRED}. Because F_{NLM} and F_G are several times larger than F_{EXP}, F_{EXP}/F_{PRED} approaches zero asymptomatically so large fluctuations in F_{EXP} do not produce large fluctuations in F_{EXP}/F_{PRED}.

Comparisons of the test results of experiments with Traffic Histories 1, 2 and 3 produce information concerning the relation between the fatigue damage produced by a segment of loading alone and as part of a larger stress history. The concept being investigated is that the fatigue damage caused by each segment of a loading history can be summed to predict the fatigue damage produced by the entire history. To check this concept, the complex effective stress range, S_{REC} was calculated for Traffic Histories 2 and 3 using their average F_{EXP} as follows:

$$S_{REC} = (F_{EXP})^{1/3.76} (S_{RMAX}) \qquad (4.1)$$

as part of Traffic History 1, S_{RMAX} for the segments representing Traffic Histories 2 and 3 are 16.1 and 35 ksi respectively. Assuming a linear summation of fatigue damage, S_{REC} for Traffic History 1 was calculated with Eq. (4.2) is 41.79 ksi while the actual S_{REC} from Eq. 4.1) is 41.30 ksi. The difference between the predicted and actual values (1.2%) is negligible. This demonstrates that the interaction between the two segments is negligible and that summation of damage of individual events may be a viable analysis technique.

To further investigate the method of analysis by which the damage produced by individual segments are summed, Traffic Histories 1 and 2 were studied. For both histories each event was defined as a segment. As before, S_{REC} was calculated using Eq. (2.3). However, F_{EXP} was not available for each individual event, so F_M and F_{NLM} were calculated and used instead of F_{EXP}. The values of S_{REC} for each event of Traffic History 1 and Traffic History 2 are presented in Tables 4.3 and 4.4 respectively. As before, the values of S_{REC} were summed linearly to predict the damage produced by Traffic Histories 1 and 2. The results of this calculation are presented in Table 4.5.

From the values of F_{EXP}/F_{PRED} presented in Table 4.5, it is apparent that the summation of damage by events using Miner's theory is very accurate while the same method using nonlinear Miner's theory is grossly overconservative. A comparison of the values of F_{EXP}/F_M in Table 4.5 with those in Table 4.2 indicates that the summation of damage by events is more accurate than summing the damage caused by each individual cycle using Miner' theory. This difference in accuracy is a result of the reservoir counting procedure. The counting method tends to count cycles across the boundaries of events; thus, the histograms produced by a reservoir cycle counting across the entire history differs from the sum of the histograms of the individual events. Figures 4.5 and 4.6 illustrate the differences in the histograms produced by a reservoir count of the entire history (global) and of each individual event (summation) for Traffic Histories 1 and 2 respectively. It should be noted that the major cycle in Traffic History 2 is superimposed

TABLE 4.3 S_{REC} for Events in Traffic History 1

Event No.	S_{RMAX} (ksi)	F_M	$S_{REC}(M)$ (ksi)	F_{NLM}	$S_{REC}(NLM)$ (ksi)
1	8.77	2.36	11.02	6.39	14.37
2	12.71	1.05	12.87	1.75	14.75
3	15.74	1.71	18.15	3.90	22.60
4	12.21	1.50	13.60	4.86	18.60
5	16.10	2.31	20.11	7.19	27.20
6	35.00	1.49	38.92	4.18	51.20
7	12.29	1.17	12.82	2.27	15.29
8	14.47	1.22	15.26	2.83	19.09
9	13.56	1.26	14.43	3.33	18.68
10	15.56	2.41	19.66	7.46	26.55

TABLE 4.4 S_{REC} for Events in Traffic History 2

Event No.	S_{RMAX} (ksi)	F_M	$S_{REC}(M)$ (ksi)	F_{NLM}	$S_{REC}(NLM)$ (ksi)
1	16.28	2.36	20.46	6.39	26.67
2	23.58	1.05	23.89	1.75	27.37
3	29.21	1.71	33.69	3.90	41.95
4	22.66	1.50	25.24	4.86	34.51
5	29.88	2.31	37.33	7.19	50.49
7	22.82	1.17	23.79	2.27	28.38
8	26.86	1.22	28.32	2.83	35.42
9	25.18	1.26	26.78	3.33	34.67
10	28.87	2.41	36.48	7.46	49.27

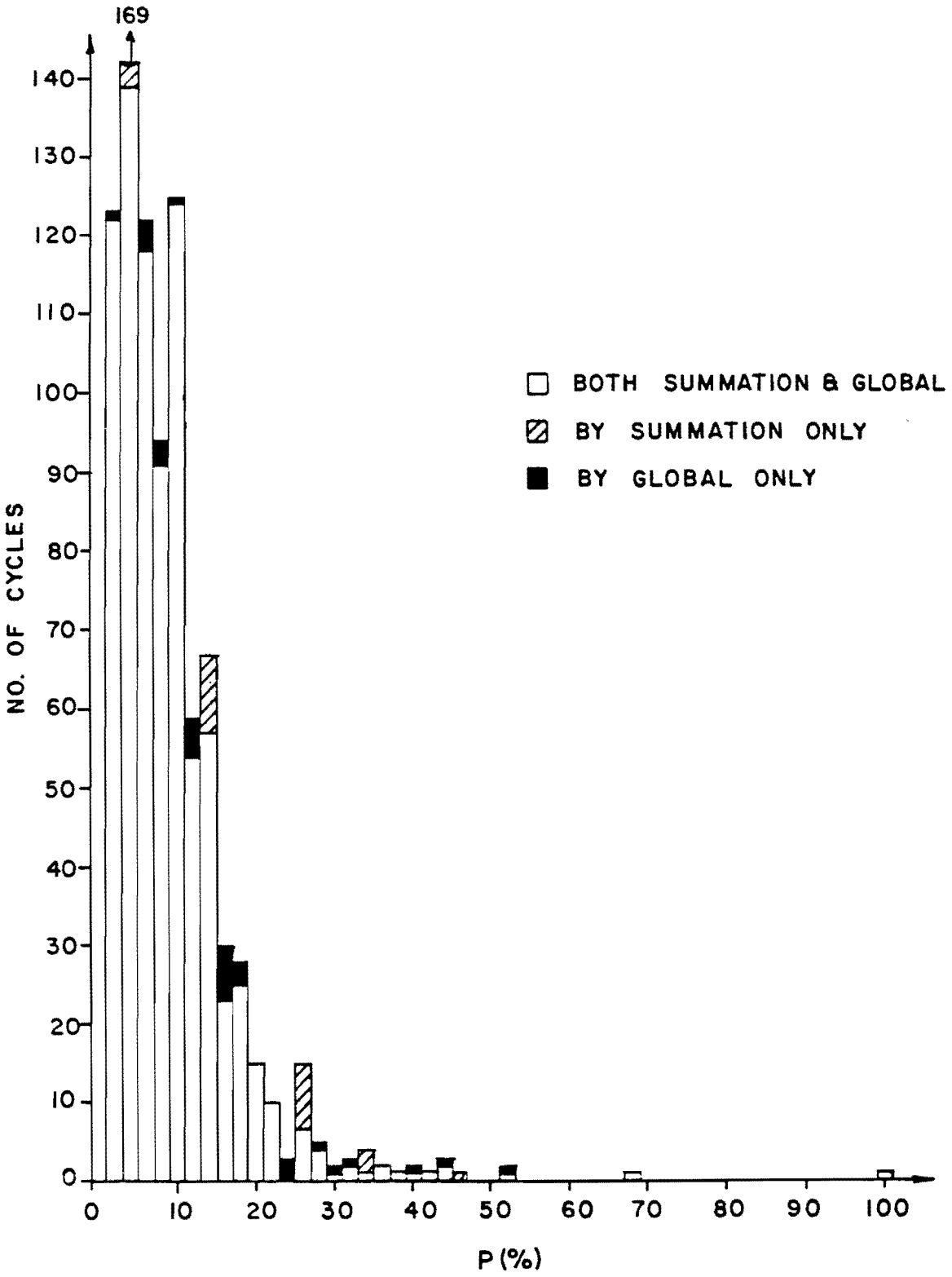

Fig. 4.5 Comparison of stress range histograms from global and by event cycle counting for Traffic History 1.

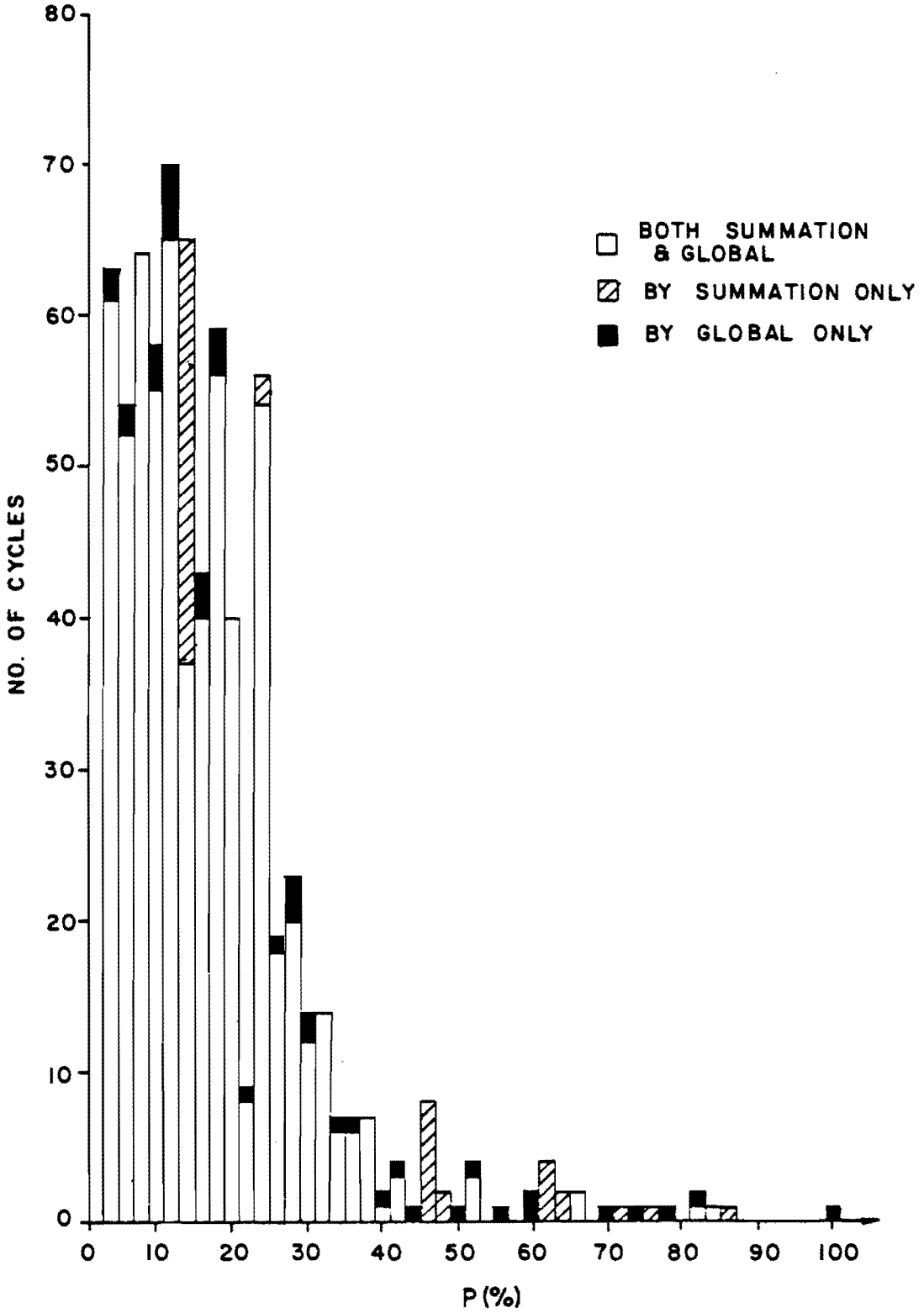

Fig. 4.6 Comparison of stress range histograms from global and by event cycle counting for Traffic History 2.

across events and is not accounted for in the analysis by summation of events.

To investigate the amount of damage produced by the minor cycles in each event, F_{PRED} was calculated using the method of summation of fatigue damage by events neglecting the minor cycles. If the minor cycles are neglected, S_{REC} becomes S_{RMAX} as F becomes unity. Repeating the analysis presented above with $S_{REC} = S_{RMAX}$ produced the values of F_{PRED} presented in Table 4.6. From the values of F_{EXP}/F_{PRED} presented in Table 4.6, it is apparent that neglecting the damage caused by minor cycle results in an underestimation of fatigue damage by Miner's theory while neglecting minor cycles improves the damage prediction by non-linear Miner's theory.

4.1.4 Constant Minimum Stress Histories.

Constant Minimum Stress History 1. CMS History 1 is a random discrete loading pattern with the same stress range histogram as the test truck loading. The development of CMS History 1 is discussed in Section 3.1.3. Two tests were included in this test series. Both tests were run with a maximum stress range of 35 ksi and a constant minimum stress of 5 ksi. The results of these two tests along with the values of F_{EXP}/F_{PRED} are shown in Table 4.7.

The values of F_{EXP} for the four test truck specimens are plotted along with those for the tests with CMS History 1 in Fig. 4.7. Comparison of F_{EXP} for the two test histories indicates that the random discrete loading produces less fatigue damage than the actual test truck loading. The average F_{EXP} produced by the test truck history is 1.89

TABLE 4.5 F_{EXP}/F_{PRED} from Summation of Fatigue Damage by Events

Traffic History	F_{EXP} (avg)	F_M	F_{NLM}	$\frac{F_{EXP}}{F_M}$	$\frac{F_{EXP}}{F_{NLM}}$
1	1.92	2.08	13.73	0.92	0.14
2	5.57	5.94	28.59	0.94	0.19

TABLE 4.6 F_{EXP}/F_{PRED} from Summation of Fatigue Damage by Events--Minor Cycles Neglected

Traffic History	F_{EXP} (avg)	F_M	F_{NLM}	$\frac{F_{EXP}}{F_M}$	$\frac{F_{EXP}}{F_{NLM}}$
1	1.92	1.32	3.12	1.45	0.62
2	5.57	2.99	4.87	1.86	1.14

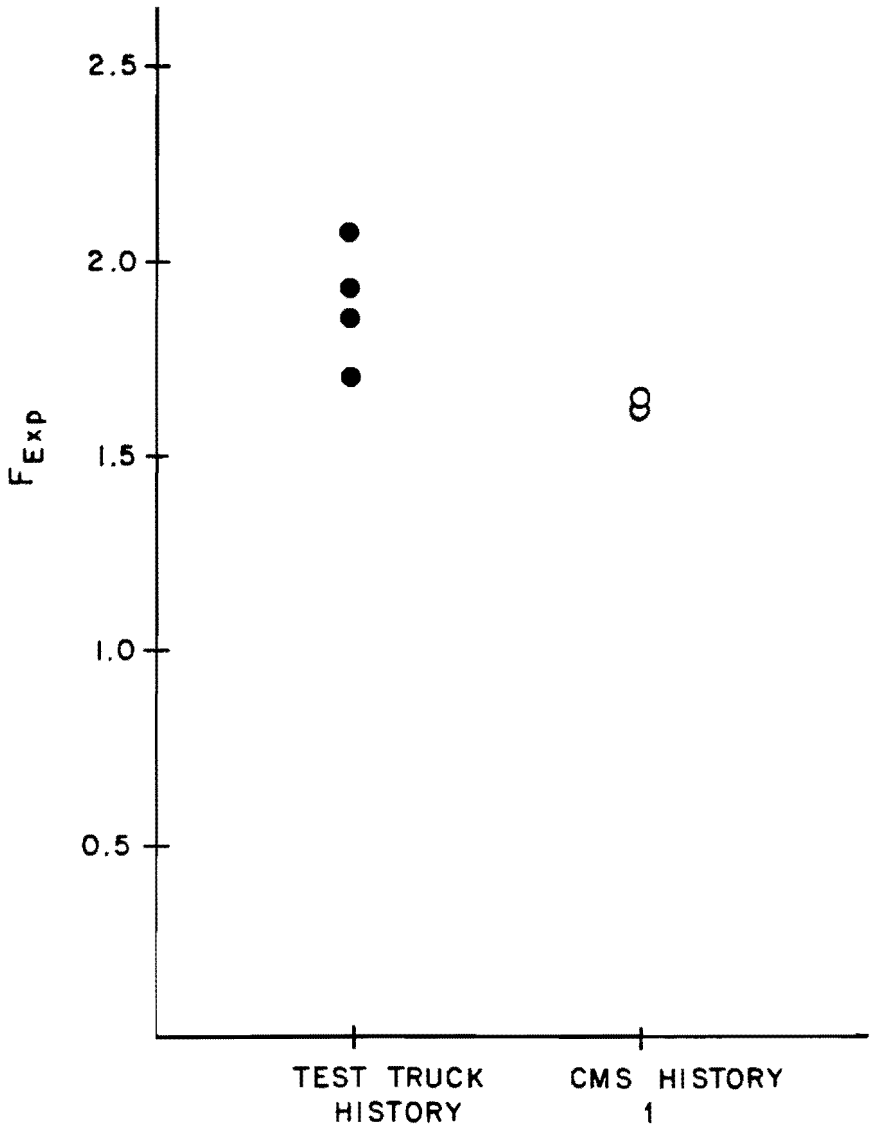

Fig. 4.7 Comparison of F_{EXP} for the test truck history and CMS History 1.

while the average F_{EXP} produced by CMS History 1 is 1.63. This indicates that the random discrete loading pattern is an unconservative model of the actual test truck loading. However, this conclusion must be qualified because there are only two replicates of CMS History 1. The difference in the test results of the two models could be due to by the mean stress effect documented by Zwerneman [1].

Constant Minimum Stress History 2. CMS History 2 is a random discrete loading developed to model a loading used in the U.S. Steel study completed for NCHRP Project 12-12 [12]. CMS History 2 has the same stress range histogram as the loading used in the U.S. Steel study with S_{RD}/S_{RM} = 1.0. The only difference in the loadings is the random sequences of cycles. Two tests were completed using CMS History 2 which is described in Section 3.1.3. Both tests were run with a maximum stress range of 35 ksi and a constant minimum stress of 5 ksi. The results of the two tests are shown in Table 4.8.

Figure 4.8 presents a plot of F_{EXP} CMS History 2 along with the values of F_{EXP} calculated from the U.S. Steel study on full sized bridge girders [12]. Only data from the U.S. Steel experiments using S_{RD}/S_{RM} = 1.0 are included in Fig. 4.8. Each data point from the U.S.S. study is the average of the results of three replicate tests. It can be observed from Fig. 4.8 that the values of F_{EXP} from the present study fall well within the range of F_{EXP} values from the U.S. Steel study. In fact, the F_{EXP} from the present study is very close to the mean of the U.S. Steel data which is shown by the dotted line in Fig. 4.8. This indicates that

TABLE 4.7 CMS 1 Test Resuls

Specimen	N_c x 10^3	F_{EXP}	$\frac{F_{EXP}}{F_M}$	$\frac{F_{EXP}}{F_{NLM}}$	$\frac{F_{EXP}}{F_G}$
BL6610	200.2	1.63	1.35	0.65	0.60
BL6611	202.3	1.62	1.33	0.65	0.60

TABLE 4.8 CMS 2 Test Results

Specimen	N_c x 10^3	F_{EXP}
USS612	5.3	62.3
USS713	5.9	55.5

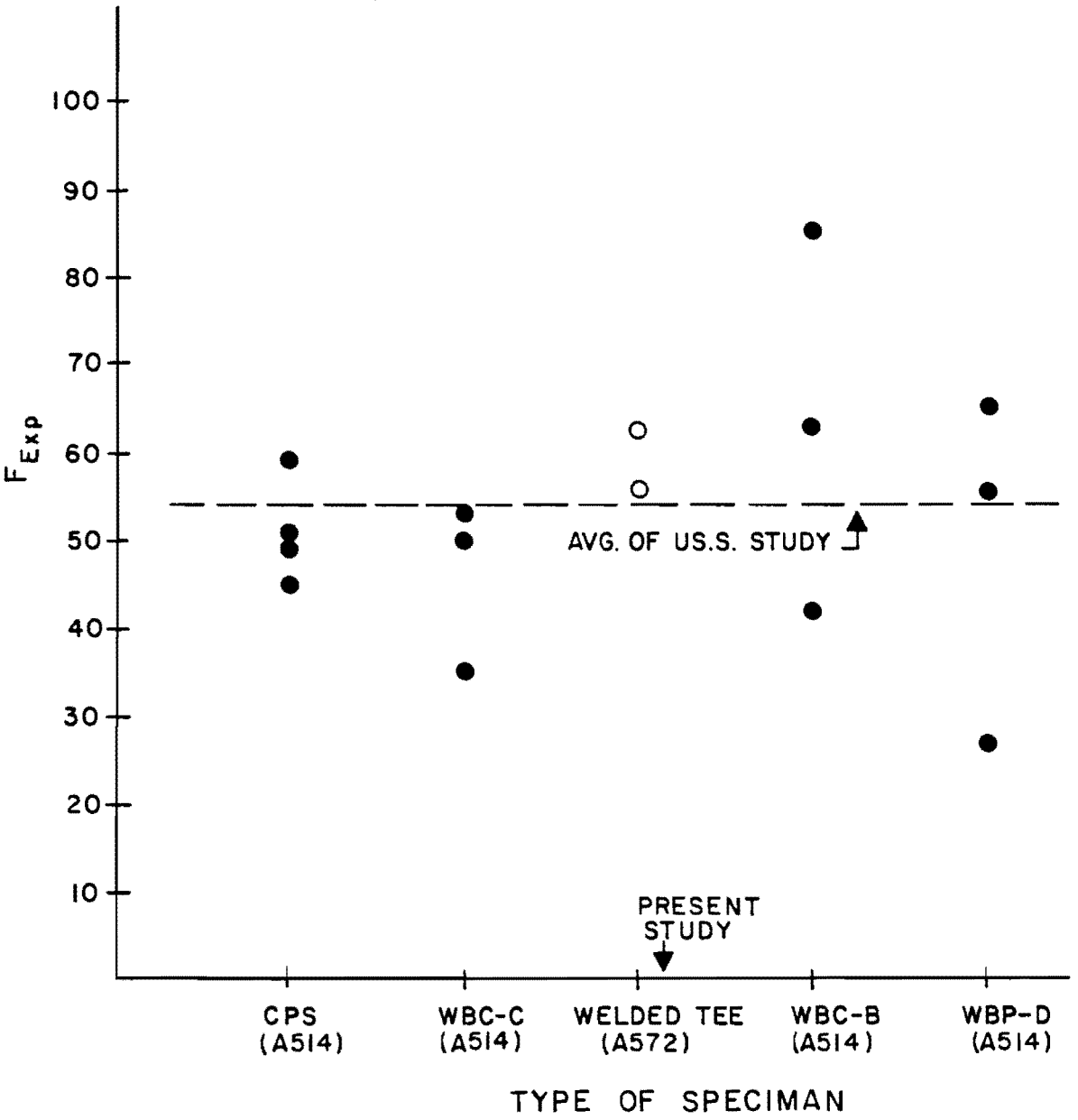

Fig. 4.8 Comparison of F_{EXP} for U.S.S. study and CMS History 2 tests.

the welded tee specimen can be used to predict the fatigue damage produced by a certain loading on full sized bridge girders.

4.2 U.S. Steel Study

To expand the data on which to base the conclusions of this study, the results of fatigue experiments done by U.S. Steel laboratories for NCHRP Project 12-12 were reanalyzed for comparison with the results of the present study. The analysis of the U.S. Steel data consisted of calculating 1) the slope and intercept of the log-log S-N curve for each specimen type, 2) F_M and F_{NLM} for each specimen type and loading, and 3) F_{EXP} based on the experimental fatigue life of each specimen.

The research program of the U.S. Steel study included experiments on 156 welded beams with partial length cover plates and 60 welded beams without cover plates. The variable amplitude loadings used were random discrete loadings based on a Rayleigh spectrum which is described in Section 3.1.4. Three basic forms of the Rayleigh spectrum with S_{Rd}/S_{RM} values of 0.25, 0.50, and 1.00 were included in the experimental program. Figure 4.9 illustrates the respective shapes of the three spectrums. It should be noted that all loadings were applied with a constant minimum stress, but the level of the minimum stress was varied between tests. A more detailed description of the specimens, experimental procedure and individual test results is given in Ref. 12.

Table 4.9 presents the results of the first two steps of the analysis, the values of m, A, F_M, and F_{NLM} for each specimen type and loading history. The specimens with detail type "A" are not included in

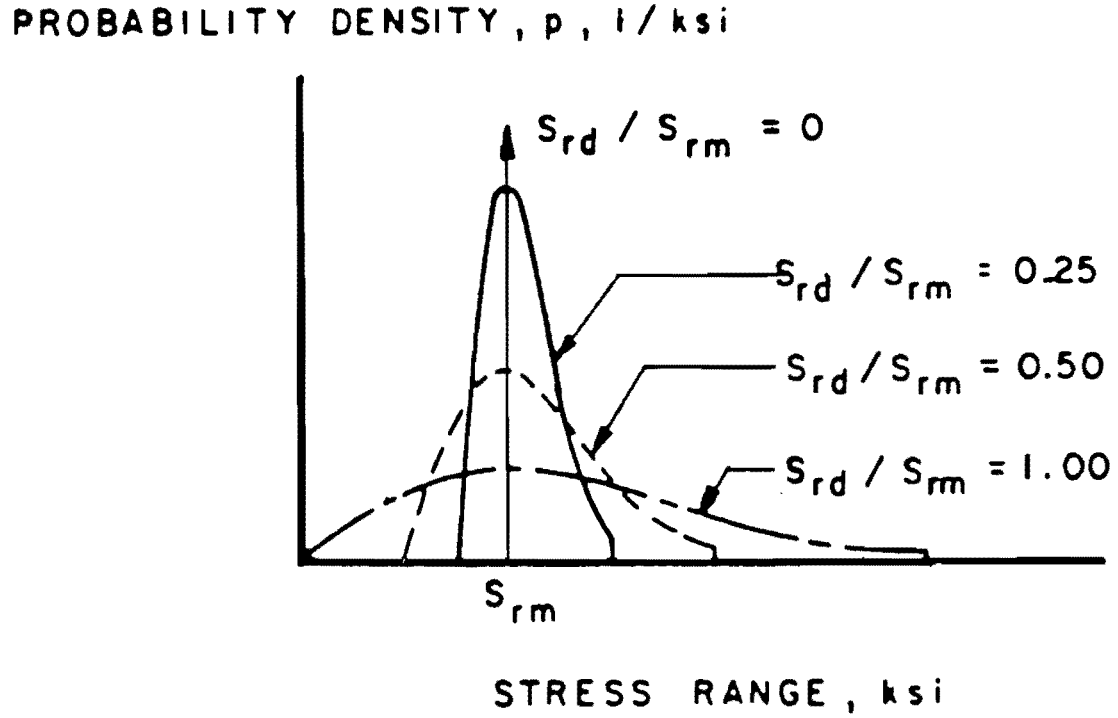

Fig. 4.9 Probability densities of the Rayleigh spectrums used in U.S.S. study.

TABLE 4.9 Predicted Damage Factors for U.S.S. Study

Specimen Type*	Steel Grade	m	A x 10^9	S_{Rd}/S_{RM}	F_M	F_{NLM}
CPS	A514	2.817	3.534	0.50	116.7	224.9
				1.00	69.0	153.5
WBC-B&C	A514	2.692	0.734	0.50	123.0	232.3
				1.00	73.3	160.2
WBP-D	A514	3.459	99.28	0.50	90.2	191.4
				1.00	51.8	124.7
WBC-C	A36	3.121	1.667	0.25	180.7	292.9
				0.50	103.7	208.2
WBP-D	A36	3.214	52.86	0.25	175.9	288.5
				0.50	99.2	203.4

* CPS - cover plate specimen

WBC-B&C - welded seam with either cover plate detail "B" or "C"

WBP-D - welded beams without cover plates

WBC-C - welded beam with cover plate detail "C"

this analysis because the fabrication technique used in the detail produced results which do not correlate with other studies [12]. Tables 4.10 through 4.12 contain the results of the analysis of the experimental data for S_{Rd}/S_{RM} = 0.25, 0.50, and 1.00 respectively. Each table presents the specimen type, S_{RMAX}, minimum stress (S_{MIN}), ; maximum, minimum and average F_{EXP}; F_{EXP}/F_M, and F_{EXP}/F_{NLM} for each set of tests. The value of F_{EXP} used in F_{EXP}/F_M and F_{EXP}/F_{NLM} is the average F_{EXP} for each set of tests. The values of F_{EXP}/F_M and F_{EXP}/F_{NLM} are plotted against the specimen type for S_{Rd}/S_{RM} = 0.25, 0.50 and 1.00 in Figs. 4.10 through 4.12 respectively.

Two general observations can be made from the results shown in Figs. 4.10 through 4.12. First, Miner's cumulative damage rule predicts the fatigue damage caused by the loadings better than nonlinear Miner's. Second, Miner's rule is not very accurate in predicting F_{EXP}. The value of F_{EXP}/F_M ranges from 0.48 (52% conservative) to 1.37 (37% unconservative). Part of this inaccuracy is a result of the scatter which can be expected in a fatigue study of this magnitude. A plot of the average values of F_{EXP}/F_{PRED} for each S_{Rd}/S_{RM} (Fig. 4.13) indicates that Miner's rule on the average produces good predictions of fatigue damage and is slightly conservative (F_{EXP}/F_M average = 0.94).

The results of the U.S. Steel study are useful in studying the applicability of various damage models. However, the application of any conclusion based on these results in design must be qualified because all tests were run with a constant minimum stress. The comparison of a constant minimum stress and an actual test truck loading presented in

TABLE 4.10 U.S.S. Study Results with $S_{Rd}/S_{RM} = 0.25$

Spcmn. Type	Steel Grade	S_{RMAX} (ksi)	S_{MIN} (ksi)	F_{EXP} (max)	F_{EXP} (min)	F_{EXP} (avg)	$\frac{F_{EXP}(avg)}{F_M}$	$\frac{F_{EXP}(avg)}{F_{NLM}}$
WBC-C	A36	15.0	0.0	244.0	197.0	214.3	1.19	0.73
WBC-C	A36	30.0	0.0	170.4	145.1	159.1	0.88	0.54
WBP-D	A36	30.0	0.0	277.7	104.1	180.8	1.03	0.63
WBP-D	A36	30.0	0.0	220.9	119.9	186.3	1.06	0.65
WPB-D	A36	40.0	0.0	193.7	175.0	184.4	1.05	0.64
WPB-D	A36	45.0	10.0	230.9	163.7	192.0	1.09	0.67

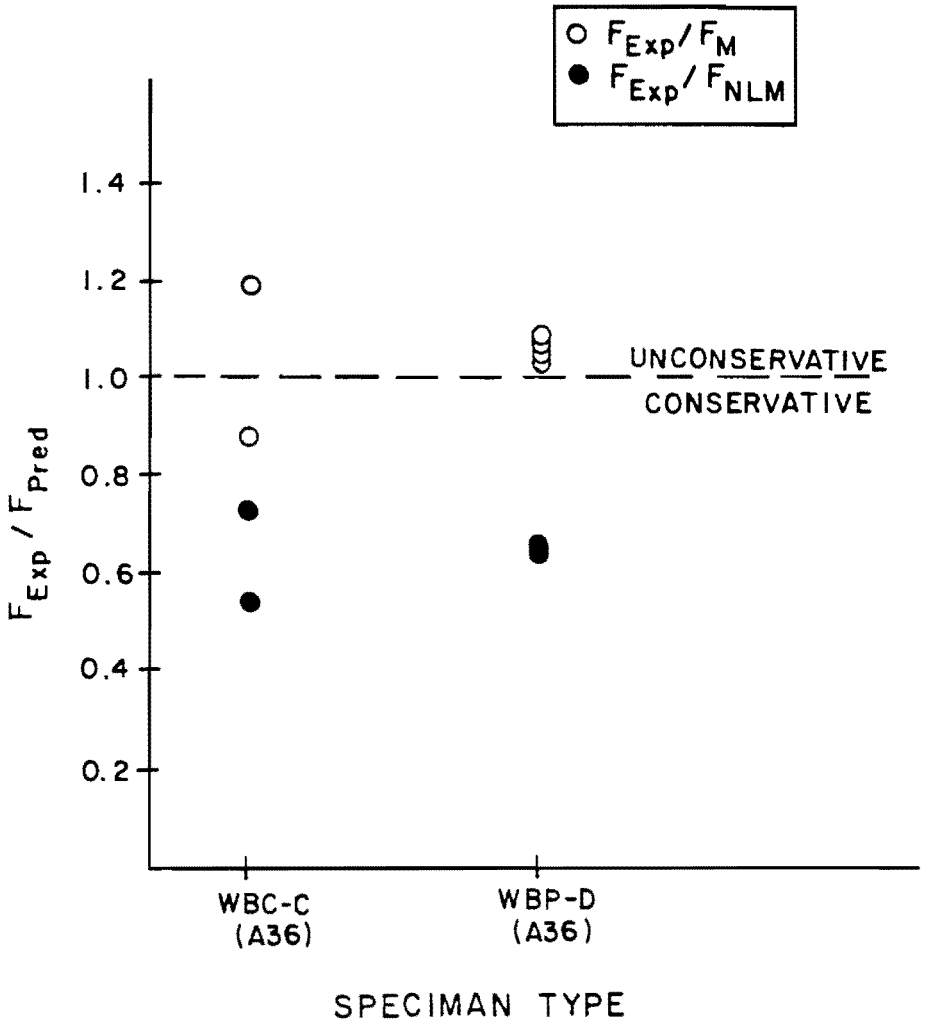

Fig. 4.10 F_{EXP}/F_{PRED} for U.S.S. study; S_{Rd}/S_{RM} = 0.25.

TABLE 4.11 U.S.S. Study Results with $S_{Rd}/S_{RM} = 0.50$

Spcmn. Type	Steel Grade	S_{RMAX} (ksi)	S_{MIN} (ksi)	F_{EXP} (max)	F_{EXP} (min)	F_{EXP} (avg)	$\frac{F_{EXP}(avg)}{F_M}$	$\frac{F_{EXP}(avg)}{F_{NLM}}$
WBC-C	A36	10.0	0.0	160.9	66.8	112.7	1.09	0.54
CPS	A514	20.0	0.0	120.1	76.2	98.5	0.84	0.44
WBC-C	A36	20.0	0.0	127.3	113.5	118.4	1.15	0.57
CPS	A514	20.0	10.0	156.0	70.5	113.0	0.97	0.50
WBC-C	A514	20.0	10.0	114.8	80.6	99.5	0.85	0.43
WBC-C	A36	20.0	10.0	143.4	125.1	136.8	1.33	0.66
CPS	A514	20.0	40.0	187.5	109.1	159.6	1.37	0.71
WBP-D	A36	40.0	0.0	162.6	92.6	120.6	1.34	0.63
WBC-C	A36	40.0	0.0	116.8	59.2	86.4	0.84	0.41
WBP-D	A36	40.0	0.0	177.5	68.6	112.9	1.14	0.59
WBP-C	A514	40.0	10.0	134.6	87.0	108.6	0.88	0.47
WBP-D	A36	40.0	10.0	127.6	107.1	119.3	1.20	0.59
CPS	A514	60.0	0.0	107.1	86.5	95.2	0.82	0.42
WBP-D	A514	60.0	0.0	59.2	58.8	59.0	0.65	0.31
CPS	A514	60.0	10.0	101.4	84.9	94.0	0.81	0.42
WBC-C	A514	60.0	10.0	94.8	68.5	79.2	0.64	0.34
CPS	A514	60.0	40.0	158.0	106.9	126.4	1.08	0.56
WBP-D	A514	80.0	0.0	50.0	42.4	45.3	0.50	0.24

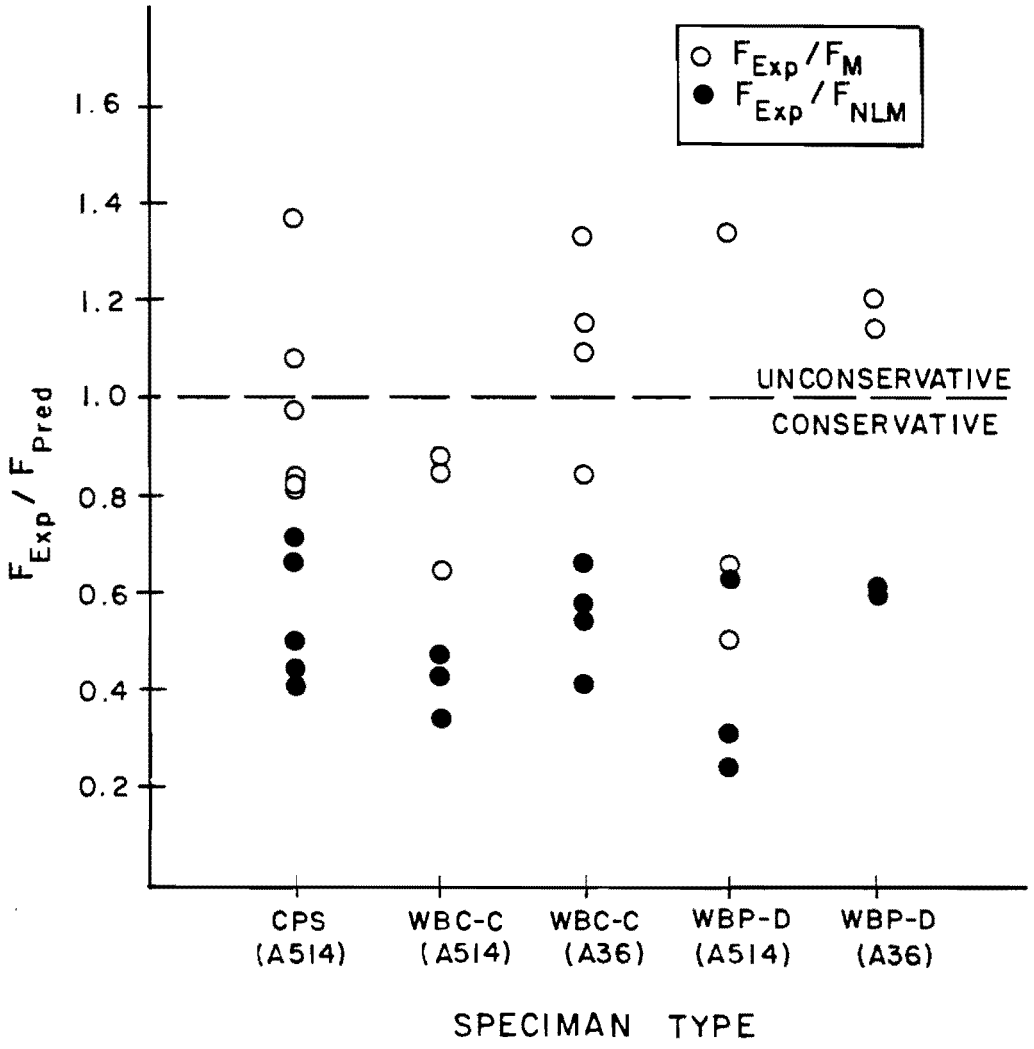

Fig. 4.11 F_{EXP}/F_{PRED} for U.S.S. study; S_{Rd}/S_{RM} = 0.50.

TABLE 4.12 U.S.S. Study Results with S_{Rd}/S_{RM} = 1.00

Spcmn. Type	Steel Grade	S_{RMAX} (ksi)	S_{MIN} (ksi)	F_{EXP} (max)	F_{EXP} (min)	F_{EXP} (avg)	$\frac{F_{EXP}(avg)}{F_M}$	$\frac{F_{EXP}(avg)}{F_{NLM}}$
WBC-C	A514	6.0	10.0	49.0	28.4	35.3	0.48	0.22
WBC-C	A514	9.0	15.0	58.3	45.1	49.7	0.68	0.34
CPS	A514	30.0	0.0	53.1	49.8	50.9	0.74	0.33
WBC-C	A514	30.0	0.0	59.2	46.5	52.9	0.72	0.33
WBC-B	A514	30.0	0.0	45.2	35.9	41.9	0.57	0.26
WBP-D	A514	30.0	0.0	67.5	38.3	55.4	1.07	0.44
CPS	A514	30.0	10.0	63.9	52.7	58.9	0.85	0.38
WBC-B	A514	30.0	10.0	115.4	69.7	85.0	1.16	0.53
WBP-D	A514	60.0	0.0	72.4	58.0	65.2	1.26	0.52
WBC-B	A514	60.0	10.0	81.6	32.3	62.9	0.86	0.39
CPS	A514	90.0	0.0	68.5	33.0	49.5	0.72	0.32
WBP-D	A514	90.0	0.0	29.0	25.3	26.7	0.52	0.21
CPS	A514	90.0	10.0	46.5	43.1	44.8	0.65	0.28

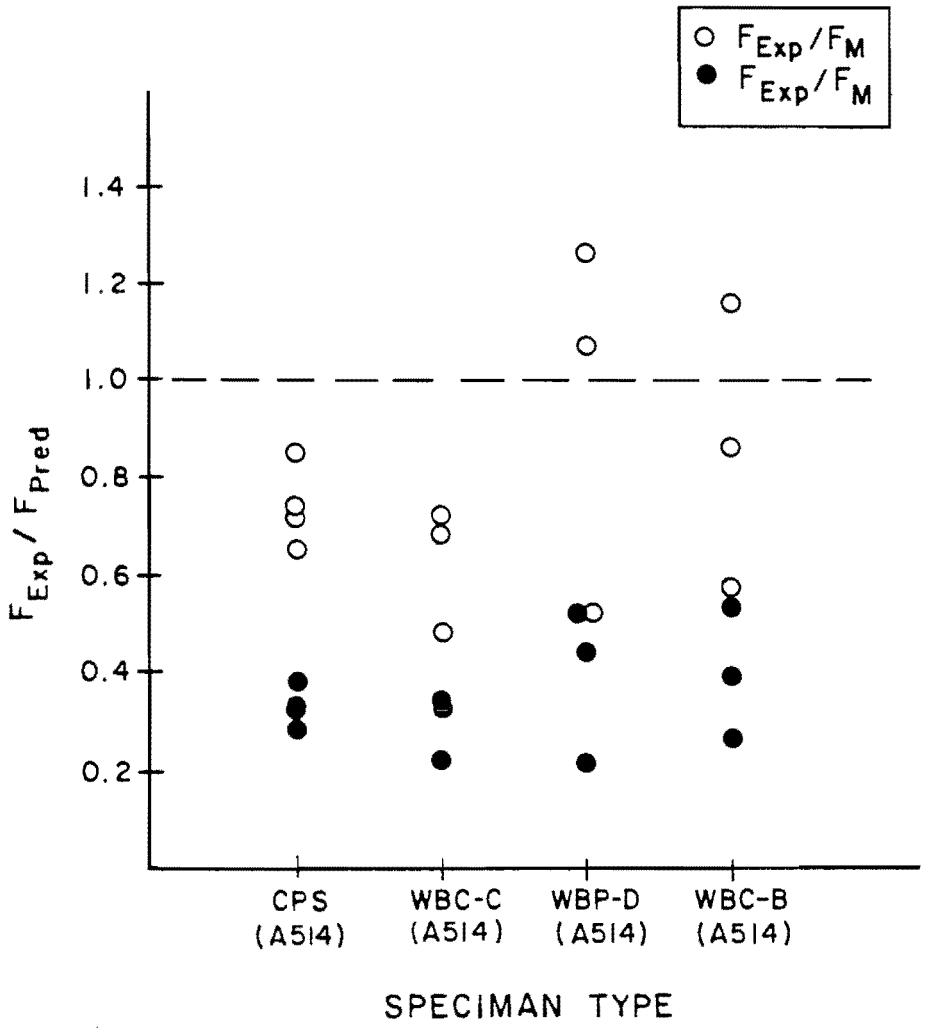

Fig. 4.12 F_{EXP}/F_{PRED} for U.S.S. study; S_{Rd}/S_{RM} = 1.0.

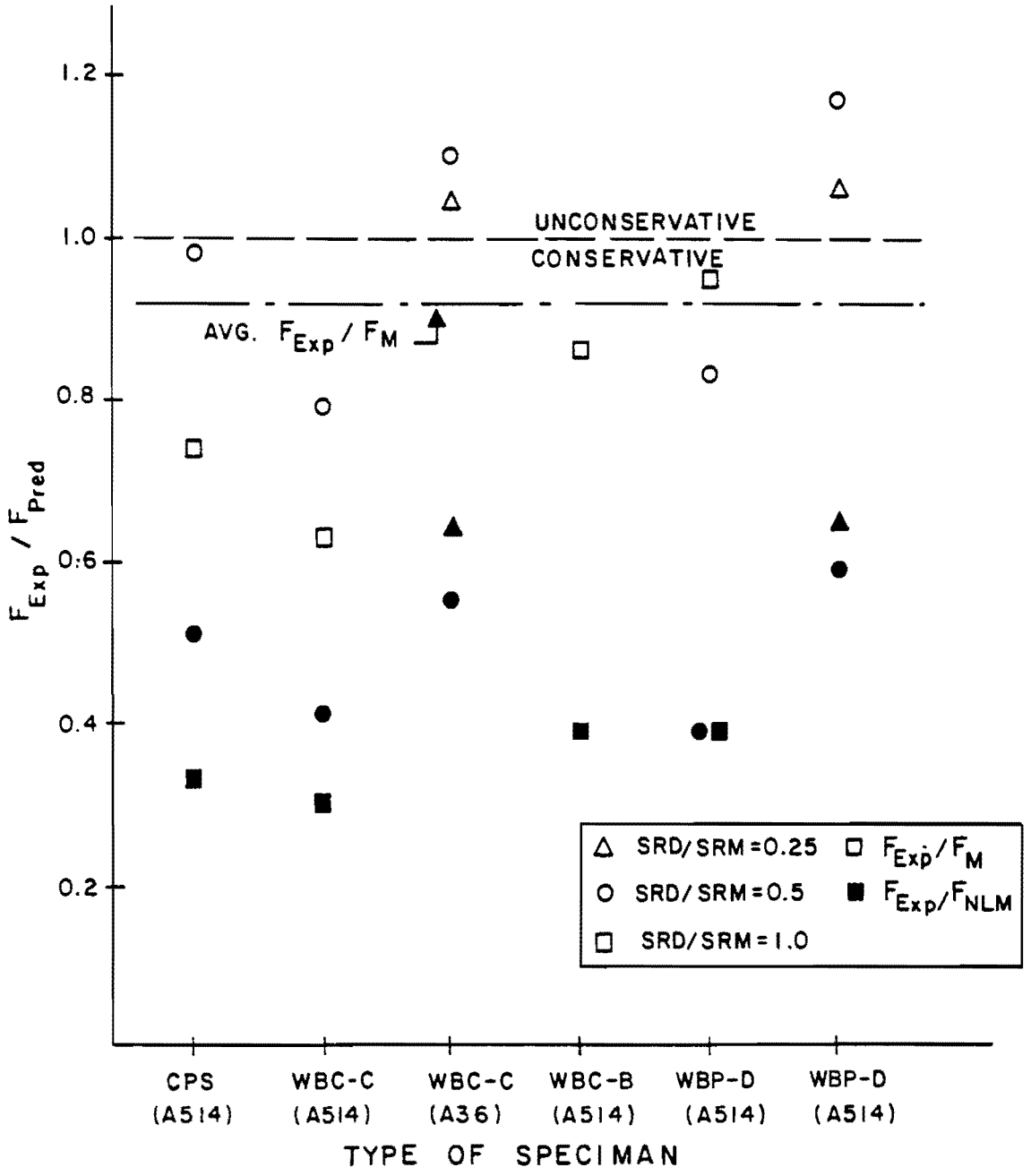

Fig. 4.13 Avg. F_{EXP}/F_{PRED} for each detail in U.S.S. study.

Section 4.14 indicates that a constant minimum stress history is an unconservative model of actual bridge loadings.

4.3 Stress Interaction Effects

The comparisons of nonlinear Miner's and Miner's fatigue damage models presented in Figs. 2.14 through 2.21 illustrate that nonlinear Miner's theory assumes that the minor cycles are more damaging then Miner's theory assumes. Thus, the accuracy of each model in predicting the damage factor is a measure of the fatigue damage produced by the minor cycles.

The experimental results of this study as well as the studies done by Gurney [13], Joehnk [14], Zwerneman [1], and U.S. Steel [12] presented in Table 4.13 indicate a trend in the accuracy of the two models. In general, the stress histories which are simulated correctly by Joehnk's (NLM) model are short and the average mean stress of the minor cycles is equal to the mean stress of the major cycle. The histories which follow Miner's assumption of linearity are generally long histories with the average mean stress of the minor cycles below that of the major cycle. The effect of the average mean stresses is explained well by Zwerneman's mean stress tests [1]. The results of the mean stress tests indicate that the damage caused by the minor cycles decreases with the ratio of $S_{MEAN(minor)}/S_{MEAN\ (major)}$ as shown in Fig. 4.14.

This linear relationship between the effectiveness of the minor cycles and their mean stresses predicts the general trends in data, but it is inaccurate for several loadings. Table 4.14 presents the ratio of

TABLE 4.13 Summary of Results

Study	Waveform	$\frac{F_{EXP}}{F_M}$	$\frac{F_{EXP}}{F_{NLM}}$	Comments
Gurney [14]	Fig. 2.12	1.25	1.00	1. Short history (n_c=2.16) 2. $S_{MEAN(minor)} = S_{MEAN(major)}$
Joehnk [13]	Superimposed sine	2.04	1.09	1. Short history (n_c=3.16) 2. $S_{MEAN(minor)} = S_{MEAN(major)}$
Zwerneman [1]	Mean stress	1.69	0.90	1. Short history (n_c=10) 2. $S_{MEAN(minor)}$ varies
U.S.S. [12]	Rayleigh	0.92	0.47	1. Long history (n_c=500) 2. $S_{MEAN(minor)} < S_{MEAN(major)}$
Present	Test truck	1.56	0.76	1. Short history (n_c=27) 2. $S_{MEAN(minor)} < S_{MEAN(major)}$
	Traffic 1	0.87	0.12	1. Long history (n_c=850) 2. $S_{MEAN(minor)} < S_{MEAN(major)}$
	Traffic 2	0.82	0.16	1. Long history (n_c=710) 2. $S_{MEAN(minor)} < S_{MEAN(major)}$
	Traffic 3	1.06	0.38	1. Medium history (n_c=99) 2. $S_{MEAN(minor)} < S_{MEAN(major)}$
	CMS 1	1.33	0.65	1. Short history (n_c=27) 2. $S_{MEAN(minor)} < S_{MEAN(major)}$
	CMS 2	1.29	0.52	1. Long history (n_c=50) 2. $S_{MEAN(minor)} < S_{MEAN(major)}$

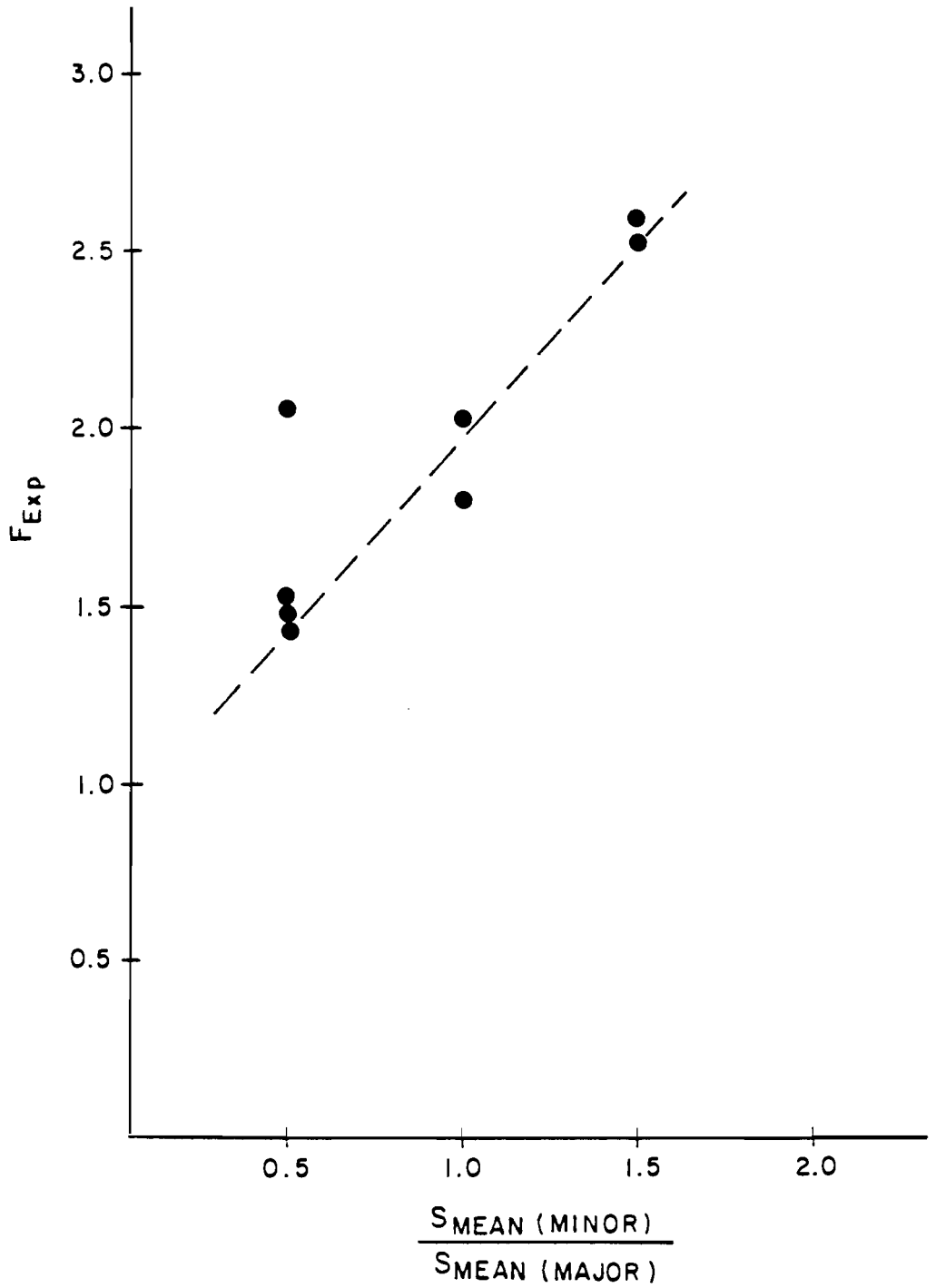

Fig. 4.14 F_{EXP} vs. mean stress level for Zwerneman's mean stress tests.

TABLE 4.14 F_{EXP}/F_{PRED} for Tests on Welded Tee Specimen

Waveform	$\frac{S_{MEAN}(minor)}{S_{MEAN}(major)}$	$\frac{F_{EXP}}{F_M}$	$\frac{F_{EXP}}{F_{NLM}}$
Mean Stress 1	1.50	2.25	1.19
Superimposed Sine*	1.00	2.04	1.09
Mean Stress 2	1.00	1.68	0.89
Test Truck	0.92	1.56	0.76
Traffic 2	0.90	0.82	0.16
Traffic 3	0.81	1.06	0.38
CMS 2	0.54	1.29	0.52
Mean Stress 3	0.50	1.39	0.69
CMS 1	0.36	1.33	0.65

* average of 8 tests

the average mean stress of the minor cycles to the mean stress of the major cycle and the corresponding values of F_{EXP}/F_M and F_{EXP}/F_{NLM}. Since the values of F_{EXP}/F_M and F_{EXP}/F_{NLM} are a measure of the effectiveness of the minor cycles, these values should vary with $S_{MEAN(minor)}/S_{MEAN(major)}$. Only the experiments on the welded tee specimen are included in Table 4.14 to eliminate any variables due to material properties or weld geometry. From Fig. 4.15, which is a plot of the data in Table 4.14, the exceptions to the mean stress relation are the traffic histories. These exceptions to the mean stress relation indicate that other properties of the stress history play a role in fatigue damage.

The variation in fatigue damage caused by the minor cycles is probably a result of stress interaction effects. In order to predict how the stress interactions alter the fatigue damage produced by the minor cycles, the variables which are involved in stress interactions must be identified. Research by Jacoby [23] on stress interaction effects caused by variations in mean stress and by overloads provides some insight. Jacoby proposed that the crack growth rate at any point in a loading is determined by the deformations caused by previous fatigue damage. The deformations influence the crack growth rate by producing residual stresses and by altering the material properties at the crack tip. Jacoby determined that the deformations caused by a propagating crack and thus the crack growth rate depend on the following factors:

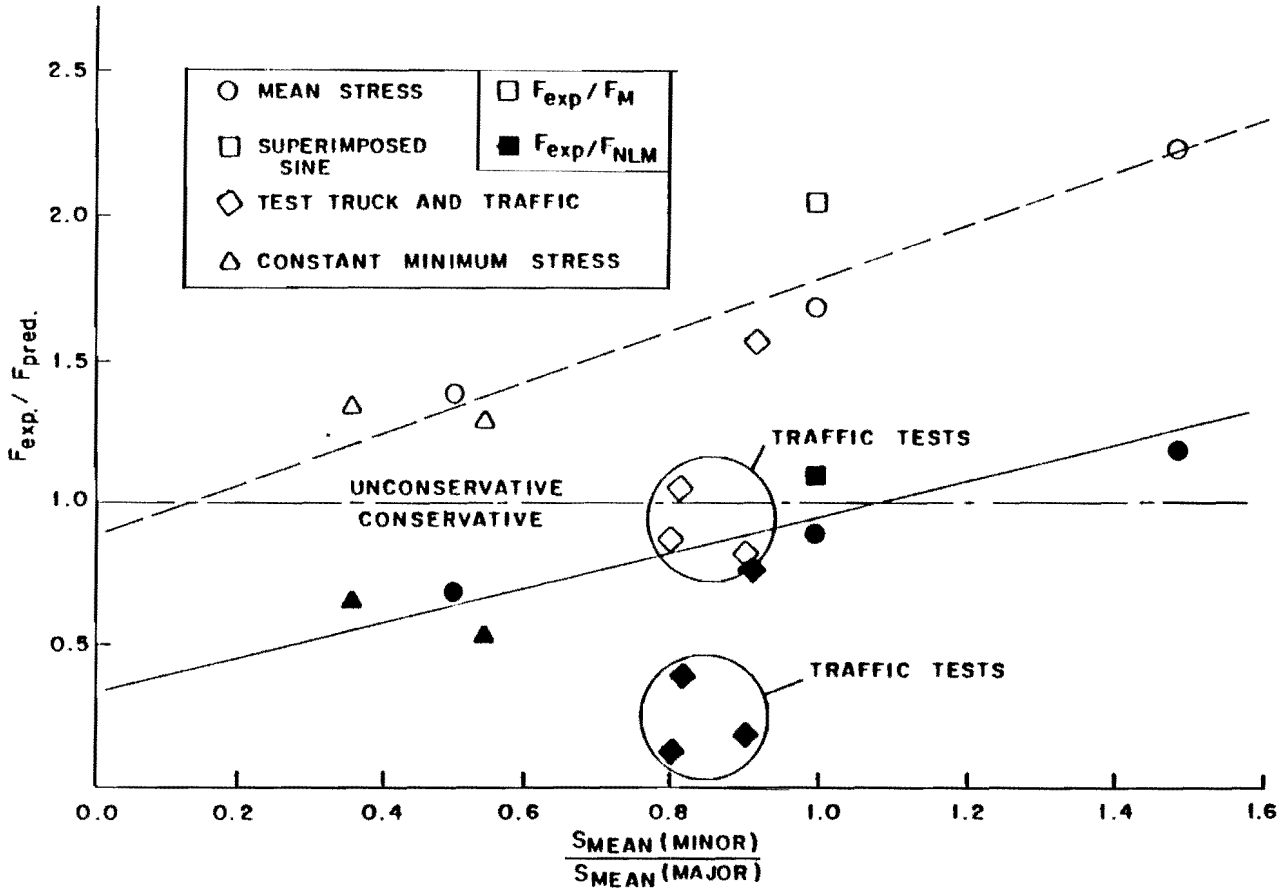

Fig. 4.15 F_{EXP}/F_{PRED} vs. mean stress level for tests on welded tee.

1. maximum stress intensity factor;
2. variation in stress intensity during a cycle;
3. stress intensity history; and
4. monotonic and cyclic deformation characteristics of the material.

From comparisons of the tests on the welded tee specimen, the major variables appear to be the relative level (mean stress), magnitude and number of the minor cycles. The minor cycles cause more damage as the level of the minor cycles increases relative to the major cycle. This relation is shown in Fig. 4.14. Nonlinear Miner's theory, which assumes the minor cycles produce a large amount of fatigue damage, becomes more accurate ($F_{EXP}/F_{NLM} = 1.0$) as $S_{MEAN(minor)}/S_{MEAN(major)}$ approaches 1.0. Miner's theory, which assumes minor cycles produces little fatigue damage, is accurate ($F_{EXP}/F_{M} = 1.0$) as $S_{MEAN(minor)}/S_{MEAN(major)}$ approaches 0.0. The exception to this relation is presented by the traffic tests. The difference between the traffic histories and the other histories under investigation is their large number of small minor cycles ($P_i < 0.25$). The results presented in Fig. 4.15 indicate that Miner's rule accurately predicts the damage produced by these cycles without accounting for their relative mean stress level. In addition, nonlinear Miner's model grossly overpredicts the damage produced by these smaller minor cycles.

4.4 Damage Model Development

Since the accuracy of the damage models is altered by stress interaction effects, the proposed damage model will consist of one of

the damage models already presented modified by a correction factor. This correction factor will be based on the characteristics of a stress history which affect the stress interactions. The correction will be known as the stress interaction correction and will be denoted as CF. In order to keep the analysis simple, each term used will be based on the entire stress history, not on the relationship between individual cycles. Thus, the proposed stress interaction damage model would produce a damage factor, F_{si}, which may be represented by

$$F_{si} = F(CF) \tag{4.1}$$

where F is given by F_M, F_{NLM}, or F_G.

At this point, it is not known which damage factor F_{NLM}, F_G, or F_M used in Eq. (4.1) will produce the best result. Thus, a CF will be determined for each case. The proposed model will be chosen from the three resulting equations.

4.4.1 Correction Factor. Because a correction factor is based on empirical data, the choice of which data to use in the development of the correction is crucial. In deciding which test results to use in determining CF, the main criterion was that the stress histories included in the calculation have some similarity with measured stress histories. Based on this criterion, the stress histories included were the superimposed sine histories developed by Joehnk, Gurney's stress histories 1 and 2, and test truck stress history, and the traffic stress histories. The reason for including the histories developed by Joehnk

and Gurney is that the superimposed sine type histories are very similar to actual truck loadings.

Based on the conclusions presented in Jacoby's report [23] and observations of the results of the present study, the effect of the following variables was investigated in the developemtn of CF.

1. $S_{MEAN(minor)}/S_{MEAN(major)}$
2. $S_{MAX(minor)}/S_{MEAN(major)}$
3. $S_{MAX(minor)}/S_{MEAN(minor)}$
4. $S_{RES}/S_{RMAX} = P_{EFF}$
5. $S_{R(AVG)}/S_{RMAX} = P_{AVG}$

The first three variables were included in the study to account for the effect of the mean stress level as described by Zwerneman, and the effect of the maximum stress described by Jacoby. It should be noted that the values of S_{MAX} and S_{MEAN} for the minor cycles are determined by the arithmatic average for all the minor cycles in the history. In addition, the values of S_{MAX} and S_{MEAN} are based on the actual applied stress; therefore, variables 1, 2 and 3 will vary depending on the minimum stress of the applied stress history. The fourth and fifth variables were included to account for the effect of the magnitude of the minor cycles as shown in the traffic test results. P_{EFF} which is defined as the ratio of the simple effective stress range, S_{RES}, and S_{RMAX}, provides a measure of the magnitude of the minor cycles based on their fatigue behavior. It also includes the fatigue behavior of the material through m. S_{RES} can be determined using Miner's, nonlinear Miner's or Gurney's fatigue model. $S_{R(AVG)}/S_{RMAX}$, or P_{AVG}, is the

arithmatic average of the magnitudes of the stress cycles in the stress history.

Given the definition of CF in the proposed damage model (Eq. (4.1)), the value of CF can be determined from experimental results with the following expression:

$$CF = F_{EXP}/F \tag{4.2}$$

where F is given by F_M, F_{NLM}, and F_G. To minimize confusion, the terms CF(M), CF(NLM) and CF(G) will denote the correction factor to be used with F_M, F_{NLM}, and F_G respectively.

The following observations concerning stress interaction effects were presented in the previous section: 1) the damage caused by minor cycles varies with the relative mean stress level of the minor cycles, and 2) the damage caused by small minor cycles is predicted well by a linear damage model (Miners') and overpredicted by nonlinear Miner's model. From these observations, it follows that CF(NLM) and CF(G) should vary with a term accounting for minor cycle stress level and approach zero as the variable accounting for the minor cycle magnitude approaches zero. In addition, CF(M) should vary with a variable accounting for the minor cycle stress level and approach 1.0 as the variable accounting for the magnitude of the minor cycle approaches 0.0.

Because the effects of the mean stress level and magnitude of the minor cycle were not understood before testing, the experimental program was not designed to determine the statistical significance of each parameter presented earlier . Thus, the development of an

expression for CF was a combination of intuition and trial and error in order to match experimental results. The values of each of the five variables presented earlier along with the corresponding values of F_{EXP}/F_M and F_{EXP}/F_G are presented in Table 4.15. In addition, the values of m used in all calculations are presented in Table 4.16.

First, trial and error was used to develop a term λ(NLM) which varied with CF(NLM) to use in an expression for CF(NLM). After experimenting with several combinations of the variables presented, the following term was found to have the best agreement with experimental values of CF(NLM):

$$\lambda(NLM) = \left(\frac{S_{MAX}}{S_{MEAN}}\right)_{MINOR} \left[\frac{1.0}{P_{EFF}(M)}\right] \qquad (4.3)$$

where $P_{EFF(M)}$ is determined using Miner's cumulative damage theory. The limits of λ(NLM) are difficult to define as $(S_{MAX}/S_{MEAN})_{minor}$ is dependent on the minimum stress used in each application. However, $(S_{MAX}/S_{MEAN})_{minor}$ can be no less than 1.0 as the maximum stress of any cycle is always larger than its mean stress. In addition, $(S_{MAX}/S_{MEAN})_{minor}$ can never be greater than 2.0 as the maximum stress of any cycle can never be more than twice its mean stress, assuming all loadings are in tension. Thus, the range of P_{EFF} is from a maximum of 1.0, as S_{RES} cannot be larger than S_{RMAX}, to a minimum of 0.0. Therefore, the term $(1.0/P_{EFF})$ has a range of from 1.0 to infinity. Given these ranges for $(S_{MAX}/S_{MEAN})_{minor}$ and $(1.0/P_{EFF})$, λ(NLM) can range from 1.0 to infinity.

To give the variable λ(NLM) some physical significance, the limits of λ(NLM) must be described in terms of the properties of a

TABLE 4.15 Stress Interaction Variables

Stress History	$S_{MEAN(min)}$ / $S_{MEAN(maj)}$	$S_{MAX(min)}$ / $S_{MEAN(maj)}$	S_{MAX} / $S_{MEAN\ min}$	P_{AVG}	P_{EFF} (NLM)	P_{EFF} (M)	P_{EFF} (G)	F_{EXP} / F_M	F_{EXP} / F_{NLM}
SS1	1.00	1.12	1.12	0.24	0.58	0.54	0.60	1.63	1.30
SS2	1.00	1.33	1.33	0.46	0.69	0.54	0.66	2.7	1.71
SS3	1.00	1.44	1.44	0.62	0.80	0.68	0.79	1.38	0.74
SS4	1.00	1.25	1.25	0.40	0.66	0.56	0.66	2.87	1.53
SS5	1.00	1.37	1.37	0.55	0.75	0.62	0.74	2.20	1.60
SS6	1.00	1.49	1.49	0.70	0.84	0.73	0.82	1.62	0.93
SS7	1.00	1.39	1.39	0.60	0.78	0.65	0.76	1.55	0.76
SS8	1.00	1.42	1.42	0.68	0.84	0.74	0.84	2.14	1.33
Test Truck	0.92	1.09	1.18	0.24	0.53	0.45	0.54	1.56	0.76
Traf. 1	0.80	0.88	1.10	0.09	0.35	0.21	0.28	0.87	0.12
Traf. 2	0.90	1.03	1.14	0.16	0.45	0.29	0.39	0.82	0.16
Traf. 3	0.81	0.91	1.12	0.14	0.42	0.35	----	1.06	0.38
G11	1.00	1.75	1.75	0.83	0.92	0.85	0.91	1.27	1.03
G12	1.00	1.50	1.50	0.67	0.82	0.74	0.82	1.33	0.97
G13	1.00	1.33	1.33	0.66	0.77	0.70	0.77	1.33	1.01
G14	1.00	1.08	1.08	0.39	0.69	0.68	0.70	1.26	1.19
G15	1.00	1.38	1.38	0.58	0.78	0.70	0.78	1.02	0.76
G16	1.00	1.60	1.60	0.73	0.87	0.78	0.86	1.13	0,84
G17	1.00	1.75	1.75	0.83	0.92	0.85	0.91	1.03	0.84
G21	1.00	1.75	1.75	0.80	0.89	0.81	0.87	1.16	0.88
G22	1.00	1.50	1.50	0.60	0.78	0.66	0.75	1.33	0.83
G23	1.00	1.33	1.33	0.46	0.71	0.59	0.68	1.48	0.95
G24	1.00	1.13	1.13	0.30	0.60	0.57	0.61	1.26	1.03
G25	1.00	1.40	1.40	0.52	0.73	0.62	0.71	1.27	0.79
G26	1.00	1.67	1.67	0.73	0.86	0.75	0.83	1.13	0.79

TABLE 4.16 Values of m for Each Specimen

Specimen	Study	m
Welded Tee	Present, Zwerneman, Joehnk	3.76
Plate with Longitudinal Fillet Weld	Gurney	2.83
CPS (A514)	U.S.S.	2.83
WBC-B&C (A514)	U.S.S.	2.69
WBP-D (A514)	U.S.S.	3.46
WBC-C (A36)	U.S.S.	3.12
WBP-D (A36)	U.S.S.	3.21

stress history. Assuming all stresses are tensile, as the minimum stress decreases the value of $(S_{MAX}/S_{MEAN})_{minor}$ increases from 1.0 to 2.0. In addition, if the minor cycles were near the maximum stress of a stress history, $(S_{MAX}/S_{MEAN})_{minor}$ would be closer to 1.0. If the minor cycles were near the minimum stress of a stress history, $(S_{MAX}/S_{MEAN})_{minor}$ would be closer to 2.0. Thus, the term $(S_{MAX}/S_{MEAN})_{minor}$ is a measure of the mean stress of the entire stress history, and the level of the minor cycles. As the magnitude of the minor cycles approaches the magnitude of the major cycles, P_{EFF} approaches 1.0 and $(S_{MAX}/S_{MEAN})_{minor}$ moves closer to 2.0. As the magnitude of the minor cycles approaches 0.0, P_{EFF} approaches 0.0 and $(1/P_{EFF})$ approaches infinity. Therefore, a value of λ(NLM) of 1.0 results from a stress history with large minor cycles and a high mean stress. A value of λ(NLM) of infinity results from any stress history with a large number of small minor cycles, as in traffic histories. From this description of λ(NLM) it follows that CF(NLM) should approach 0.0 as λ(NLM) approaches infinity.

The next step in the development of CF(NLM) based on λ(NLM) is to fit a curve to the experimental data. Figures 4.16 and 4.17 present plots of F_{EXP}/F_{NLM} and F_{EXP}/F_G against λ(NLM). As expected, the plots are very similary. Thus, the same expression for CF can be used with both F_{NLM} and F_G. The only difference between CF(NLM) and CF(G) occurs as λ(NLM) becomes large. As the number of cycles increases, F_G becomes less conservative than F_{NLM}. This occurrence is shown in the comparisons of the three damage models presented in Figs. 2.14 through

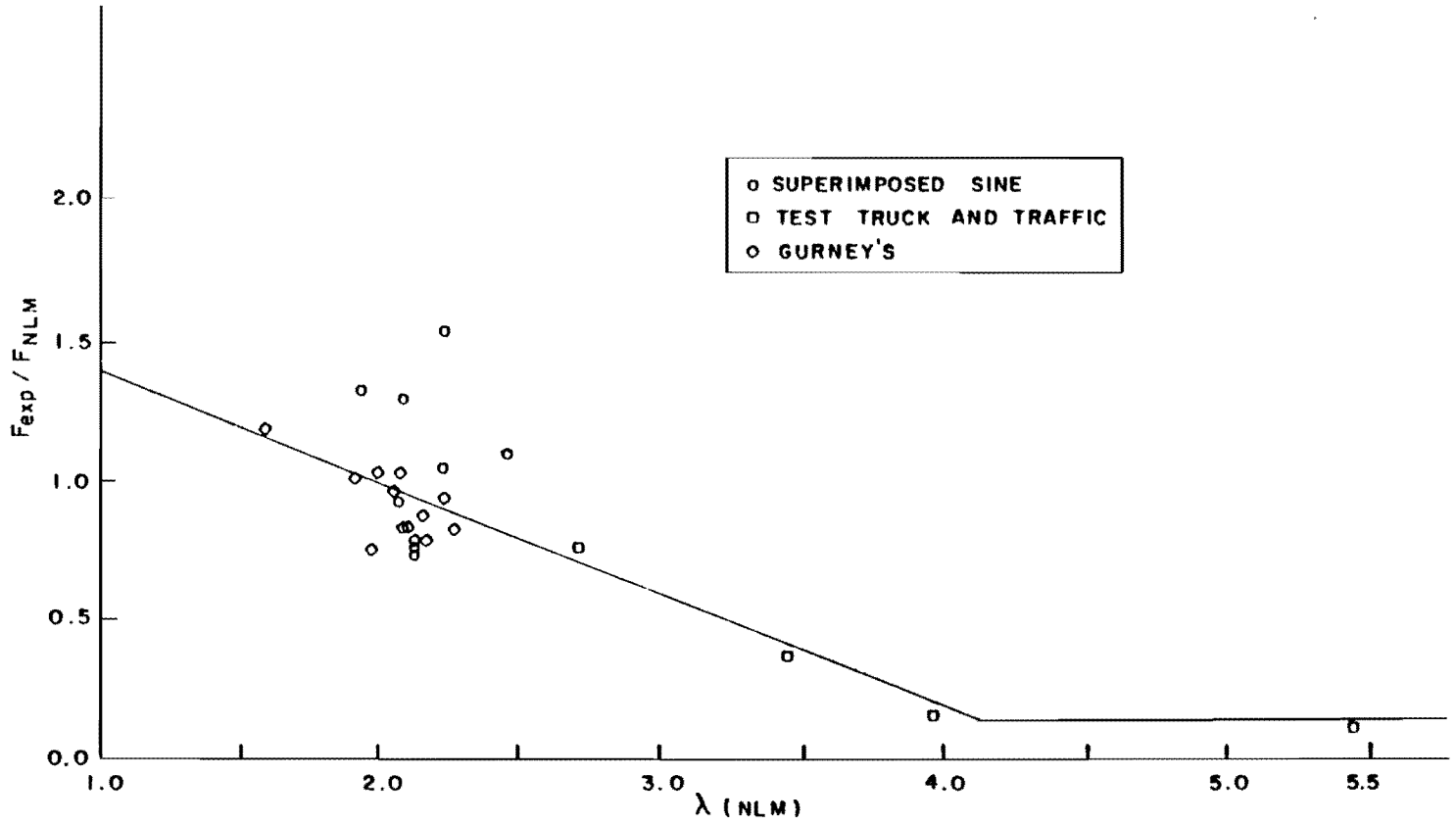

Fig. 4.16 F_{EXP}/F_{NLM} vs. λ(NLM)

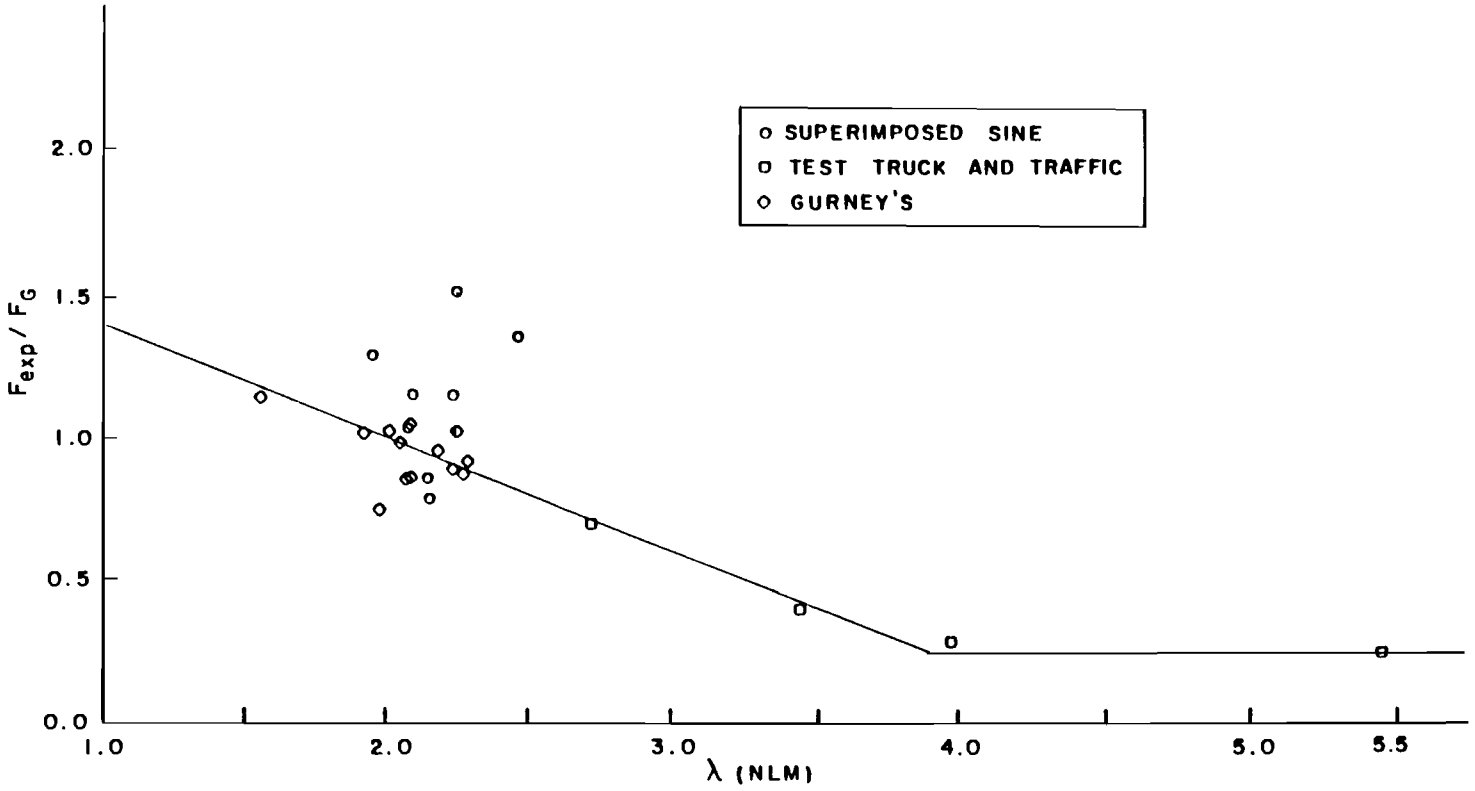

Fig. 4.17 F_{EXP}/F_G vs. λ(NLM).

2.21. Assuming a linear relation between CF and λ(NLM), the following expressions produce good predictions of experimental data:

$$CF(NLM) = 1.8 - 0.4\,\lambda(NLM) \geq 0.15 \qquad (4.4)$$

$$CF(G) = 1.8 - 0.4\,\lambda(NLM) \geq 0.25 \qquad (4.5)$$

Next, CF for use with F_M was developed. Using the same procedure, λ(M) was developed for use in an expression for CF(M):

$$\lambda(M) = P_{EFF}(NLM)(S_{MAX}/S_{MEAN})^{-2}_{MINOR} \qquad (4.6)$$

where $P_{EFF}(NLM)$ is determined using nonlinear Miner's cumulative damage theory. $(S_{MAX}/S_{MEAN})_{minor}$ varies from 1.0 to 2.0 so the term $(S_{MAX}/S_{MEAN})^{-2}_{MINOR}$ will vary from 0.25 to 1.0. $P_{EFF}(NLM)$ varies from 0.0 to 1.0. Therefore, λ(M) varies from a minimum of 0.0 to a maximum of 1.0.

The physical significance of the ratio $(S_{MAX}/S_{MEAN})_{minor}$ was discussed in the development of CF(NLM). From that discussion, it follows that $(S_{MAX}/S_{MEAN})^{-2}_{MINOR}$ will approach 0.25 in stress histories where 1) the level of the minor cycles is at a minimum and 2) the mean stress of the entire history is at a minimum. When the mean stress level of the minor cycles and the entire history are at a maximum, $(S_{MAX}/S_{MEAN})^{-2}_{MINOR}$ will approach 1.0. The value of $P_{EFF}(NLM)$ will approach 1.0 as the magnitude of the minor cycles approaches a maximum. $P_{EFF}(NLM)$ will approach 0.0 as the magnitude of the minor cycles approaches 0.0. Therefore, a value of λ(M) of 0.0 results from a stress history in which the magnitude of the minor cycles approaches 0.0. A

value of $\lambda(M)$ of 1.0 results from a stress history in which 1) the level of the minor cycles and the mean stress of the entire history are at a maximum and 2) the magnitude of the minor cycles is at a maximum. Based on observations of experimental data, CF(M) should be 1.0 when $\lambda(M) = 0.0$ and should increase from 1.0 as $\lambda(M)$ approaches 1.0.

Figure 4.18 presents a plot of F_{EXP}/F_M against $\lambda(M)$. Assuming a linear relation between CF(M) and $\lambda(M)$, the following expression represents a best fit to the experimental data:

$$CF(M) = -0.8 + 5.9\ \lambda(M) = 1.0 \qquad (4.7)$$

The minimum value of 1.0 is not based on experimental data because there is no data below $\lambda(M) = 0.29$. The minimum value of CF(M) is based on the assumption that Miner's cumulative damage rule is accurate as $P_{EFF}(NLM)$ approaches 0.0

4.4.2 Proposed Damage Model. At this point, three equations for the damage factor have been developed using the correction factor CF. These equations will be known as stress interaction damage models. The damage factor calculated using a stress interaction damage model will be designated as F_{SI} and:

$$F_{SI}(M) = F_M\ [CF(M)]$$

$$F_{SI}(NLM) = F_{NLM}\ [CF(NLM)]$$

$$F_{SI}(G) = F_G\ [CF(G))]$$

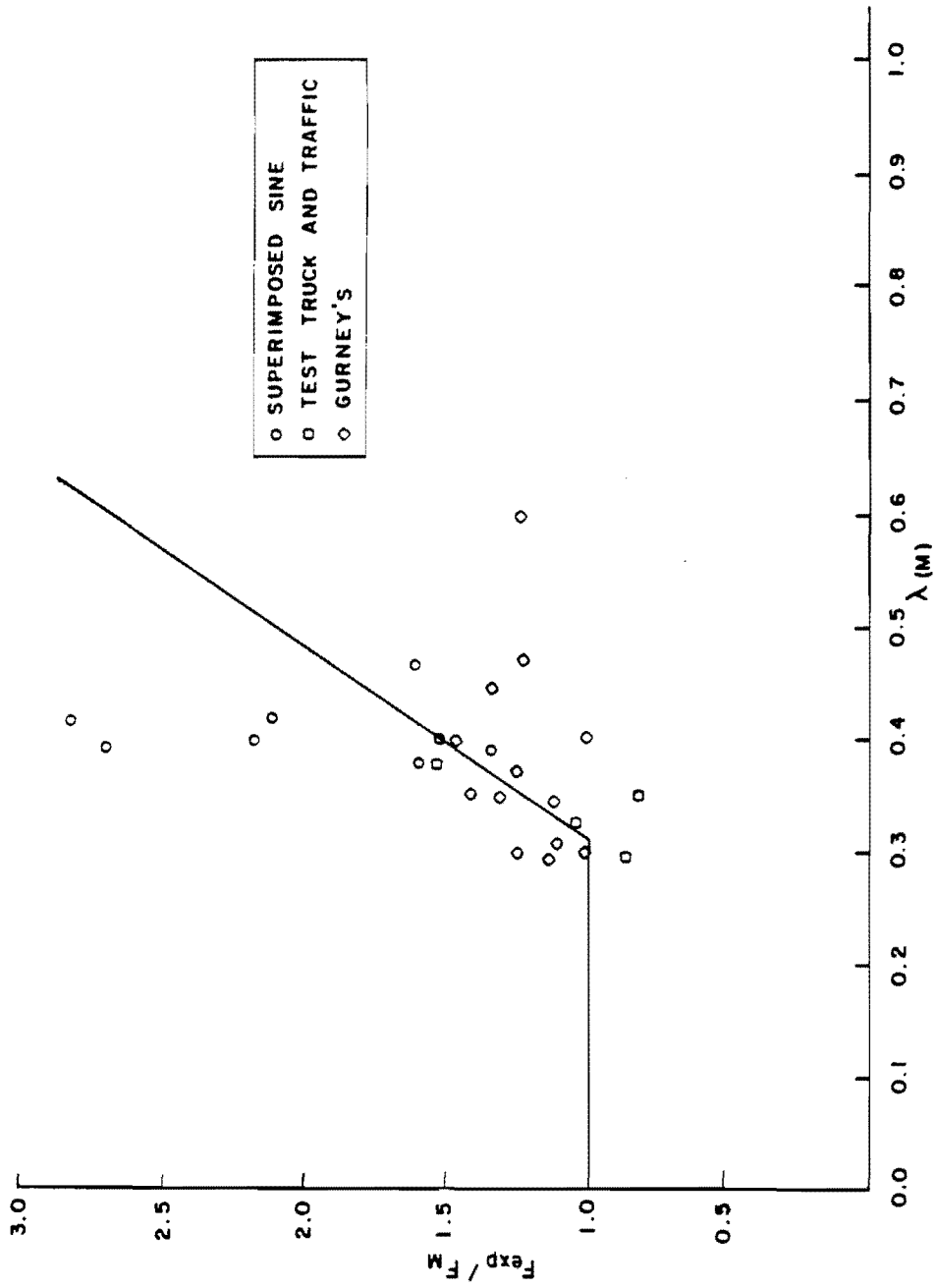

Fig. 4.18 F_{EXP}/F_M vs $\lambda(M)$.

A comparison of the damage models using CF are presented in Table 4.17. This comparison indicates that the use of F_{NLM} with CF(NLM) in the proposed damage model will produce the best results. The accuracy of all three models is comparable with average values of F_{EXP}/F_{PRED} of 1.02, 1.00, and 1.05 for $F_{SI}(M)$, $F_{SI}(NLM)$, and $F_{SI}(G)$ respectively. However, $F_{SI}(M)$ produces more scatter. $F_{SI}(NLM)$ and $F_{SI}(G)$ produce almost equivalent predictions of fatigue damage. Since F_{NLM} is simpler to calculate, $F_{SI}(NLM)$ is recommended. Therefore, from this point F_{SI} shall be taken as $F_{SI}(NLM)$, CF = CF(NLM) and $\lambda = \lambda(NLM)$.

4.4.3 Evaluation of Proposed Model. In order to investigate the overall applicability of the proposed model, CF was calculated for the stress histories used by Gurney, Joehnk, Zwerneman, U.S. Steel and the present study. Figure 4.19 presents a plot of the experimental values of CF vs. λ with the predicted values of CF represented by the solid line. Points above the predicted value of CF represent unconservative predictions, while points below the line represent conservative results. The results shown in Fig. 4.19 represent more than 175 experiments using 21 different stress histories on 7 different specimens.

One major exception was found to the relationship between CF and λ. These test results are indicated by a plus sign (+) on Fig. 4.19. The common factor between these tests is that the mean stress of the history was higher in relation to the maximum stress range than in the other tests. The increase in the mean stress causes the ratio of $(S_{MAX}/S_{MEAN})_{minor}$ to approach 1.0 as discussed in the previous section. As the ratio of S_{MAX} to S_{MEAN} of the minor cycles approaches 1.0, the

TABLE 4.17 Comparison of Proposed Damage Models

Stress History	$\frac{F_{EXP}}{F_{SI(M)}}$	$\frac{F_{EXP}}{F_{SI(NLM)}}$	$\frac{F_{EXP}}{F_{SI(G)}}$
SS1	0.86	1.39	1.24
SS2	1.85	1.34	1.66
SS3	0.93	0.78	0.82
SS4	1.73	1.67	1.67
SS5	1.41	1.16	1.18
SS6	1.12	0.94	1.05
SS7	0.99	0.82	0.91
SS8	1.28	1.33	1.25
Test Truck	1.08	1.05	0.97
Traf. 1	0.87	0.89	1.00
Traf. 2	0.65	0.76	1.08
Traf. 3	0.92	0.88	0.91
G11	1.27	1.05	1.07
G12	1.00	0.98	0.99
G13	0.75	0.98	0.97
G14	0.47	0.90	0.86
G15	0.63	0.75	0.74
G16	0.94	0.86	0.88
G17	1.03	0.86	0.88
G21	1.16	0.94	1.02
G22	1.05	0.92	1.03
G23	0.95	1.04	1.12
G24	0.64	1.04	1.03
G25	0.92	0.88	0.97
G26	1.10	0.86	0.96
Avg	1.02	1.00	1.05
Max	1.85	1.67	1.67
Min	0.47	0.75	0.74

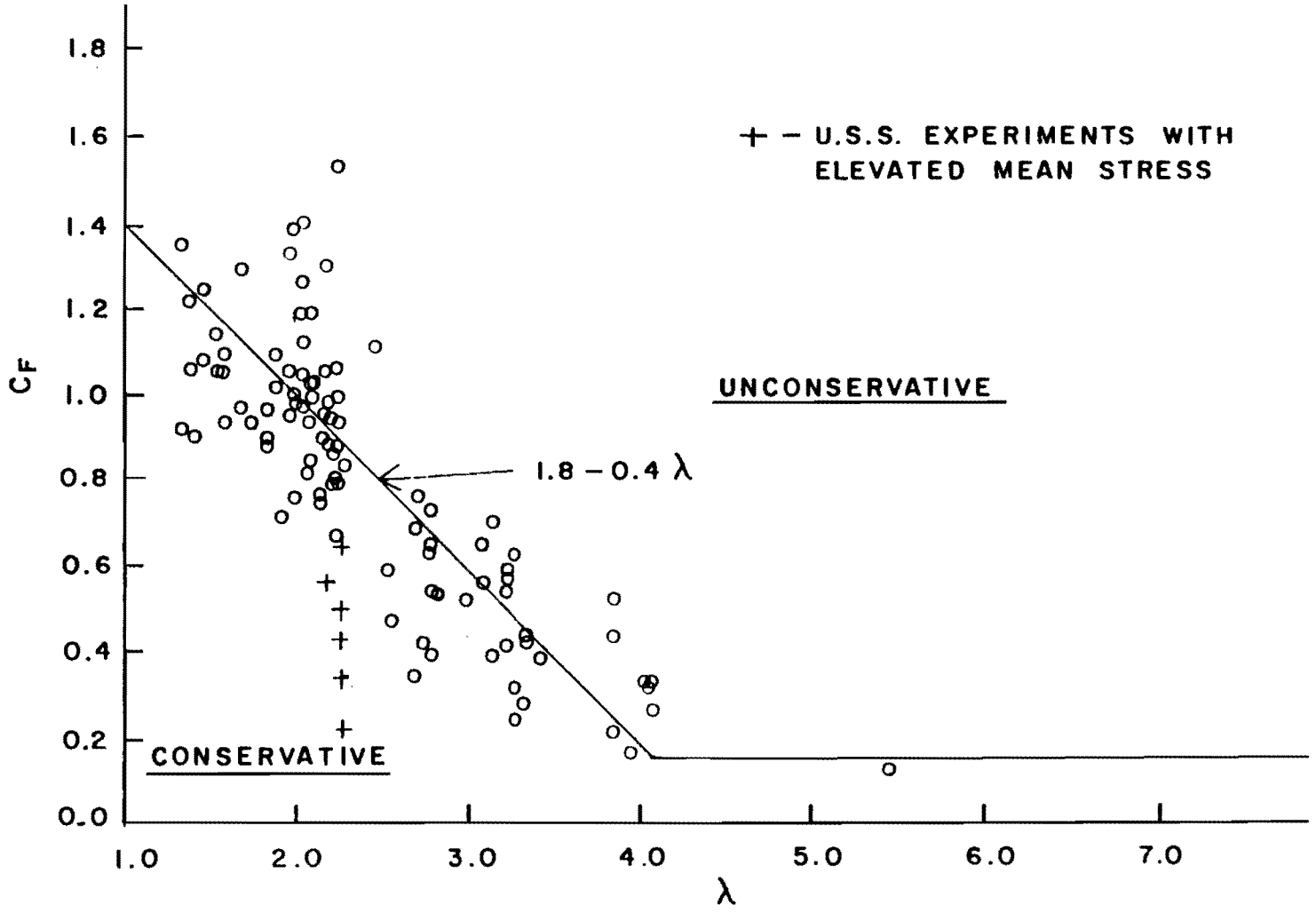

Fig. 4.19 CF vs λ for all test results.

value of λ decreases. A decrease in λ produces an increase in CF. However, these test results indicate that CF should not vary in this case. Therefore, the effect of the mean stress level of the stress history on CF may be exaggerated in the variable $(S_{MAX}/S_{MEAN})_{MINOR}$. It should be noted that all of these tests were part of the U.S. Steel study and were run at a constant minimum stress.

A comparison of the predictions made by Miner's, nonlinear Miner's, Gurney's and the proposed stress interaction model for all the stress histories is presented in Table 4.18. The average values of F_{EXP}/F_{PRED} for each set of fatigue tests are plotted in Fig. 4.20. The proposed stress interaction model is applicable in almost all the stress histories tested. The stress interaction model produced fatigue damage predictions which were on average grossly unconservative (> 20%) when applied to three stress histories (Gurney's waveform 8, Mean Stress 1, U.S.S. with $S_{Rd}/S_{RM} = 1.0$).

From Fig. 2.11 Gurney's waveform 8 has only 5 cycles; however, the experimental damage factor was greater than 5.0 which is the maximum theoretical value of F. Since only three tests were conducted with this stress history and the behavior is very unexpected, the results are attributed to experimental scatter. Mean Stress History 1 is the only stress history in which the mean stress of the minor cycles was above the mean stress of the major cycle. Thus, the error in F_{SI} may result from an error in the use of the $(S_{MAX}/S_{MEAN})_{minor}$ term in λ. The U.S. Steel history using S_{Rd}/S_{RM} was different from all other histories being investigated because it contained a continuous spectrum of stress cycles

TABLE 4.18 Comparison of Damage Models

Stress History	F_{EXP} / F_M			F_{EXP} / F_G			$F_{EXP} / \bar{F}_{NLM}$			F_{EXP} / F_{SI}		
	Max	Min	Avg	Max	Min	Avg	Max	Min	Avg	Max	Min	Avg
Gurney 1	1.33	1.02	1.22	1.14	0.75	0.98	1.19	0.76	0.98	1.05	0.75	0.91
Gurney 2	1.48	1.13	1.29	1.03	0.87	0.97	1.04	0.79	0.91	1.04	0.86	0.95
Gurney 3	1.50	1.03	1.23	1.24	0.85	1.06	1.29	0.88	1.09	1.14	0.81	0.93
Gurney 4	1.38	1.09	1.16	1.33	0.89	1.02	1.35	0.93	1.05	1.07	0.83	0.92
Gurney 5	1.66	1.42	1.54	1.08	0.93	1.01	0.65	0.65	0.61	1.14	0.98	1.06
Gurney 6	1.47	1.02	1.27	1.22	0.81	0.99	1.26	0.80	0.98	1.27	0.83	1.02
Gurney 7	1.66	1.13	1.32	1.15	0.88	0.98	1.14	0.87	0.98	1.22	0.92	1.02
Gurney 8	1.48	1.17	1.36	1.37	1.10	1.27	1.40	1.12	1.30	1.40	1.13	1.29
Superimposed Sine	3.01	1.14	2.04	1.60	0.72	1.14	1.69	0.68	1.09	1.67	0.78	1.18
MS1			2.25			1.19			1.19			1.23
MS2			1.68			0.89			0.89			0.97
MS3			1.29			0.69			0.69			0.94
USS-S_{RD}/S_{RM}=0.25	1.19	0.88	1.05				0.73	0.54	0.64	1.06	0.74	0.89
USS-S_{RD}/S_{RM}=0.50	1.37	0.50	0.97				0.71	0.24	0.49	1.29	0.47	0.83
USS-S_{RD}/S_{RM}=1.0	1.26	0.48	0.79				0.53	0.21	0.35	2.00	0.56	1.22
Test Truck	1.71	1.40	1.56	0.77	0.63	0.70	0.83	0.68	0.76			1.05
CMS1			1.34			0.60			0.65			1.60
CMS2			1.34			0.60			0.65			1.00
Traffic 1			1.28						0.52			0.87
Traffic 2			0.87			0.25			0.12			0.88
Traffic 3			1.06			0.39			0.38			0.89

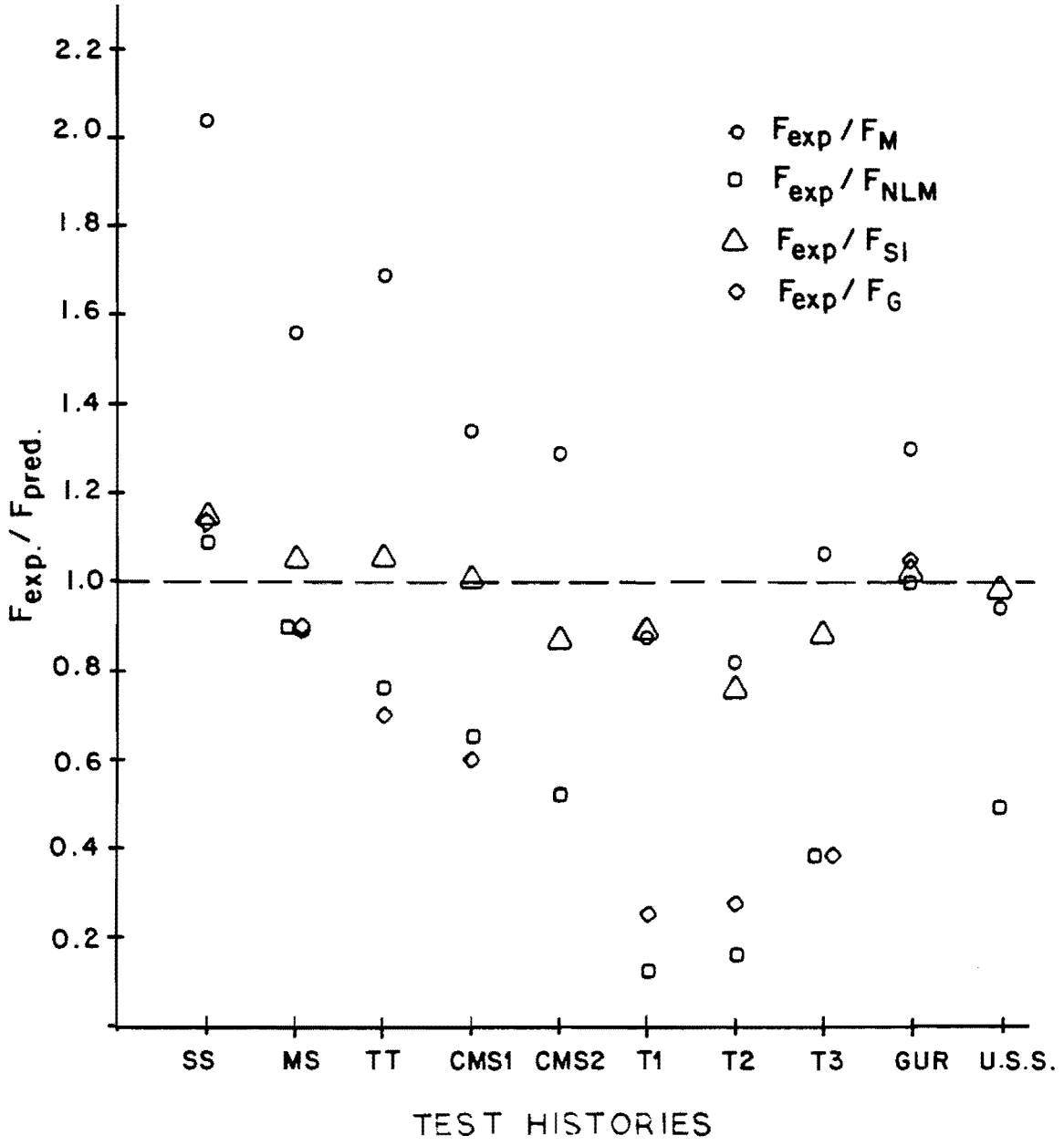

Fig. 4.20 Comparison of damage models.

from P = 0.0 to P = 1.0. Therefore, the error may result from underestimating the fatigue damage caused by the minor cycles with P values close to 1.0. In addition, the values of λ for this stress history fall very close to the break in the curve for CF. Thus, more experimental data is required for values of λ of 4.0 and greater to better define the values of CF.

4.5 Proposed Highway Bridge Fatigue Analysis

At the beginning of Chapter II variable amplitude fatigue design was divided into the following three procedures: 1) development of a finite load history which represents the loads imposed on the structure, 2) calculation of an equivalent constant amplitude load history, and 3) determination of the fatigue life based on constant amplitude fatigue tests. The results of this study are directly applicable to procedures 1 and 2.

Presently, the finite load histories used in highway bridge fatigue analysis are based on the assumption of one stress cycle per truck passage. The fatigue damage caused by the minor cycles is neglected. The results of the tests using the test truck and traffic histories indicate that the minor cycles produced by a truck passage cause a significant amount of fatigue damage. Neglecting the minor cycles resulted in an overprediction of the fatigue life of between 40 and 50 percent. Therefore, the finite load histories used in highway bridge fatigue analysis should include the effect of the minor cycles.

Comparisons of the fatigue damage done by Traffic Histories 1, 2 and 3 demonstrate that fatigue damage of a stress history can be

predicted by linearly summing the fatigue damage caused by each segment. Therefore, it follows that the fatigue life of a bridge detail can be determined by simply summing the damage caused by each individual truck passage. However, the effectiveness of the minor cycles varies with properties of the stress history. Thus, even though nonlinear Miner's theory fairly accurately models an individual truck passsage, it produces grossly overconservative fatigue life predictions for a series of truck passages. Miner's cumulative damage model, on the other hand, accurately predicted the fatigue damage caused by the minor cycles when applied to all three traffic histories. In addition, the trends in the experimental results indicate that Miner's rule accurately simulates the fatigue behavior of stress histories with a large percentage of small minor cycles (< 20% of S_{RMAX}), as is found in most bridge traffic stress histories. Therefore, the equivalent constant amplitude load history can be calculated using Miner's cumulative damage theory.

In the proposed analysis technique, the finite load history is developed by calculating an effective stress cycle to represent each truck passage and placing these cycles in series. The magnitude of the effective stress cycle is determined by the GVW of the truck, the geometry of the bridge, and the fatigue damage caused by the minor cycles. The maximum stresses in the stress cycle can be determined, as described in Eq. (1.2), by applying an impact fraction to the static component of the stress cycle. However, the impact fraction does not account for the fatigue damage caused by the minor cycles. Therefore, an additional factor is required to account for the fatigue damage

produced by the minor cycles. Since the effective stress cycle can be described as the complex effective stress range for the complex cycle produced by a truck passsage, the effective stress cycle can be calculated using Eq. (2.3):

$$S_{REFF} = S_{RMAX} (F)^{1/m} \tag{2.3}$$

where S_{RMAX} is given by Eq. (1.2) and $(F)^{1/m}$ is the additional factor used to account for the fatigue damage produced by the minor cycles. Thus, the effective stress cycle produced by a truck passage can be expressed as:

$$S_{REFF} = \delta(GVW)\ (1.0 + I)\ (I_F) \tag{4.8}$$

where I is the impact fraction given by Eq. (1.1) and I_F is the fatigue factor given by $(F)^{1/m}$. Since Miner's rule most accurately models the fatigue behavior of the minor cycles in highway bridge loadings, F will be taken as F_M.

At this point, the bridge loading history can be simulated by a distribution of S_{REFF} based on Eq. (4.8) and a GVW distribution of trucks which will cross the bridge. Finally, an equivalent constant amplitude history can be calculated by applying Miner's cumulative damage model to determine the simple effective stress range (S_{RES}) (Eq. (2.9)) for the loading distribution. This S_{RES} would represent the design stress range of the loading history.

The only difference between the proposed analysis and the analysis used in the AASHTO Specifications (see Chapter I) is the

addition of a factor to account for the fatigue damage produced by the minor cycles. This difference can be easily assimilated into present design by requiring the designer to increase the calculated design stress range by I_F.

4.5.1 Fatigue Factor. Given the definition of F_M presented by Eq. (2.11), I_F is calculated for a given truck loading using the following equation:

$$I_F = (\Sigma n_i P_i^m)^{1/m} \tag{4.9}$$

Because no two truck passages will produce the exact same stress history, it is inefficient to calculate I_F for every truck loading. A representative stress history can be developed using a superimposed sine waveform, as shown in Fig. 1.2, with minor cycles of a single magnitude. In this way, Eq. (4.9) can be simplified to:

$$I_F = (1 + n_c P_E^m)^{1/m} \tag{4.10}$$

where P_E is the single magnitude of the minor cycles in a superimposed sine loading which replace the minor cycles in the truck loading. P_E is given in terms of F_M by:

$$P_E = \left(\frac{F_M - 1}{n_c} \right)^{1/m} \tag{4.11}$$

The variable n_c is primarily determined by the natural frequency of the individual bridge, the length of the span, and the speed of the truck. P_E is primarily dependent on the bridge's structural response to load.

The sensitivity of I_F to n_c, P_E and m is shown in Fig. 4.21 which is a plot of I_F against P_E for three values of n_c (10, 25, 50) and

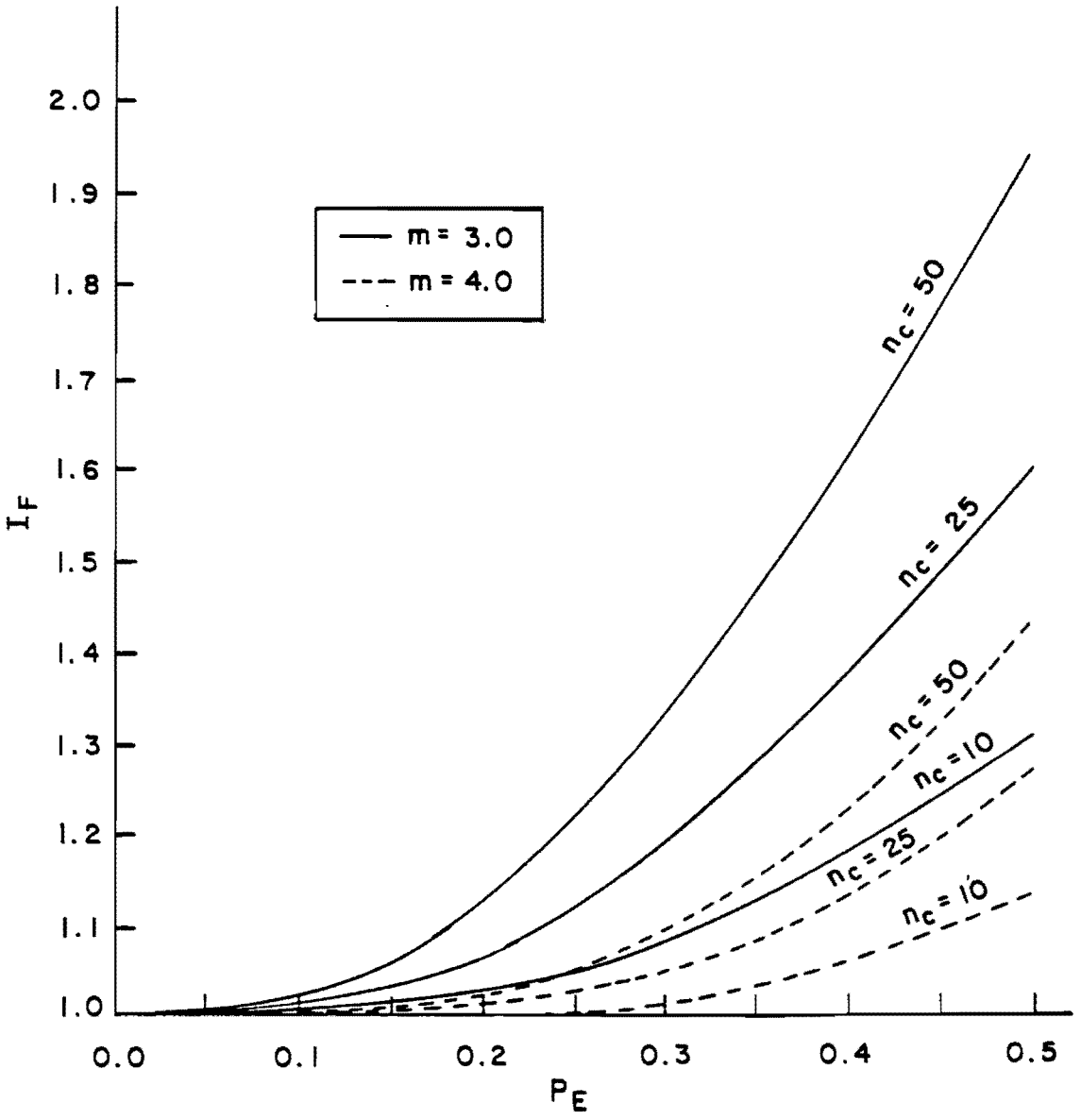

Fig. 4.21 Variation of I_F with P_E, n_c, and m.

two values of m (3.0, 4.0). The curves are terminated at P_E = 0.50 because values of P_E larger than 0.50 are not likely in bridge loadings. From Fig. 4.26 it can be observed that the sensitivity of I_F to n_c and P_E are interrelated. I_F is more sensitive to changes in P_E as n_c increases from 10 to 50, and I_F becomes more sensitive to changes in n_c as P_E increases from 0.0 to 0.5. A shift in m from 3.0 to 4.0 decreases I_F approximately 15, 20, and 25 percent for n_c = 10, 25, and 50 respectively.

To obtain an estimate of I_F for use in design, an average P_E was calculated for the ten events used in the traffic histories and the test truck using Eq. (4.11). The average value of P_E was 0.31. The other variables required to determine I_F are n_c and m. Because all design details presented in the AASHTO specifications are given an m = 3.0, this value will be used to determine I_F. From Hoadley's measurements of four test truck loadings at 50 mph, the average number of cycles in a truck loading was 16.5. Therefore, n_c will be assumed as 17. Given these values of n_c, m and P_E, I_F = 1.15.

As a comparison, I_F was estimated using F_{NLM} instead of F_M. The average value of P_E for the ten events used in the traffic histories and the test truck history using Eq. (4.11) with F_{NLM} instead of F_M was 0.47. Assuming m = 3.0 and n_c = 17 as before, I_F = 1.40. This represents a 22 percent increase in the value of the fatigue factor calculated using F_M. Thus, using F_{NLM} instead of F_M in Eq. (4.11) will result in a conservative estimation of the fatigue damage caused by the minor cycles.

It should be noted at this point that this 15 percent increase in the calculated stress range represented by $I_F = 1.15$ is very dependent on the dynamic qualities of the bridge used in this study. On other types of bridges, the number and magnitude of the minor cycles in each truck loading will vary with the span length and type of construction. Because the construction of this bridge tends to amplify stress fluctuations as it had a low level of redundancy, the 1.15 value of I_F should be an upper bound.

4.5.2 Evaluation of Proposed Analysis. The use of the fatigue factor is supported well by the experimental results of this research; however, the true test of the proposed analysis is in its application to actual bridges. Two different case studies were chosen on which to test the use of the proposed analysis in design. In the first there was no detectable cracking, while in the second there was considerable cracking.

The first bridge was the one on which the measurements used in this study were taken. The bridge is located near downtown Dallas, Texas. It is composed of two large steel girders which support a concrete deck. A more detailed description of the bridge is presented in Appendix B and Reference 18. The second case dealt with the Yellow Mill Pond Bridge which has been the subject of sevral studies which were concluded in research done by Fisher and Slockbower at Lehigh University [30]. The Yellow Mill Pond Bridge was located on a heavily traveled section of the Connecticut Turnpike. The bridge was constructed of

rolled wide flange steel girders with cover plates. A more detailed description of the bridge is given in Reference 30.

The analysis procedure is composed of three steps: 1) determination of the maximum stress range applied by the heaviest truck passasge; 2) calculation of an equivalent design stress range using Miner's theory based on a loading distribution and accounting for the fatigue factor; and 3) calculation of the fatigue life of a specific detail based on its constant amplitude S-N curve. From the definition of S_{RES} given in Eq. (2.9) and assuming I_F will remain constant for the range of truck loadings, the fatigue factor can be applied directly to the design stress range calculated neglecting I_F.

Test loadings of the Dallas Bridge completed by Hoadley [18] with a test truck weighing 52 kips at 50 mph produces a maximum stress range of 2.8 ksi in the tension flange. Because no loading distribution was constructed for this bridge, one had to be assumed. From the 1970 FHWA Loadometer Survey, the maximum GVW = 100 kips. Thus, the maximum stress range in the distribution is given by:

$$S_{RMAX} = (2.9 \text{ ksi})\ (100 \text{ kips}/52 \text{ kips}) = 5.38 \text{ ksi}$$

This value of S_{RMAX} correlates well with data collected by Hoadley during normal traffic loadings. From the GVW distribution developed from the 1970 FHWA Loadometer Survey, the ratio of the simple effective stress range to the maximum strss range (S_{RES}/S_{RMAX}) is 0.70. Another probable distribution of loadings was developed as part of NCHRP Project 12-12 [12]. This is a Rayleigh distribution which produces a value of

S_{RES}/S_{RMAX} = 0.50. Given that I_F = 1.15 the design stress range, S_{RD}, is 4.33 ksi based on the distribution given by the FHWA Loadometer Survey and is 3.09 ksi based on the Rayleigh distribution. All stress ranges are given at the tension flange.

The critical detail in the Dallas bridge was at the intersection of a longitudinal and a transverse stiffener (LTSI detail). This intersection was located 15 in. above the bottom flange. Therefore, assuming a linear stress distribution, S_{RD} at the detail is 2.53 ksi and 1.80 ksi for the FHWA and Rayleigh distribution respectively. The S-N curve for the LTSI detail which was developed by Platten [31] and experimentally verified in constant amplitude testing [32], has m = 3.0 and A = 1.66 x 10^8. Based on this S-N curve the predicted number of trucks required to produce cracking is 10 million and 28 million for the FHWA and Rayleigh distribution respectively. From average daily traffic data, the number of truck passages experienced by the bridge at the time of the study was approximately 4 million. If I_F based on F_{NLM} had been assumed, the predicted life would have been 6 million and 15 million respectively. Since no cracking had occurred in the detail, the predicted fatigue lives (using I_F) based on F_M and for both loading distributions seem reasonable.

From the stress history studies completed on the Yellow Mill Pond Bridge in 1971, 1973 and 1976, Fisher determined that the maximum truck load produced a stress range of 5.4 ksi [30]. Since the Dallas bridge and the Yellow Mill Pond Bridge are of comprable span length and construction, I_F will be assumed as 1.15 as with the Dallas bridge.

With S_{RD} calculated as before, S_{RD} is 4.35 ksi and 3.11 ksi based on the FHWA and Rayleigh distributions.

Several cracks in the structured were detected in welds at the end of the cover plates on the tension flanges. This detail has been designated as a category E' in the AASHTO Specifications and A = 4.24 x 10^8. Based on this S-N curve, the predicted number of truck passages to failure are 5 million and 14 million using the FHWA and Rayleigh distribution respectively.

The first crack in the structure was discovered after approximately 21 million truck loadings. The prediction made using the FHWA distribution seems overly conservative as the detail would have survived four times its predicted life before detection. Even without applying I_F, the predicted life using the FHWA distribution would be 8 million truck passages, which also appears conservative. The prediction made based on the Rayleigh distribution with the fatigue factor seems more reasonable. The predicted life based on the Rayleigh distribution without the fatigue factor applied is 22 million truck passages. This analysis would not predict the cracks which occurred. However, if the fatigue damage caused by the minor cycles is accounted for through I_F, the fatigue cracks would have been predicted.

To further investigate how I_F will vary with bridge type, loading study done on the Silver Memorial Bridge [33] was used to calculate I_F1 The Silver Memorial Bridge is a long span (approximately 700 ft) truss bridge which crosses the Ohio River at Point Pleasant, West Virginia. In the study, several truss members were instrumented with

strain gages and strains were measured as a loaded test truck crossed the bridge. From these strain histories, the average size of the superimposed stress cycles was P = 0.37. The frequency of these cycles was approximately 6.0 cps. With a test truck velocity of 35 mph, the instrumented member was loaded for 7.0 secs. Thus, n_c can be estimated as 42. Assuming m = 3.0, I_F for this member is 1.46. This analysis indicates that I_F is sensitive to the span length of the bridge and truck velocity.

From the analyses of the Dallas and Yellow Mill Pond bridges, the value of I_F = 1.15 seems reasonable for medium span girder bridges. However, the variation in predictions between the two assumed GVW distributions indicates that the distribution of traffic may be a more important factor. The investigation of the Silver Memorial Bridge, a long-span truss bridge, showed that I_F is sensitive to the span length and truck velocity.

C H A P T E R V

SUMMARY AND CONCLUSIONS

This research project had three main objectives: 1) determine the ability of random discrete loadings to simulate actual bridge loadings; 2) determine the applicability of Miner's comulative fatigue damage model to the design of highway bridges; and 3) develop a design method which accounts for the fatigue damage produced by the minor cycles in a truck loading. The experimental program used to obtain these objectives included fatigue tests on welded tee specimens with six different loading histories. Four of these histories were developed from strain data measured on an in service highway bridge.

The results of testing with a random discrete loading pattern indicate that this loading produces unconservative estimates of fatigue damage produced by actual loadings. This result may be explained by the effect which the mean stress level of the minor cycles has on the damage these cycles produce. Only two replicate tests were completed in this test series, and only one stress range distribution was utiized in the testing of this hypothesis. However, the stress level effect was also documented by Zwerneman [1]. Thus, the conclusion has some justification, but more research on this question is needed.

The abiilty of Miner's cumulative damage theory, as well as two others proposed by Joehnk and Gurney, to predict fatigue damage varied with each load history tested. Joehnk's and Gurney's theories produced

good results on short stress histories where the average mean stress of the minor cycles was the same as the major cycle. For these histories, Miner's theory produced unconservative predictions. Miner's theory worked well with the measured traffic loadings, while Gurney's and Joehnk's models were grossly overconservative. The traffic loadings contained large numbers of small minor cycles ($P < 0.25$) and the average mean stress of these cycles was below that of the major cycle. From these results, it was concluded that Miner's damage theory is accurate and applicable in highway bridge fatigue design.

Research by Joehnk [14], Gurney [13], and the present study indicate the minor cycles in a stress history produce a significant amount of fatigue damage. Specific experimentation in this study using measured loadings indicate the minor cycles present in truck loadings produce significant damage even if they are below the threshold stress range. Thus, this additional fatigue damage must be accounted for in design. The proposed design method is similar to present analysis except for the addition of a fatigue factor, I_F, in the calculation of the stress cycle produced by a truck passage. I_F is dependent on the number and size of the minor cycles present in a truck loading. Therefore, I_F is affected by the span, and the dynamic and structural response of the bridge as well as the speed of the truck loading the bridge. From analyses of the bridge used in this study, I_F has been estimated at 1.15. This represents a 15 percent increase in the calculated stress cycle due to fatigue damage of the minor cycles. Application of this design method in two field cases produced reasonable

results. However, the assumed distributions of loadings proved to be as important as the fatigue factor in the analysis.

In addition to the objectives stated above, an additional fatigue damage model was proposed. The proposed damage model applies a correction factor to Joehnk's theory based on the properties of the loading being analyzed. The stress interaction correction factor, CF, is based on the average level, magnitude, and number of minor cycles as well as the fatigue characteristics of the detail. The proposed stress interaction damage model produces good results for a wide range of stress histories and specimen types. The exception to the model occurs for loadings with a high mean stress. In this case, the model becomes overly conservative.

The most important findings of this research are that 1) the minor cycles in a truck loading produce a significant amount of fatigue damage, and 2) the damage produced by the minor cycles varies with the stress histories which surround them. Further research is required to quantify the amount of fatigue damage produced by minor cycles. The research should use strain data measured in the field on various bridge types. In addition, basic fracture mechanics research on loadings which more closely resemble actual loadings is required to determine how stress interaction affects the fatigue life of highway bridges. An extension of this project which is being done by Dr. K. H. Frank and Farrel Zwerneman at The University of Texas at Austin deals with this basic fracture mechanics problem. The results of this research should be enlightening.

A P P E N D I X A

DERIVATION OF EFFECTIVE STRESS RANGES AND DAMAGE FACTOR

A P P E N D I X A

DERIVATION OF EFFECTIVE STRESS RANGES AND DAMAGE FACTOR

Any variable amplitude stress history can be converted to an equivalent constant amplitude stress history by a cumulative damage theory and cycle counting technique. The equivalent constant amplitude stress history is important in design because it allows the use of the vast amount of constant amplitude test data. The equivalent constant stress history is characterized by an effective stress range or damage factor.

Combining a cumulative damage rule and the linear relationship between Log N and Log S_R yields expressions for the effective stress ranges and the damage factor. The development of these expressions is shown below.

Given

$$\text{Log } N_i = A - m \text{ Log } S_{Ri} \qquad (A.1)$$

where S_{Ri} = constant amplitude stress range

N_i = number of cycles to failure at S_{RI}

A = N axis intercept on Log S_R-Log N curve

m = slope of Log S_R - Log N curve

Rearranging (A.1) yields

$$N_i = 10^A \, S_{Ri}{}^{-m} \qquad (A.2)$$

The simple effective stress range, S_{RES}, is defined as the constant amplitude stress range which causes the same fatigue damage as the variable history in the same number of cycles. The fatigue damage done by the variable history or complex cycle can be expressed as:

$$n_c/N = W_c \tag{A.3}$$

where N_c = number of variable cycles in the complex cycle

N = total number of variable cycles to failure

W_c = fatigue damage or work done by a complex cycle.

From the relation shown in Eq. (A.2) and the definition of a simple effective stress range, it follows that

$$N = 10^A \, S_{RES}^{-m} \tag{A.4}$$

Combining Eqs. (A.3) and (A.4) yields an expression for the fatigue damage done by a complex cycle as a function of S_{RES}.

$$W_c = n_c \; / \; 10^A \, S_{RES}^{-m} \tag{A.5}$$

The complex effective stress range, S_{REC}, is defined as the constant amplitude stress range which causes the same fatigue damage as the variable history in one cycle. Using this defintion of S_{REC}, the fatigue damage done by one complex cycle can be expressed as

$$1 \; / \; N_c = W_c \tag{A.6}$$

where N_c = number of complex cycles at failure.

From the relation shown in Eq. (A.2) and the definition of a complex effective stress range, it follows that:

$$N_c = 10^A \, S_{REC}^{-m} \qquad (A.7)$$

Combining Eqs. (A.6) and (A.7) yields

$$1 / 10^A \, S_{REC}^{-m} = W_c \qquad (A.8)$$

The damage factor as developed by Zwerneman [1] is defined by the following expression:

$$F = N_{MAX} / N_c \qquad (A.9)$$

where N_{MAX} = number of cycles to failure at the maximum stress range in the complex cycle

Using the relation in Eq. (A.2), F can be expressed as

$$F = 10^A \, S_{RMAX}^{-m} / N_c \qquad (A.10)$$

where S_{RMAX} = maximum stress range in the complex cycle

Combining Eqs. (A.6) and (A.10) results in the following expression for W_c in terms of F:

$$W_c = F \, (S_{RMAX})^{-m} / 10^A \qquad (A.11)$$

Since $N_c = N/n_{ci}$. F can be related to the simple effective stress range by the expression

$$F = (S_{RMAX} / S_{RES})^{-m} \, (n_c) \qquad (A.13)$$

or $$S_{RES} = S_{RMAX} (F / n_c)^{-1/m} \quad (A.14)$$

Replacing N_c in Eq. (A.10) with the expression for N_c in Eq. (A.7) yields the following relation between F and S_{REC}:

$$F = (S_{RMAX} / S_{REC})^{-m} \quad (A.15)$$

or $$S_{REC} = S_{RMAX} F^{1/m} \quad (A.16)$$

In this study three cumulative damage models are investigated. The developments of the effective stress ranges and damage factor based on each theory follow.

1. Miner's Cumulative Damage Model:

Using Miner's damage model, the fatigue damage caused by a complex cycle is given by

$$\sum_{1}^{n_c} \frac{n_i}{N_i} = W_c \quad (A.17)$$

Replacing N_i in Eq. (A.17) with the expression for N_i given by Eq. (A.2) yields

$$\sum_{1}^{n_c} \frac{n_i}{A S_{Ri}^{-m}} = W_c \quad (A.18)$$

The following expressions for S_{RES} and S_{REC} are given by equating Ea. (A.18) with Eqs. (A.15) and (A.8) respectively:

$$S_{RES} = \left(\frac{1}{n_c} \sum_{1}^{n_c} n_i S_{Ri}^{\ m} \right)^{1/m} \quad (A.19)$$

$$S_{REC} = \left(\sum_{1}^{n_c} n_i S_{Ri}^{\ m} \right)^{1/m} \quad (A.20)$$

Equating Eqs. (A.11) and (A.18) yields the following expression for F:

$$F = \sum^{n_c} n_i \left(\frac{S_{Ri}}{S_{RMAX}} \right)^m \qquad (A.21)$$

or

$$F = \sum^{n_c} n_i \, P_i^{\,m} \qquad (A.22)$$

where $P_i = S_{Ri} / S_{RMAX}$

2. Nonlinear Miner's Cumulative Damage Model

Nonlinear Miner's theory replaces S_{Ri} in Eq. (A.18) with an increased stress range given by

$$Z_{EFF} = (S_{RMAX} / S_{Ri})^{1/2} \, S_{Ri} \qquad (A.23)$$

Thus, nonlinear Miner's theory produces the following expression for W_c:

$$\sum^{n_c} \frac{n_i}{10^A} \left[\left(\frac{1}{P_i} \right)^{1/2} S_{Ri} \right]^m = W_c \qquad (A.24)$$

Equating Eq. (A.24) with Eqs. (A.15) and (A.8) yields the following expressions for S_{RES} and S_{REC} respectively:

$$S_{RES} = \left\{ \sum^{n_c} \frac{n_i}{n_c} \left[\left(\frac{1}{P_i} \right)^{1/2} S_{Ri} \right]^m \right\}^{1/m} \qquad (A.25)$$

$$S_{REC} = \left\{ \sum^{n_c} n_i \left[\left(\frac{1}{P_i} \right)^{1/2} S_{Ri} \right]^m \right\}^{1/m} \qquad (A.26)$$

Equating Eqs. (A.11) and (A.24) yields the following equation for the damage factor F:

$$F = \sum_{i}^{n_c} n_i P_i^{m/2} \tag{A.27}$$

3. Gurney's Cumulative Damage Model

Gurney's cumulative damage model predicts fatigue life in complex cycles using the following equation:

$$N_c = \left[\frac{K}{2} \pi \left(\frac{x_{(i-1)}}{x_i} \right)^{P_i} \right] N_{MAX} \tag{A.28}$$

Combining Eqs. (A.6) and (A.28) yields the expression for W_c based on Gurney's model:

$$W_c = \left[\frac{K}{2} \pi \left(\frac{x_{(i-1)}}{x_i} \right)^{P_i} \right] \frac{1}{10^A S_{RMAX}^{-m}} \tag{A.29}$$

Equating Eq. (A.28) with Eqs. (A.5) and (A.8) yields the following expressions for S_{RES} and S_{REC} respectively:

$$S_{RES} = \left\{ \left[\frac{K}{2} \pi \left(\frac{x_{(i-1)}}{x_i} \right)^{-P_i} \right] n_c \right\}^{1/m} S_{RMAX} \tag{A.30}$$

$$S_{REC} = \left[\frac{K}{2} \pi \left(\frac{x_{(i-1)}}{x_i} \right)^{-P_i} \right]^{1/m} S_{RMAX} \tag{A.31}$$

Rearranging Eq. (A.28) yields the expression for F

$$F = \frac{K}{2}\pi \left(\frac{x_{(i-1)}}{x_i} \right)^{-P_i} \qquad (A.32)$$

A P P E N D I X B

ACQUISITION AND REDUCTION OF THE TEST TRUCK AND TRAFFIC STRAIN DATA

A P P E N D I X B

ACQUISITION AND REDUCTION OF THE TEST TRUCK AND TRAFFIC STRAIN DATA

B.1 Acquisition of Strain Data

The test truck and traffic load histories were generated from strain data measured on an in-service highway bridge in Dallas, Texas. The bridge is composed of two longitudinal steel girders supporting transverse floor beams which, in turn, support a post-tensioned concrete deck. The basic bridge dimensions and geometry are shown in Fig. B.1. The strains were measured with 3/8 in. long, 120 ohm strain gages attached to the steel girder flanges at the four locations indicated in Figs. B.2 and B.3. The strain readings were collected and stored on magnetic tape with a high speed Vidar data acquisition system. A more detailed description of the bridge and the instrumentation used in the study is provided by Hoadley [18].

Because more traffic passed over the east girder, and because strains in the west girder were not measured during the passage of the test truck, only strains from the east girder are used in this study. This girder was instrumented at sections A and D. During passage of the test truck, three gages at section D malfunctioned [18]. At section A, all gages performed well. The strain-time history used to develop the test truck history was taken from section A. During measurements of normal traffic, the gages at section D performed well, and the strain history at section D contained much larger minor cycles. Thus, the load

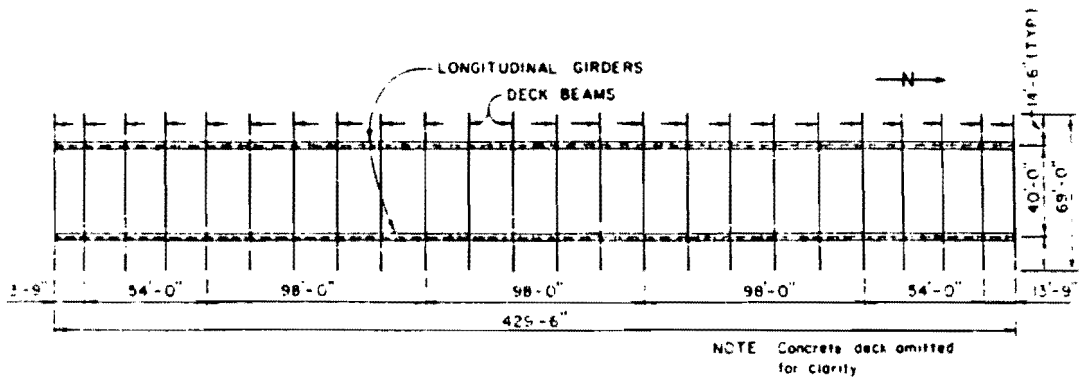

(a) PLAN

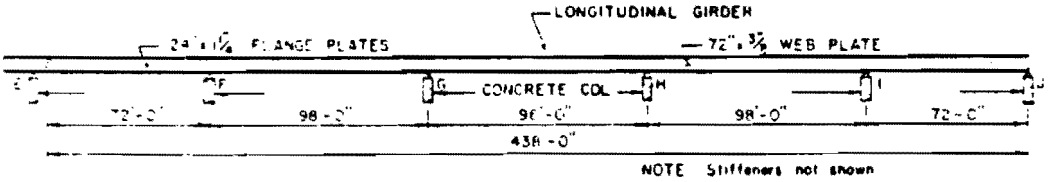

(b) ELEVATION

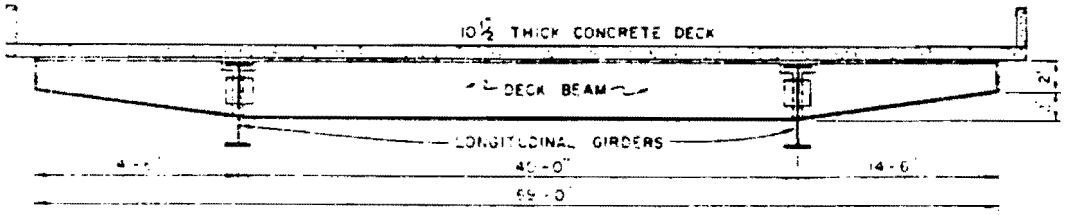

(c) CROSS SECTION
(TYPICAL)

Fig. B.1 Dimensions and geometry of instrumented bridge

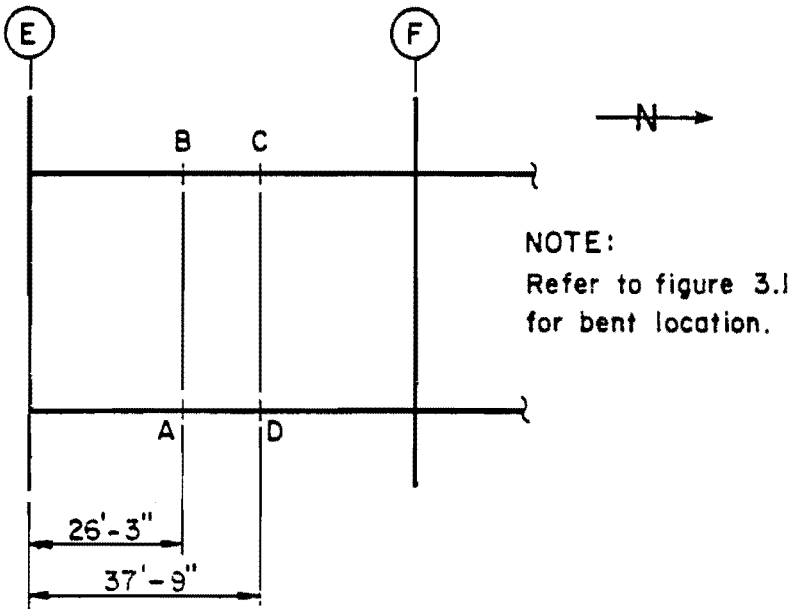

Fig. B.2 Locations of strain gages in plan

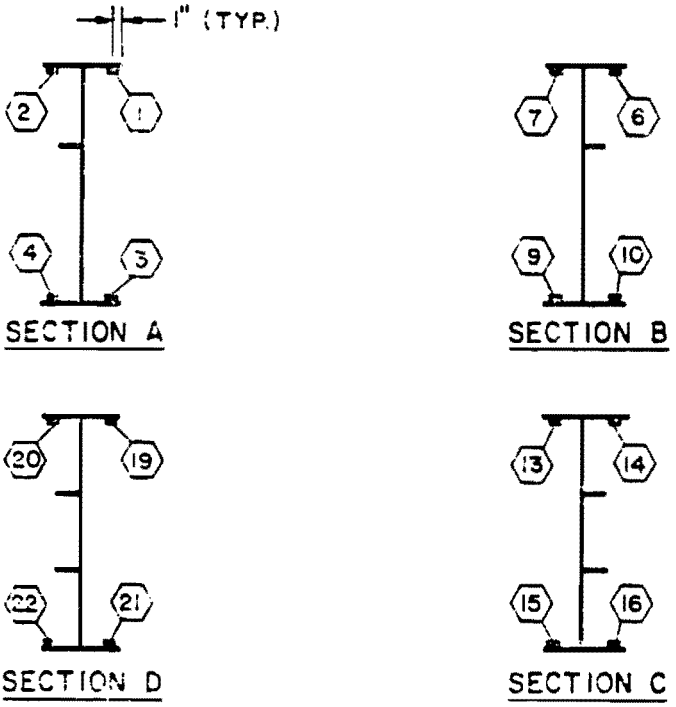

Fig. B.3 Location of strain gages in cross section

history for the traffic tests was developed from measurements taken at section D.

B.2 Reduction of Strain Data

The data reduction began by selecting the most appropriate strain-time histories from Hoadley's field data [18]. Hoadley collected two types of strain histories: 1) the passage of a single truck, and 2) normal traffic flow. Both types of strain histories are used in this study.

Three histories were generated by the test truck at speeds of 5, 35, and 50 mph. The 50 mph truck passage caused much larger secondary strain cycles than the 5 and 35 mph passages. This reduces the relative importance of random electronic noise in the strain readings, and the 50 mph speed more accurately models highway speeds. Therefore, the 50 mph strain data was used to generate the test truck load history. A comparison of the strain data histories from the 5 pmh and 50 mph passings is shown in Fig. B.4.

Measurements on normal traffic were taken during eight tests over a period of two days. Hoadley's study of the effect of record length showed that the histograms tend to remain constant after approximately 10 minutes. Thus, a test of 10-minute duration is suffucient to model highway traffic. Three of Hoadley's tests had a duration of 10 minutes. Of these three tests, measurements taken during test number 8 were of higher quality than the other two. Therefore, test number 8 was used to generate the traffic test histories used in this study.

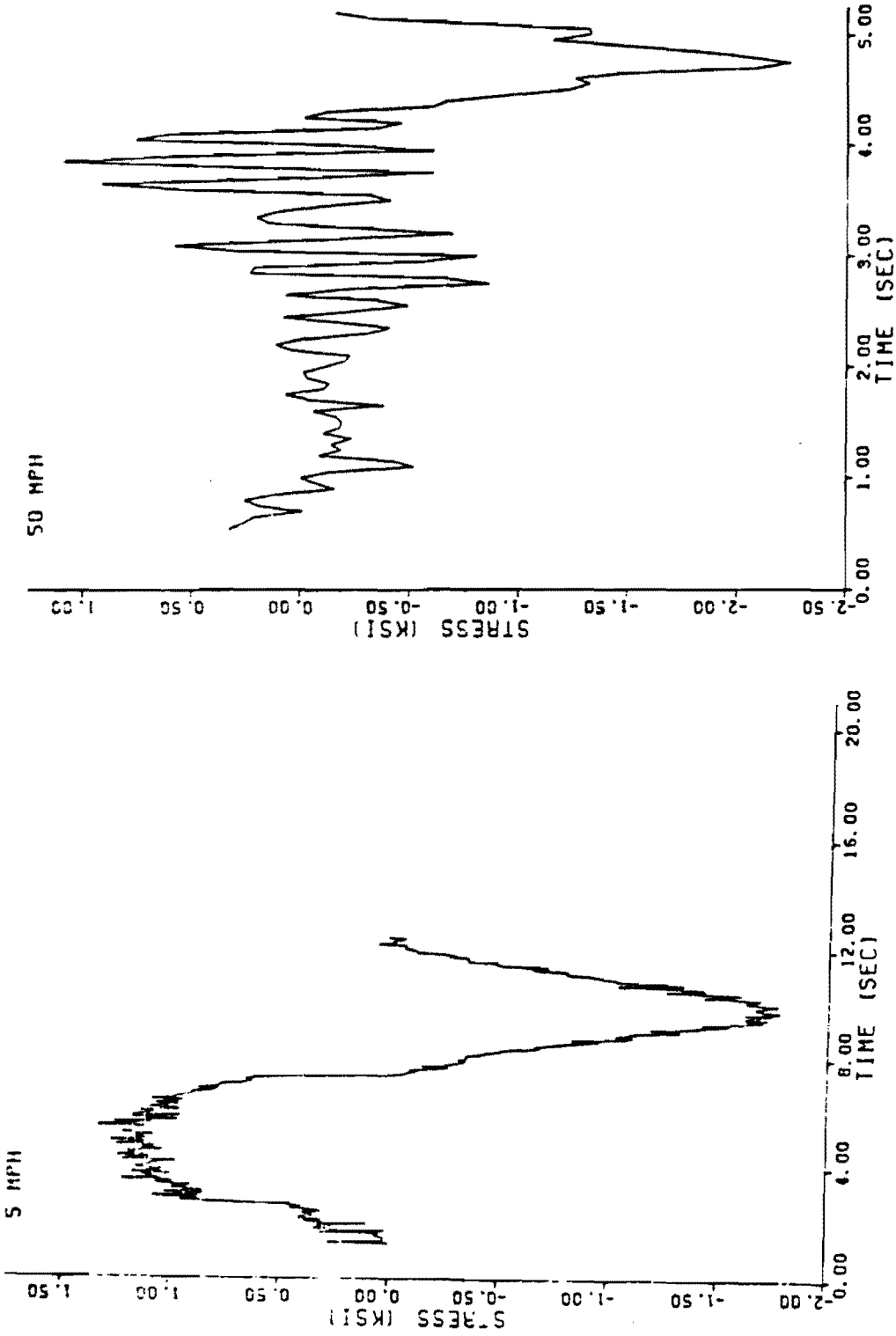

Fig. B.4 Sample stress-time histories for 5mph and 50mph truck velocities

Reducing the data from the test truck and traffic test into a single strain time history required four steps:

1. Change sign of all values from the strain gage on the top flange.
2. Normalization of the data so that each set of strain data began with a zero reading.
3. Eliminate grossly incorrect strain values by visual inspection of a strain-time plot.
4. Average the three strain-time histories to eliminate random signal noise.

Figure B.5 illustrates the four steps required in producing a single strain-time history.

To produce a manageable load history from the traffic data, a visual inspection of the strain-time plot was made to determine which sections were significant. Ten "significant" segments of the history were retained to use in testing. An example of a significant segment is shown in Fig. 3.4. A full description of the traffic load histories used in testing can be found in Section 3.1.2. This procedure was not required for the test truck data because record length was already manageable.

To reduce the number of points required to produce the desired strain-time history, only peaks in the history were counted as endpoints. A peak is defined as a relative maximum or relative minimum in the strain-time history. The definition is illustrated by Fig. B.6. Omission of non-peaks does not affect the magnitude or number of load

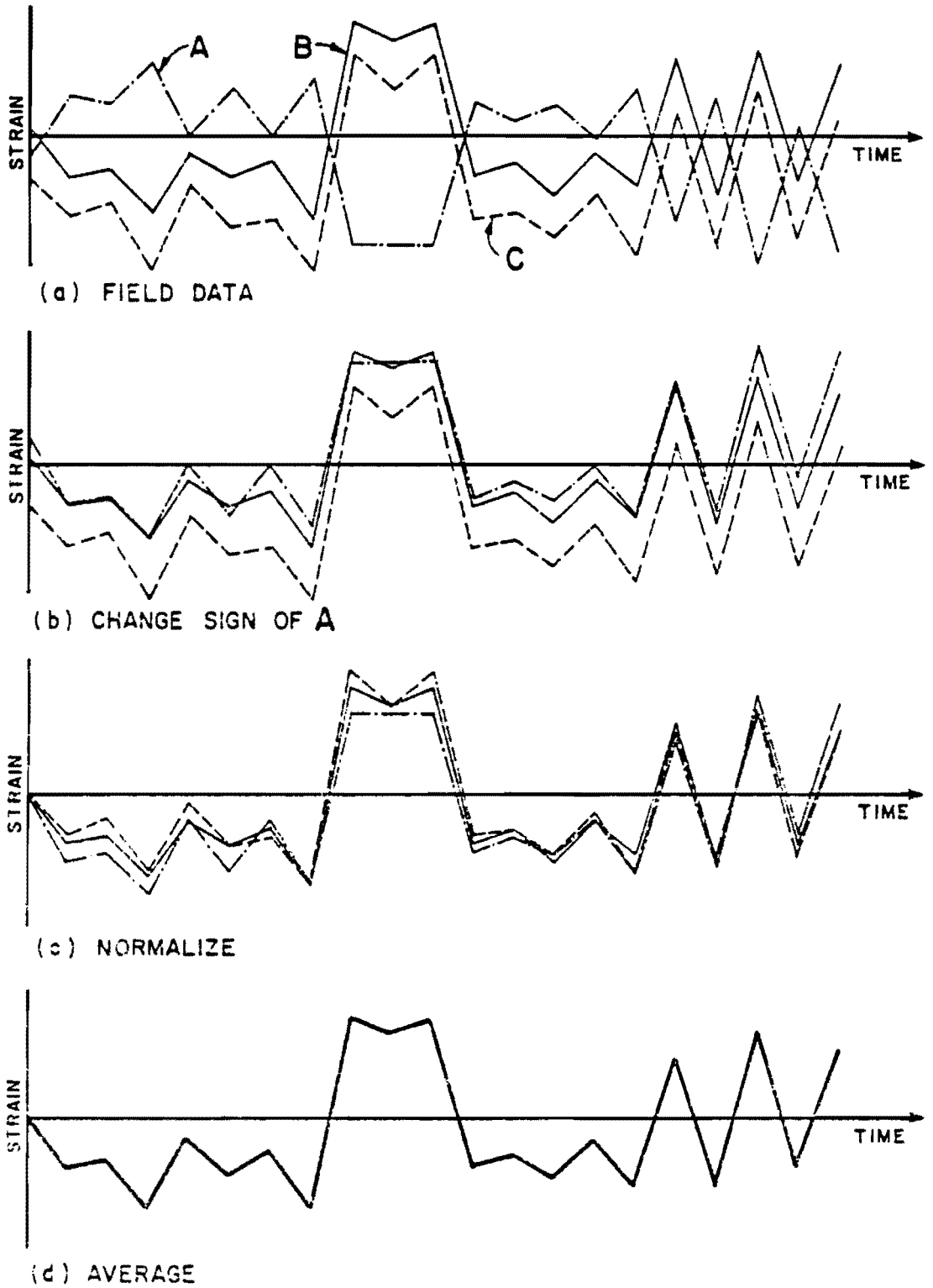

Fig. B.5 Reduction of strain-time field data

cycles in the history, as shown by comparing Figs. B.6 and B.7. Thus, it is assumed in this study that omission of non-peak endpoints does not affect fatigue behavior.

At this point, the strain-time history was transformed into a program for use in the microcomputer-based function generator. The function generator allowed the use of 512 unique endpoint values and 3715 program steps. This presented a problem because if each endpoint or peak is given a unique value, only 512 program steps may be used. To eliminate this problem, the range of available endpoint values from -100% to 100% of full load was divided into 510 intervals. The mean values of each interval was defined as the endpoint value. The value of any peak which fell in an interval was changed to the endpoint value of the interval. Since each interval accounted for only 0.392 percent of the maximum load, the greatest possible difference between the actual and assigned value of a peak is 0.196% of maximum load. This difference is negligible.

A Haversine loading function was used to connect the endpoints of the load history. The Haversine was used for two reasons: 1) hydraulic equipment produces continuous Haversines better than the discontinuous curves caused by ramping, and 2) a Haversine curve represents the actual loading better than ramping.

A final step was included in the data reduction to reduce testing time. The lag of the hydraulic response behind the command signal tends to limit the testing speed as discussed in Section 3.3. However, if the command load and the load rate are adjusted such that

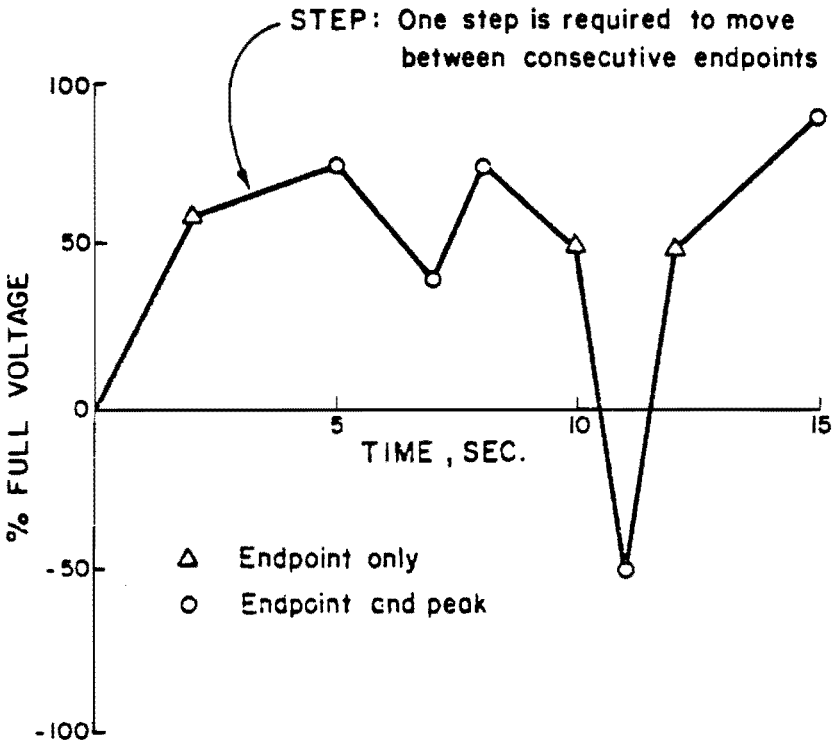

Fig. B.6 Sample programmed waveform

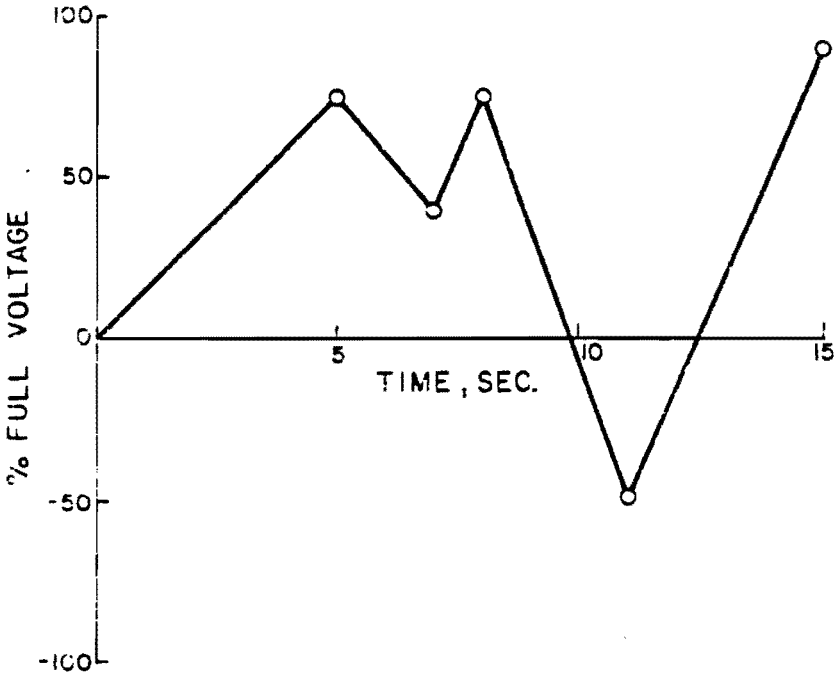

Fig. B.7 Sample programmed waveform with non-peak endpoints omitted

the difference between the command and desired loads is equal to the lag in response, testing speed can be increased. This type of adjustment in the command load is only accurate if the loading rate is constant throughout the history. Therefore, a constant loading rate was determined and the elapsed time between endpoints in the history was altered to produce the desired loading rate. The loading rate was much greater than any which would occur in service; however, the change in loading rate should not significantly affect the fatigue life of the specimen.

A P P E N D I X C

DESCRIPTIONS OF SIGNIFICANT EVENTS

A P P E N D I X C

DESCRIPTIONS OF SIGNIFICANT EVENTS

Figures C.1 through C.19 (odd) present the stress histories for each event used in the construction of traffic histories 1, 2, and 3. The use of these events is described more fully in Section 3.1.2. The scale used for the stress term in the stress history plots is based on the maximum stress recorded at 100 percent. This maximum stress occurred in Event 6. All other stresses in all events are scaled to this maximum. The time scale used in the stress history plots has no physical significance. The time scale was determined so that all events could be presented on the same scale to make comparisons easier.

Figures C.2 through C.20 (even) present the stress range histograms for each event. These histograms were developed from the results of a reservoir cycle count on each individual event. The maximum stress range in each event is given the value of 100 percent in that histogram. Included in each histogram is the record length in number of cycles, N, and the simple effective stress range calculated using Miner's and nonlinear Miner's theories.

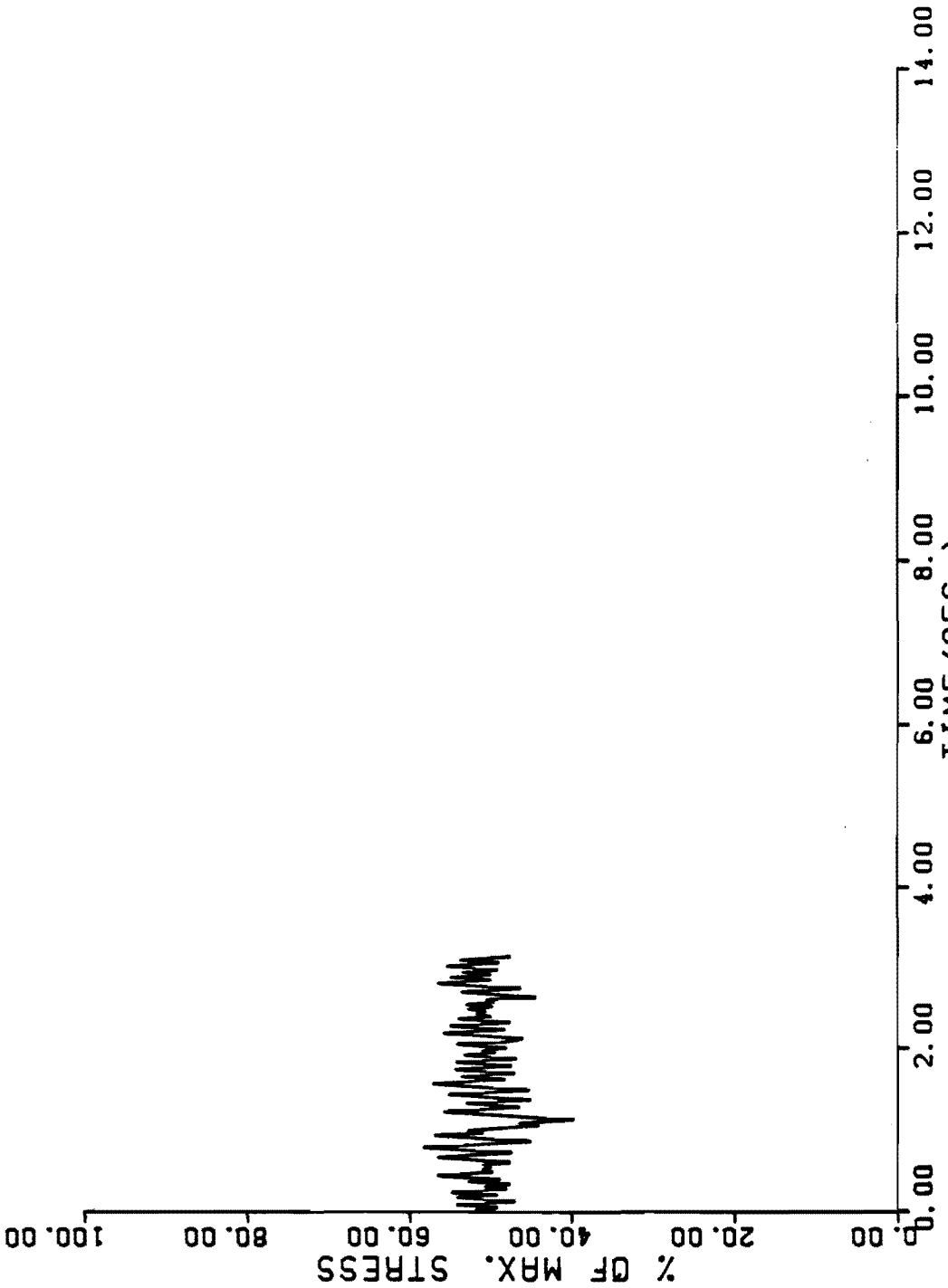

Fig. C.1 Plot of stress history of Event 1.

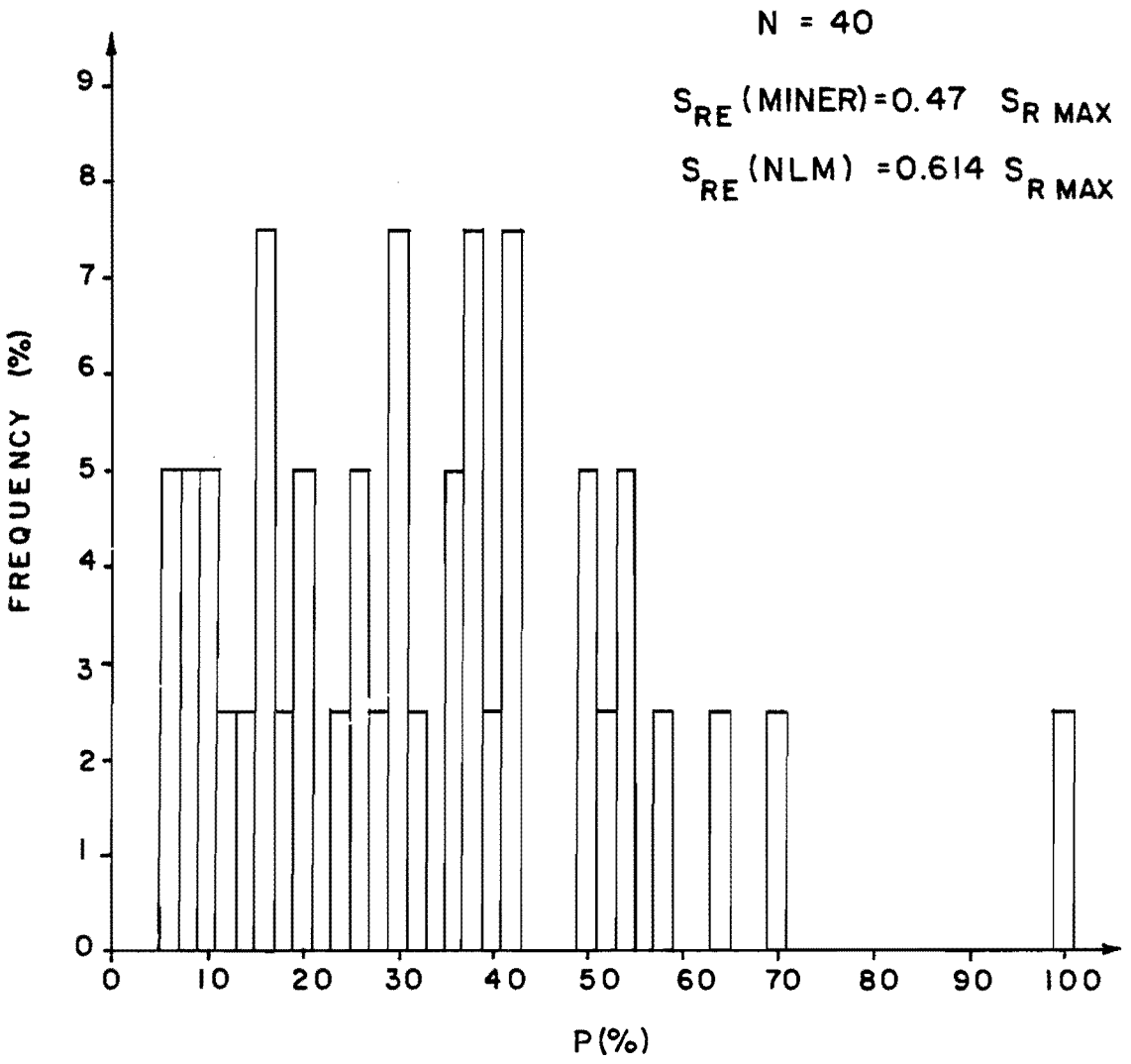

Fig. C.2 Stress range histogram of Event 1.

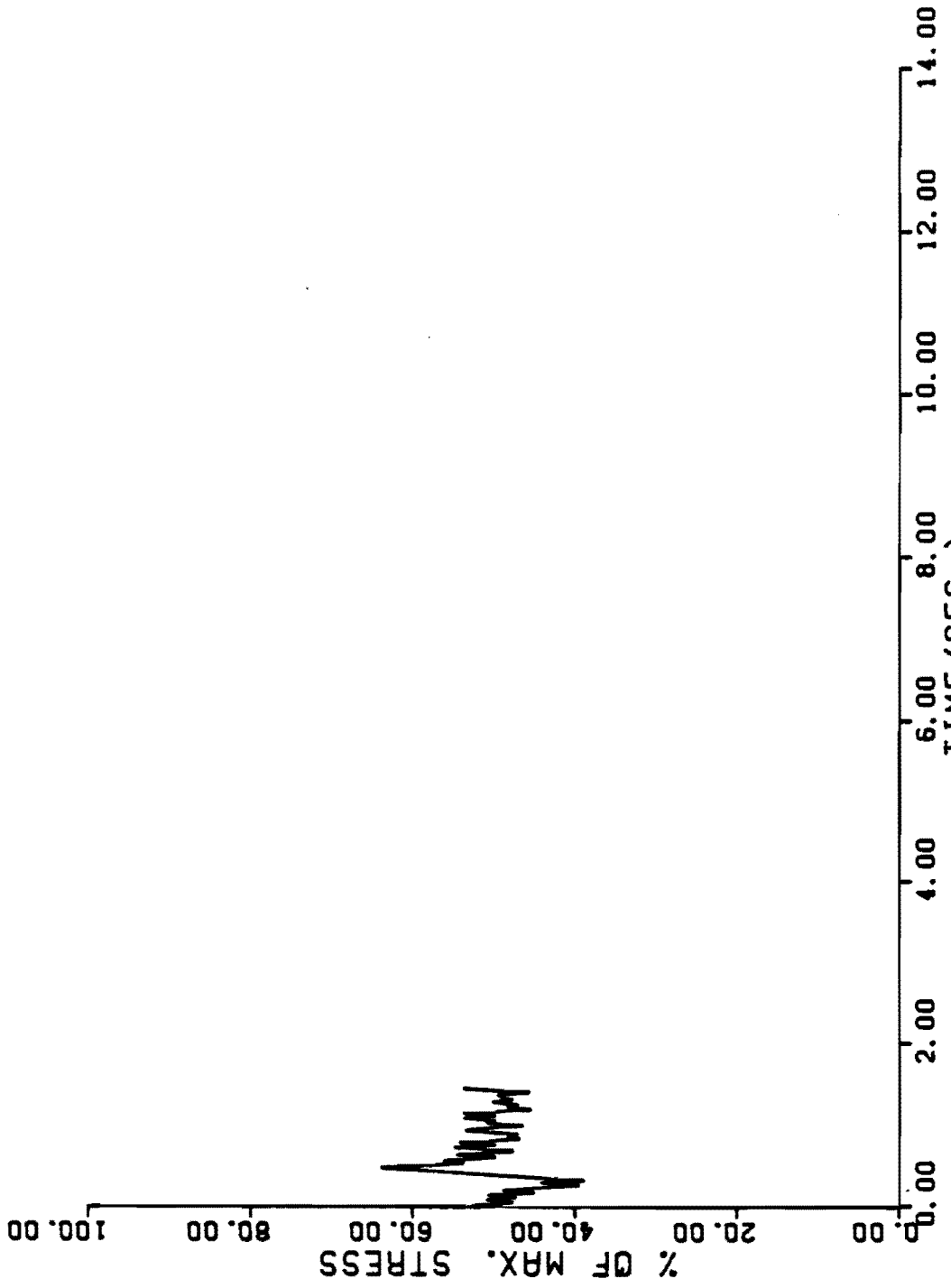

Fig. C.3 Plot of stress history of Event 2.

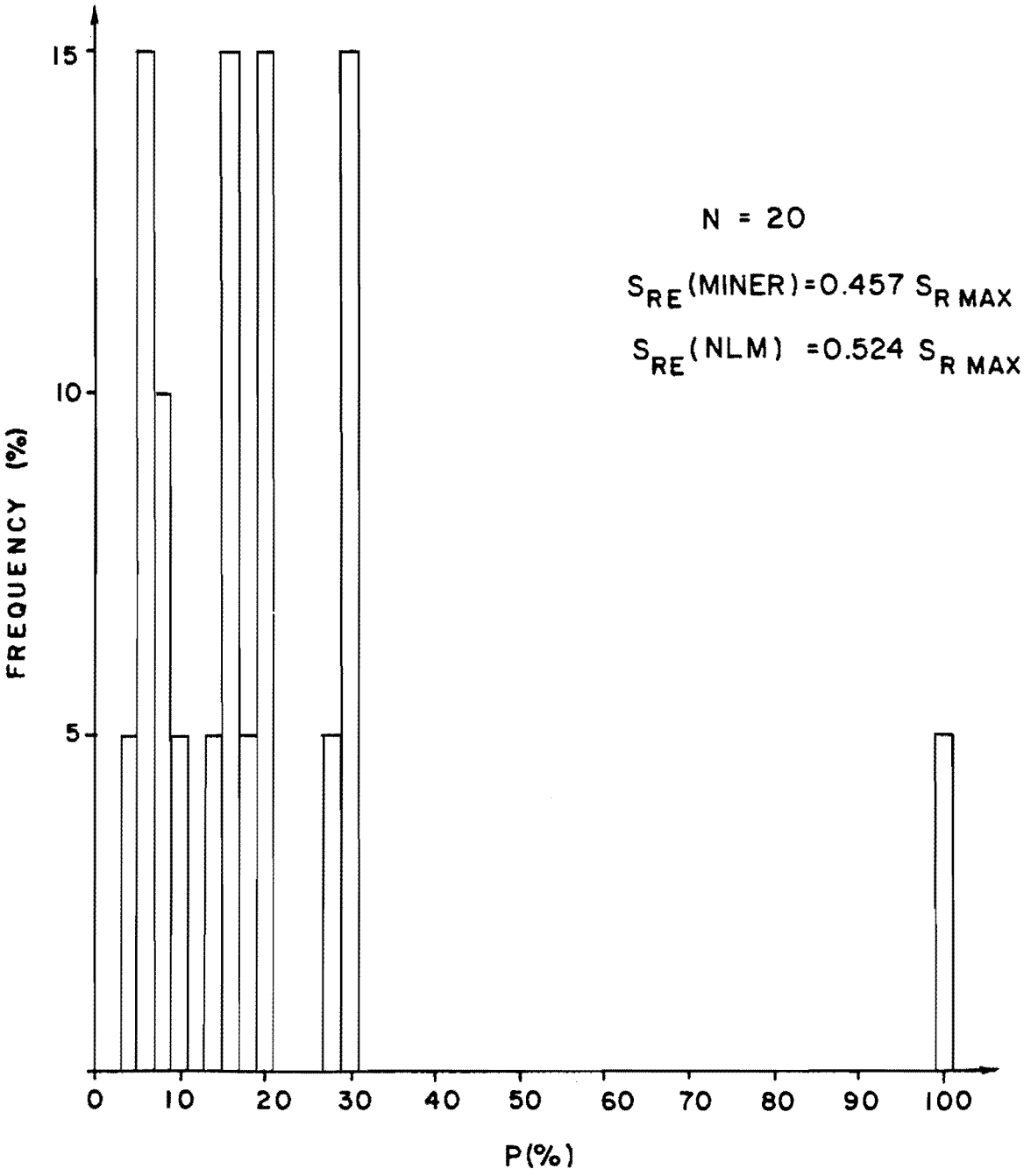

Fig. C.4 Stress range histogram of Event 2.

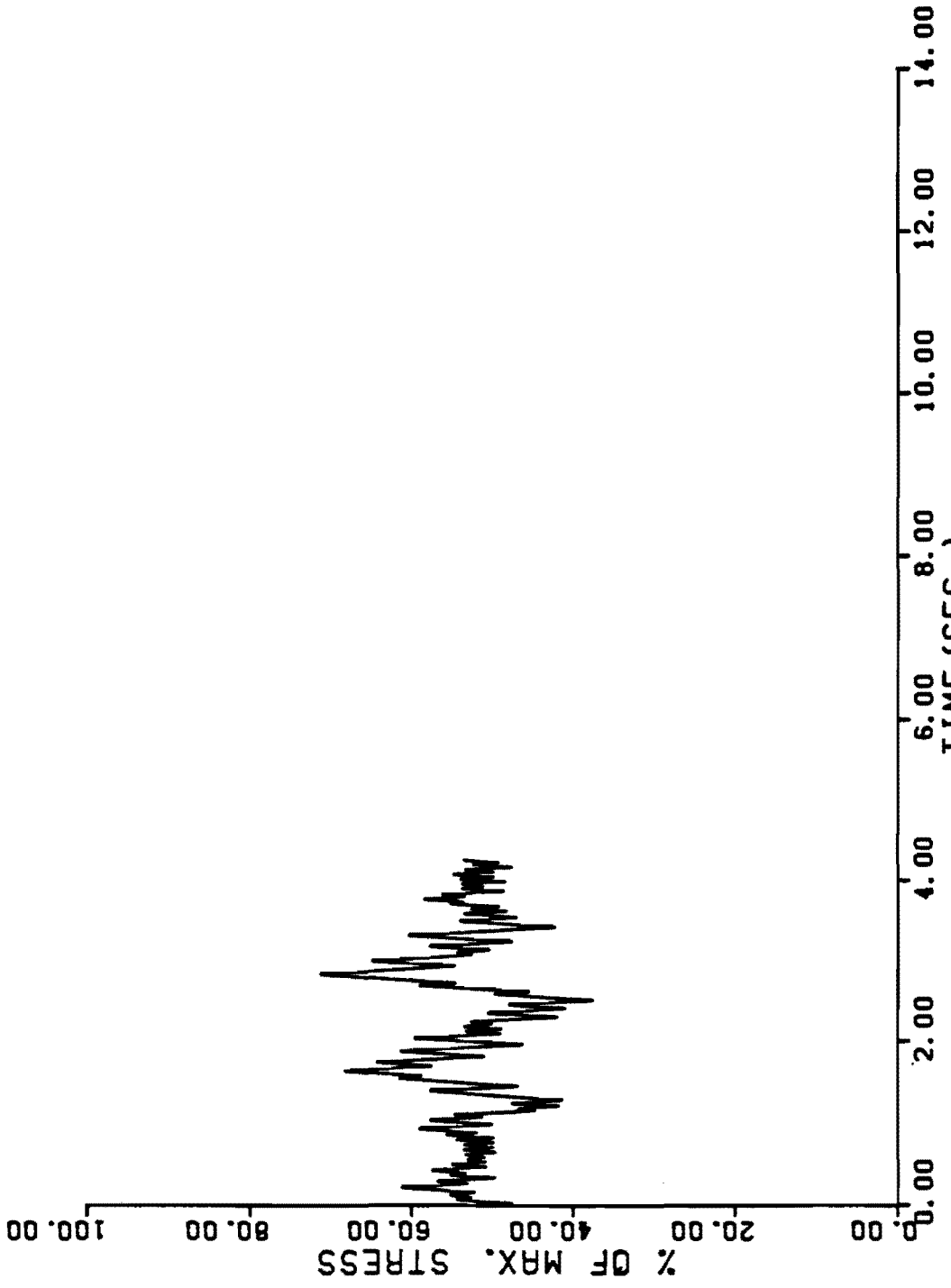

Fig. C.5 Plot of stress history of Event 3.

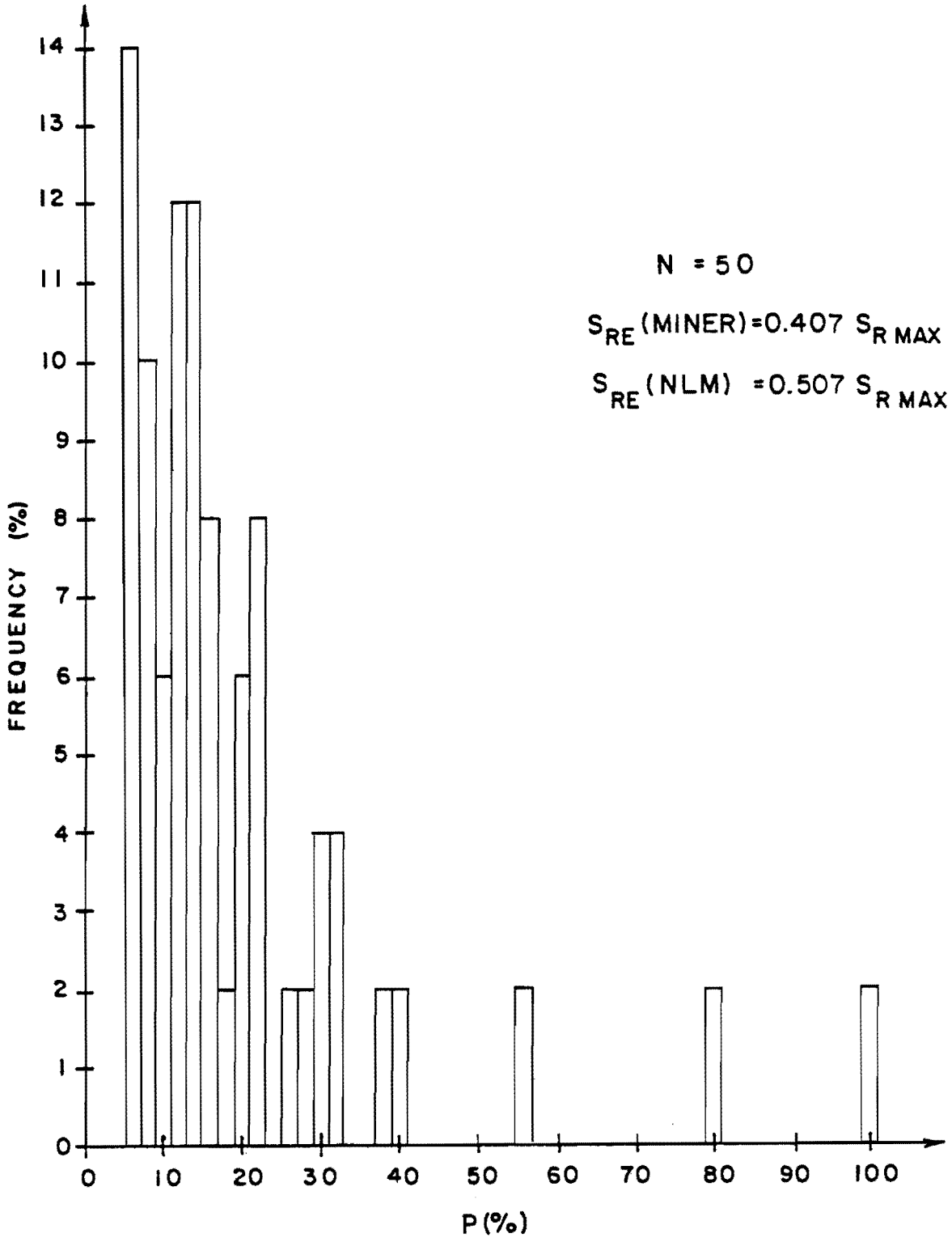

Fig. C.6 Stress range histogram of Event 3.

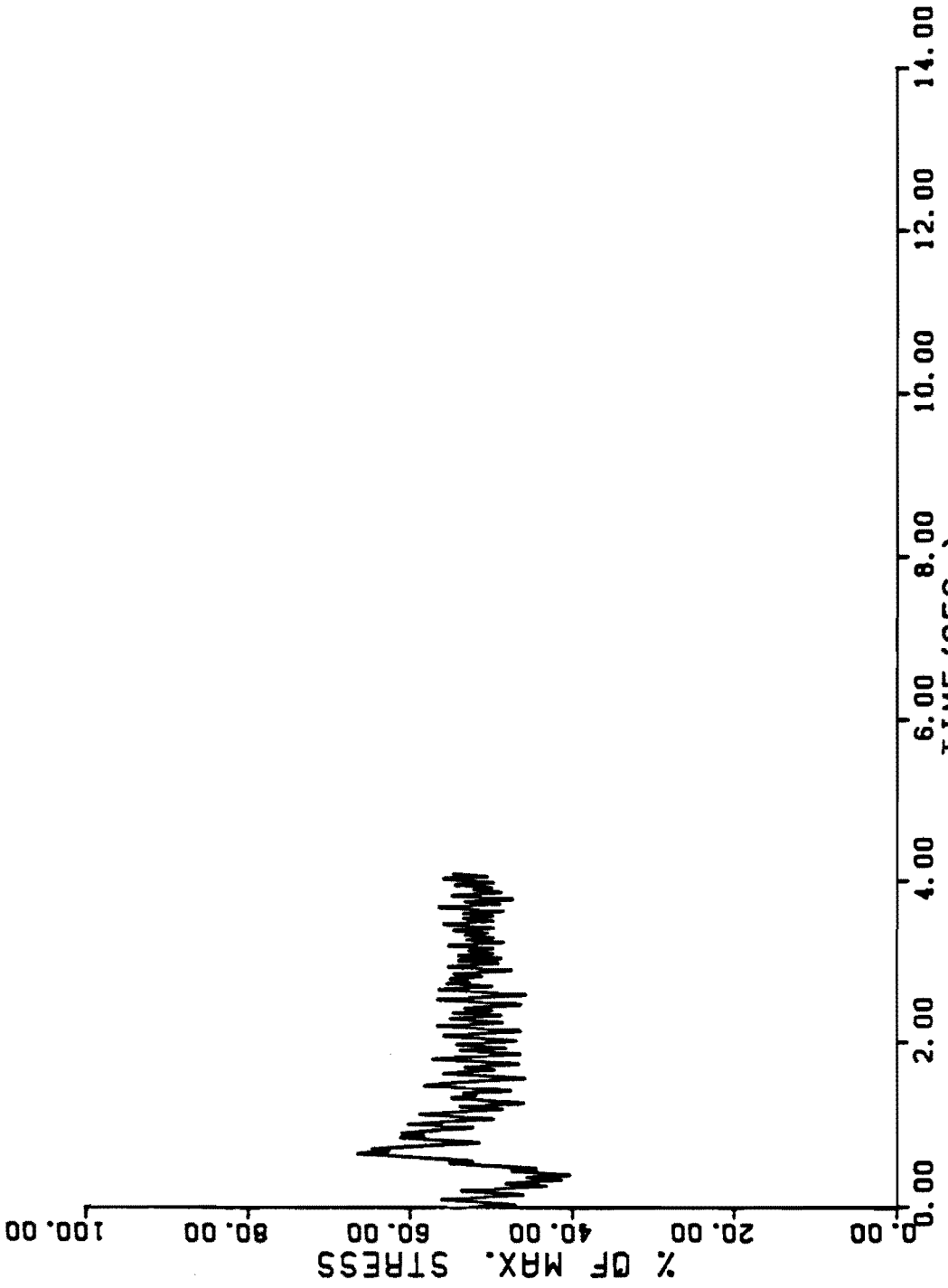

Fig. C.7 Plot of stress history of event 4.

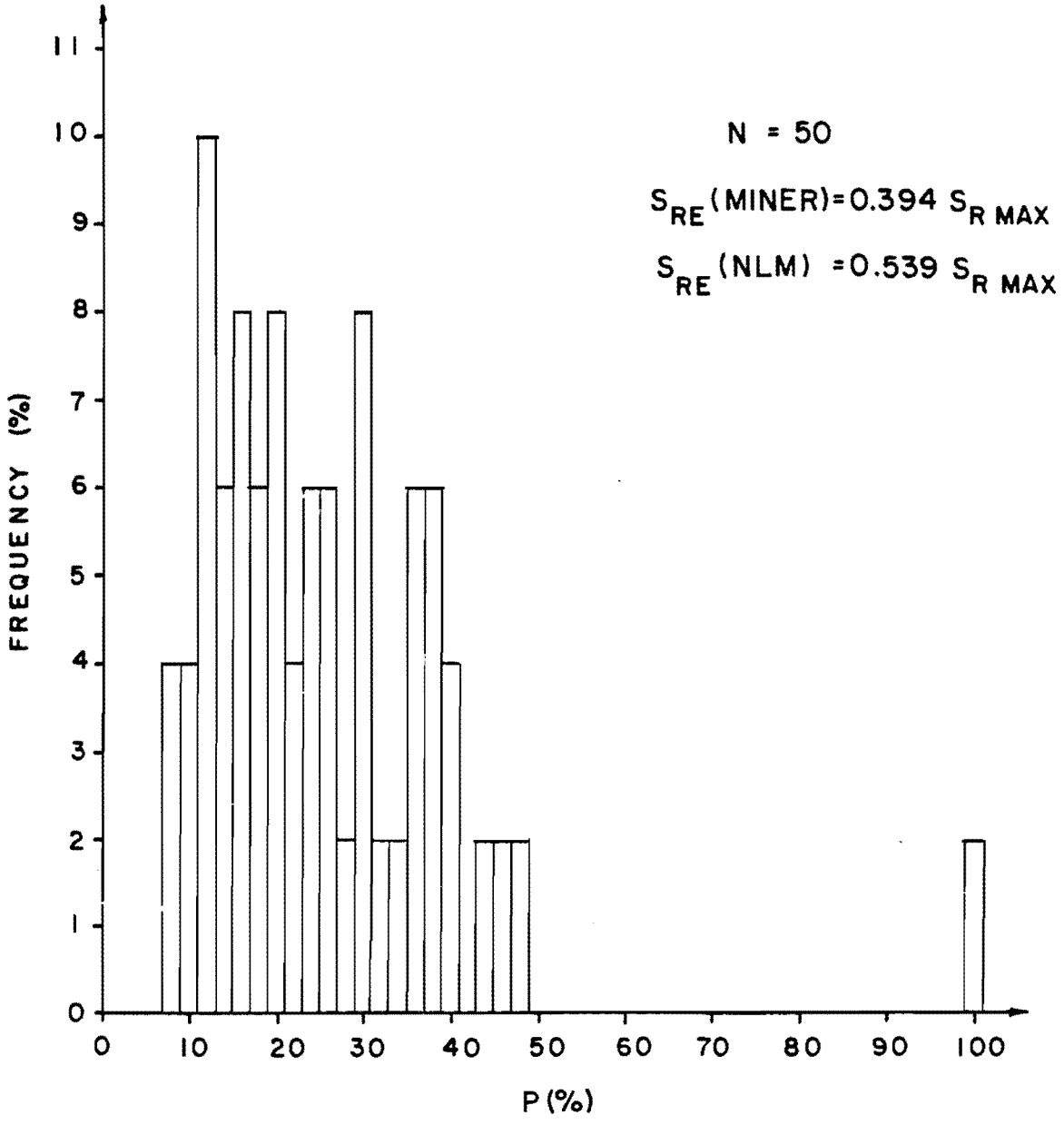

Fig. C.8 Stress range histogram of Event 4.

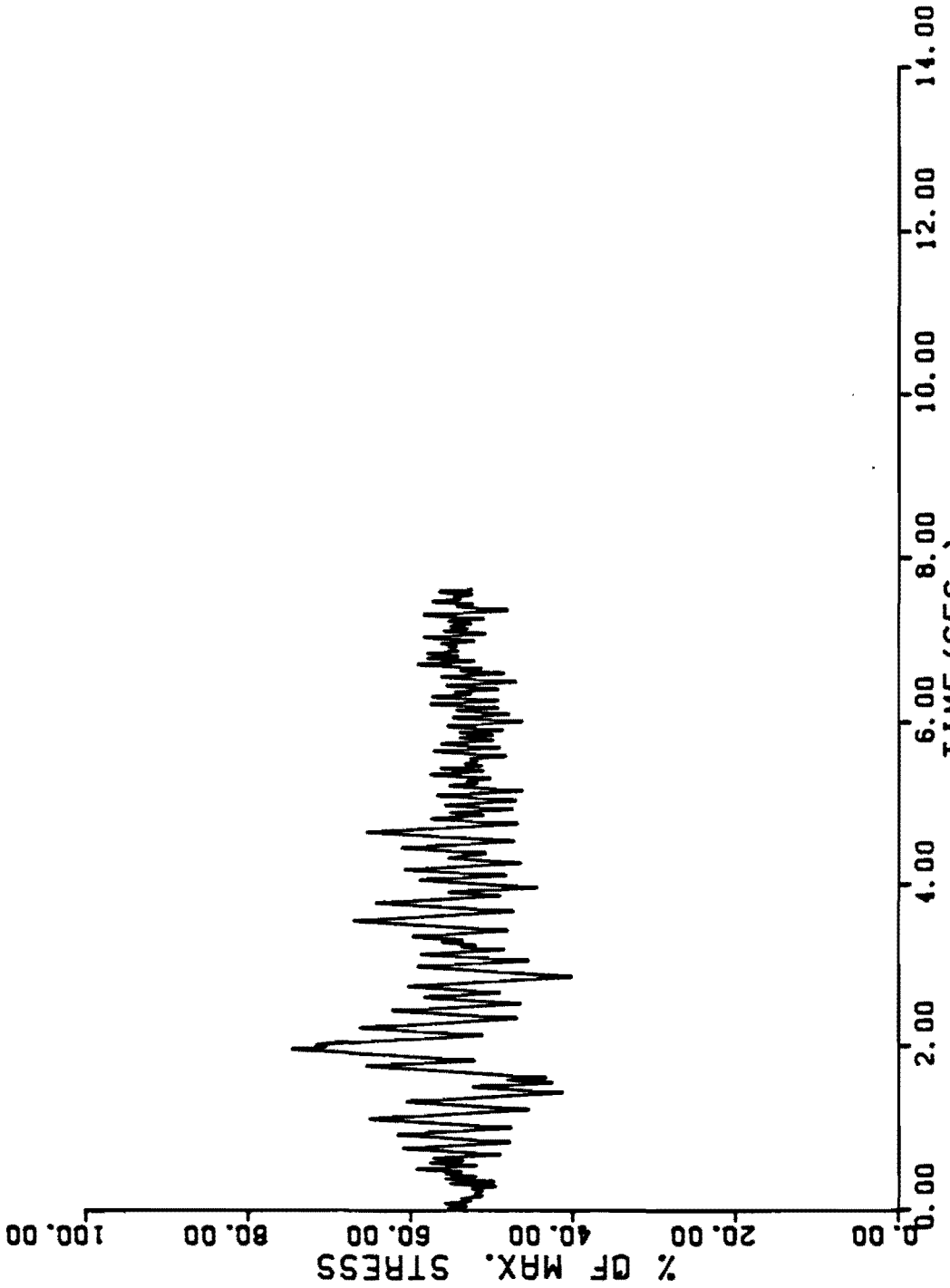

Fig. C.9 Plot of stress history of Event 5.

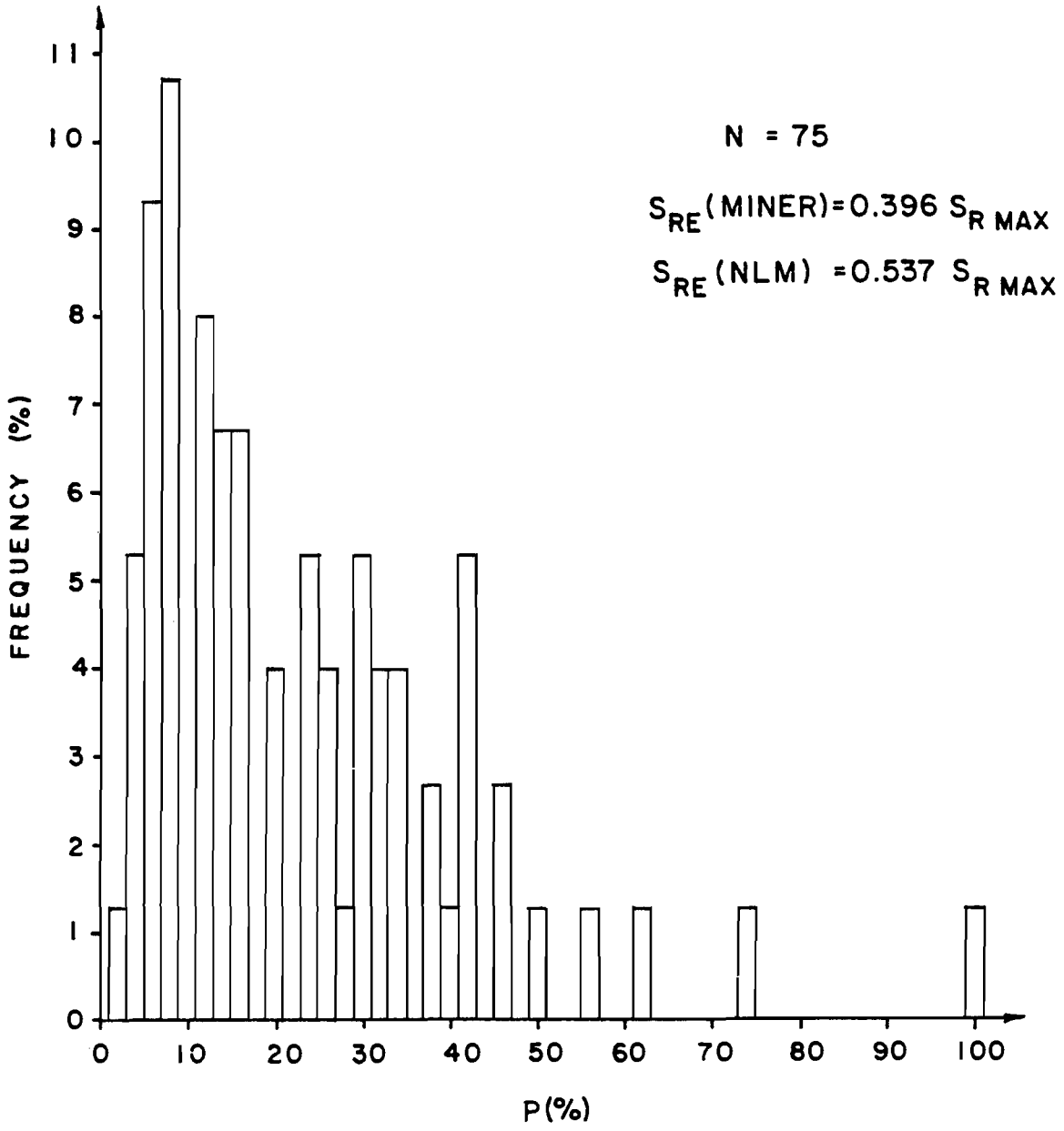

Fig. C.10 Stress range histogram of Event 5.

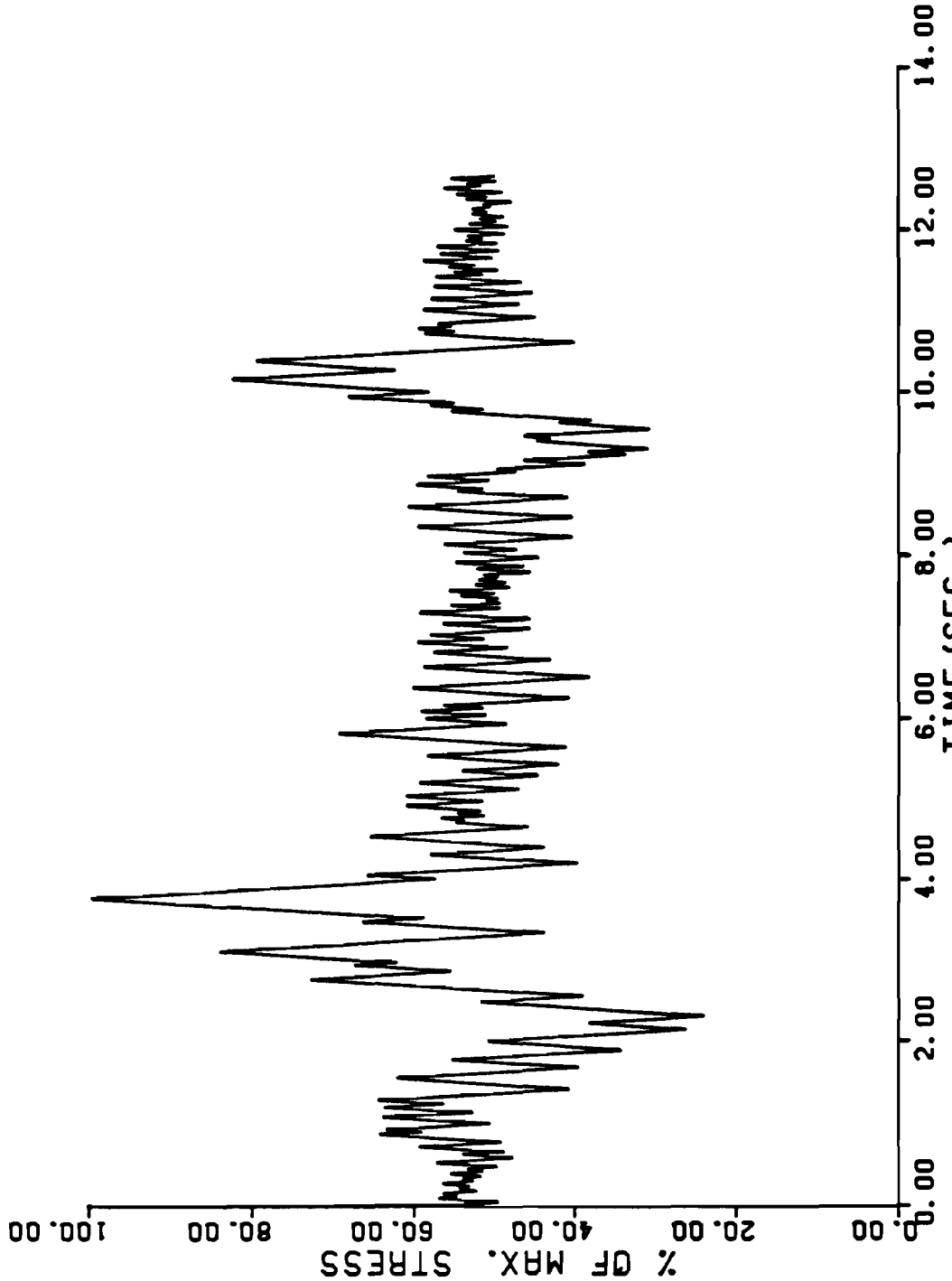

Fig. C.11 Plot of stress history of Event 6.

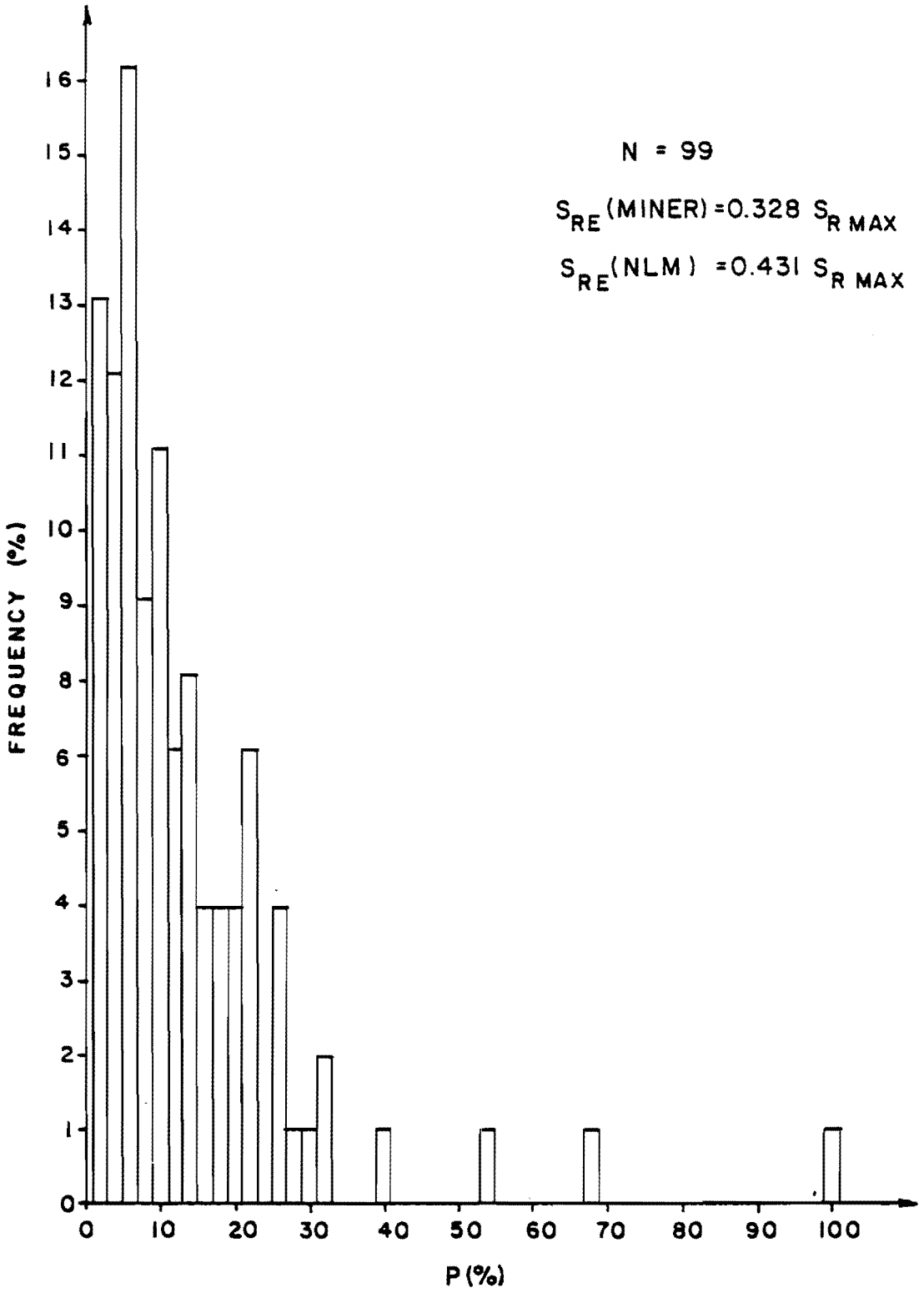

Fig. C.12 Stress range histogram of Event 6.

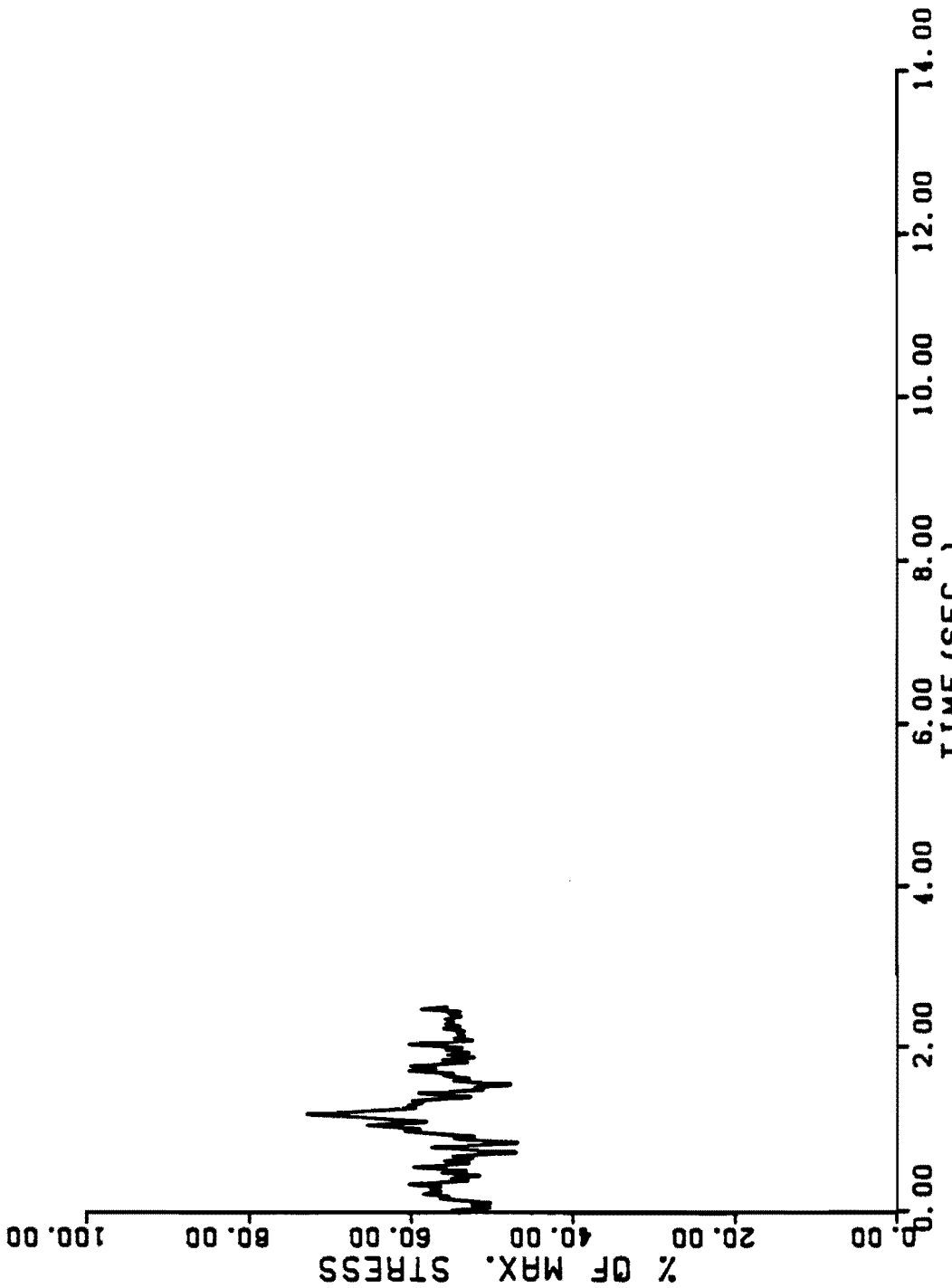

Fig. C.13 Plot of stress history of Event 7.

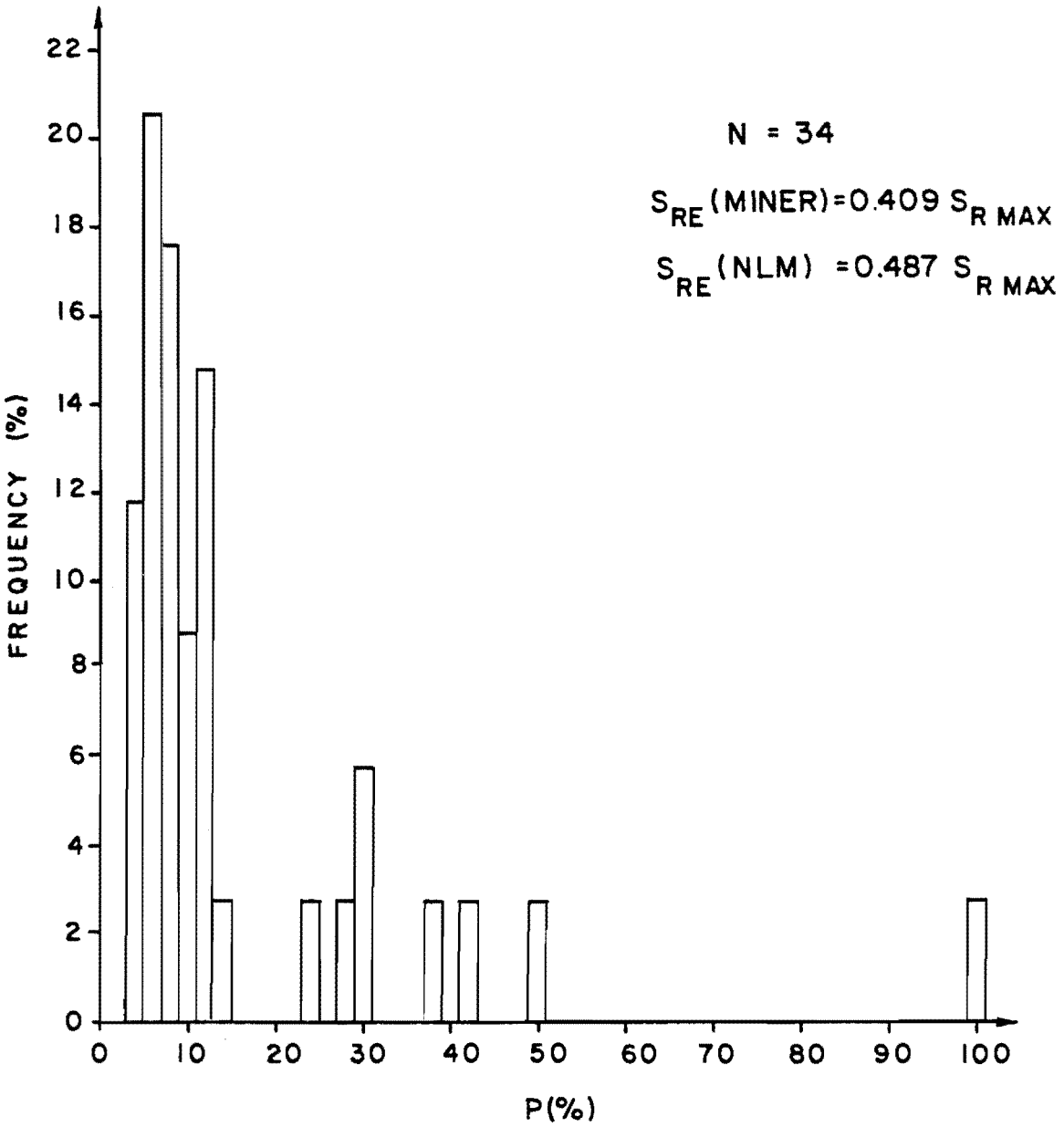

Fig. C.14 Stress range histogram of Event 7.

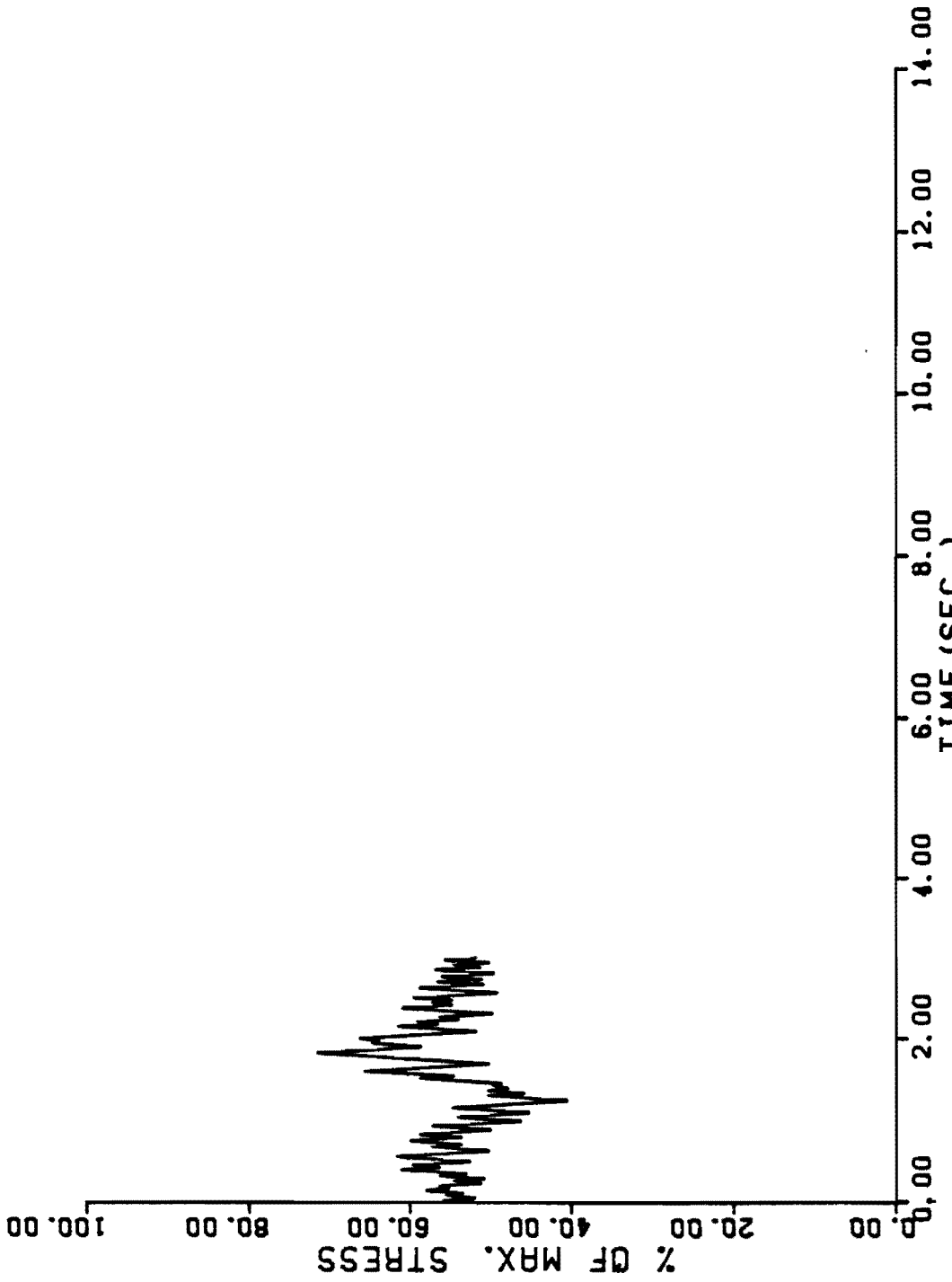

Fig. C.15 Plot stress history of Event 8.

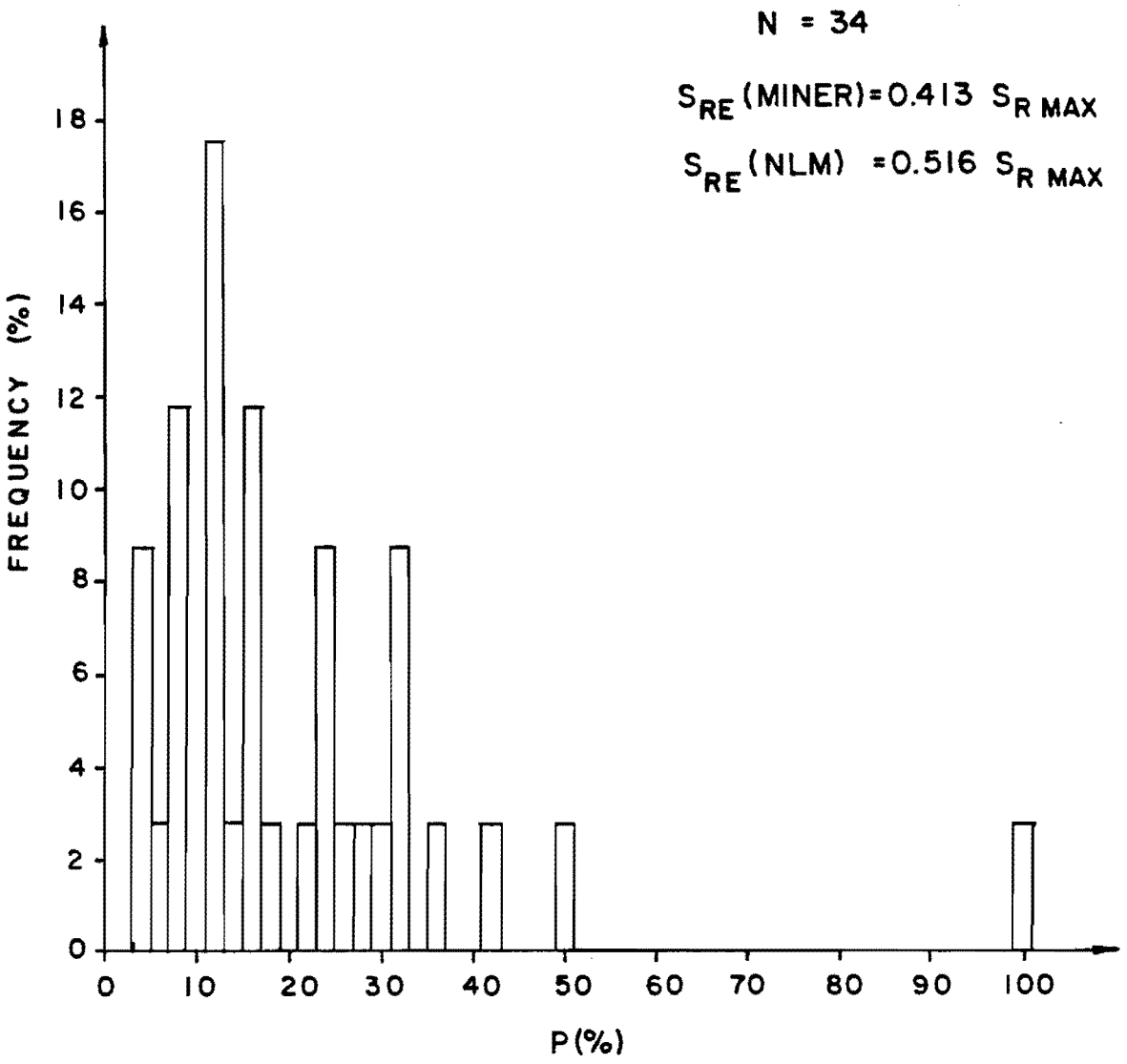

Fig. C.16 Stress range histogram of Event 9.

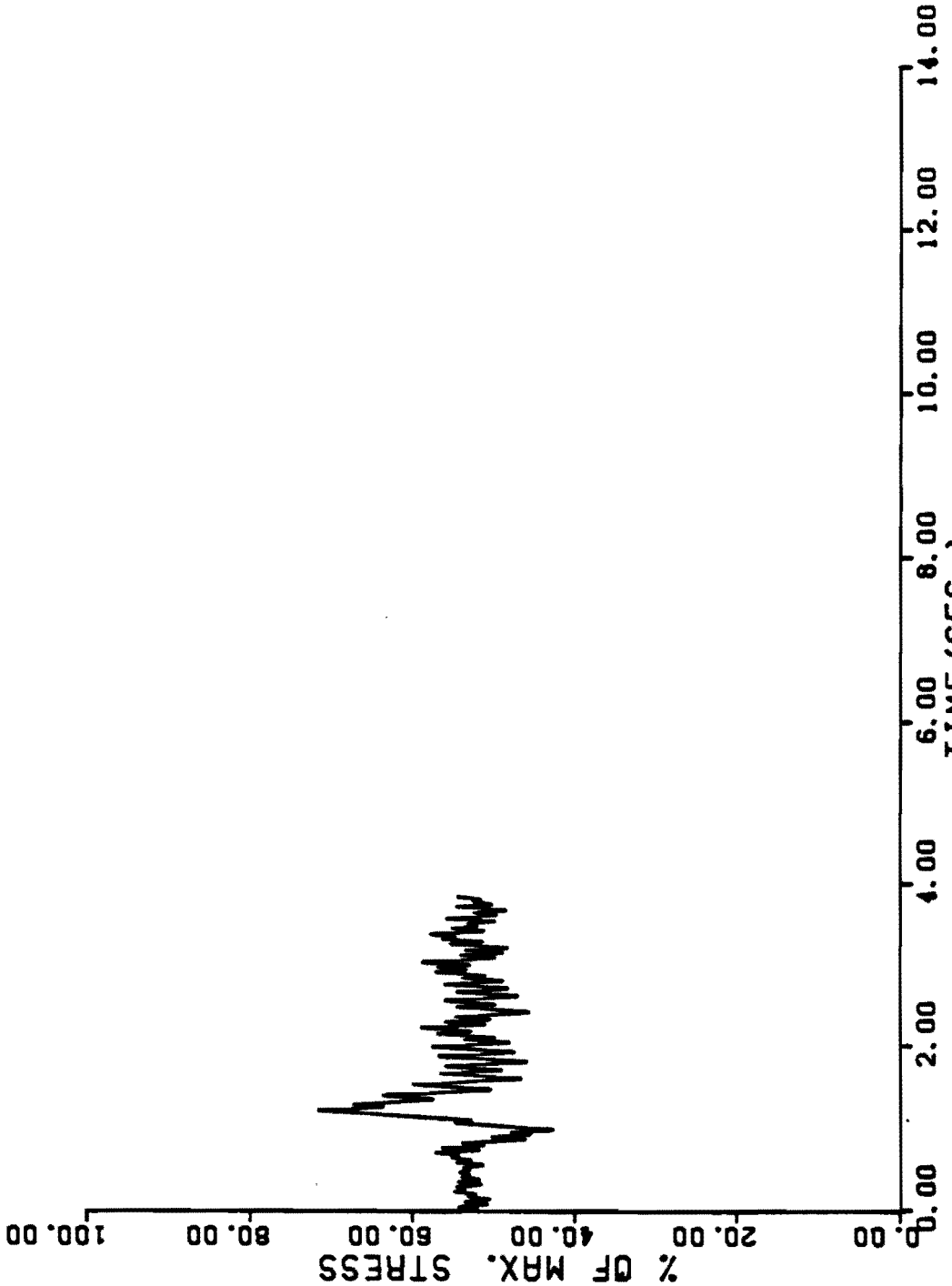

Fig. C.17 Plot of stress history of Event 9.

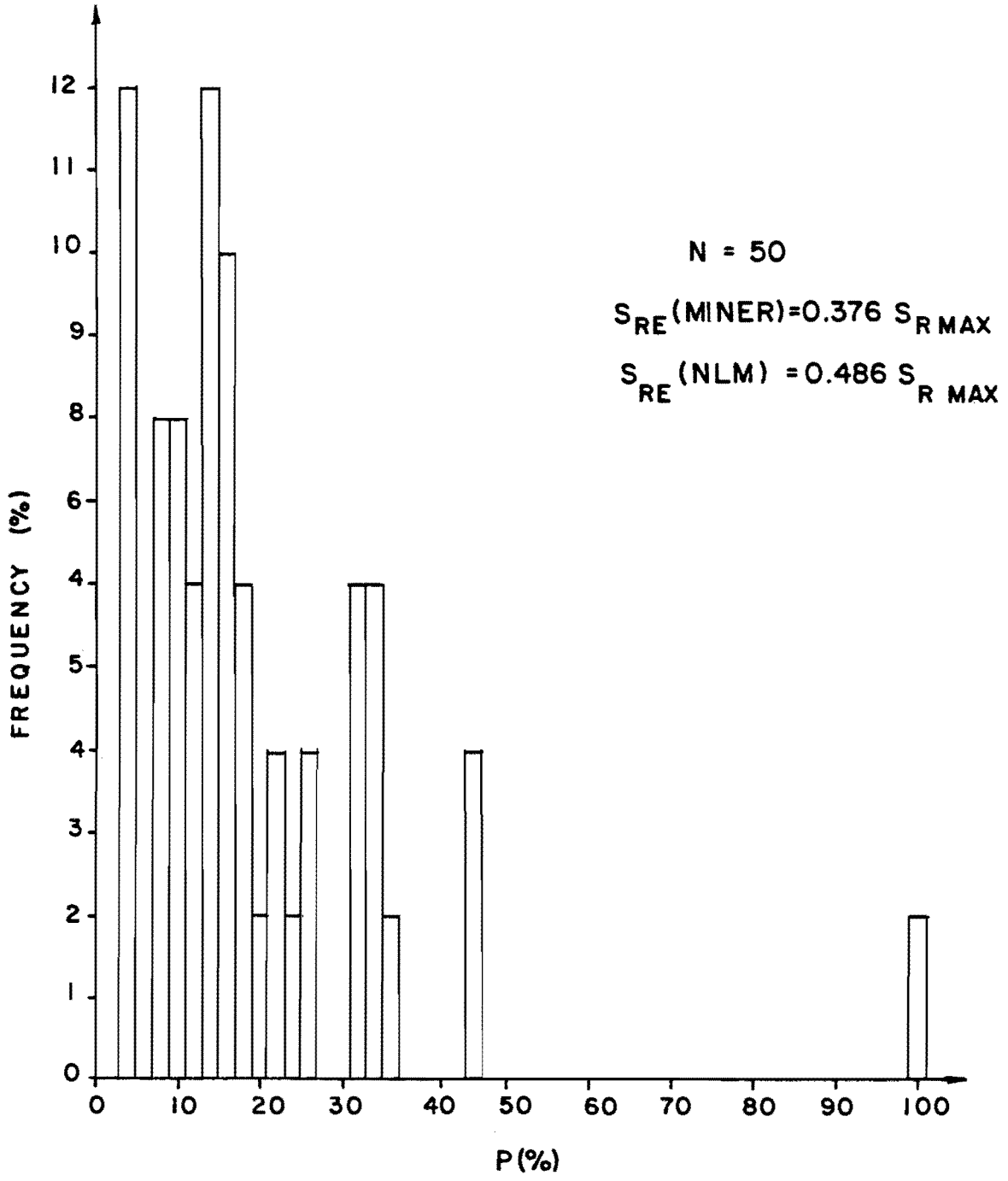

Fig. C.18 Stress range histogram of Event 9.

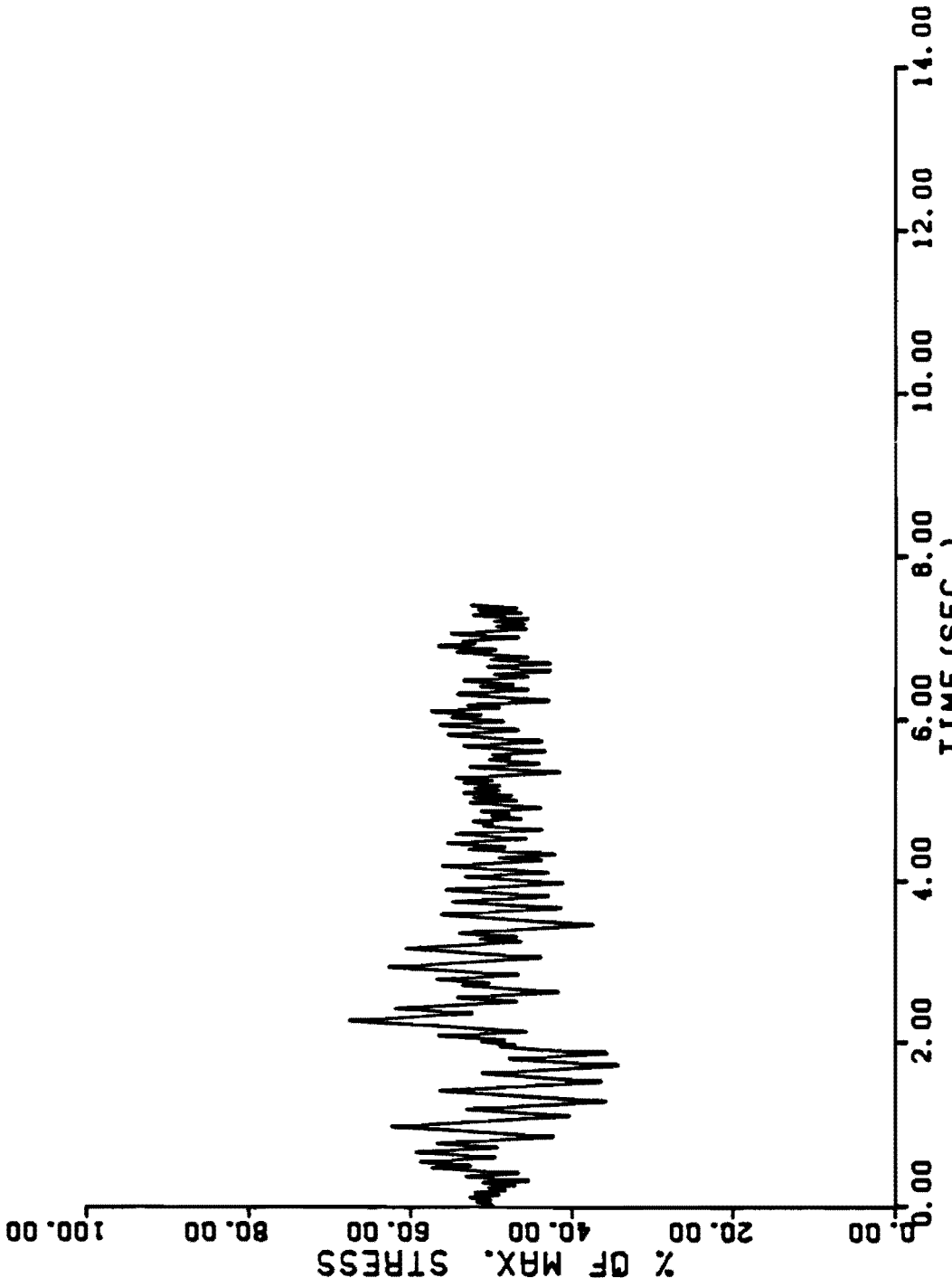

Fig. C.19 Plot of stress history of Event 10.

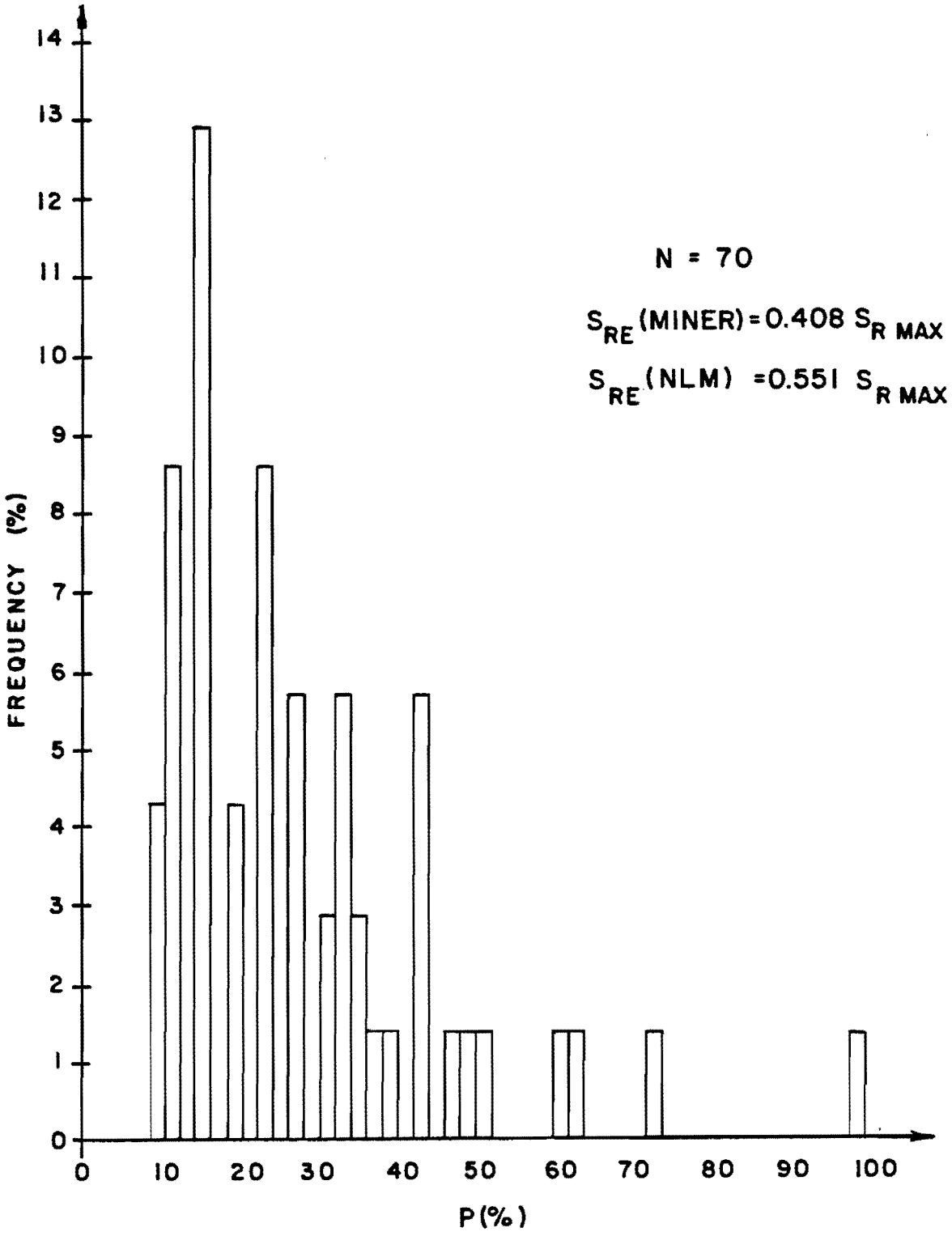

Fig. C.20 Stress range histogram of Event 10.

REFERENCES

1. Zwerneman, F. J., "Influence of the Stress Level of Minor Cycles on the Fatigue Life of Steel Weldments," unpublished M.S. thesis, The University of Texas at Austin, May 1983.

2. Fisher, J. W., Bridge Fatigue Guide--Design and Details, AISC, 1977.

3. Dowling, N. E., "Fatigue Failure Predictions for Complicated Stress-Strain Histories," Journal of Maerials, Vol. 7, No. 1, March 1972, pp. 71-87.

4. Wirshing, P. H., and Shehata, A. M., "Fatigue under Wide Band Random Stresses Using the Rainflow Method," Journal of Engineering Materials and Technology, July 1977, pp. 205-211.

5. End, T., Mitsunaga, K., Takahashi, K., Kobayashi, M., and Matsuishi, M., "Damage Evaluation of Metals for Random or Varying Load--Three Aspects of Rainflow Method," Mechanical Behavior of Materials, Proceedings of the 1974 Symposium on Mechanical Behavior of Materials, The Society of Materials Science, Japan.

6. The Committee on Fatigue and Fracture Reliability of the Committee on Structural Safety and Reliability of the Structural Division, "Fatigue Reliability: Variable Amplitude Loading," Journal of the Structural Division, ASCE, ST1, January 1982, pp. 47-66.

7. Willenborg, J. D., Engle, R. M., and Wood, H. A., A Crack Growth Retardation Model Using an Effective Stress Concept, AFFDL-TM-FBR-71-1, Air Force Flight Dynamics Laboratory, 1971.

8. Wheeler, O. E., "Spectrum Loading and Crack Growth, Journal of Basic Engineering, ASME, March 1972, pp. 181-186.

9. Bell, P. D., and Wolfman, A., "Mathematical Modeling of Crack Growth Interaction Effects," Fatigue Crack Growth Under Spectrum Loads, ASTM STP 595, 1976, pp. 157-171.

10. Schive, J., "Observations on the Prediction of Fatigue Crack Growth Under Variable Amplitude Loading," Fatigue Crack Growth Under Spectrum Loads, ASTM STP 575, American Society of Testing and Materials, 1976, pp. 3-23.

11. Miner, M. A., "Cumulative Damage in Fatigue," Journal of Applied Mechanics, Transactions, ASME, Vol. 67, September 1945, pp. A159-A164.

12. Schilling, C. G., Klippstein, K. H., Barsom, J. M., and Blake, G. T., "Fatigue Life of Welded Steel Bridge Members under Variable-Amplitude Loadings," National Cooperative Highway Research Report Program Report 188, Transportation Research Board National Research Council, Washington, D.C., 1978.

13. Gurney, T. R., "Some Fatigue Tests on Fillet Welded Joints under Simple Variable Amplitude Loadings," Research Report, The Welding Institute, 144/1981, May 1981.

14. Joehnk, J. M., "Fatigue Behavior of Welded Joints Subjected to Variable Amplitude Stresses," unpublished Master's thesis, The University of Texas at Austin, August 1982.

15. Abtahi, A., Albrecht, P., and Irwin, G. R., "Fatigue Behavior of a Periodically Overloaded Transverse Stiffener Detail," Journal of the Structural Division, ASCE, Vol. 102, No. ST11, Proc. Paper 12516, November 1976, pp. 2103-2119.

16. Albrecht, P., and Yamada, K., "Simulation of Service Fatigue Loads for Short-Span Highway Bridges," in P. R. Abelkis and J. M. Potter, Eds., Service Fatigue Loads Monitoring, Simulation and Analysis, ASTM STP 671, American Society of Testing and Materials, 1979, pp. 255-277.

17. Broek, David, Elementary Engineering Fracture Mechanics, Third Edition. The Hague: Martinus Nijhogg, 1982, pp. 250-283.

18. Hoadley, Peter W., "Estimation of the Fatigue Life of a Welded Steel Highway Bridge from Traffic Data," unpublished MS thesis, The University of Texas at Austin, May 1982.

19. Fisher, J. W., Yen, B. T., and Frank, K. H., "Minimizing Fatigue and Fracture in Steel Bridges," Journal of Engineering Materials and Technology, Vol. 102, Jan. 1980, pp. 20-25.

20. Alder, J. F., "Cumulative Damage in Fatigue of Welded Structures," British Welding Journal, October 1964, pp. 501-506.

21. Fisher, J. W., Mertz, D. R., Zhong, A., "Steel Bridge Members under Variable Amplitude, Long Life Fatigue Loading," NCHRP Project 12-15(4), September 1983.

22. Schilling, C. G., Klippstein, K. H., "Fatigue of Steel Beams by Simulated Bridge Traffic, Journal of the Structural Division, ASCE, ST8, August 1977, pp. 1561-1575.

23. Jacoby, G. H., Norwalk, H., and Van Upzig, H. T. M., "Experimental Results and a Hypothesis for Fatigue Crack Propagation under Variable-Amplitude Loadings, Fatigue Crack Growth Under Spectrum Loads, ASTM STP 595, 1976, pp. 47-60.

24. Booth, G. S., "Constant Amplitude Fatigue Tests on Welded Steel Joints Performed in Air," Proceedings, European Offshore Steels Research Seminar, Cambridge, U.K., 27-29 November 1978.

25. Maeda, Yukio, "Fatigue Cracks of Deep Thin-Walled Plate Girders," Transportation Research Record 664, Bridge Engineering, Vol. 1, 1978, pp. 120-128.

26. Ouchida, H., and Nishioka, A., "A Study of Fatigue Strength of Fillet Welded Joints," U.D.C. 620.178.3:621.791.053.26, Hitachi Review, April 1964.

27. Wildschut, Back, Dortland, and Van Leeuween, "Fatigue Behavior of Welded Joints in Air and Sea Water," Proceedings, European Offshore Steels Research Seminar, Cambridge, U.K., 27-29 November 1978.

28. Tilly, G. P., and Nunn, D. E., "Variable Amplitude Fatigue in Relation to Highway Bridges," The Institute of Mechanial Engineers, Applied Mechanics Group, Proceedings, 1980, Vol. 194, No. 27, pp. 258-267.

29. Alzos, W. X., Skat, A. C., Jr., and Hillberry, B. M., "Effect of Single Overload/Underload Cycles on Fatigue Crack Propagation," Fatigue Crack Growth Under Spectrum Loads, ASTM STP 595, American Society for Testing and Materials, 1976, pp. 41-60.

30. Slockbower, R. E., and Fisher, J. W., "Fatigue Resistance of Full Scale Cover-Plated Beams," Penn DOT Research Project 72-3, June 1978.

31. Platten, D. A., "Analytical Study of Fatigue Behavior of a Longitudinal-Transverse Stiffener Intersection," unpublished M.S. Thesis, University of Texas at Austin, May 1980.

32. Pass, J. D., Frank, K. H., and Yura, J. A., "Fatigue Behavior of Longitudinal Transverse Stiffener Intersection," Research Report 247-2F, Center for Transportation Research, Bureau of Engineering Research, University of Texas at Austin, October 1982.

33. Kohutek, T. L., and Frank, K. H., "Anaysis of Truck and Wind Loadings on the Silver Memorial Bridge," Research Report CESRL-WV-1, University of Texas at Austin, August 1979.